Anglia Ruskin University

DYNAMIC FINITE ELEMENT ANALYSIS OF HIP RESURFACING ARTHROPLASTY AND THE INFLUENCE OF RESTING PERIODS

CARLOS JIMENEZ-BESCOS

A Thesis in partial fulfilment of the requirements of Anglia Ruskin University for the award of a Doctor of Philosophy

This research was sponsored by the Engineering and Physical Sciences Research Council (EPSRC)

Submitted: April, 2013

ANGLIA RUSKIN UNIVERSITY

ABSTRACT

FACULTY OF SCIENCE & TECHNOLOGY

DOCTOR OF PHILOSOPHY

DYNAMIC FINITE ELEMENT ANALYSIS OF HIP RESURFACING ARTHROPLASTY AND THE INFLUENCE OF RESTING PERIODS

By CARLOS JIMENEZ-BESCOS

April 2013

The third generation of hip resurfacing commenced in the U.K. in the 1990's with the *Birmingham Hip Resurfacing* system and is now becoming more commonplace as an attractive alternative for young and active patients due to premature failure in total hip replacement in this patient group. However the Swedish National Hip Arthroplasty Register (2010) suggests that premature failure of resurfacing arthroplasty may be more prevalent than first expected. The aim of this study is to investigate, through Finite Element Analysis, the short, medium and long term performance of Poly Methyl Methacrylate (PMMA) bone cement of the femoral component in hip resurfacing arthroplasty. The study takes a forensic engineering approach, analysing the performance of PMMA bone cement in order to provide understanding, awareness and an insight into lifestyle options.

Finite Element Analysis explores and models the effect of resting periods during daily activities, patients' bone quality and PMMA bone cement Young's modulus on the PMMA bone cement stresses within the femoral hip resurfacing component. Mechanical tests are used to illustrate the use of the Finite Element Analysis results.

Contributing to knowledge, this study verifies the significance of high metal-on-metal friction due to resting periods, developing a dynamic FEA model to quantify the premature fatigue failure of PMMA bone cement, within the femoral component of hip resurfacing arthroplasty. A decrease in bone quality added to the effect of resting periods increase the risk of PMMA fatigue failure and PMMA-metal interface failure due to an increase of PMMA tensile and shear stresses, suggesting that patients with low bone quality should avoid hip resurfacing procedures. The use of low PMMA Young's modulus could greatly enhance the long term success of hip resurfacing arthroplasty generally and specifically reduce the risk of interface failure and PMMA bone cement failure due to resting periods and patient bone quality. Moreover, this study shows that the consequence of PMMA fatigue failure and PMMA-metal interface failure must be included in the design, patient selection, screening process, post-operative rehabilitation and long term lifestyle attributes.

This study suggests that occupational therapists and patients with hip resurfacing arthroplasty should be aware of high metal-on-metal friction situations, which could lead to early failure indicated by this research. The deleterious effect of resting periods indicated by this research could be alleviated by appropriate re-initiation of synovial lubrication by movement prior to full loading. Recommendations for further work include the compilation of a PMMA bone-cement fatigue properties database and further development of the FEA modelling technique for application upon other arthroplasty procedures.

Keywords: Hip resurfacing, PMMA bone cement, resting periods, Finite Element Analysis, fatigue.

Acknowledgments

All pictures, sketches and diagrams belong to the author unless otherwise referenced.

Many people have helped me to get here today, directly or indirectly. I would like to thank each of them here but that would mean adding a second volume to my thesis.

I would like to thank my Mum and Dad for all their hard work during so many years to get me to school, university and to this point in my life. I just hope I can make you proud one day of all your efforts.

Thanks to Claire McCauley for being there when I needed her the most and give me strength to finish this endeavour keeping my head.

Thanks to all the members of the Medical Engineering Research Group for their support along all these years. I am particularly grateful to: Professor Kevin Cheah FRCS for all his advice and sharing his knowledge in the operating theatre with me; Prof Paul Ingle for all his support and guidance.

Dr Mario Cortina-Borja for all his help, support and understanding especially with statistics; Dr. Bruce Murphy for supplying very gladly the raw fatigue data; Dr. Markus Wimmer for sharing his raw data on frequency of resting periods; Dr. Andrew Hopkins for all his advice in dynamic Finite Element Analysis; Prof. Mark Taylor and Prof. Patrick Prendergast for being very kind to advise me on my work during conferences.

I would like to thank every member of staff in the Built Environment Department for all their support and words of encouragement. It is a pleasure and a privilege to share an office with all of you. Further thanks to Philip Langstone and Steve Read for all their help to keep my computers running and keeping me safe in the workshop.

John Buchanan and Lyndis Reynolds for proof reading this thesis and listening to so many things about my ordeal over a glass of wine. Thanks to Ian Frame for all his encouragement and support during all this years and for being there every time I needed him.

I am very grateful to the Engineering and Physical Science Research Council (EPSRC) for supporting this research.

Particular thanks go to my supervisors for all their support, trust and encouragement through this adventure. I will always be in debt to all of you. First to Dr Alan Coday, who has been very patient with me and shown me new ways in research and writing to explore. Alan, Thursdays will not be the same again without our long morning meetings and even better, we got here without crashing the car. Dr David Reid, who was very kind to support me in this adventure and for always believing in me. Dr Robert Walker, who inspired me to embrace the path of Finite Element Analysis and share so many days of simulations and mechanical testing.

"Never was any mountain ever conquered without the first step being taken"

Abbreviations used in this Thesis

Abbreviation	Full Meaning
BHR	Birmingham Hip Resurfacing
BQ	Bone Quality
Co-Cr	Cobalt-Chrome
COF	Coefficient of Friction
DEXA	Dual Energy X-ray Absorptiometry
DVT	Deep Venous Thrombosis
EPSRC	Engineering and Physical Science Research Council
FEA	Finite Element Analysis
FRCS	Fellow Of The Royal College Of Surgeons
ICLH	Imperial College London Hospital
ISO	International Organization for Standardization
MoM	Metal on Metal
MoP	Metal on Polyethylene
NAFEMS	National Agency for Finite Element Methods and Standards
NJR	National Joint Registry
PMMA	Poly Methyl Methacrylate
SAE	Society of Automotive Engineers
TARA	Total Articular Replacement Arthroplasty
THARIES	Total Hip Articular Replacement by Internal Eccentric Shells
THR	Total Hip Replacement
UHMWPE	Ultra High Molecular Weight Polyethylene
UCS	Ultimate Compressive Stress
UTS	Ultimate Tensile Stress

Symbols used in this Thesis

Symbol	Meaning
F_X	Force in the x direction
F_y	Force in the x direction
F_z	Force in the x direction
E	Young's modulus
ρ	Density
P	Force applied
R	Relative radius of curvature
R1	Radius of hole
R2	Radius of pin
a	Contact radius
α	Half the angle subtended by the contact radius.
Po	Maximum pressure
ν	Poisson's ratio
E*	Effective Young's modulus
n_i	number of applied stress cycles
N_f	cycles to failure at that stress level
S_{max}	Maximum stress
S_{min}	Minimum stress
S_r	Stress range
$S_{amp} = S_a$	Stress amplitude
$S_{mean} = S_m$	Mean stress
R	Stress ratio
$S_{a\|sm}$	0
$S_{amp\text{-}eq}$	Stress amplitude for zero mean
S_{TS}	Tensile strength of the material
$S_{max\text{-}eq}$	Maximum stress for zero mean
$S_{min\text{-}eq}$	Minimum stress for zero mean
$S_{mean\text{-}eq}$	Mean stress for zero mean
R^2	Coefficient of determination
μ	Metal on metal friction coefficient
E_{PMMA}	PMMA Young's modulus

Specialist Nomenclature used in this Thesis

Acetabular (Acetabulum)	Concave surface of the pelvis, where the femur sits.
Arthroplasty	Orthopaedic surgery where the articular surface of a musculoskeletal joint is replaced, remodeled, or realigned.
Aseptic loosening	Failure in the lack of any disease-causing contaminants.
Avascular necrosis	Death of bone cells due to lack of blood supply.
Bone cement	Tissue compatible material (PMMA) used for artificial joints fixation.
Cancellous bone	Soft or spongy tissue forming the inner part of bone.
Cementless (uncemented)	Artificial joint fixation in the absent of bone cement.
Cortical bone	Hard tissue forming the outer part of bone.
Interdigitation	Process to describe the penetration of bone cement into the spongy cancellous bone to form a solid bonding.
Meshless	An FEA model with a adaptive mesh generation.
Orthopaedic	Branch of surgery related to conditions of the musculoskeletal system.
Osteoarthritis	Degradation of the joint due to wear and tear of the joints developing into damage to the contact surfaces in the joint with the consequent pain when moving the joint
Osteolysis	Bone resorption due to wear particles in the joint.
Rainflow counting method	Analytical technique used in fatigue studies to reduce variable stress levels into simple stress reversal cycles.
Resorption	Degeneration of bone tissue resulting in bone loss.
Sawbone	Synthetic composite bone used in orthopaedic research with similar properties to natural bone.
Varus positioning	Positioning of an implant with a smaller angle between the femoral stem and the femur shaft after the procedure compared to the original angle between the femoral neck and femur shaft.
Valgus position	Positioning of an implant with a bigger angle between the femoral stem and the femur shaft after the procedure compared to the original angle between the femoral neck and femur shaft.

Table of Contents

ABSTRACT i
Acknowledgments ii
Abbreviations used in this Thesis iii
Symbols used in this Thesis iv
Specialist Nomenclature used in this Thesis v
Table of Contents vi
List of Figures x
List of Tables xviii
Copyright xx
Chapter 1 1
Introduction 1
1.1 Research Aim and objectives 4
1.2 Preliminary Research 5
1.2.1 Initial methodology 5
1.2.2 Finite Element Analysis conundrum 5
1.3 Initial Research Question 7
Chapter 2 8
Literature Review 8
2.1 Hip Anatomy 8
2.2 Hip Resurfacing Compared with the Natural Hip 9
2.3 Hip Resurfacing Compared to Total Hip Replacement 10
2.4 Reasons for Hip Resurfacing Operations 11
2.4.1 Osteoarthritis 11
2.4.2 Avascular necrosis 11
2.5 History of Hip Resurfacing 12
2.5.1 Early development of hip resurfacing 13
2.5.2 Modern era of hip resurfacing 14
2.6 Surgical Technique for Hip Resurfacing 17
2.7 Short Term Failure 21
2.7.1 Femoral neck fracture 21
2.7.2 Thrombophlebitis and infections 22
2.7.3 Bone necrosis 23
2.8 PMMA Cementing Technique 23

2.9 PMMA Failure Mode *25*
2.10 PMMA Fatigue Data *27*
2.11 Resting Periods *27*
2.12 Gait Data *30*
2.13 Biological Variables *31*
2.13.1 Bone quality 31
2.13.2 Patient selection 32
2.14 Combination of Factors *34*
Chapter 3 ..... **36**
Methodology **36**
3.1 Conceptual Framework *36*
3.2 The Use of the Conceptual Framework and the Evolution of the Research Aim *38*
3.3 Methodology *38*
3.4 Controlling Key Variables *40*
3.5 Drivers *42*
3.6 Research Paradigm *42*
3.7 Limitations of this Research *44*
Chapter 4 ..... **45**
Building and Corroborating the Finite Element Model **45**
4.1 Introduction *45*
4.2 The Model *46*
4.3 Boundary Conditions *48*
4.3.1 Contact interfaces and restraints 48
4.3.2 Hip contact forces and flexion-extension rotation 50
4.4 Material Properties *53*
4.4.1 Cortical bone and cancellous bone 53
4.4.2 PMMA bone cement 53
4.4.3 Hip resurfacing femoral implant and acetabular cup 54
4.5 Meshing *54*
4.6 Sensitivity Analysis *58*
4.6.1 Mass scaling 58
4.6.2 Sensitivity to metal-PMMA friction 62
4.6.3 Sensitivity to metal-bone friction 65
4.7 Corroboration of Finite Element Analysis Model *68*
4.7.1 Contact mechanics 70

4.7.2 Corroboration of simulation by comparison with clinical data and published work....71
4.8 Conclusion....74
Chapter 5 75
Applying the Model to Explore the Role of Resting Periods 75
5.1 Effect of Metal-on-Metal Friction Coefficient Due to Resting Periods During Daily Activities on PMMA Bone Cement Fatigue....76
5.1.1 Finite Element Analysis results for walking....80
5.1.2 Finite Element Analysis results for descending stairs....85
5.1.3 Finite Element Analysis results for standing up....91
5.1.4 Fatigue analysis....97
5.1.4.1 PMMA fatigue data....99
5.1.4.2 Rainflow counting method....102
5.1.4.3 Results....108
5.2 Effect of Bone Quality on PMMA Bone Cement Stresses....115
5.2.1 Finite Element Analysis results for walking....115
5.2.2 Finite Element Analysis results for descending stairs....122
5.2.3 Finite Element Analysis results for standing up....128
5.3 Effect of PMMA Young's Modulus on PMMA Bone Cement Stresses....134
5.3.1 Finite Element Analysis results for walking....134
5.3.2 Finite Element Analysis results for descending stairs....142
5.3.3 Finite Element Analysis results for standing up....150
5.4 PMMA Mechanical Testing....158
5.4.1 PMMA - metal interface....159
5.4.2 Torque testing....164
Chapter 6 168
Discussion....168
6.1 Effect of Metal-on-Metal Friction Coefficient Due to Resting Periods During Daily Activities on PMMA Bone Cement Fatigue....170
6.2 Effect of Bone Quality on PMMA Bone Cement Stresses....174
6.3 Effect of PMMA Young's Modulus on PMMA Bone Cement Stresses....176
6.4 PMMA Mechanical Testing....178
Chapter 7 180
Conclusions and Recommendations....180
7.1 Effect of Metal-on-Metal Friction Coefficient Due to Resting Periods During Daily Activities on PMMA Bone Cement Fatigue....180
7.2 Effect of Bone Quality on PMMA Bone Cement Stresses....182

7.3 Effect of PMMA Young's Modulus on PMMA Bone Cement Stresses 182
7.4 PMMA Mechanical Testing 183
Chapter 8 184
Recommendations for further work 184
8.1 Developing the Application to Other Procedures 184
8.2 Fatigue, Torque and Mechanical Test Databases 184
8.3. Limitations and Refinement of the Finite Element Model 185
References 186
Appendix A 195
Personal Reflection 195

List of Figures

Figure 1.1. Birmingham hip resurfacing (St Nicholas Hospital, accessed in 2012) 1
Figure 1.2. Comparison of hip resurfacing arthroplasty and total hip arthroplasty regarding femoral bone preservation (left) and components (right) (The McMinn Centre (left) and Active Joints Orthopedics (sic) (right), accessed in 2012) 2
Figure 1.3. Hemispherical reamed femoral head (left) and a chamfered cylindrical reamed femoral head (right) (*Biomet*, 2005) 3
Figure 1.4. Risk of revision following primary hip replacement according to bearing surface (NJR, 2011) 6
Figure 2.1. Hip joint (Orthoteers, 2007) 8
Figure 2.2. Hip joint movements (https://courses.stu.qmul.ac.uk/smd/kb/grossanatomy/basic_anat/movements_of_the_hip_joint.htm, accessed in October 2010) 9
Figure 2.3. Early hip resurfacing components. Smith Petersen's mould arthroplasty (top left), THARIES (top right) (Amstutz and Le Duff, 2006) and Warner (Amstutz et al., 1998). 12
Figure 2.4. McMinn hip resurfacing component (Amstutz et al., 1998) 14
Figure 2.5. Guide pin and guide wire (Adapted from *Biomet*., 2005). 17
Figure 2.6. Drilling and guide rod (Adapted from *Biomet*., 2005) 18
Figure 2.7. Cylindrical reaming (left) and spherical reaming (right) (Adapted from *Biomet*., 2005) 19
Figure 2.8. Cementing process (left) and final section with PMMA cement mantle (right) (Adapted from *Biomet*.,2005). 20
Figure 2.9. PMMA cement mantle areas (Adapted from *Biomet*., 2005). 25
Figure 2.10.Friction coefficient after resting periods according to bearing surfaces (Nassutt et al., 2003) 29
Figure 2.11.Coefficient of friction (COF) after resting periods (Wimmer et al., 2006). 30
Figure 2.12. Type of primary hip replacement procedure between 2005 and 2010 (NJR, 2011) 32
Figure 2.13. Age and gender for primary hip replacement patients in 2010 (NJR) 33
Figure 3.1. Conceptual Framework for this thesis. 37
Figure 3.2. Research Paradigm 43

Figure 4.1. Right angle end drill bit (5 mm) used to accommodate the femoral peg in the cancellous bone (Cheah, 2007) 46
Figure 4.2. Finite Element model rotation to vertical position (http://www.rkm.com.au/anatomy/femur.html) 47
Figure 4.3.Boundary conditions in *I-Deas NX 11*. 49
Figure 4.4. Hip contact forces and flexion-extension rotation for daily activities (Bergmann, 2001) 52
Figure 4.5. Meshed finite element model. 55
Figure 4.6.a. Maximum tensile stresses during walking gait for fine mesh and meshless models. 56
Figure 4.6.b. tensile stress distribution 0.165 seconds after heel strike during walking gait for fine mesh and meshless models. 57
Figure 4.6.c. Maximum shear stresses during walking gait for fine mesh and meshless models. 57
Figure 4.6.d. Shear stress distribution 0.165 seconds after heel strike during walking gait for fine mesh and meshless models. 58
Figure 4.7.a. Maximum tensile stresses during walking gait for different material densities. 59
Figure 4.7.b. Tensile stress distribution 0.165 seconds after heel strike during walking gait for different material densities. 60
Figure 4.7.c. Maximum shear stresses during walking gait for different material densities. 60
Figure 4.7.d. Shear stress distribution 0.165 seconds after heel strike during walking gait for different material densities. 61
Figure 4.8.a. Maximum tensile stresses during walking gait for different metal-PMMA coefficient of friction. 63
Figure 4.8.b. Tensile stress distribution 0.165 seconds after heel strike during walking gait for different metal-PMMA coefficient of friction. 63
Figure 4.8.c. Maximum shear stresses during walking gait for different metal-PMMA coefficient of friction. 64
Figure 4.8.d. Shear stress distribution 0.165 seconds after heel strike during walking gait for different metal-PMMA coefficient of friction. 64
Figure 4.9.a. Maximum tensile stresses during walking gait for different metal-bone coefficient of friction. 65
Figure 4.9.b. Shear stress distribution 0.165 seconds after heel strike during walking gait for different metal-bone coefficient of friction. 66

Figure 4.9.c. Maximum shear stresses during walking gait for different metal-bone coefficient of friction. 66
Figure 4.9.d. Shear stress distribution 0.165 seconds after heel strike during walking gait for different metal-bone coefficient of friction. 67
Figure 4.10. PMMA bone cement tensile and shear stress (top) and hip contact force and flexion-extension rotation for normal walking gait. 69
Figure 4.11. Comparison of contact pressure between Finite Element Analysis model and Hertzian mechanics. 71
Figure 4.12. Retrieved specimen after femoral neck failure (left) (Falez, 2007) and Von Mises PMMA bone cement stress (Pa) during normal walking at 0.165 seconds after heel strike during walking gait. 72
Figure 4.13. Von Mises cancellous bone stress (Pa) during normal walking at 0.165 seconds after heel strike during walking gait. 73
Figure 5.1. Hip contact force and flexion-extension rotation for normal walking gait. 81
Figure 5.2. PMMA bone cement tensile stresses (Pa) 0.165 seconds into the walking gait for four different metal-on-metal friction coefficients. 82
Figure 5.3. PMMA bone cement shear stresses (Pa) 0.165 seconds into the walking gait for four different metal-on-metal friction coefficients. 83
Figure 5.4.a. Maximum tensile stresses during walking gait for different MoM friction coefficient. 83
Figure 5.4.b. Tensile stress distribution 0.165 seconds after heel strike during walking gait for different MoM friction coefficient. 84
Figure 5.4.c. Maximum shear stresses during walking gait for different MoM friction coefficient. 84
Figure 5.4.d. Shear stress distribution 0.165 seconds after heel strike during walking gait for different MoM friction coefficient. 85
Figure 5.5. Hip contact force and flexion-extension rotation for descending stairs gait. 86
Figure 5.6. PMMA bone cement tensile stresses (Pa) 1.152 seconds into the descending stairs gait for three different metal-on-metal friction coefficients. 87
Figure 5.7. PMMA bone cement shear stresses (Pa) 1.152 seconds into the descending stairs gait for three different metal-on-metal friction coefficients. 88
Figure 5.8.a. Maximum tensile stresses during descending stairs for different MoM friction coefficient. 89
Figure 5.8.b. Tensile stress distribution 1.152 seconds into the descending stairs gait cycle for different MoM friction coefficient. 89

Figure 5.8.c. Maximum shear stresses during descending stairs for different MoM friction coefficient. 90
Figure 5.8.d. Tensile stress distribution 1.152 seconds into the descending stairs gait cycle for different MoM friction coefficient. 90
Figure 5.9. Hip contact force and flexion-extension rotation for normal standing up. 91
Figure 5.10. PMMA bone cement tensile stresses (Pa) 1.245 seconds into the standing up gait for two different metal-on-metal friction coefficients. 93
Figure 5.11. PMMA bone cement shear stresses (Pa) 1.245 seconds into the standing up gait for two different metal-on-metal friction coefficients. 94
Figure 5.12.a. Maximum tensile stresses at standing up cycle for different MoM friction coefficient. 95
Figure 5.12.b. Tensile stress distribution 1.245 seconds into the standing up cycle for different MoM friction coefficient. 95
Figure 5.12.c. Maximum shear stresses at standing up cycle for different MoM friction coefficient. 96
Figure 5.12.d. Shear stress distribution 1.245 seconds into the standing up cycle for different MoM friction coefficient. 96
Figure 5.13. Cyclic stress load (Lee et al, 2005)....98
Figure 5.14. Stress versus number of cycles to failure curves for vacuum-mixed and hand-mixed *Cemex Rx* bone cement for average $\log_{10}$ (Nf) values for the four stress levels (Murphy and Prendergast, 2000)....100
Figure 5.15. Stress versus number of cycles to failure curves for vacuum-mixed and hand-mixed *Cemex Rx* for zero mean stress....101
Figure 5.16. Maximum tensile stress for walking with MoM coefficient of friction of 0.098. 102
Figure 5.17. Maximum tensile stress reduced to low and high peaks. 103
Figure 5.18. Maximum tensile stress reduced after first cycle has been calculated. 104
Figure 5.19. Regression lines and equations for first cycle amplitude tensile stress and mean stress for walking. 105
Figure 5.20. Total damage per year for hand and vacuum mixed PMMA bone cement. 113
Figure 5.21. Damage per year for hand and vacuum mixed PMMA bone cement for walking due to metal-on-metal friction. 114
Figure 5.22. Damage per year for hand and vacuum mixed PMMA bone cement for descending stairs due to metal-on-metal friction. 114

Figure 5.23. Comparison of PMMA maximum tensile stress (MPa) according to different metal-on-metal friction coefficients and patient bone quality during walking gait. 117
Figure 5.24. Comparison of PMMA maximum shear stress (MPa) according to different metal-on-metal friction coefficients and patient bone quality during walking gait. 118
Figure 5.25. Two dimensional PMMA bone cement tensile stresses (MPa) due to walking for varying metal-on-metal friction coefficient and bone quality. 119
Figure 5.26. Two dimensional PMMA bone cement shear stresses (MPa) due to walking for varying metal-on-metal friction coefficient and bone quality. 120
Figure 5.27. PMMA maximum tensile stresses during walking gait for different MoM friction coefficient and respective patient bone qualities 0f 60% and 120%. 121
Figure 5.28. PMMA maximum shear stresses during walking gait for different MoM friction coefficient and respective patient bone qualities 0f 60% and 120%. 121
Figure 5.29. Comparison of PMMA maximum tensile stress (MPa) according to different metal-on-metal friction coefficients and patient bone quality during descending stairs. 123
Figure 5.30. Comparison of PMMA maximum shear stress (MPa) according to different metal-on-metal friction coefficients and patient bone quality during descending stairs. 124
Figure 5.31. Two dimensional PMMA bone cement tensile stresses (MPa) due to descending stairs for varying metal-on-metal friction coefficient and bone quality. .125
Figure 5.32. Two dimensional PMMA bone cement shear stresses (MPa) due to descending stairs for varying metal-on-metal friction coefficient and bone quality. .126
Figure 5.33. PMMA maximum tensile stresses during descending stairs for different MoM friction coefficient and respective patient bone qualities of 60% and 120%. ..127
Figure 5.34. PMMA maximum shear stresses during descending stairs for different MoM friction coefficient and respective patient bone qualities of 60% and 120%. ..127
Figure 5.35. Comparison of PMMA maximum tensile stress (MPa) according to different metal-on-metal friction coefficients and patient bone quality during standing up. 129
Figure 5.36. Comparison of PMMA maximum shear stress (MPa) according to different metal-on-metal friction coefficients and patient bone quality during standing up. 130
Figure 5.37. Two dimensional PMMA bone cement tensile stresses (MPa) due to descending stairs for varying metal-on-metal friction coefficient and bone quality. .131

Figure 5.38. Two dimensional PMMA bone cement shear stresses (MPa) due to descending stairs for varying metal-on-metal friction coefficient and bone quality. .132
Figure 5.39. PMMA maximum tensile stresses during standing up for different MoM friction coefficient and respective patient bone qualities of 60% and 120%. 133
Figure 5.40. PMMA maximum tensile stresses during standing up for different MoM friction coefficient and respective patient bone qualities of 60% and 120%. 133
Figure 5.41. Two dimensional PMMA bone cement tensile stresses (MPa) due to walking for varying metal-on-metal friction coefficient and PMMA Young's modulus for 60% bone quality. 135
Figure 5.42. Two dimensional PMMA bone cement tensile stresses (MPa) due to walking for varying metal-on-metal friction coefficient and PMMA Young's modulus for 80% bone quality. 136
Figure 5.43. Two dimensional PMMA bone cement tensile stresses (MPa) due to walking for varying metal-on-metal friction coefficient and PMMA Young's modulus for 100% bone quality. 136
Figure 5.44. Two dimensional PMMA bone cement tensile stresses (MPa) due to walking for varying metal-on-metal friction coefficient and PMMA Young's modulus for 120% bone quality. 137
Figure 5.45. Two dimensional PMMA bone cement shear stresses (MPa) due to walking for varying metal-on-metal friction coefficient and PMMA Young's modulus for 60% bone quality. 138
Figure 5.46. Two dimensional PMMA bone cement shear stresses (MPa) due to walking for varying metal-on-metal friction coefficient and PMMA Young's modulus for 80% bone quality. 138
Figure 5.47. Two dimensional PMMA bone cement shear stresses (MPa) due to walking for varying metal-on-metal friction coefficient and PMMA Young's modulus for 100% bone quality. 139
Figure 5.48. Two dimensional PMMA bone cement shear stresses (MPa) due to walking for varying metal-on-metal friction coefficient and PMMA Young's modulus for 120% bone quality. 139
Figure 5.49. Comparison of PMMA tensile stress (MPa) according to different metal-on-metal friction coefficients, patient bone quality and PMMA Young's modulus during walking. 141
Figure 5.50. Comparison of PMMA shear stress (MPa) according to different metal-on-metal friction coefficients, patient bone quality and PMMA Young's modulus during walking. 142

Figure 5.51. Two dimensional PMMA bone cement tensile stresses (MPa) due to descending stairs for varying metal-on-metal friction coefficient and PMMA Young's modulus for 60% bone quality.....143
Figure 5.52. Two dimensional PMMA bone cement tensile stresses (MPa) due to descending stairs for varying metal-on-metal friction coefficient and PMMA Young's modulus for 80% bone quality.....144
Figure 5.53. Two dimensional PMMA bone cement tensile stresses (MPa) due to descending stairs for varying metal-on-metal friction coefficient and PMMA Young's modulus for 100% bone quality.....144
Figure 5.54. Two dimensional PMMA bone cement tensile stresses (MPa) due to descending stairs for varying metal-on-metal friction coefficient and PMMA Young's modulus for 120% bone quality.....145
Figure 5.55. Two dimensional PMMA bone cement shear stresses (MPa) due to descending stairs for varying metal-on-metal friction coefficient and PMMA Young's modulus for 60% bone quality.....146
Figure 5.56. Two dimensional PMMA bone cement shear stresses (MPa) due to descending stairs for varying metal-on-metal friction coefficient and PMMA Young's modulus for 80% bone quality.....146
Figure 5.57. Two dimensional PMMA bone cement shear stresses (MPa) due to descending stairs for varying metal-on-metal friction coefficient and PMMA Young's modulus for 100% bone quality.....147
Figure 5.58. Two dimensional PMMA bone cement shear stresses (MPa) due to descending stairs for varying metal-on-metal friction coefficient and PMMA Young's modulus for 120% bone quality.....147
Figure 5.59. Comparison of PMMA tensile stress (MPa) according to different metal-on-metal friction coefficients, patient bone quality and PMMA Young's modulus during descending stairs. 149
Figure 5.60. Comparison of PMMA shear stress (MPa) according to different metal-on-metal friction coefficients, patient bone quality and PMMA Young's modulus during descending stairs. 150
Figure 5.61. Two dimensional PMMA bone cement tensile stresses (MPa) due to standing up for varying metal-on-metal friction coefficient and PMMA Young's modulus for 60% bone quality.....151
Figure 5.62. Two dimensional PMMA bone cement tensile stresses (MPa) due to standing up for varying metal-on-metal friction coefficient and PMMA Young's modulus for 80% bone quality.....152

Figure 5.63. Two dimensional PMMA bone cement tensile stresses (MPa) due to standing up for varying metal-on-metal friction coefficient and PMMA Young's modulus for 100% bone quality.....152
Figure 5.64. Two dimensional PMMA bone cement tensile stresses (MPa) due to standing up for varying metal-on-metal friction coefficient and PMMA Young's modulus for 120% bone quality.....153
Figure 5.65. Two dimensional PMMA bone cement shear stresses (MPa) due to standing up for varying metal-on-metal friction coefficient and PMMA Young's modulus for 60% bone quality.....154
Figure 5.66. Two dimensional PMMA bone cement shear stresses (MPa) due to standing up for varying metal-on-metal friction coefficient and PMMA Young's modulus for 80% bone quality.....154
Figure 5.67. Two dimensional PMMA bone cement shear stresses (MPa) due to standing up for varying metal-on-metal friction coefficient and PMMA Young's modulus for 100% bone quality.....155
Figure 5.68. Two dimensional PMMA bone cement shear stresses (MPa) due to standing up for varying metal-on-metal friction coefficient and PMMA Young's modulus for 120% bone quality.....155
Figure 5.69. Comparison of PMMA tensile stress (MPa) according to different metal-on-metal friction coefficients, patient bone quality and PMMA Young's modulus during standing up. 157
Figure 5.70. Comparison of PMMA shear stress (MPa) according to different metal-on-metal friction coefficients, patient bone quality and PMMA Young's modulus during standing up. 158
Figure 5.71. Interface testing jigs after testing. 159
Figure 5.72. Interface testing jig during mechanical testing in *Instron* testing machine. 161
Figure 5.73. Ultimate interface shear stress for *Palacos LV* PMMA bone cement. .162
Figure 5.74. PMMA shear stress during walking gait.....162
Figure 5.75. Ultimate interface shear stress for *Simplex P* PMMA bone cement. ...163
Figure 5.76 Torque testing results for ten testing samples. 165
Figure 5.77. Test sample during inspection. 165
Figure 5.78. Torque testing results for eight testing samples. 166

List of Tables

Table 3.1.Research methods advantages and disadvantages (After Fellows and Liu, 2008). 39
Table 4.1. Force factor to apply to LS-Dyna for walking gait 51
Table 4.2. Material properties 53
Table 5.1. Frequency of everyday activities (Morlock et al., 2001). 76
Table 5.2. Duration and frequency of resting periods. 77
Table 5.3. Metal-on-metal friction for resting periods (Nassutt et al., 2003). 78
Table 5.4. Finite element models to solve according to MoM friction coefficient. 78
Table 5.5. Cycles per year according to MoM friction coefficient and activity. 79
Table 5.6. Adjusted cycles per year according to MoM friction coefficient and activity. 80
Table 5.7. MoM friction due to resting periods for walking. 81
Table 5.8. PMMA maximum tensile and shear stresses for different MoM friction coefficients during walking. 82
Table 5.9. MoM friction due to resting periods for descending stairs. 86
Table 5.10. PMMA maximum tensile and shear stresses for different MoM friction coefficients during descending stairs. 87
Table 5.11. MoM friction due to resting periods for standing up. 92
Table 5.12. PMMA maximum tensile and shear stresses for different MoM friction coefficients during walking. 92
Table 5.13. Tensile stress for points in Figure 5.17. 102
Table 5.14. Equations for amplitude and mean tensile and shear stress cycles in MPa for everyday activities due to metal-on-metal friction coefficient. 106
Table 5.15. Amplitude and mean tensile stress cycles in MPa for walking due to resting periods. 107
Table 5.16. Amplitude and mean tensile stress cycles in MPa for descending stairs due to resting periods. 107
Table 5.17. Amplitude and mean tensile stress cycles in MPa for standing up due to resting periods. 107
Table 5.18. Damage per year calculation for hand mixed bone cement during running in phase. 109

Table 5.19. Damage per year calculation for hand mixed bone cement after running in phase. 110
Table 5.20. Damage per year calculation for vacuum mixed bone cement during running in phase. 111
Table 5.21. Damage per year calculation for hand mixed bone cement after running in phase. 112
Table 5.22. Cancellous and cortical bone Young's modulus according to different bone quality.....115
Table 5.23. PMMA maximum tensile and shear stresses due to varying MoM friction coefficient and bone quality during walking. 116
Table 5.24. PMMA maximum tensile and shear stresses due to varying MoM friction coefficient and bone quality during descending stairs. 122
Table 5.25. PMMA maximum tensile and shear stresses due to varying MoM friction coefficient and bone quality during standing up.....128
Table 5.26. PMMA tensile and shear stresses due to varying MoM friction coefficient, bone quality and PMMA Young's modulus during walking. 140
Table 5.27. PMMA tensile and shear stresses due to varying MoM friction coefficient, bone quality and PMMA Young's modulus during descending stairs. 148
Table 5.28. PMMA tensile and shear stresses due to varying MoM friction coefficient, bone quality and PMMA Young's modulus during standing up.....156
Table 5.29. Interface testing jigs areas. 160

Copyright

Chapter 1

Introduction

The third generation of hip resurfacing commenced in the U.K. in the 1990's with the *Birmingham hip resurfacing* system accounting for 10% of all primary hip replacement procedures in England and Wales in 2010 and now becoming a procedure in decline with only 3% of all primary hip replacement procedures in England and Wales (National Joint Registry, 2011). Mainly due to the latest revision rates of 11.8% at 7 years for hip resurfacing and 13.6% revisions at 7 years for stemmed metal-on metal bearings (total hip replacement) published by the National Joint Registry (2011). Furthermore, the voluntary recall by DePuy in August 2010 of its ASR Hip Resurfacing System, due to a revision rate of 12% after 5 years (DePuy, 2011) and higher revision risks reported in the literature (Seppanen et al., 2012)

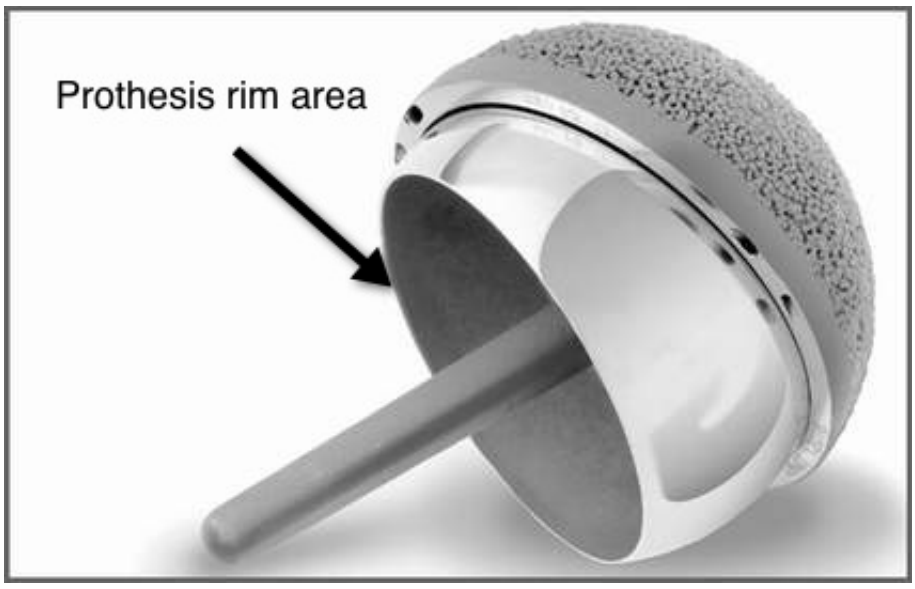

Figure 1.1. Birmingham hip resurfacing (St Nicholas Hospital, accessed in 2012)

Hip resurfacing looks an attractive alternative for young and active patients mainly due to premature failure in total hip replacement in this patient group (Callaghan et al., 2000) and due to preservation of the femoral bone stock as shown in Figure 1.2.

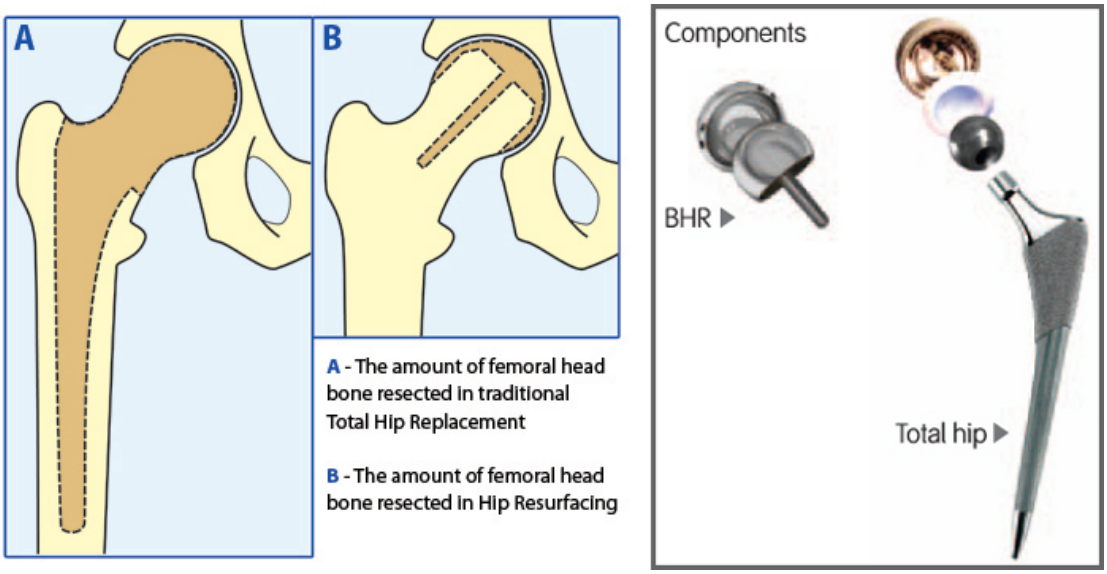

Figure 1.2. Comparison of hip resurfacing arthroplasty and total hip arthroplasty regarding femoral bone preservation (left) and components (right) (The McMinn Centre (left) and Active Joints Orthopedics (sic) (right), accessed in 2012)

Discriminatory patient selection is an important part of an effective hip resurfacing process, putting attention into bone quality for young and active patients (Amstutz et al., 2004, Pollard et al., 2006, Siebel et al., 2006, Nunley et al., 2009 and Kordas et al., 2012).

After several years of trials and manufacturing testing with different options for hip resurfacing designs, implantation options and materials, a metal-on-metal bearing with a cemented femoral component and press-fit uncemented acetabular component was chosen as the preferred design (McMinn, 2003). The femoral component is cemented into a chamfered cylindrical reamed femoral head as shown in Figure 2.1. Different orthopaedic implant manufacturers are producing their own hip resurfacing arthroplasty systems, most of them based on a chamfered cylindrical reamed femoral head as in the Birmingham hip resurfacing system. A different approach for the reamed femoral head is the *Biomet ReCap* hip resurfacing system, which is based on a hemispherical reamed femoral head (*Biomet*, 2005).

Figure 1.3 shows an illustration of a hemispherical reamed femoral head (left), as use in the *ReCap* hip resurfacing system and a chamfered cylindrical reamed femoral head (right) as used in the Birmingham hip resurfacing for example.

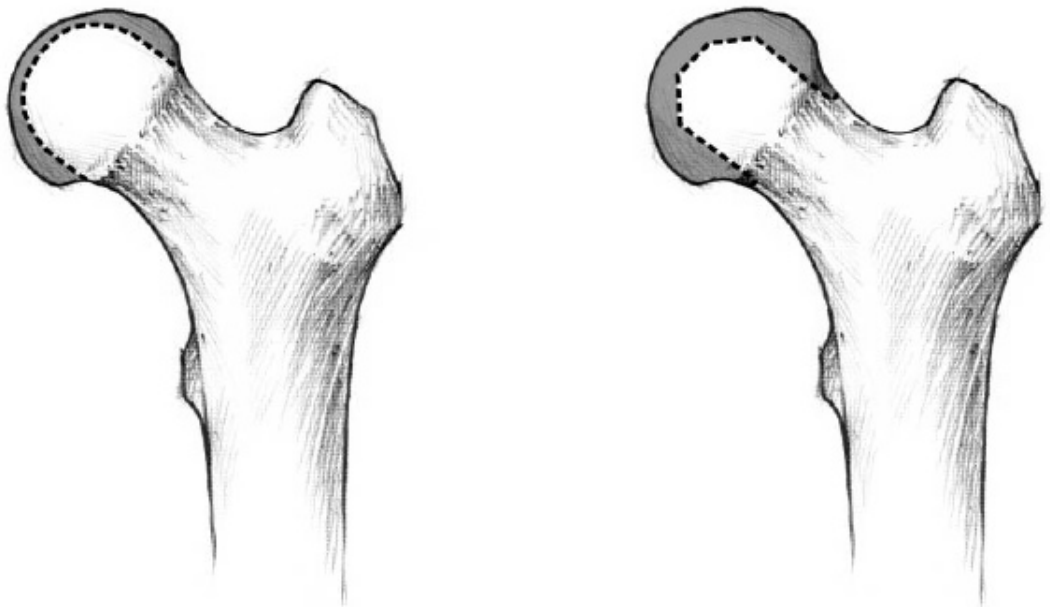

Figure 1.3. Hemispherical reamed femoral head (left) and a chamfered cylindrical reamed femoral head (right) (*Biomet*, 2005)

The short-term performance of hip resurfacing arthroplasty is reported by Treacy et al. (2005) to be very encouraging although, as it happened in the second generation of hip resurfacing, femoral neck fracture has been identified as a mechanism for short-term failure (Shimmin and Back, 2005, Beaule et al., 2006 and Gross et al., 2012). As previously reported in this introduction, the current performance and rate of revision is not as satisfactory (NJR, 2011 and Reito et al., 2013)

Poly Methyl Methacrylate (PMMA) bone cement is used in the femoral hip resurfacing component to achieve initial stability and facilitate early weight bearing as it was used in total hip replacement (Goodman, 2005). PMMA bone cement shows a range of different properties according to the combination of ingredients by different manufacturers (Lewis, 1997).

PMMA bone cement could be responsible for aseptic loosening of the femoral component due to fatigue in the long term.

Findings from Nassutt et al. (2003) on metal-on-metal bearings have shown a stick phenomenon after resting periods, a tendency to temporary immobility and restarting of gait movement, which increases the static metal-on-metal friction coefficient.

This thesis addresses issues related to the effect of resting periods and higher metal-on-metal friction on hip resurfacing and the next section introduces the aim and objectives.

1.1 Research Aim and objectives

The aim of the study is to investigate, through modelling and simulation, the short, medium and long term performance of PMMA bone cement of the femoral component in hip resurfacing arthroplasty from the point of view of analysing the failure of the bone cement to provide understanding, awareness and potentially inform upon lifestyle options following hip resurfacing arthroplasty.

The following objectives will be used to achieve the aim:

- Investigate the effect of high metal-on-metal friction coefficients due to resting periods on femoral hip resurfacing components by PMMA bone cement fatigue.

- Investigate the effect of bone quality on PMMA bone cement stresses.

- Analyse the effect of different PMMA bone cement on PMMA bone cement stresses.

- Test the torque play role in the loosening of femoral hip resurfacing components.

- Assess the implications of lifestyle options and hip resurfacing arthroplasty.

1.2 Preliminary Research

1.2.1 Initial methodology

The methodology for the preliminary research was a triangulation approach using literature, qualitative data and quantitative data (Fellows and Liu, 2008):

- The literature provides an overview of previous experiences with hip resurfacing and the current state of the modern era of hip resurfacing. Preliminary reviews suggested a problem worthy of future investigation.

- Qualitative data was collected through observation of hip resurfacing operations and interviews with orthopaedic surgeons, such as Professor Kevin Cheah FRCS (Capio Springfield Hospital) and Mr. Ron Treacy FRCS (Royal Orthopaedic Hospital Birmingham).

- Quantitative data was collected following initial mechanical testing and ultimately through Finite Element Analysis (FEA) models of hip resurfacing.

These three-dimensional Finite Element Analysis models simulated a cylindrical-chamfer femoral hip resurfacing component used by BHR Birmingham Hip Resurfacing and a hemispherical femoral hip resurfacing component, as used by *Biomet* in the *ReCap* hip resurfacing system (Figure 1.3). The Finite Element Analysis models were solved using a static simulation.

1.2.2 Finite Element Analysis conundrum

Preliminary Finite Element Analysis by others suggested that tensile and shear stresses in the bone cement and the PMMA-prosthesis interface have a similar pattern for cylindrical-chamfer and hemispherical femoral hip resurfacing components. The highest stresses in the PMMA bone cement were reported at the rim area of the femoral component, where the metal femoral component joins the femoral neck. This area has been reported in the literature after femoral neck fractures and associated with component failure (Amstutz et al., 2004, Cuckler et al., 2004, Kwon et al., 2010 and Mellon et al., 2011). The rim area of the hip resurfacing femoral component is shown in Figure 1.1.

Jimenez-Bescos et al. (2005) investigated the effect of a decrease of bone quality by reducing the Young's modulus of the cortical and cancellous bone. The Finite Element Analysis results showed that a reduction of bone quality produced an increase in tensile and shear stresses in the PMMA, which agreed with concerns in the literature on patient selection and bone quality (Sehatzadeh et al., 2012, Corten et al., 2010, Maguire et al., 2009, Schmalzried et al., 2005).

Observations and interviews for the current research showed the difficulties of the surgical technique for hip resurfacing, such as those with Professor Kevin Cheah FRCS (Capio Springfield Hospital) and Mr. Ron Treacy FRCS (Royal Orthopaedic Hospital Birmingham), and allowed the author to learn valuable insights into possible failure mechanisms for the medium and long-term.

According to Silva et al. (2002), a healthy person hip can withstand 2 million walking cycles a year and duration and frequency of daily activities were collected by Morlock et al. (2001).

An important finding in the literature was the suggestion that resting periods may affect the friction coefficient for different surface bearings, with metal-on-metal bearing surface being the worse affected by the resting periods (Nassutt et al., 2003). This fact may explain the poor performance of metal-on-metal bearing surfaces according to the National Joint Registry (2011) and shown in Figure 1.4.

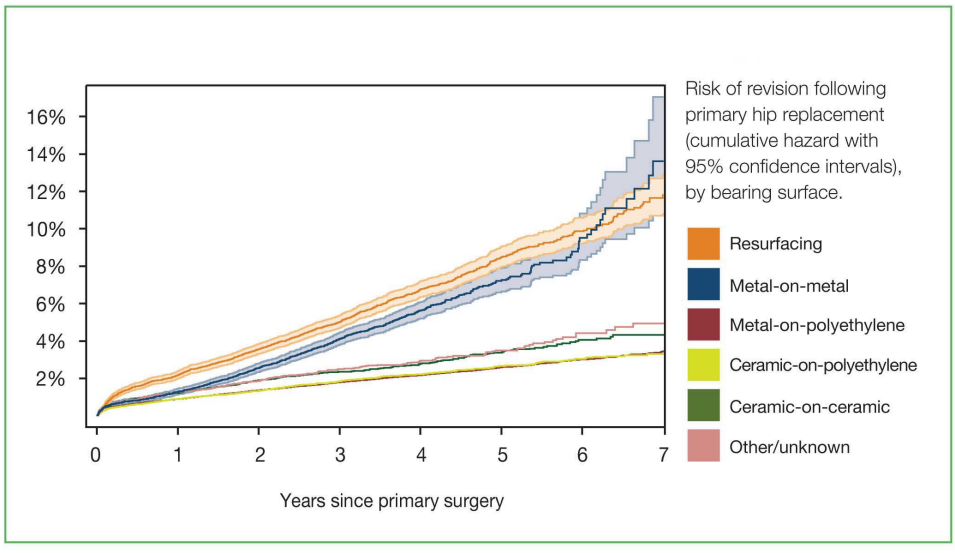

Note: 95% confidence intervals are not shown for all groups due to overlap obscuring plot.

Figure 1.4. Risk of revision following primary hip replacement according to bearing surface (NJR, 2011)

The triangulation of literature, qualitative data and Finite Element Analysis of the preliminary research drove the development of the aim and objectives of this thesis and the postulation of the following initial research questions.

1.3 Initial Research Question

The following initial research questions are postulated to answer the research aim presented in Section 1.1:

- Could high metal-on-metal friction coefficient due to resting periods cause aseptic loosening of femoral hip resurfacing components by PMMA bone cement fatigue?

- Could bone quality affect the stability of the femoral hip resurfacing components due to PMMA stresses?

- Could different PMMA bone cement affect the stability of the femoral hip resurfacing components due to PMMA stresses?

- Could the torque play a role in the loosening of femoral hip resurfacing components?

- What are the implications of lifestyle options and hip resurfacing arthroplasty?

In order to explore these issues, the following literature review provides information from secondary sources.

Chapter 2

Literature Review

This section sets out to resolve the initial research questions introduced in Section 1.3 concerning the design, performance and surgical technique in hip resurfacing arthroplasty. This section provides an understanding of the variables affecting hip resurfacing arthroplasty, such as resting periods, PMMA bone cement, patient bone quality, metal-on-metal friction, PMMA fatigue and torque.

2.1 Hip Anatomy

The hip joint is a ball and socket synovial joint, which main function is to connect the upper body to the legs. The hip joint is formed by the femur, which is a long bone ending the femoral head with a ball shape, and the pelvis, which has a socket shape to accommodate the ball shape from the femur. Both ball and socket pair together to form the hip joint. Figure 2.1 shows an image of the hip joint.

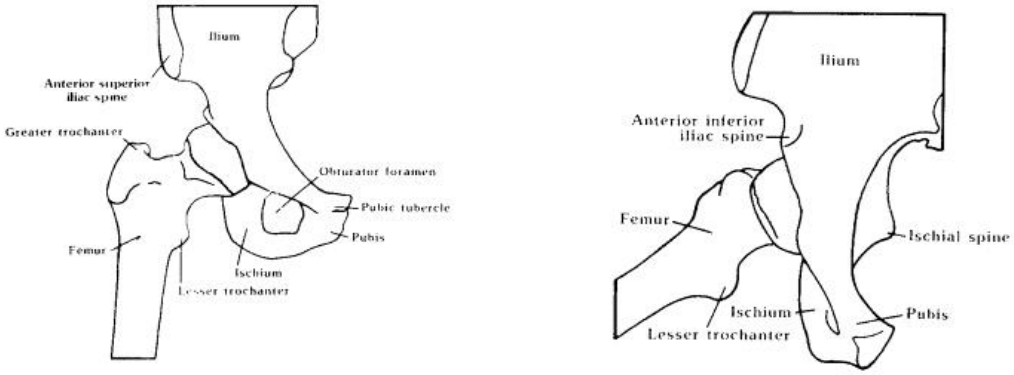

Figure 2.1. Hip joint (Orthoteers, 2007)

The hip joint is lubricated by synovial fluid, which provides a low friction articulation between the ball and socket. The contact areas in the ball and socket are covered by a soft spongy material called cartilage. The cartilage is responsible for the good lubrication in the joint because when no load is applied to the joint, the cartilage accumulates the synovial fluid. As soon as load is applied, the cartilage releases

synovial fluid as a sponge providing instant lubrication in the right place (Walker, 2007 and Fisher, 2002).

The hip joint has three degrees of freedom with six movements that can be done by the joint as picture in Figure 2.2. Flexion and extension can reach on average 120 and 20 degrees respectively giving the biggest range of movement. Abduction and adduction can reach on average 40 and 25 degrees respectively and 45 degrees of rotation in the external and internal rotation.

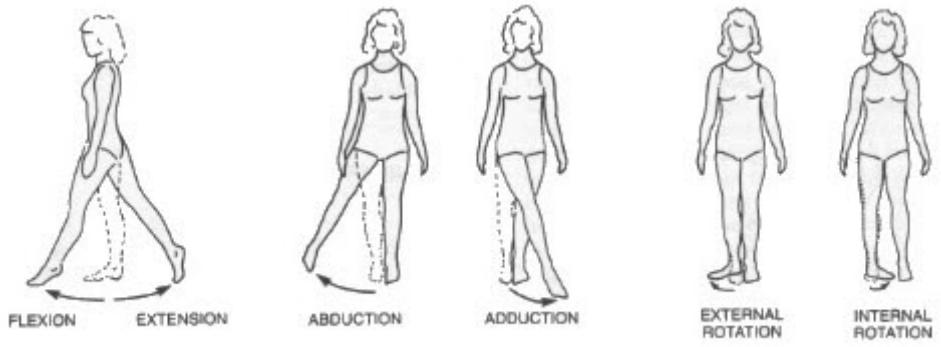

Figure 2.2. Hip joint movements
(https://courses.stu.qmul.ac.uk/smd/kb/grossanatomy/basic_anat/movements_of_the_hip_joint.htm, accessed in October 2010)

2.2 Hip Resurfacing Compared with the Natural Hip

The natural hip joint is lubricated by synovial fluid, which can be stored in the cartilage to have a fast release of synovial fluid in the moment of loading as explained in Section 2.1. This provides a good lubrication of the joint and low wear properties.

After hip resurfacing implantation, although achieving fluid film (hydrodynamic) lubrication with metal-on-metal bearing surfaces due to large diameter, surface roughness and clearance, the lubrication of the hip joint suffers some changes compare to the natural hip joint. While in the natural joint, the cartilage should be able to accumulate the synovial fluid and store it to be delivered at the moment of joint loading (Fisher, 2002 and Walker, 2007). In the Hip Resurfaced joint, the synovial fluid cannot be stored anywhere inside the joint; instead the synovial fluid will slide down the metal surfaces leaving the hip joint contact surfaces without lubricant.

The implications of this phenomenon are higher friction values after resting periods. This ‘stick phenomenon’ after resting period was studied by Nassutt et al. (2003) and

Wimmer et al. (2006) for different bearing surfaces, finding that the higher friction coefficients due to resting periods appeared in metal-on-metal bearing surfaces. Furthermore, higher friction for bigger head diameters will generate higher moments and torques, which could damage the stability of the implants.

2.3 Hip Resurfacing Compared to Total Hip Replacement

This section contrasts hip resurfacing with Total Hip Replacement (THR) as a UHMWPE acetabular component with a small diameter metal femoral head.
The advantages of hip resurfacing over Total Hip Replacement are:

- Alternative for active and young patients. High rate of failure has been reported for young patients after Total Hip Replacement (Dorr et al., 1994), this may be related to being active and subsequently wearing the UHMWPE faster (inducing osteolysis). On the contrary, hydrodynamic lubrication benefits from active patients, the more you use the joint, the better the lubrication.

- 45% of patients receiving a hip resurfacing in 2010 were fit and healthy, while 52% were had mild disease not incapacitating according to the National Joint Registry (NJR, 2011)

- Hydrodynamic or fluid film lubrication producing a low friction – low wear joint.

- Avoidance of polyethylene wear debris in the joint, which could initiate osteolysis and aseptic loosening.

- Easy revision to metal-on-metal total Hip Replacement with a big diameter head. This is due to the good preservation of femoral bone stock.

- More natural loading of the femur, avoiding stress shield in the femur shaft.

- Reduce the risk of dislocation due to bigger head diameter.

2.4 Reasons for Hip Resurfacing Operations

Hip resurfacing is still a recent alternative to Total Hip Replacement accounting for only 3% of all primary hip replacement procedures performed in 2010 in England and Wales (NJR, 2011). The procedure is an alternative for young and active patients achieving the younger average age for all the procedures with 54.2 years for females and 54.98 years for males.

According to the physical status of patients before the procedure, 45% of hip resurfacing patients qualify as P1 (fit and healthy) and 52% as P2 (mild disease not incapacitating) for hip resurfacing in 2010 (NJR, 2011).

According to the NJR for England and Wales data (2011), primary or secondary osteoarthritis is the main indicator for hip resurfacing as compared to other indicators such as trauma or avascular necrosis.

2.4.1 Osteoarthritis

Osteoarthritis is due to wear and tear of the joints developing into damage to the contact surfaces in the joint with the consequent pain when moving the joint. Osteoarthritis is influenced by many different factors, such as family history, trauma or surgery. The effect of osteoarthritis gets worse through the day with activity levels.

Although osteoarthritis is very common in older patients, it can affect young patient for whom hip resurfacing is used. 96% of hip resurfacing procedures in 2010 were due to osteoarthritis and a further 3% to congenital dislocation (secondary osteoarthritis)(National Joint Registry, 2011).

2.4.2 Avascular necrosis

NJR (2011) attributes avascular necrosis to a temporary or permanent supply of blood to the bone and affects all age group, being responsible for 2% of hip resurfacing procedures in 2010, although avascular necrosis is a contraindication due to the probability of bone quality damage. The main effect of avascular necrosis is that when the blood supply is stopped the bone dies and this will provoke the bone breaking or collapsing (Krause et al., 2012).

2.5 History of Hip Resurfacing

The idea of hip resurfacing was developed from the work of Smith Petersen with the mould arthroplasty technique (Smith Petersen, 1948) shown on Figure 2.3 and was revisited by Charnley in the 1950s, when he developed a teflon-on-teflon hip resurfacing prosthesis incorporating low friction capabilities of teflon. Early results were very good but due to the low wear capabilities of teflon, the prostheses failed very rapidly and patients need revisions (Ebied and Journeaux, 2002). Later on, Charnley abandoned the pursuit of hip resurfacing in favour of the low friction total hip arthroplasty using a Ultra High Molecular Weight Polyethylene (UHMWPE) cup and small metal head (Charnley, 1979)

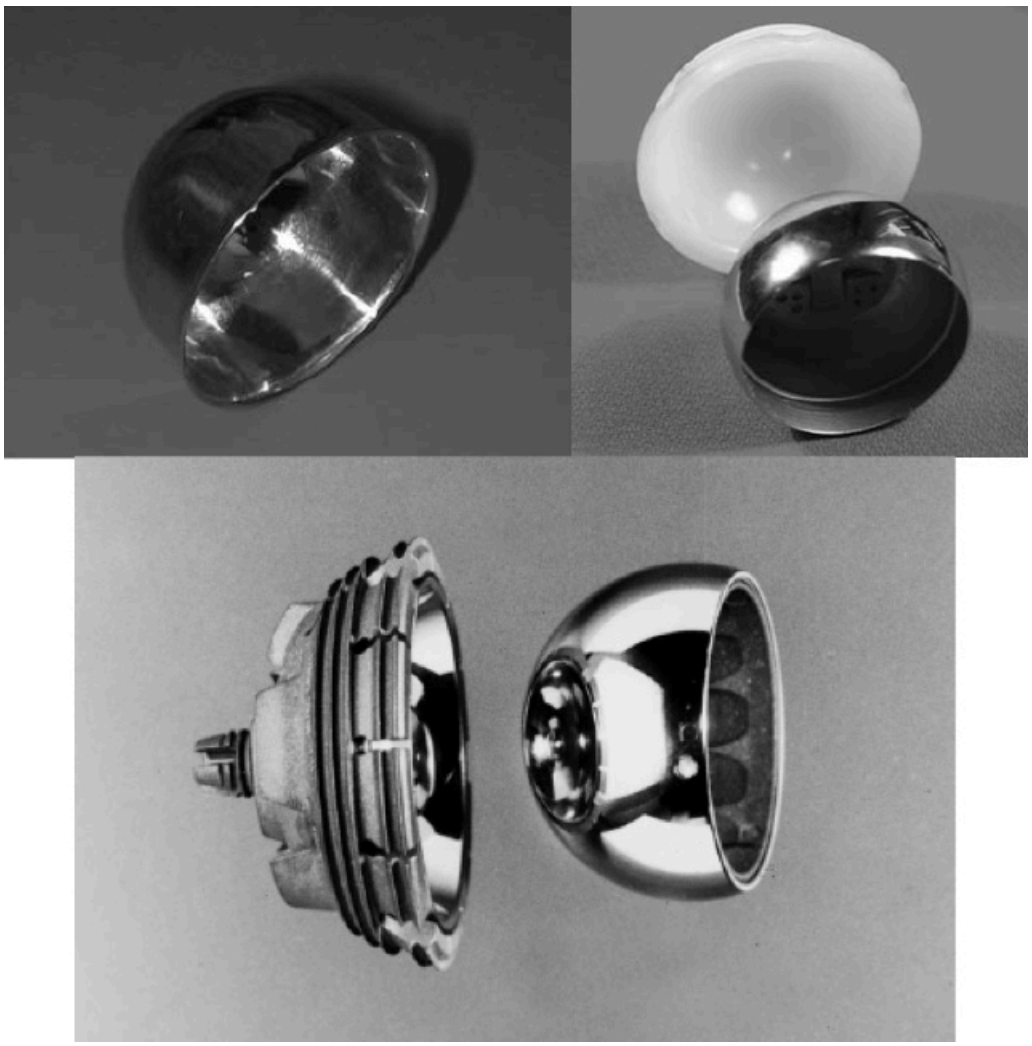

Figure 2.3. Early hip resurfacing components. Smith Petersen's mould arthroplasty (top left), THARIES (top right) (Amstutz and Le Duff, 2006) and Warner (Amstutz et al., 1998).

2.5.1 Early development of hip resurfacing

During the late 1960s and 1970s many hip resurfacing prostheses were developed, some of them are: *Total Articular Replacement Arthroplasty* (TARA), Freeman's ICLH, Wagner and Amstutz's *Total Hip Articular Replacement by Internal Eccentric Shells* (THARIES). Some of the components are shown in Figure 2.3 for illustration.

The majority of these prostheses were designed with a cemented UHMWPE acetabular cup and a cemented metal femoral head.

This was a very different approach to Charnley's low friction total hip arthroplasty, mainly due to the size of the femoral component. While Charnley's total hip arthroplasty prosthesis would be using a 22.2 millimetres femoral head, THARIES prosthesis would have a femoral head size in the range of 36 to 54 millimetres (Amstutz and Le Duff, 2006) with the consequent increment in size of the acetabular component. According to Murtha et al. (2008), the average acetabular diameter is 50 millimetres for female and 53.4 millimetres for male

There were several reasons for the early failure rate in these hip resurfacing prostheses. The main reason for failure was the high rate of UHMWPE wear and the osteolysis due to the interaction of the wear debris and the living bone tissue provoking acetabular and femoral aseptic loosening of the components.

Another mode of failure was a high incidence of femoral neck fracture, mainly due to the incorrect positioning of the femoral component. (Adams and Quigley, 2005).

At the time, due to limited knowledge around osteolysis, the loosening failure was attributed to avascular necrosis but studies suggest that bone stock is healthy under the metal femoral component (Howie et al., 1993).

Bell et al (1985) identified failure at the cement-bone interface due to mechanical loosening at the cement interface and fracture of the cement in Wagner components. They argued the case for the production of cement debris provoking the loosening factor at the interface.

Due to poor performance of these prostheses and the early revision rate. All the procedures were abandoned by the mid 1980s (Grigoris et al, 2006).

Some lessons were to be learned from the development of hip resurfacing in this era as stated by Amstutz and Le Duff (2006):

- Preservation of femoral neck stock, facilitating an easy revision to total hip replacement (Sandiford et al., 2010).

- Reduce the risk of dislocation due to the bigger femoral head size.

- Switching to using a cementless acetabular component improved the performance. As oppose to the femoral side, hip resurfacing do not preserve acetabular bone stock due to the increase size of the cup.

- Failure mechanisms in the acetabular and femoral prostheses already described in this section.

2.5.2 Modern era of hip resurfacing

The first hip resurfacing devices of the modern era were developed almost simultaneously by Wagner in Germany and McMinn in the United Kingdom (Figure 2.4) (Amstutz and Le Duff, 2006).

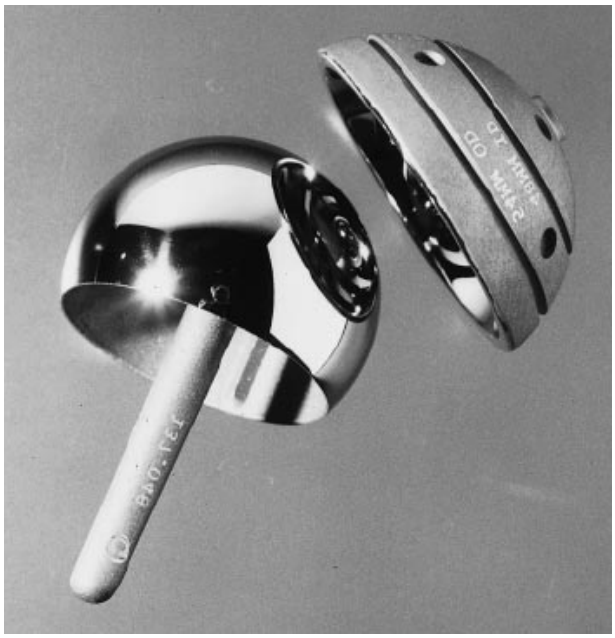

Figure 2.4. McMinn hip resurfacing component (Amstutz et al., 1998).

The reason behind this reinvention of interest into hip resurfacing is due to two main factors. Firstly, the high rate of failure in Total Hip Replacement for young patients (under 55 years old), mainly related to higher levels of activities and higher wear of the UHMWPE (Dorr et al., 1994). Secondly, the development and innovations in metallurgy and manufacture of metal-on-metal bearing surface.

Metal-on-metal is not a new concept to hip resurfacing, McMinn noticed the long survival of the Ring Total Hip Replacement based on metal-on-metal and decided to start a revolution using large diameter metal-on-metal bearing for the modern era of hip resurfacing.

The success of metal-on-metal bearing surfaces relies on the hydrodynamic lubrication effect (McMinn & Daniel, 2006). Hydrodynamic lubrication happens due to the head diameter, roundness, surface finish and the clearance achieved between femoral and acetabular component (Jin et al., 1997 and Liu et al., 2006). These factors allow the creation of a thin film of lubrication separating the femoral and acetabular component and reducing the wear rate compared to UHMWPE-metal bearing surfaces (Ebied and Journeaux, 2002).

Wear rates for metal-on-metal bearing surfaces has two phases, a first phase with high wear known as ‘running in’ phase or pre-wear, lasting between 0.5 - 2 million cycles. After the running in phase, the wear rate remains steady at a much lower value (Isaac et al., 2006) and is known as post-wear phase. This is basically until the bearing surfaces paired each other. This could be a concern regarding a late revision on the femoral side having a new femoral surface with a worn acetabular surface.

After several years of trials and manufacturing testing with different options for hip resurfacing designs, implantation options and materials to achieve the best performance and the lesson learnt throughout the implantation of these trial implants resulting in the BHR system. Nowadays, most manufactures have developed a hip resurfacing arthroplasty using ‘as cast’ Co-Cr alloy as a bearing surface (Grigoris et al., 2006). The majority of hip resurfacing components are hybrid, incorporating an uncemented acetabular component coating in hydroxyapatite matched with a cemented femoral component as the Birmingham hip resurfacing shown in Figure 1.1. Although some hip resurfacings are already investigating the use of uncemented

femoral components, the interest of this thesis focus on the use of cemented femoral components in Hip Resurfacing.

The following extract from the Swedish National Hip Arthroplasty Register (2010) raises concerns regarding levels of the understanding of modern era hip resurfacing arthroplasty:

> "In general the use of resurfacing prostheses are associated with an increased risk of early revision. This problem could mainly be related to the design of certain prostheses or related factors such as the design of the instrumentation and the training of individual surgeons, factors that cannot be evaluated in the registry."

In summary, the current concerns over hip resurfacing are:

- The lack of independent medium and long term follow-ups. Currently the National Joint Registry (NJR) for England and Wales has a follow-up for hip resurfacing of 7 years and starts to draw the picture of the performance of hip resurfacing with a revision rate of 11.8% at 7 years, almost four times higher than cemented prostheses (3% at 7 years). Further adding to the lack of clarity in the performance of stemmed metal-on metal bearings (total hip replacement) with a revision rate of 13.6% at 7 years. Furthermore, the Swedish National Hip Arthroplasty Register (2011) has reported the risk of revision within five years to be more than doubled in the use of resurfacing.

- Unknown aseptic loosening mechanism in the medium and long term. (Sharma et al., 2005).

- Release of metallic ions into the body systems due to wear with unknown long-term consequences (Macpherson and Breusch, 2011).

- Stability of the acetabular component, where the bone stock is not preserved.

- Femoral neck fracture.

- Bone necrosis.

- Stress shielding in the femoral neck (Taylor, 2006 and Radcliffe and Taylor, 2007).

- Demanding surgical technique requiring a surgeon learning curve (Amstutz et al., 2012).

2.6 Surgical Technique for Hip Resurfacing

This section focuses on the surgical technique used for hip resurfacing arthroplasty from the point of view of the femoral component, which is the interest of this research. The described technique is taken from the *ReCap* operative technique by *Biomet* (2005).

The first step is templating the anatomy of the patient using hip resurfacing templates from the implant manufacturer. The process involves sizing the patient through an anterior/posterior X-ray to find out the optimum size and position of the implant. The implant is positioned in neutral position or slightly valgus. A varus position must be avoided due to high stresses arising from such positioning, that leads to femoral neck fractures.

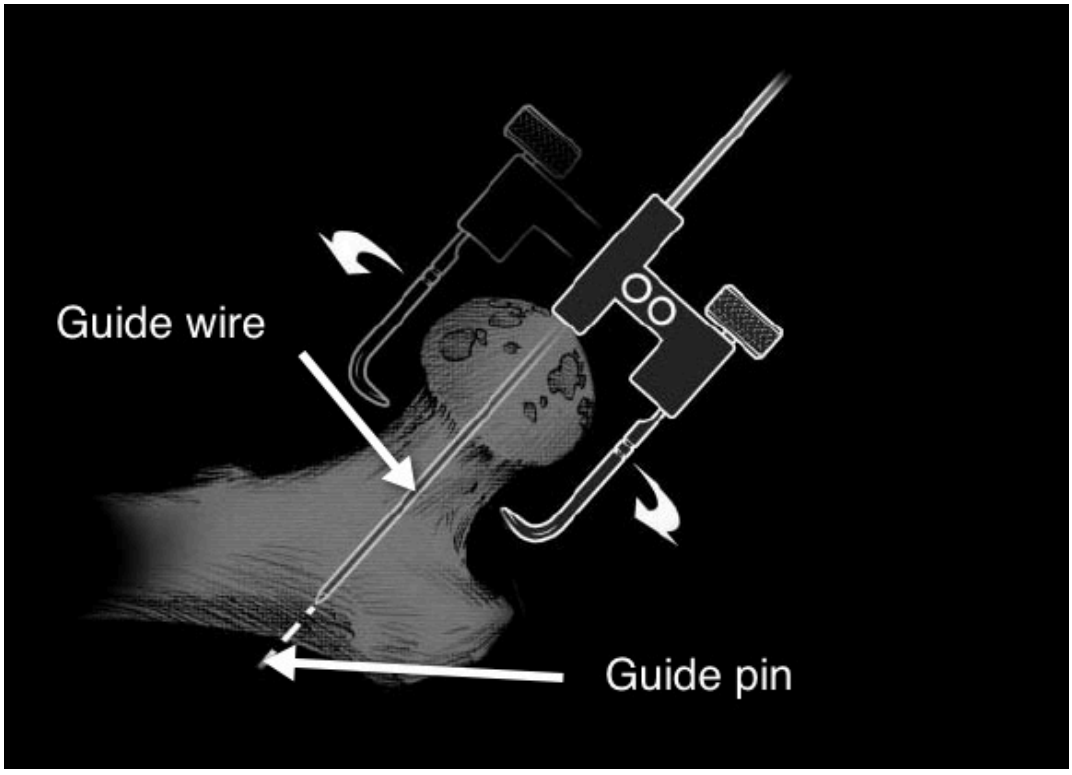

Figure 2.5. Guide pin and guide wire (Adapted from *Biomet*., 2005).

A guide pin is position below the trochanter, which will be used as guidance to place a guide wire through the centre of the femoral neck. The position of the guide pin is measured on the X ray in relation to the greater trochanter. The guide pin positioning is shown in Figure 2.5.

Following surgical exposure and dislocation of the hip to make the femoral head accessible to work on, the femoral head and neck is sized in vivo to verify or rectify the sizing during templating. It must be said that after dislocation of the hip to expose the femoral head, the blood supply to the femoral head is affected. For this reason, the less time the hip is dislocated the better for the vascularity of the femoral head and the survival of the implant. It is very important to verify that the implant size for the femoral head is big enough to not to damage the femoral neck. If the femoral neck is damaged during the reaming process, known as notching of the femoral neck, this will produce a stress concentration point in the femoral neck which will result ultimately in failure due to femoral neck fracture (Davis et al., 2009).

The next step is to find the femoral neck centre, it must be noticed that the femoral neck centre is different to the femoral head centre. Specialised instruments have been engineered to find the femoral neck centre. After being located, a guide wire is placed by drilling through the femoral head and neck. Using the guide wire, the femoral head size is checked again to verify that the femoral neck will not be damaged.

After this point, all the tools are colour coded for the particular size of femoral head to avoid any confusion during the operation.

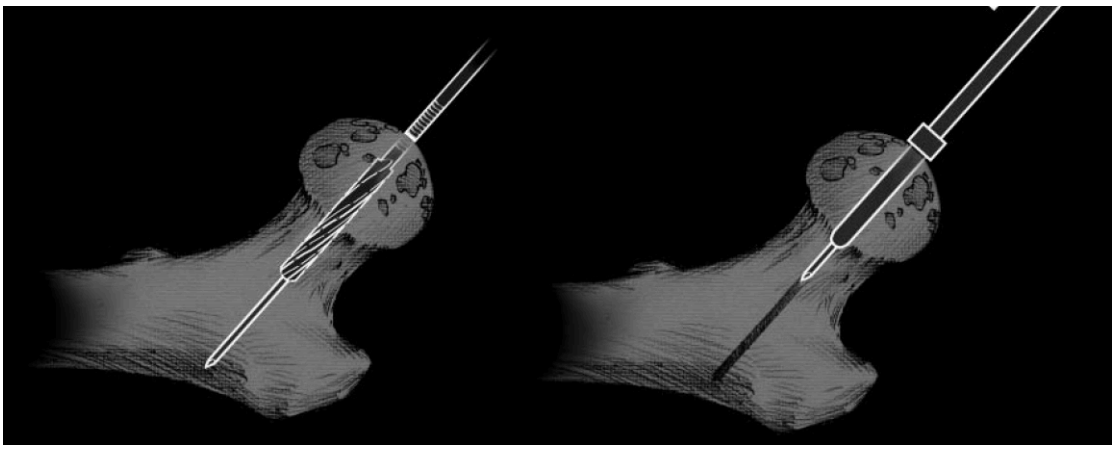

Figure 2.6. Drilling and guide rod (Adapted from *Biomet*., 2005).

The femoral head is drilled to the final size, which will accommodate a guide rod as shown in Figure 2.6. This guide rod will be used through the rest of the operation to facilitate guidance and positioning of the tooling. Different guide rod sizes are available for the surgeons to restore the patient original hip anatomy.

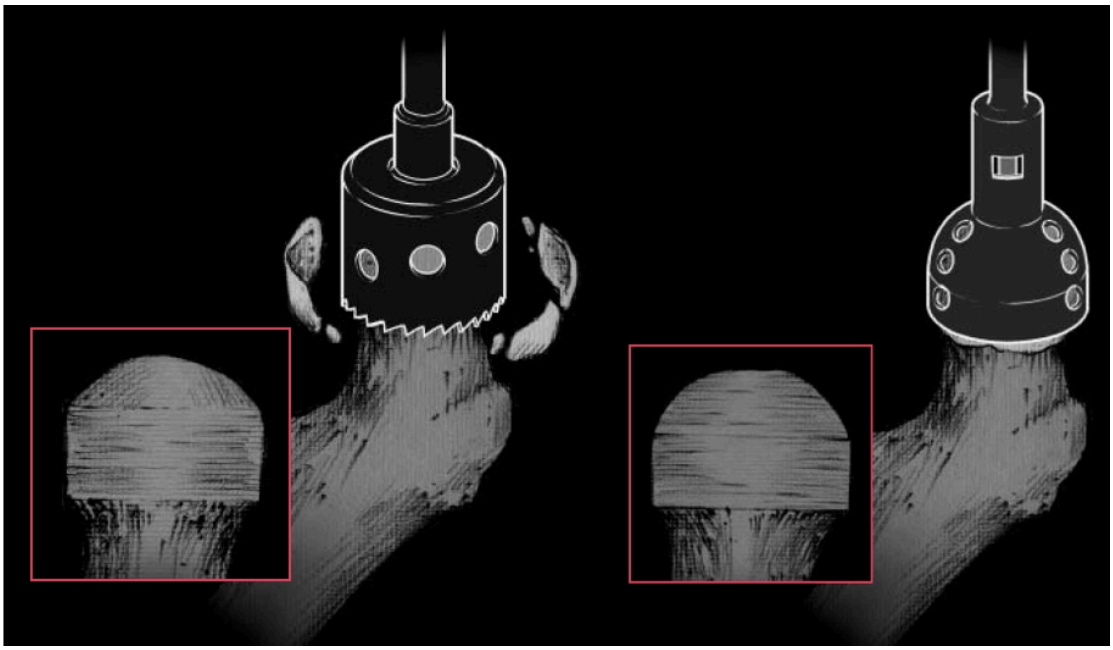

Figure 2.7. Cylindrical reaming (left) and spherical reaming (right) (Adapted from *Biomet*., 2005).

The femoral head is cylindrically reamed to the selected femoral head size as shown in Figure 2.7. Notching of the femoral neck must be avoided. If the femoral neck is notched during the reaming, the patient will receive a total hip arthroplasty instead of a hip resurfacing arthroplasty.

Following the cylindrical reaming, the femoral head is spherically reamed finalising the reaming process as shown in Figure 2.7.

The final preparation of the femoral head includes the removal of any cyst or defect from the femoral head. The surgeons must evaluate if the defects are big enough to produce complication for hip resurfacing arthroplasty, such as increased thickness of PMMA bone cement, which could cause thermal necrosis or compromise the primary stability of the implant after the operation. Small keyholes are drilled in the femoral head to improve cement interdigitation.

The femoral hip resurfacing component is fixed in position using low viscosity PMMA bone cement or high viscosity PMMA bone cement depending on the cementing technique selected by the surgeon performing the procedure.

The hip resurfacing femoral component is placed on the reamed femoral head and impacted until fully seated in position. Care must be taken to avoid PMMA bone cement getting attached to the stem of the femoral component. All excess of bone cement must be removed from the joint before reduction of the hip joint into position. The hip resurfacing femoral component features a series of critical stages during the surgical technique, which could affect the survival of the procedure.

Figure 2.8 shows the cementing process and a section of the hip resurfacing component showing the PMMA cement mantle.

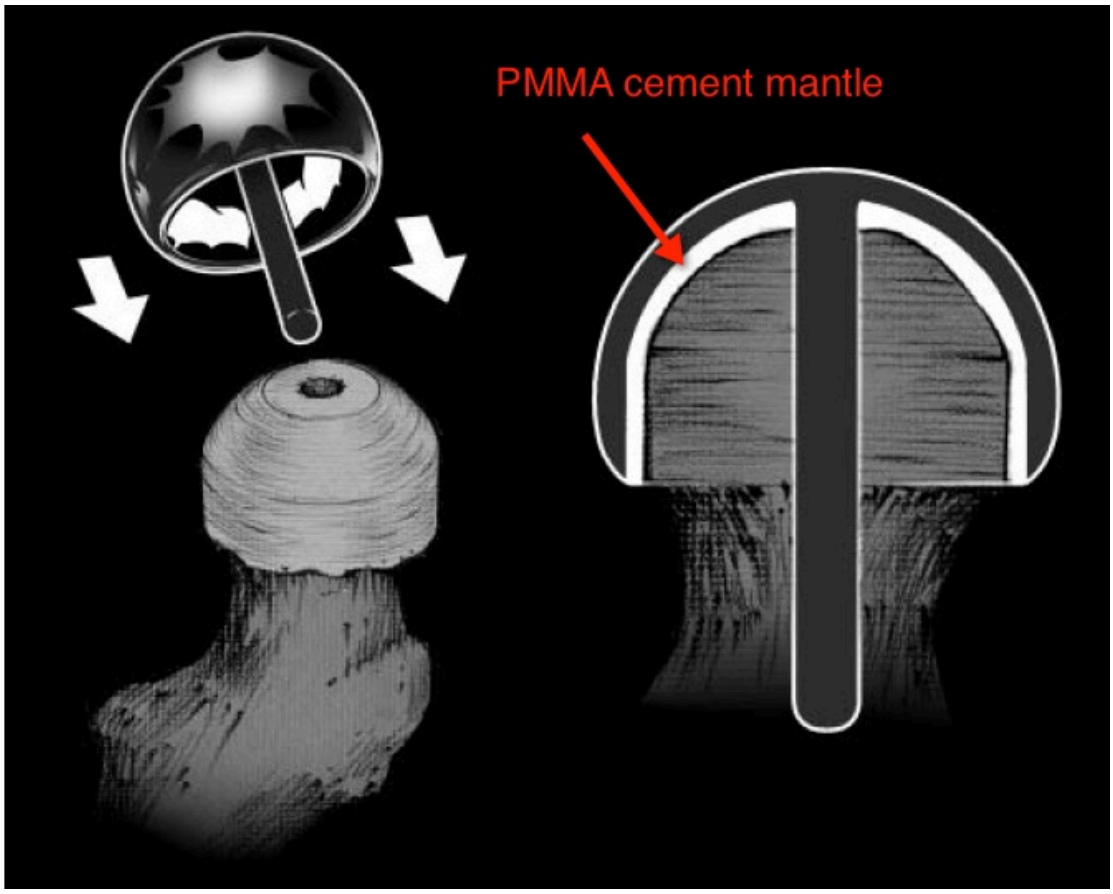

Figure 2.8. Cementing process (left) and final section with PMMA cement mantle (right) (Adapted from *Biomet*.,2005).

The surgical technique has driven the Swedish National Hip Arthroplasty Register (2011) to recommend hip resurfacing procedures to be performed by centres with good surgical competence and continuous follow up of patients.

2.7 Short Term Failure

2.7.1 Femoral neck fracture

This section describes how hip resurfacing is becoming the procedure of choice to treat young and active patients suffering from osteoarthritis or related diseases. However, as more procedures are performed, there appears to be the potential for short term failure mechanism. As it happened in the 1970s and 1980s (Adams and Quigley, 2005), femoral neck fractures may dominate the short term failure mechanism following hip resurfacing in the current modern era of hip resurfacing surgery (Gross et al., 2012).

Several reasons have emerged to explain the reason behind femoral neck fractures. Shimmin and Back (2005) reviewed 50 femoral neck fracture cases with an average time to fracture of 15.4 weeks. They found 21 of the cases showing notching of the femoral neck in after operation radiographs, 71.1% of cases having a varus positioning of more than 5 degrees for the femoral component and raised awareness regarding patient selection for hip resurfacing. Varus positioning refers to a smaller angle between the femoral stem and the femur shaft after the procedure compared to the original angle between the femoral neck and femur shaft

Femoral neck notching in hip resurfacing was studied by Beaule et al. (2006) from a vascularity point of view. Their results argue that notching of the femoral head would damage the blood supply causing avascular necrosis, which will be responsible for aseptic loosening of the femoral component or femoral neck fracture. Little et al. (2005) showed similar findings of avascular necrosis in retrieved femoral heads.

Hip resurfacing is a challenging procedure compared to Total Hip Replacement due to the surgical technique as explained in Section 2.6. As pointed out by Beaule et al. (2006) and Little et al. (2005), surgeons should put attention during the reaming of the femoral head to avoid notching and operation time should be as short as possible to avoid long interruption of the blood supply to the femoral head.

Davis et al. (2009) found out increasing stress and strain distributions in the femoral neck due to notching.

Femoral heads studied after femoral neck fracture appear to have thick PMMA cement mantle (Amstutz et al., 2004 and Little et al., 2005) suggesting thermal necrosis due to high polymerisation temperature during curing of PMMA, adding arguments to the discussion on cementing techniques in hip resurfacing (Falez et al., 2010, Falez et al., 2011 and Janssen et al., 2012).

Varus positioning of the femoral component has been identified as a cause of femoral neck fracture (Shimmin and Back, 2005 and Sharma et al., 2005). Schnurr et al. (2009) and Beaule et al. (2004) studied the orientation of the femoral component finding that a valgus orientation reduces stresses in the femoral head-neck region and prevent femoral neck fracture. These results were corroborated by Finite Element Analysis (Radcliffe and Taylor, 2007) arriving to similar conclusions that a valgus positioning of the femoral component was desirable.

As argued by Radcliffe and Taylor (2007) and this review, femoral neck fracture seems to be a combination of different factors, such as load, surgical technique, cementing technique and bone quality.

This information points towards the greater needs for understanding of the potential initiation failure mechanisms in hip resurfacing arthroplasty.

2.7.2 Thrombophlebitis and infections

Thrombophlebitis, known as well as Deep Venous Thrombosis (DVT), can occur after surgery on the hip, pelvis, or knee. DVT occurs when the blood in the large veins of the leg forms blood clots within the veins. This may cause the leg to swell and become warm to the touch and painful. The main risk is if the blood clots in the veins break apart because then it can travel to the lung and it will cause a pulmonary embolism. There are many ways to reduce the risk of DVT, but probably the most effective is getting the patient moving around as soon as possible, which will also benefit the remodelling bone process by having a reduced weight load on the joint and reducing the post operation recovery time to the minimum possible.

Some of the commonly used preventative measures include:

- Pressure stockings to keep the blood in the legs moving.

- Medications to thin the blood and consequently preventing the formation of blood clots.

Infection can be a very serious complication following an artificial joint replacement. Infection is a reaction of the human body to a foreign object, such as a hip resurfacing implant. Infections can appear early after the operation or months after even if patients have high doses of antibiotic to avoid rejection before, during and after the operation.

Infections are so serious that patients are advised to avoid any kind of dental work after the operation for a year at least, because infections from other parts of the body could travel to the implant and cause rejection.

2.7.3 Bone necrosis

Poly Methyl Methacrylate (PMMA) polymerisation is a very exothermic reaction, being able to reach up to 90 °C (ISO, 2002). The main cause of concern is if the temperature of PMMA in contact with the bone rises above the threshold for bone necrosis. If the temperature threshold is passed, the bone in contact with the PMMA will die due to bone necrosis. The dead bone is less elastic and weaker than living bone and is easier to fracture, hugely increasing the risk of failure of the implant. Furthermore, cellular remodelling of the dead bone continues happening, which leads to additional weakening of the implant-bone interface (Revell, 1986).

2.8 PMMA Cementing Technique

Two different cementing techniques have emerged for implanting the cemented femoral hip resurfacing component.

The first technique (low viscosity) was developed by McMinn (McMinn et al., 1996) and comprised using low viscosity cement in a liquid state, which is poured into the femoral head and then the femoral implant is inserted into the reamed femoral head. This technique is very broadly spread between the different hip resurfacing implants.

This is the technique used for the *Biomet ReCap* hip resurfacing system as explained in Section 2.6.

Using the bone cement in liquid state and thanks to the design of the femoral component, the bone cement should be able to easily flow into the cancellous bone and provide an even cement mantle.

The second technique (high viscosity) was developed by Amstutz (Amstutz and Le Duff, 2006) and uses bone cement in a viscous state. The bone cement in this state is malleable and easy to apply by the surgeon's hand. The surgeon can create a bone cement 'pancake' of uniform thickness, which will be covering the femoral head and the surgeon can apply pressure with the thumbs to allow interdigitation in the cancellous bone. This technique should allow more control of the thickness of the cement mantle in the femoral head and thinner cement mantle (Radcliffe and Taylor, 2007).

Beaule et al. (2009) and Chandler et al. (2006) pointed out the effect that different hip resurfacing designs play upon the characteristics of the cement mantle. Furthermore, their results showed that a low viscosity technique provide a thicker cement mantle at the top of the femoral head with little penetration around the rim of the femoral component (Scheerlinck et al., 2010 and Bitsch et al., 2013), while a high viscosity technique achieved a more consistent and uniform thickness for the cement mantle as it was reported by Janssen et al (2012) recently.

Bitsch et al. (2007) used different porosity models of the femoral head to investigated different variations of the cementing techniques. They found the high viscosity technique the only technique to avoid over penetration of the bone cement (Bitsch et al., 2010 and Bitsch et al., 2011).

A thick cement mantle could be leading to thermal osteonecrosis disease (Chandler et al. 2006, Falez et al., 2010, Falez et al., 2011, Jansenn et al., 2012 and Krauser et al., 2012) and stress shielding in the proximal section of the femur (Radcliffe and Taylor, 2007).

Using the low viscosity technique could allow cement to fall into the stem hole, which will result in the stem being cemented while it was originally designed for guidance (Chandler et al. 2006).

The outer wall of the femoral head provides the resistance to torque (Bitsch et al., 2007), maybe cementing the stem would help in this matter. Amstutz et al. (2004) cemented the stem in small femoral heads to achieve better initial stability.

Figure 2.9 shows the terminology for different areas of the PMMA cement mantle in hip resurfacing arthroplasty.

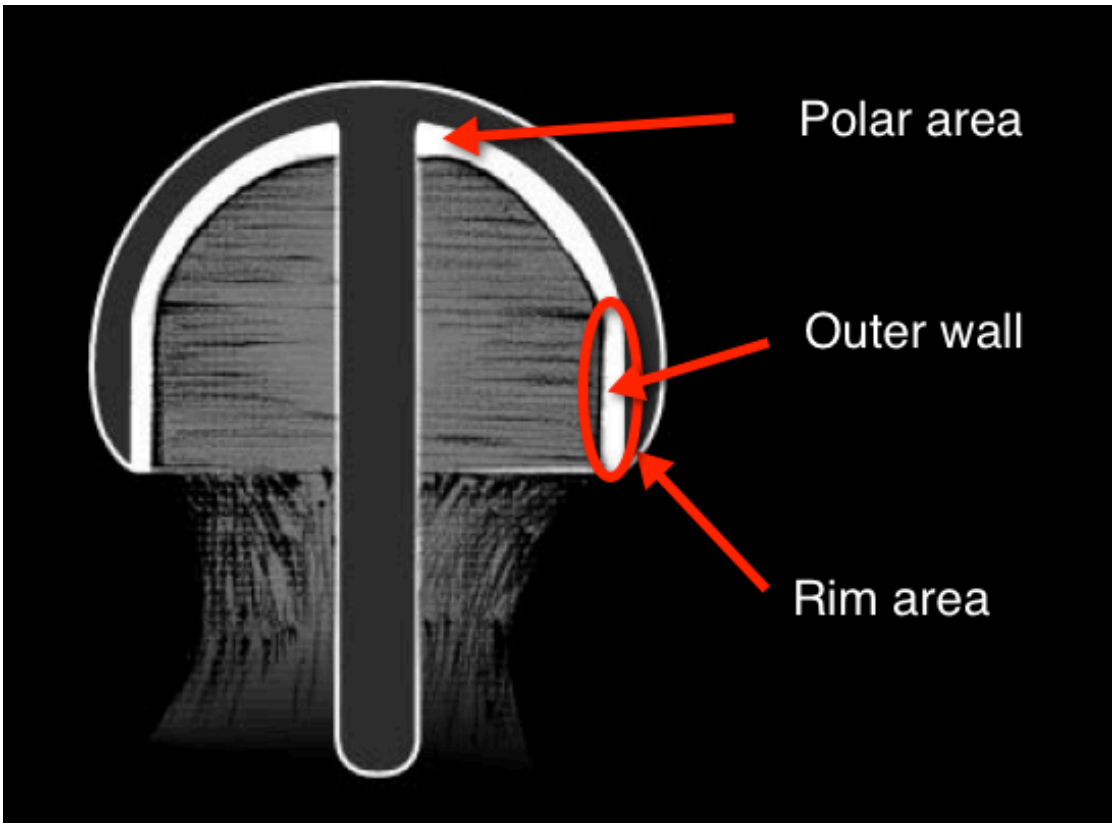

Figure 2.9. PMMA cement mantle areas (Adapted from *Biomet*., 2005).

On the other side of the coin, Radcliffe and Taylor (2007) suggested that cementing the stem could lead to bone resorption through strain shielding.

2.9 PMMA Failure Mode

Given all the benefits of improved Poly Methyl Methacrylate (PMMA) mixing techniques, the fact remains that PMMA is responsible for aseptic loosening mainly due to mechanical failure as presented by Huiskes et al (1985).

Lewis (1997), Davies et al. (1987) and Kindt-Larsen et al. (1995) showed that Ultimate Tensile Stress (UTS) for PMMA bone cement for different PMMA

configurations, different mixing techniques and curing techniques has a range between 25 and 49.2 MPa.

Lewis (1997), Krauser et al. (1980) and Krauser et al.(1989) showed that Ultimate Compressive Strength (UCS) for PMMA bone cement for different PMMA configurations, different mixing techniques and curing techniques has a range between 72.6 and 117 MPa.

It can be seen that PMMA mechanical properties are far better in compression than in tension by a factor of more than double. For this reason, the main failure mode for PMMA is by high tensile stress potentially occurring, for example during stumbling.
In many ways, PMMA bone cement has a mechanical performance very similar to construction concrete with high strength to compression stresses but brittle against tensile stresses.

The main problems related to mechanical failure of PMMA are loosening of the implant and osteolysis disease. If PMMA bone cement fails, the implant will be free to move and these micro movements will provoke erosion of PMMA particles, which will react with the bone during the bone remodelling process. Particles of PMMA will react with the bone causing osteolysis which degenerates the bone making it weaker and weaker, ultimately causing mechanical failure of the implant by bone fracture.

Furthermore, any cracks in the PMMA bone cement structure may induce stress concentration points but more importantly damage could be caused by the infiltration of synovial fluid into the cracks and interface by hydrodynamic pressure crack propagation, which will increase mechanical damage (Stachowiak & Batchelor, 2005).

Failure at the interface between metal and PMMA bone cement can be a failure mode for aseptic loosening of hip resurfacing as observed by McMinn and Daniels (2006) during pilot studies in the early 1990s. Similar concerns regarding interface failure have been reported by Breer et al. (2012) Jansenn et al. (2012) and Krauser et al. (2012). Very little has been published regarding interface failure in hip resurfacing but due to the rotational symmetry of femoral hip resurfacing component, this is a factor to take into account for failure mode.

Fatigue failure is understood as cyclic loading in which the stress is below the UTS but the damage is produce by repetition of cycles. This phenomenon is very important for daily activities such as walking in which the stresses are low but the number of cycles per year is very high.

2.10 PMMA Fatigue Data

Fatigue is a process of damage and failure in material under cyclic loading. Cyclic loads producing fatigue are far lower than static design loads because the damage is done by the repetition of the load (Suresh, 2003).

The PMMA cement mantle in the femoral component of hip resurfacing is subjected to high cyclic loading due to our day by day activities such as walking.

While in Section 2.9 it was shown that PMMA has an ultimate tensile stress in the range of 25 and 49.2 MPa, cyclic loads as small as 20 MPa can produce PMMA fatigue failure in under 10000 cycles (Noble et al., 1995 and Furman et al., 1999).

To make matters worse, PMMA fatigue is very variable and dependent on many intrinsic (e.g. basic composition) and extrinsic factors (e.g. mixing method). Lewis (2003) compiled a review of fatigue data which accommodates all the different fatigue testing experiments carried out to date.

Murphy and Prendergast (2000) performed fatigue experiments using *Cemex Rx* bone cement (low viscosity) producing data for vacuum mixed and hand mixed bone cement. They provided a lineal fatigue equation to estimate the fatigue life of PMMA for a range of stresses under hand or vacuum mix based on the assumption of a linear relation between stress and cycles to failure.

Fatigue data from Murphy and Prendergast (2000) will be used in this thesis to carry out fatigue analysis of the finite element results of the model describe in Chapter 4.

2.11 Resting Periods

Testing of hip replacements takes place assuming continuous motion of the bearing surfaces or the patient (Wimmer, 2001). This factor applies to wear simulations and

to Finite Element Analyses. During normal daily activities, human motion is not continuous. As an example, walking from one side of an office to the opposite side may seem like a continuous motion until the patient encounters somebody or something on the way and the person stops for a moment. This is called a resting period or an interruption on the continuous movement of the joint.

As it was discussed in Section 2.1, the contact surfaces within a natural joint are protected by cartilage. Cartilage acts as a sponge during a resting period, absorbing synovial fluid when the joint is at rest. The main benefit of this phenomenon is that when the motion is restarted after a resting period, the bearing surfaces are lubricated instantly with the synovial fluid that is squeezed out from the cartilage. The synovial fluid is available at the right moment and on the right place due to the properties of cartilage.
In the case of hip resurfacing where the bearing surface is metal-on-metal, the synovial fluid slides down from the metal-on-metal contact surfaces during resting period because the synovial fluid cannot be trapped or absorbed by the metal bearing surfaces as it happens with cartilage. This means that when the motion is restarted, the bearing surfaces will be dry; causing a high friction coefficient between the metal bearing surfaces, and the synovial fluid will be pumped in between the bearing surfaces due to hydrodynamic lubrication returning the bearing surfaces to its normal low friction characteristics. The same effect that happens in the hip resurfacing bearing surfaces, happens in the engine of cars, as soon as the car is stopped the engine oil will drain into the sump and the most damaging moment for the engine is the moment it starts until the oil pump can lubricate the whole engine.

Resting periods will produce a stick phenomenon in the bearing surfaces which will be responsible for the reports by patients regarding squeaky hip replacement at the start-up of movement (Cheah, 2007). The squeaky noise seems to be more noticeable after sitting periods (longer periods of rest), longer periods of walking and the noise will disappear after a few steps (Esposito et al., 2010). Furthermore, it could explain the abrasion marks that appear in ceramics bearing surfaces. The author experienced squeaky noises while performing experimental torque testing for this study. This could be caused by the high friction coefficient during the start-up of any motion.

The effect of resting periods has been quantified by Nassutt et al (2003). These authors performed laboratory experiments with different bearing surfaces for artificial

hips to evaluate the effect of resting periods on the friction coefficient as shown in Figure 2.10. The friction coefficient for the bearing surfaces was measured at the restart of the motion after resting periods of 1, 5, 10, 30 and 60 seconds. The friction coefficient increased related to the length of the resting period but most of the bearing surfaces for artificial hips will arrive to a stabilization maximum value of friction coefficient after which an increase in resting period does not affect the friction value. For most bearing surfaces, this stabilization phenomenon happened at around 10 seconds. In the particular case of metal-on-metal bearing surfaces, the friction coefficient continues increasing with the length of the resting period and as well the increase on friction coefficient is the highest of all artificial hip bearing surfaces.

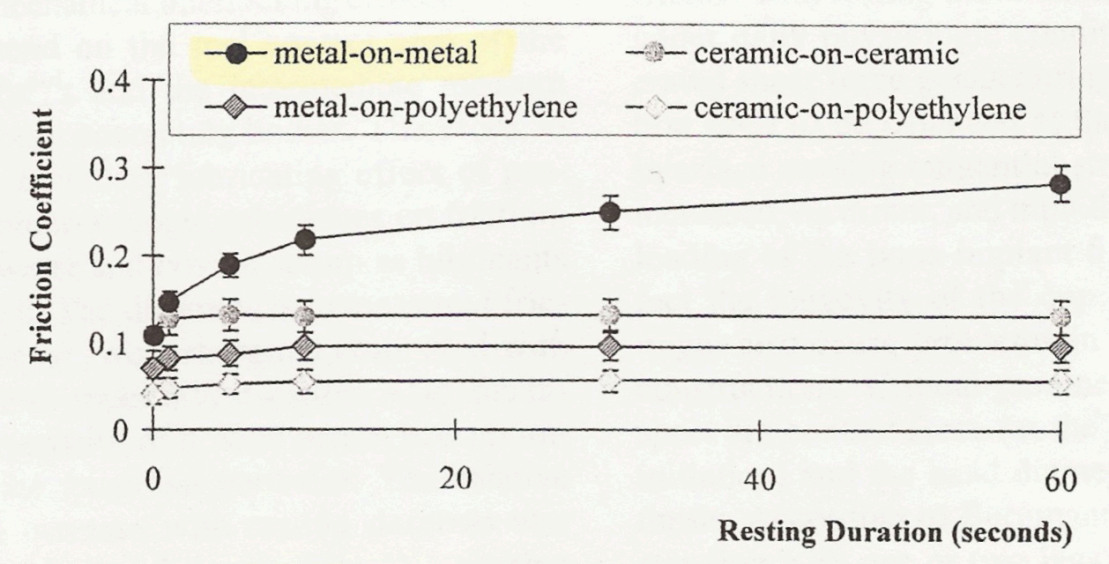

Figure 2.10.Friction coefficient after resting periods according to bearing surfaces (Nassutt et al., 2003).

The ‘stick phenomena’, described in Chapter 1, were also investigated taking into account the wear of the bearing surfaces and the effect of resting periods (Wimmer et al, 2006). Figure 2.11 shows the test results for metal-on-metal (MoM) pre-wear and post-wear (after running in process explain in section 2.5.2) compared to metal on polyethylene (MoP).

The high friction coefficients will be restored to dynamic friction values after only 2 or 3 cycles (email correspondent with Professor Michael Morlock on 15-6-2005).

The main focus of this research is to understand if the effect of resting period and the consequent increase of friction coefficient could compromise the stability of hip resurfacing due to PMMA fatigue failure and PMMA-metal interface failure.

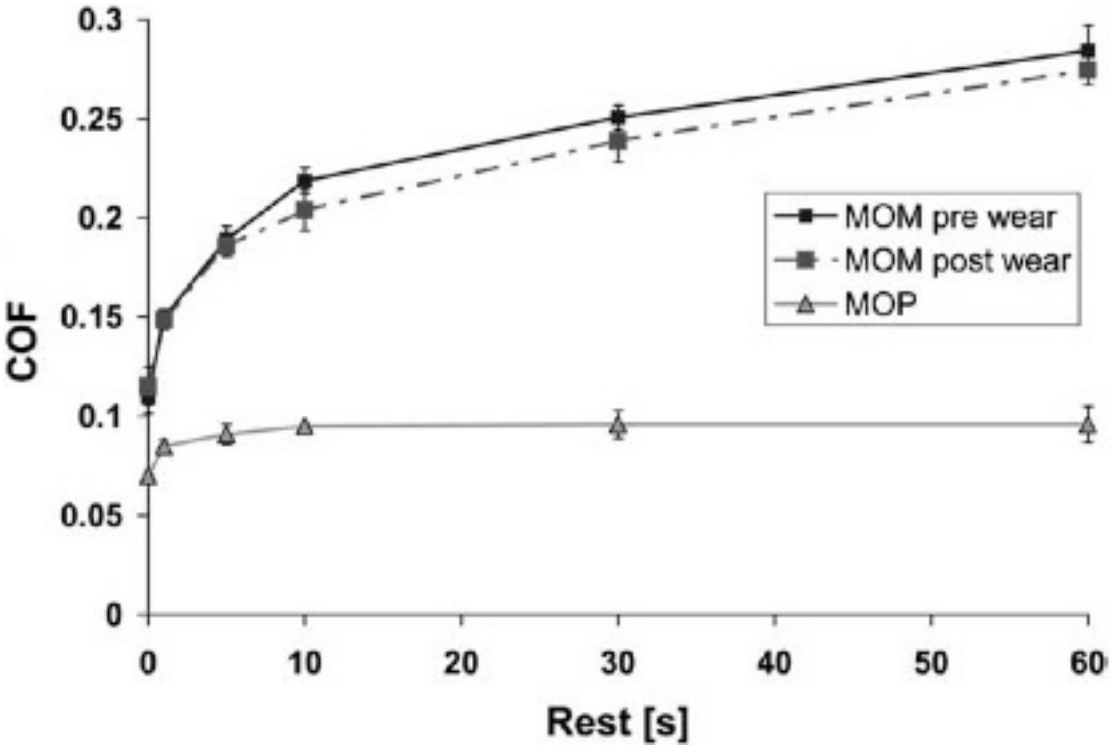

Figure 2.11.Coefficient of friction (COF) after resting periods (Wimmer et al., 2006).

2.12 Gait Data

The parameters describing the movement affecting the hip joint (gait data) proposed for this study is taken from the work of Bergman et al and published in HIP98 CD (2001). The data includes in vivo measurements in humans with instrumented hip implants that were taken at the Free University of Berlin. The data captures normal daily activities and this study focuses on the normal activities of walking at a normal speed, descending stairs and standing up from a chair. The main reason to select these activities is because they are activities in which the effect of resting periods could be very high, such as standing up, or very repetitive as in walking normally.

The data presented on the HIP98 CD includes hip contact forces in three dimensions for every activity, as well as the flexion-extension angle of rotation which will allow the simulation of the effect of resting periods in hip resurfacing.

Using this data will allow all the boundary conditions for the Finite Element Analysis to be taken from one source and will reduce any incompatibilities in matching different sets of data.

Another important data that is included in the HIP98 CD is the duration and frequency of everyday activities (Morlock et al, 2001). The importance of the duration and frequency of everyday activities account as the link for the relationship between the Finite Element Analyses results for resting periods and the PMMA fatigue data to study the effect of resting periods on the stability of hip resurfacing for middle and long term.

2.13 Biological Variables

2.13.1 Bone quality

Bone quality is a very important factor for the success of any hip replacement but even more in the case of hip resurfacing where the femoral component is seated on top of the reamed femoral head (Currey, 1998).

Bone quality is a factor that can be measure using a DEXA scan to account for the bone density of the patient and such a test is requested if the bone quality of the patient is questionable (Davis et al. 2013). Bone quality decreased with age and as well this effect is more pronounced in females than males due to menopausal processes. While surgeons will perform a hip resurfacing in almost any male regardless of any age, a common concern over bone quality and complications including osteoporosis, make the selection of female patients for hip resurfacing much less certain (Coulter et al., 2012 and Seppanen et al., 2012).

The most well-known bone degeneration is osteoporosis, which degenerate the mechanical properties of cortical and cancellous bone to the point of causing osteoporotic fractures of the bone.

Two important factors could have an impact on the bone quality for the medium and long term success of the implant. On the one-hand bone necrosis due to high temperatures during the curing of PMMA bone cement, which will damage the bone structure causing a decrease on bone quality. On the other-hand, a decrease of bone quality due to osteolysis may exist, as explain in Section 2.9, regarding potential PMMA failure mode caused by the reaction between PMMA particles and bone during the bone remodelling process. Either way, both mechanisms should be avoided to assure the stability of hip resurfacing.

It has been shown using Finite Element Analysis that the reduction on bone quality produces an increase in the stresses at the PMMA bone cement and consequently the risk of PMMA mechanical failure and bone fracture (Jimenez-Bescos et al, 2005 and Little et al, 2007).

2.13.2 Patient selection

According to the National Joint Registry (NJR) for England and Wales, 2067 hip resurfacing operations were registered in 2010 accounting for 3% of all primary hip replacement procedures. The number of hip resurfacing operations shown for the period between 2005 and 2010 seems to be following a decline in favour of other procedures such as cementless or hybrid total hip replacement as shown in Figure 2.12.

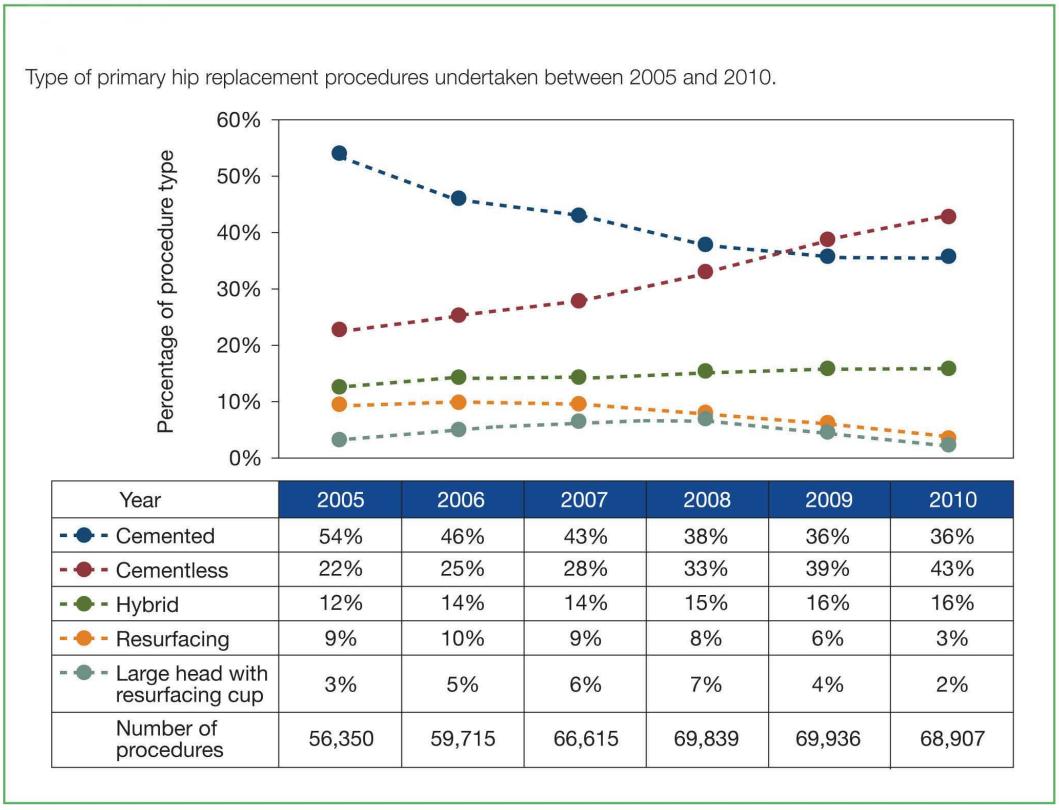

Year	2005	2006	2007	2008	2009	2010
Cemented	54%	46%	43%	38%	36%	36%
Cementless	22%	25%	28%	33%	39%	43%
Hybrid	12%	14%	14%	15%	16%	16%
Resurfacing	9%	10%	9%	8%	6%	3%
Large head with resurfacing cup	3%	5%	6%	7%	4%	2%
Number of procedures	56,350	59,715	66,615	69,839	69,936	68,907

Figure 2.12. Type of primary hip replacement procedure between 2005 and 2010 (NJR, 2011)

Having a closer look at the statistics, it can be appreciated that the hip resurfacing group is by far the youngest average age group (54.84) and note particularly that 82% of the patients were male (NJR, 2011).

As Figure 2.13 shows, hip resurfacing is mainly a procedure for young patients and mainly male gender to avoid issues related to bone quality as explained in Section 2.13.1.

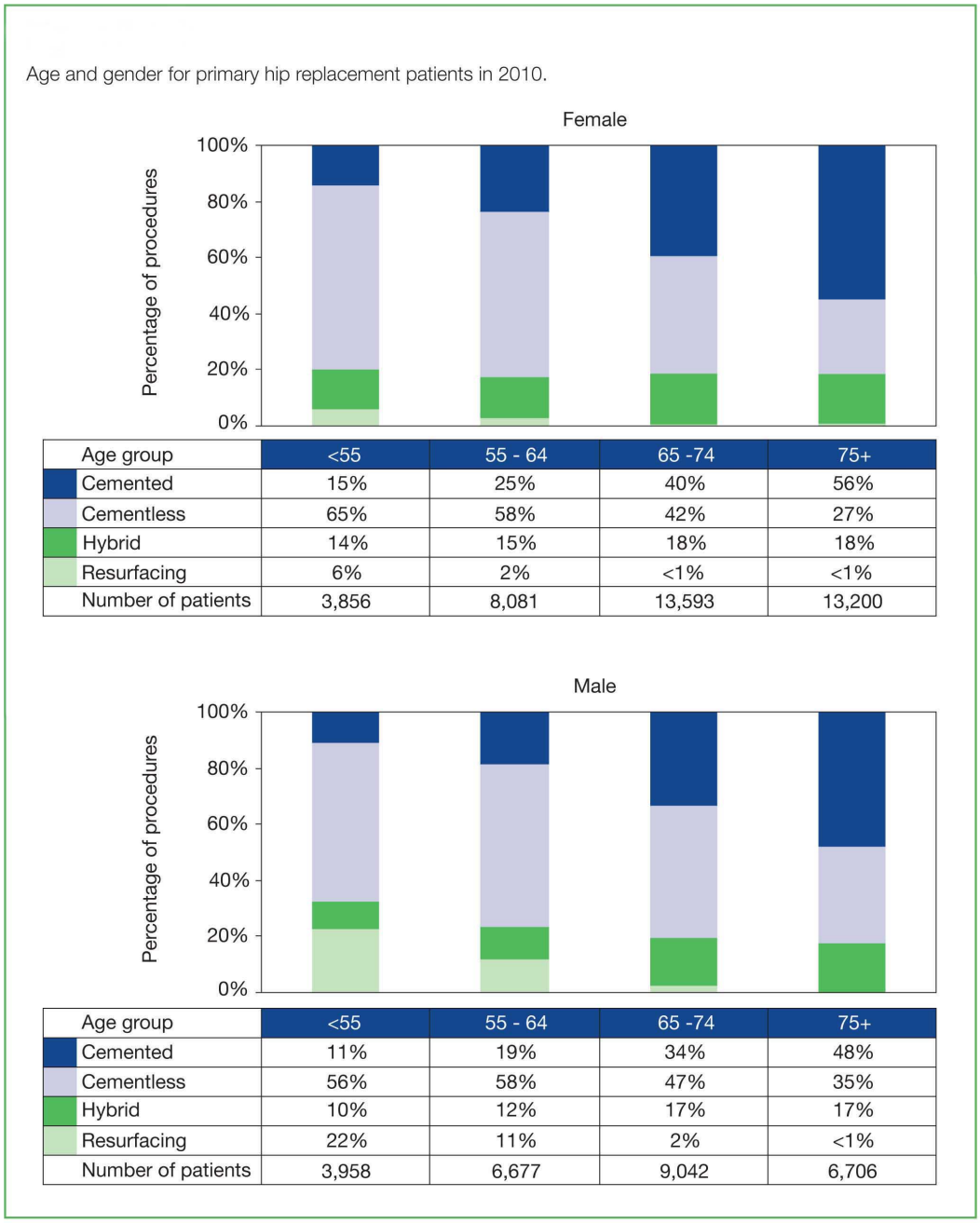

Age group	<55	55 - 64	65 -74	75+
Cemented	15%	25%	40%	56%
Cementless	65%	58%	42%	27%
Hybrid	14%	15%	18%	18%
Resurfacing	6%	2%	<1%	<1%
Number of patients	3,856	8,081	13,593	13,200

Age group	<55	55 - 64	65 -74	75+
Cemented	11%	19%	34%	48%
Cementless	56%	58%	47%	35%
Hybrid	10%	12%	17%	17%
Resurfacing	22%	11%	2%	<1%
Number of patients	3,958	6,677	9,042	6,706

Figure 2.13. Age and gender for primary hip replacement patients in 2010 (NJR)

The successful outcome of the procedure depends heavily upon patient selection for hip resurfacing, which can be observed with a higher survival of hip resurfacing procedure for young and male patients according to the National Joint Registry for England and Wales (2011).

As explained in the previous section, bone quality has a big impact in the success of the procedure so starting out with good bone quality is a bonus. For this reason most hip resurfacing patients are mainly males and young patients, older female patients has increased chances of suffering from age related bone mineral density loss, which could compromise the positive outcome of the operation with a reduction on bone quality. These patients should be avoided for hip resurfacing arthroplasty.

As stated by McMinn and Daniel (2006), the line to select appropriate patients is very fine and relies on the expertise of the surgeon. According to Schnurr et al. (2009), patient selection is absolutely imperative for the success of hip resurfacing.

Currently, the main points for patient selection are young, good bone quality and high activity levels. These parameters are commonplace in the reported literature of hip resurfacing studies. (Amstutz et al., 2004, Pollard et al., 2006, Siebel et al., 2006, Maguire et al., 2009 and Nunley et al., 2009). Schmalzried et al. (2005) used a radiographic arthritis hip grading to categorise patients according to bone density, shape, biomechanics and focal local defects.

2.14 Combination of Factors

Many different factors or variables affecting the success of hip resurfacing have been presented during the literature review.

These factors will be compiled into a combination of factors to be able to satisfy the initial research questions stated in Section 1.3.

- It is proposed that the methodology should include daily activities selected from the work of Morlock et al. (2001) according to the duration and frequency, with hip forces and rotations extracted from the work of Bergmann et al. (2001) for these daily activities.

- The daily activities selected will be split in number of cycles according to the resting period findings by Nassutt et al. (2003) and Wimmer et al. (2006), to be able to match metal-on-metal friction coefficients to numbers of cycles for the activities selected.

- PMMA stresses will be calculated according to the hip forces and rotations of the selected daily activity and for the different cases of metal-on-metal friction coefficient in every daily activity selected.
- PMMA fatigue data from Murphy and Prendergast (2000) for hand-mixed and vacuum-mixed bone cement will be used to evaluate the fatigue life of the cement mantle according to the Miner cumulative damage rule for low-cycle fatigue.

- Fatigue analysis will be performed using stress levels in PMMA to calculate the cycles to failure from the PMMA fatigue data (Murphy and Prendergast, 2000). Cycles to failure for every daily activity selected and MoM friction case can be combined with the estimated yearly number of cycles. The combination of cycle to failure and yearly cycles according to Miner's rules (Miner, 1945) will provide an estimation of the life of the cement mantle in the femoral component.

Furthermore, the effect of bone quality and bone cement properties on PMMA stresses will be evaluated using a multi-parametric approach for the selected daily activities and metal-on-metal friction cases.

Chapter 3

Methodology

This chapter describes the methodology used in the study to address the initial research questions. The chosen methodology will be justified from different methodological options. The key variables will be chosen and filtered for the study, arriving to a refinement of a predictive model and a statement of the limitations of the study.

3.1 Conceptual Framework

Figure 3.1 summarises the key components determined by the review of the literature and proposes a conceptual relationship between the parameters included in this thesis. The framework demonstrates that the theories and limitations of mechanical and simulatory investigation are integral parts of this study and, when used appropriately, may provide enhanced understanding and an insight into the lifestyle options that could affect the long term success of hip resurfacing arthroplasty.

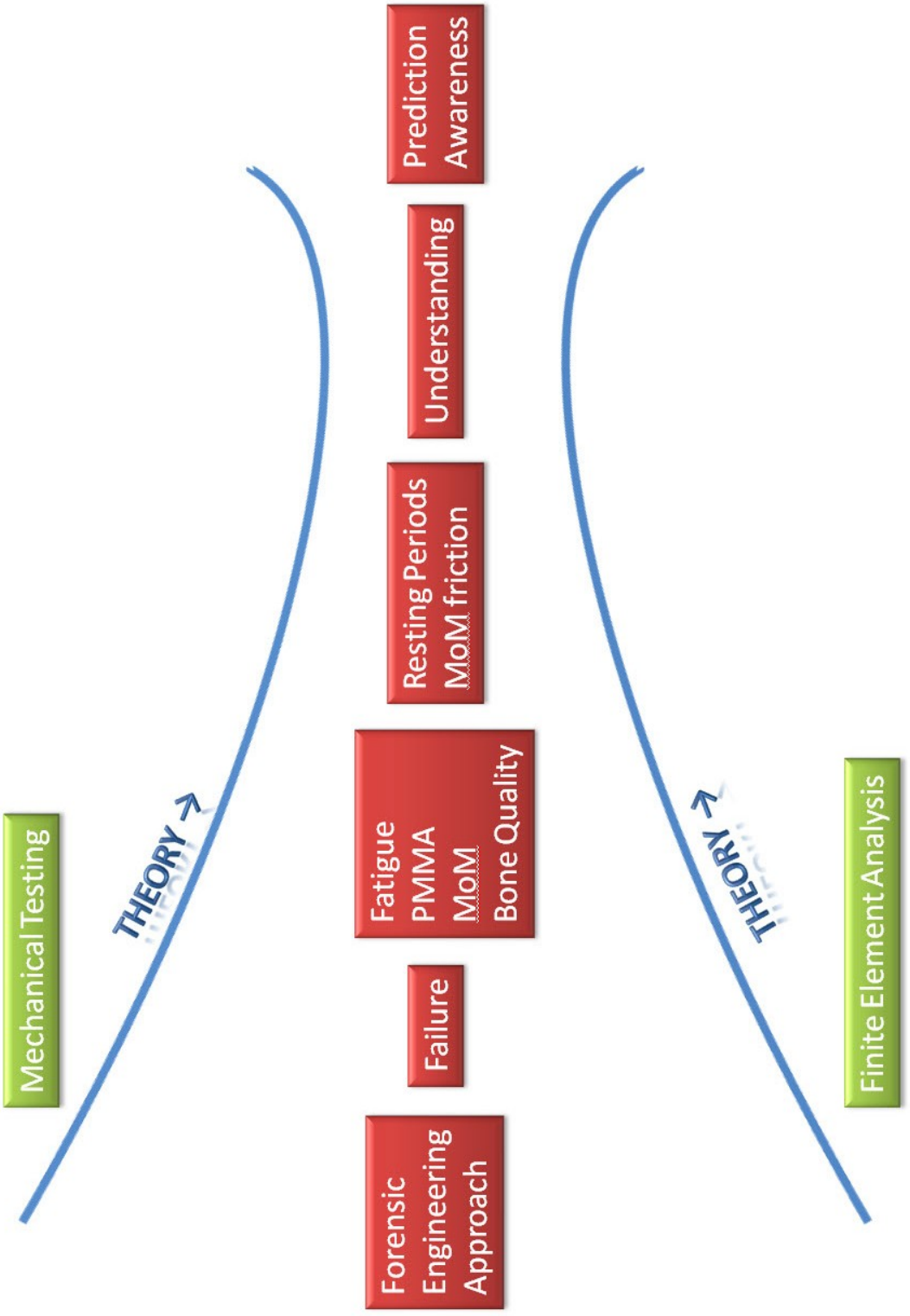

Figure 3.1. Conceptual Framework for this thesis.

3.2 The Use of the Conceptual Framework and the Evolution of the Research Aim

The initial research questions (Section 1.3) and the subsequent literature review resulted in a focus upon hip resurfacing design, surgical technique, short term failure, PMMA cementing technique, PMMA failure, gait data, resting periods and patient selection but with unresolved concerns about the failure in femoral components of hip resurfacing arthroplasty due to the effect of metal-on-metal friction due to resting period, patient bone quality and PMMA bone cement Young's modulus during daily activities.

The conceptual framework provides a logical path for the development of this thesis.

3.3 Methodology

The different methodological options are presented in Table 3.1. Each alternative is analysed in terms of advantages and disadvantages to meet the aims and objectives, revealing and justifying the preferred method.

Table 3.1.Research methods advantages and disadvantages (After Fellows and Liu, 2008).

Research Method	Advantages	Disadvantages	Conclusions
Action Research	Practical approach to professional inquiry in any social situation. Monitoring of planned change in practice.	Ethical issues due to human patients.	Not possible to make changes to parameters to be implanted in a patient to observe results.
Experiment Simulation / FEA	Variables involved are known. Facilitate cause and effect conclusions. Very accurate dimensions. Theoretical generalisation.	Reality is not so accurate. Simplifications and assumptions. (NAFEMS, 2002)	Bioengineering is a field where experiment and simulation are obvious methodology choices. Predict result of changes to variables.
Surveys Questionnaire-Interview-Observation	Produce standardised data - easy to analyse. (Biggam, 2008) Can provide facts, opinion, feelings and experiences. For certain purposes it is best to observe the reality. (Naoum, 2007) Empirical generalisation.	Can only provide relatively brief and straightforward information.(Naoum, 2007) Results harder to analyse as answers will be non-standard.(Naoum, 2007) Can lead to oversimplification of information (Denscombe, 2007)	Surveys provide a good inside as used in the initial research but it can predict changes to current practice.
Case Studies	Theoretical generalisation. Source of insights and ideas. Facilitate in-depth investigation of particular instances	Patient specific. Difficult to generalise findings.	Case studies provide an insight into survival and follow-up results but cannot predict the effect of new developments

3.4 Controlling Key Variables

After selecting *simulation* – Finite Element Analysis (FEA) as the research method to achieve the aim and objectives, the key variables of the study are selected and filtered to be able to answer the supplementary research questions.

The Finite Element Analysis will be a three dimensional dynamic simulation instead of static simulation to be able to capture the effect of hip forces, rotation and MoM friction on the PMMA stresses during the whole gait daily activities.

- Femoral and acetabular hip resurfacing components are modelled from manufacturer's templates, while only the femoral neck and head are simulated with an ideal shape. The PMMA cement mantle is simulated with a uniform thickness and in absence of porosity.

- All materials in the Finite Element Analysis model are assumed to be isotropic and homogeneous.

- Hip contact forces in the 3 degrees of freedom (x, y and z) are taken from Bergman et al. (2001). Flexion-extension rotation is selected as the most influential hip rotation during gait.

- Metal-on-metal friction coefficient is taken from the work of Nassutt et al. (2003) and Wimmer et al. (2006) to simulate the 'running in' effect of the metal bearing surface as explained in Section 2.2.2.

- The most common daily activities are taken as walking, descending steps and standing up. Number of cycles per year for each activity is collected (Morlock et al., 2001). Numbers of cycles for walking, descending stairs and standing up are divided according to resting period time during daily activities.

- Mean stresses for PMMA fatigue data from Murphy and Prendergast (2001) are adjusted using the Goodman approach to convert to a pure alternating loading (compression-tension, mean stress =0) (Gokhale et al., 2008)

- A rainflow analysis is performed for the Finite Element Analysis PMMA tensile stress results for every activity and MoM friction, followed by adjusting the

mean stress with the modify Goodman approach and finally, calculating the cycles to failure for every PMMA tensile stress level.

- Fatigue analysis is performed using Miner's cumulative damage rule (Miner, 1945) following a stress life approach, which can calculate the damage for variable amplitude loading. The fatigue life of the femoral component is calculated according to the number of cycles performed per year divided by the number of cycles to failure.

- The effect of bone quality on PMMA stresses is analysed by altering the material properties of cortical and cancellous bone in the Finite Element Analysis models.

- The effect of different PMMA bone cement on the outcome of hip resurfacing is evaluated by changing the Young's modulus of PMMA in the Finite Element Analysis models.

- Shear stress and torque mechanical testing are performed to illustrate the use of Finite Element Analysis results to understand the behaviour of the metal-bone cement interface and the implications on the stability of the implant, following an experimental methodology.

3.5 Drivers

The following drivers, identified in Section 1.3, are developed in the light of the controlled key variables:

- Could high metal-on-metal friction coefficient due to resting periods cause aseptic loosening of femoral hip resurfacing components during daily activities by PMMA bone cement fatigue?

- Could low bone quality affect the stability of the femoral hip resurfacing components due to PMMA stresses?

- Could PMMA Young's modulus affect the stability of the femoral hip resurfacing components due to PMMA stresses?

- Could the torque produce failure on the PMMA-metal interface and loosening of femoral hip resurfacing components?

3.6 Research Paradigm

Figure 3.2 provides a directional summary of the inter-relationships between key parameters and this research within the boundaries of the conceptual framework.

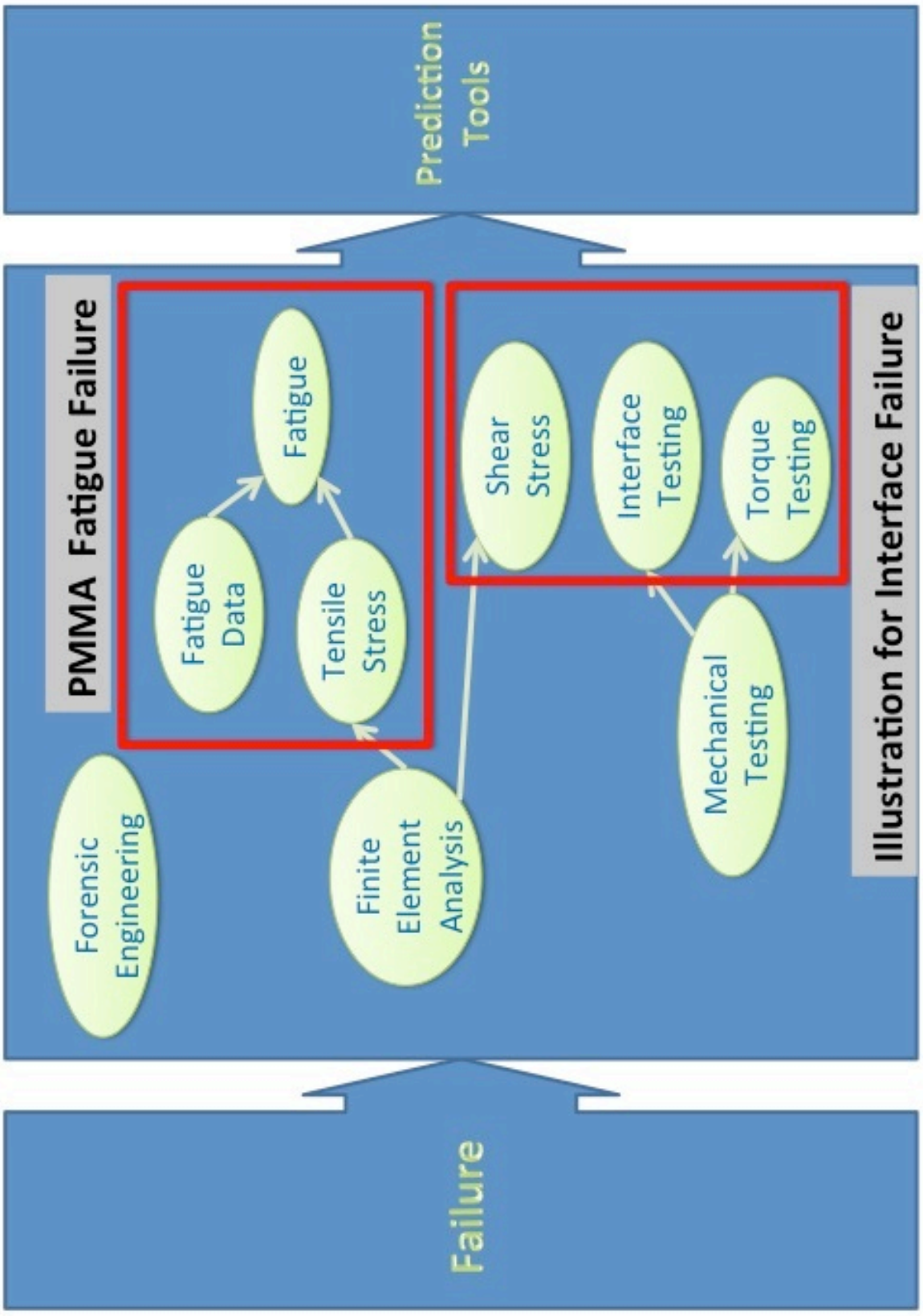

Figure 3.2. Research Paradigm

3.7 Limitations of this Research

The following limitations are taken in this study:

- Femoral neck and femoral head bone are modelled as if an ideal shape.

- Material properties are assumed to be isotropic and homogenous, not taking into account the heterogeneous properties of bone for every individual patient and porosity in PMMA bone cement.

- The application of flexion-extension is simplified in the Finite Element Analysis modelling.

- PMMA fatigue data is considerate to have a linear relationship between stress and cycles to failure (Davies et al., 1987) and no fatigue limit (Huiskes, 1993).

- No fracture or damage mechanics is considered.

Chapter 4

Building and Corroborating the Finite Element Model

This chapter describes how the Finite Element hip resurfacing model was created, boundary conditions applied and sensitivity analyses performed.

4.1 Introduction

NAFEMS (2002) describes how Finite Element Analysis (FEA) was born in the late 1940s and it was used primarily with a focus on the aerospace industry due to the high cost of digital computer at the time. Finite Element Analysis currently has potential to be applied to fields of engineering where a complex structural problem can be solved using this methodology. Finite Element Analysis can be separated into two stages. The first stage is to divide the structure into small finite elements and the second stage involves the assembly of all small finite elements to satisfy the continuity across the whole structure (NAFEMS, 1992). A Finite Element Analysis is a mathematical approximation of a real problem.

Finite Element Analysis has been applied in bioengineering for stress analysis of bone, bone-implant structures and various other tissues other than bone. Finite element studies on the reconstructed femur after hip resurfacing can be classified into three stages. The most simplified approach has been the modelling of two-dimensional (2D) plane strain models of a cross section through the bone. Axisymetric models, where the hemispherical geometry of the head of the femur is taken into account, has been used by Watanabe (2000). The final stage is the creation of accurate three-dimensional (3D) models of reconstructed bones from CT scan data as used by Taylor (2006).

4.2 The Model

The model of the reconstructed femur after hip resurfacing was developed using the software *I-Deas NX 11* finite element pre-processing. The model of a 54 mm diameter hip resurfacing femoral implant was created from operating templates supplied by Professor Cheah FRCS (*Biomet*, 2005). Furthermore, the operating templates where compared to the measurements taken from a *Biomet ReCap* hip resurfacing system using a vernier calliper. In the same way, a hip resurfacing acetabular cup of diameter 60 mm was developed. The clearance between femoral and acetabular component was fixed to 0.1125 mm according to technical data from *Biomet* (*Biomet*, 2005). Polymethyl methacrylate (PMMA) bone cement was created to fix the femoral implant to the hemispherical reamed femoral head with a uniform thickness of 1 mm for FEA simplification purposes and agreement with published data after Campbell et al. (2009). The reamed femoral head was completely covered by PMMA bone cement and the femoral implant avoiding any uncemented femoral head areas, which could result in neck fracture (Amstutz, 2005). The femoral implant peg was simulated uncemented (*Biomet*, 2005). Finally, a simplification was used to model the cancellous and cortical bone at the head and neck of the femur, the cortical bone was modelled with a uniform thickness of 1 mm. Similar simplifications to create bone models has been used by others researchers (Watanabe, 2000 & Udofia, 2004). The hole drilled in cancellous bone to accommodate the femoral peg was finished in a right angle end following instrumentation details form *Biomet* as it can be seen in Figure 4.1.

Figure 4.1. Right angle end drill bit (5 mm) used to accommodate the femoral peg in the cancellous bone (Cheah, 2007)

The cancellous and cortical bone was positioned with an angle of 120 degrees between femur shaft and femoral neck. The position of the hip resurfacing femoral implant in respect to the femoral neck was taken as neutral, so the femoral implant peg follows the geometrical centre of the femoral neck. This position of the femoral implant avoids any stress raised effect due to a varus position which has been identified as a short term concern (Freeman, 1978, Beaule, 2004 and Shimmin, 2005) as explained in section 2.7.1. The hip resurfacing acetabular cup was position with an abduction angle of 45 degrees following recommendations from *Biomet* and orthopaedic surgeons.

Prior to the meshing process, the whole Finite Element Analysis model was rotate 60 degrees to end up with a vertical position of the femoral neck bone and femoral implant, as shown in Figure 4.2, to allow a better implementation of boundary conditions to the Finite Element Analysis model. The vertical positioning allowed the flexion-extension rotation to be applied to the acetabular cup through the vertical axis.

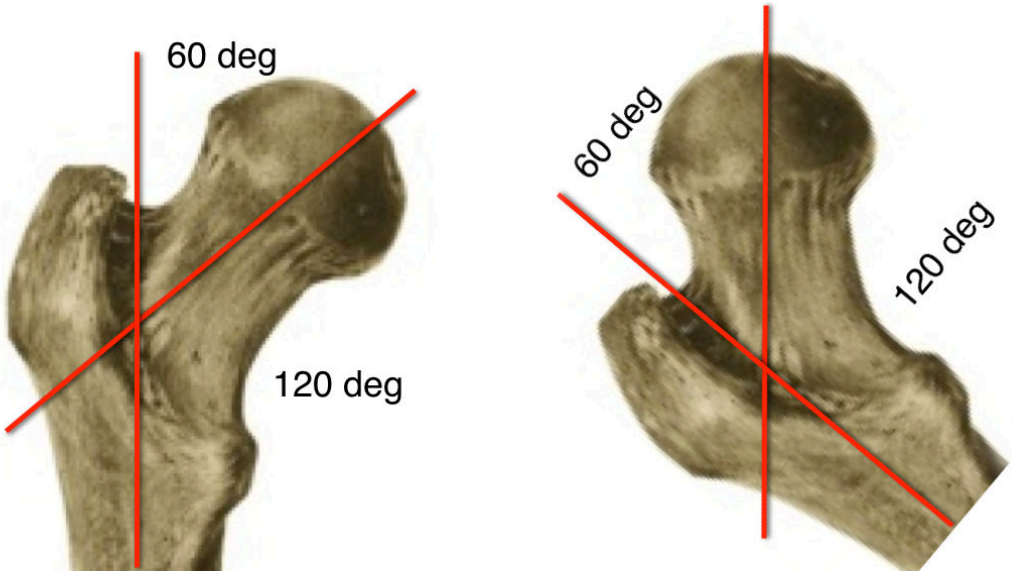

Figure 4.2. Finite Element model rotation to vertical position
(http://www.rkm.com.au/anatomy/femur.html)

4.3 Boundary Conditions

4.3.1 Contact interfaces and restraints

Nodes at the interface between cortical bone and cancellous bone were merged to represent perfect bonding. The same approach was used to simulate the interface between PMMA bone cement and cancellous bone because the interface between these surfaces was bonding due to the PMMA bone cement flowing into the sponge reamed cancellous bone and helped by the keyholes reamed to improve interdigitation of the PMMA bone cement (*Biomet*, 2005).

The contact interface between acetabular cup and femoral implant were simulated using contact elements with a metal-on-metal coefficient of friction of 0.098, according to the work of Nassutt et al in 2003.

The contact interface between femoral implant and PMMA bone cement was performed with a metal-PMMA coefficient of friction of 0.42, following mechanical testing carried out by the author previously to this research during his dissertation (Jimenez-Bescos, 2004). A sensitivity analysis for a variation of metal-PMMA coefficient of friction from the present research was performed to analyse the impact on the research.

The contact interface between the femoral implant peg and the cancellous bone was simulated using a coefficient of friction for metal-bone of 0.15 (Orthoteers, 2007). A sensitivity analysis for a variation of metal-bone coefficient of friction from the present research was performed to analyse the impact on the research.

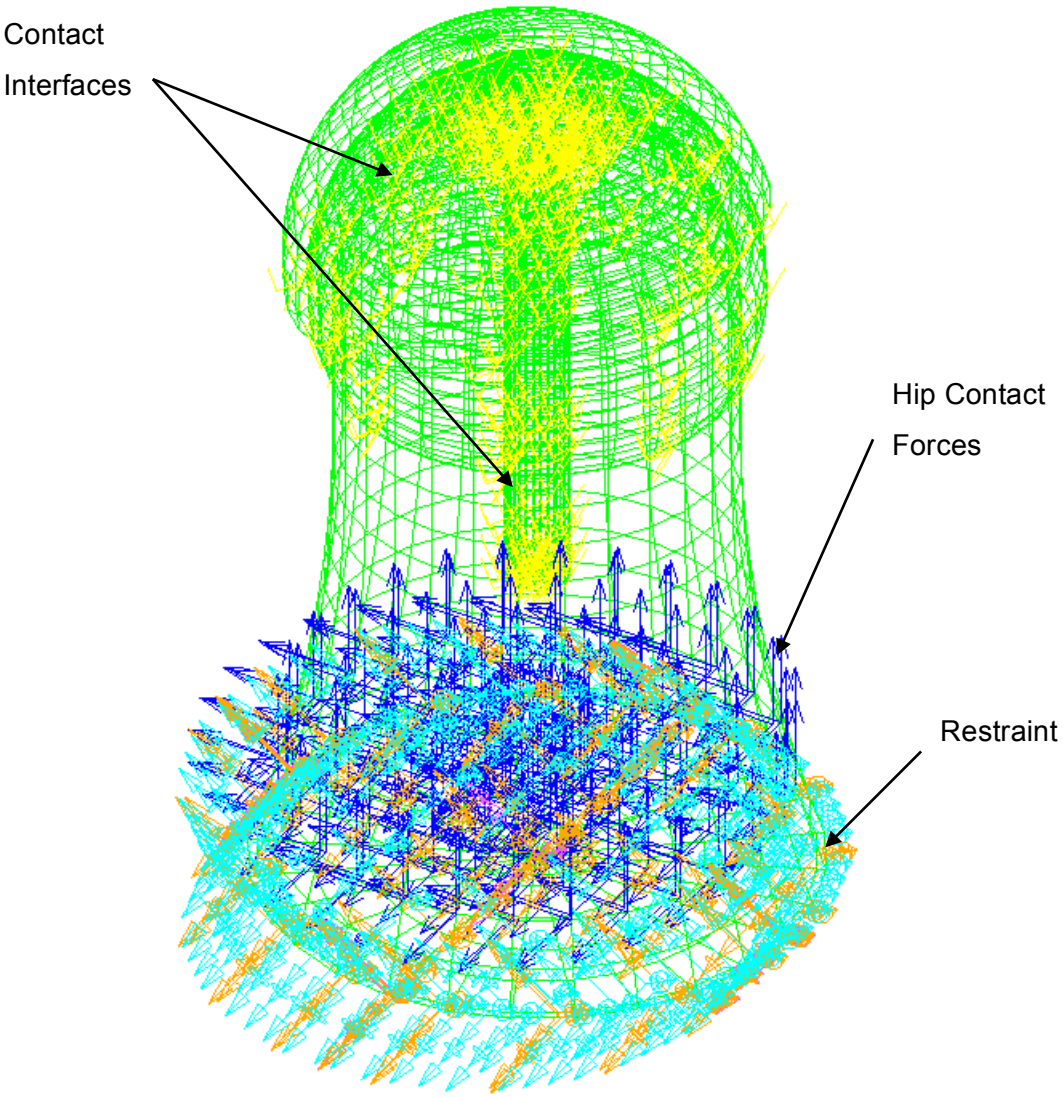

Figure 4.3.Boundary conditions in *I-Deas NX 11*.

The base of the femoral neck, including cancellous bone and cortical bone, was restrained in 5 degrees of freedom (all rotations and 2 displacements) and allow to move in the direction of the maximum hip contact force for the daily activity simulated. This restraint was applied in *I-Deas NX 11*.

The acetabular cup was modelled as a rigid body to allow the application of the flexion-extension rotation in the vertical axis in Figure 4.2. The acetabular cup was restrained in 5 degrees of freedom (all displacements and 2 rotations) and allowed to rotate around the femoral neck axis to simulate flexion-extension rotation during gait. This restraint was applied in *LS-Dyna*.

The boundary conditions are shown in Figure 4.3.

4.3.2 Hip contact forces and flexion-extension rotation

Three activities were chosen to represent the most usual daily activities and applying the higher hip contact forces. These activities were normal walking, descending steps and standing up from a chair. The hip contact forces data from the work of Bergmann and colleagues (2001) were used to specify the loads representing the daily activities. The hip flexion-extension rotation was taken from the same set of data as the hip contact forces, helping to achieve a better simulation of the activities. The body weight for normal walking and standing up was 836 N and for descending steps was 847 N.

The hip contact forces and flexion-extension rotation for the three activities are shown in Figure 4.4.

As explained in section 4.2 and shown in Figure 4.2, the Finite Element model was rotated by 60 degrees to position the femoral neck in a vertical position to allow an easier application of the rigid body movement of the acetabular cup. This rotation meant that the hip contact forces were recalculated to accommodate the 60 degrees rotation. Trigonometry was used to calculate the hip contact forces in the vertical and horizontal axes (Z-axis was unaffected by the rotation). The load was applied in *I-Deas NX 11* using unitary value forces of 100 N in the three principal directions (X, Y and Z) multiplied by a force factor to achieve the resultant hip contact force described in Figure 4.7 for every daily activity. The force factor allowed the application of a variable load with time for the dynamic simulation in *LS-Dyna*. An example of the

calculation of the force factor for walking gait is presented in Table 4.1. The load was applied through a surface of nodes at the base of the femoral neck, but at a distance of 2 elements from the base to avoid any complication with the restraints already in place at the base of the femoral neck (Figure 4.3). The final hip contact forces that will be applied during the solving process in *LS-Dyna* will be equal to:

Table 4.1. Force factor to apply to LS-Dyna for walking gait

Time	Total Hip Contact Force (Bergmann,2001)	Force Factor = Total Hip Contact Force / 100
0.000	77.66	0.777
0.055	135.94	1.359
0.110	202.66	2.027
0.166	231.63	2.316
0.221	229.79	2.298
0.276	217.56	2.176
0.331	207.41	2.074
0.386	203.39	2.034
0.441	204.52	2.045
0.497	203.62	2.036
0.552	192.64	1.926
0.607	164.23	1.642
0.662	125.19	1.252
0.717	93.62	0.936
0.772	71.31	0.713
0.828	51.75	0.518
0.883	36.17	0.362
0.932	29.38	0.294
0.993	34.08	0.341
1.048	52.71	0.527
1.103	80.00	0.800

$$F_X = \left(100 \cdot \cos(30°)/number\ of\ nodes\right) \cdot force\ factor$$
$$F_Y = \left(100 \cdot \cos(30°)/number\ of\ nodes\right) \cdot force\ factor$$
$$F_Z = \left(100/number\ of\ nodes\right) \cdot force\ factor$$

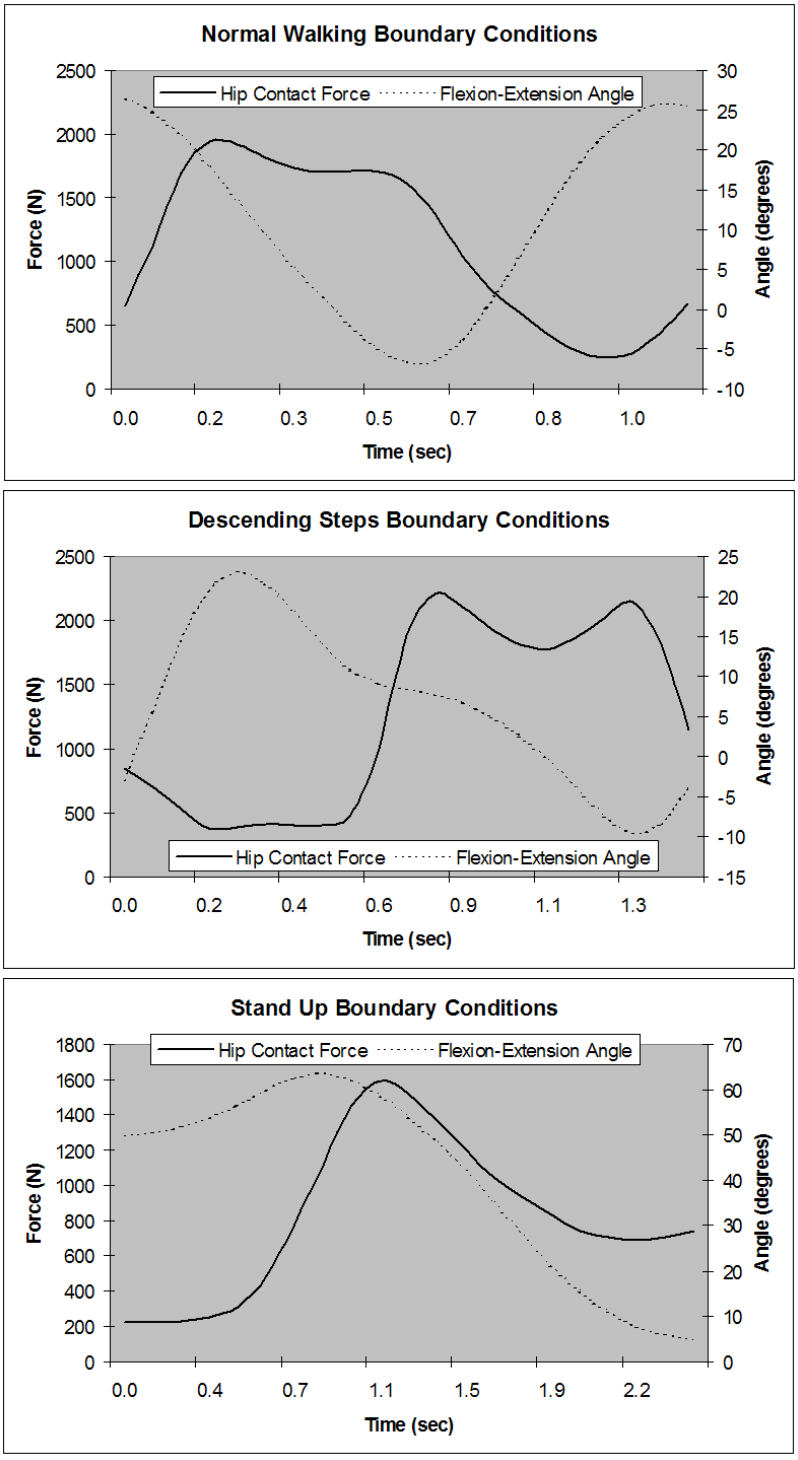

Figure 4.4. Hip contact forces and flexion-extension rotation for daily activities (Bergmann, 2001)

The flexion-extension rotation was applied in *LS-Dyna* using a boundary prescribed motion applied to the rigid body (acetabular cup). The application of the rigid body

movement meant that the Finite Element Analysis would be performed using an explicit solving approach. The rotation was specified at the same time steps as for the hip contact forces with the angles in radians. The application of torque due to the friction produce by the metal-on-metal bearing surfaces was achieved by using the rotation of the acetabular cup.

4.4 Material Properties

4.4.1 Cortical bone and cancellous bone

The material properties for cortical bone and cancellous bone were retrieved from literature (Taylor, 1995 and Udofia, 2004) and were assumed to be isotropic and homogeneous. The values for Young's modulus and Poisson's ratio are presented in Table 4.2.

Table 4.2. Material properties

	Poisson's ratio	Young's modulus (GPa)
Cancellous Bone	0.3	0.8
Cortical Bone	0.2	17
Co-Cr	0.3	210
PMMA	0.3	2

4.4.2 PMMA bone cement

PMMA bone cement has been widely used in hip resurfacing and total hip replacements to fit femoral and/or acetabular components. PMMA bone cement is supplied by different companies with slightly different constituents and molecular weight, which can subsequently produce PMMA bone cement with different mechanical behaviours. According to the work of Schmoelz in 2001, the values of Young's modulus used in finite element analyses varies between 1 GPa and 4 GPa. PMMA bone cement Young's modulus reported through mechanical testing was found to vary between 1.5 GPa and 4.1 GPa (Lewis, 1997). A Young's modulus of 2 GPa and a Poisson's ratio of 0.3 were used for the cement mantle in this study (Huiskes, 1990 and Watanabe, 2000).

4.4.3 Hip resurfacing femoral implant and acetabular cup

Femoral implants and acetabular cups for hip resurfacing are manufactured using 'as cast' CoCrMo materials in accordance with the requirements of ISO 5832-4 (ASTM F75) as stated in the *ReCap* technical design rationale published by *Biomet* in 2005. A Young's modulus of 210 GPa and a Poisson's ratio of 0.3 were used to simulate CoCr for the femoral implant and the acetabular cup (Udofia, 2004).

4.5 Meshing

The meshing of the Finite Element Analysis model was performed using the software *I-Deas NX 11* finite element pre-processing. The Finite Element Analysis model was partitioned to apply the materials properties. Furthermore, the whole model was partitioned in four quadrants following the centre axis from the femoral neck to allow the use of a mapped mesh. After partitioning, every partition is compound of six sides or five sides, which is a requirement to allow the application of a mapped mesh (brick elements). The Finite Element Analysis model was manually mapped mesh using 8 nodes low order brick elements checking the quality of the model to achieve the best accuracy at the lowest processing cost. The boundary conditions were applied in *I-Deas NX 11*. Finally, the Finite Element Analysis model was exported to *LS-Dyna 9.70* to be dynamically solved using an explicit solving approach. The Finite Element Analysis model was solved using an explicit approach due to the application of the rigid body movement to a rigid body (acetabular cup) in the model.

A rough mesh was generated using 6168 brick elements and 1254 contact elements. Contact elements were used for the interface between femoral implant and PMMA bone cement and as well, the interface between femoral peg and cancellous bone. The Finite Element Analysis model was solved for walking gait to test the accuracy of the mesh and took around three days of run analysis time, finishing the analysis without errors or warnings. After post-processing, the Finite Element Analysis was found to have singularity points in the PMMA bone cement stresses, which could affect the accuracy of the results. The singularity points were located in elements in the PMMA bone cement, where data on stresses would be collected for further analyses, so it was decide to develop a finer mesh.

A fine mesh was generated using 8960 brick elements and 3234 contact elements. The number of elements at each interface of two bodies in contact was kept equal in

order to reduce the processing time for the finite element analyses according to *I-Deas Help Library*. The Finite Element Analysis model took around nine days of run analysis time, finishing the analysis without errors or warnings. After post-processing, the Finite Element Analysis was found to be free of singularities in the PMMA bone cement stresses. The meshed Finite Element Analysis model is shown in Figure 4.5.

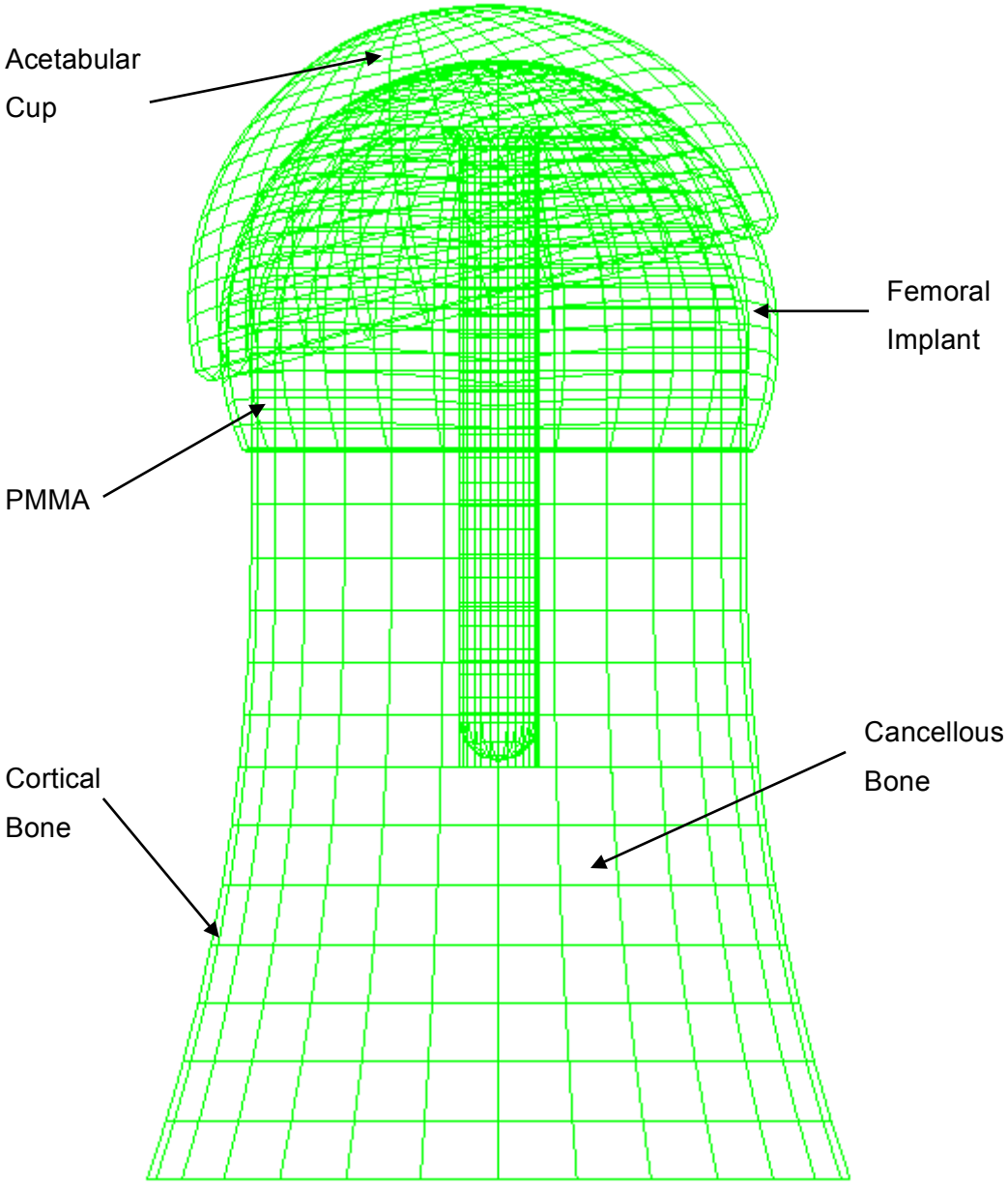

Figure 4.5. Meshed finite element model.

A third Finite Element Analysis was created using a meshless "Element Free Galerkin" method in *LS-Dyna*. The meshless model was very time consuming to

solve but it allowed verifying the mesh density of the model to be able to perform the research using the fine mesh model presented in Figure 4.5.

Figure 4.6.a and 4.6.c show the resultant maximum tensile and shear stresses respectively during walking for the fine mesh and meshless models. Furthermore, tensile and shear stress distributions for 0.165 seconds after heel strike in the walking gait are presented in Figure 4.4.b and 4.4.d respectively.

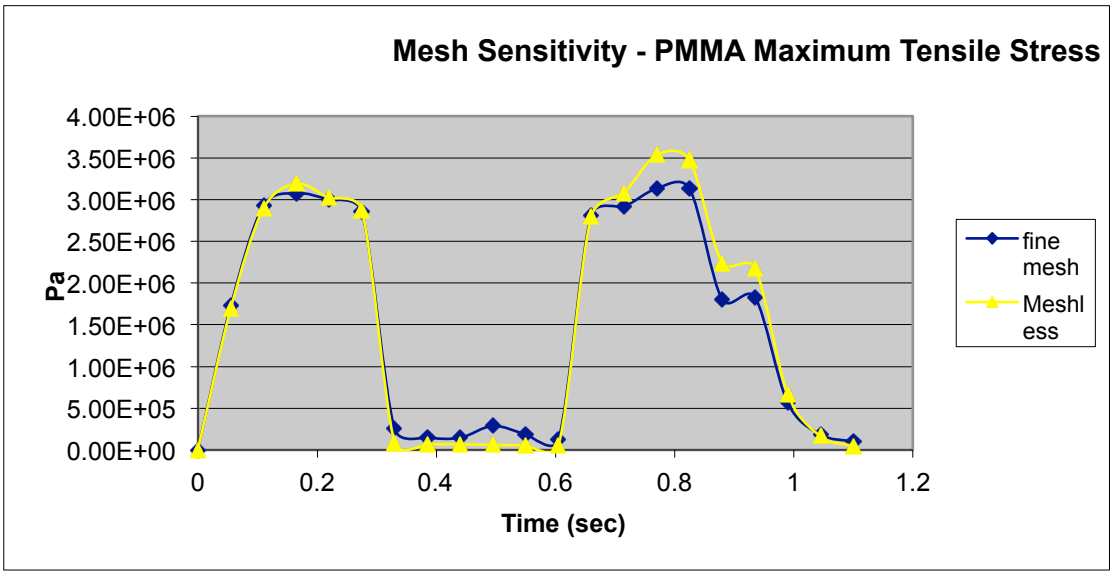

Figure 4.6.a. Maximum tensile stresses during walking gait for fine mesh and meshless models.

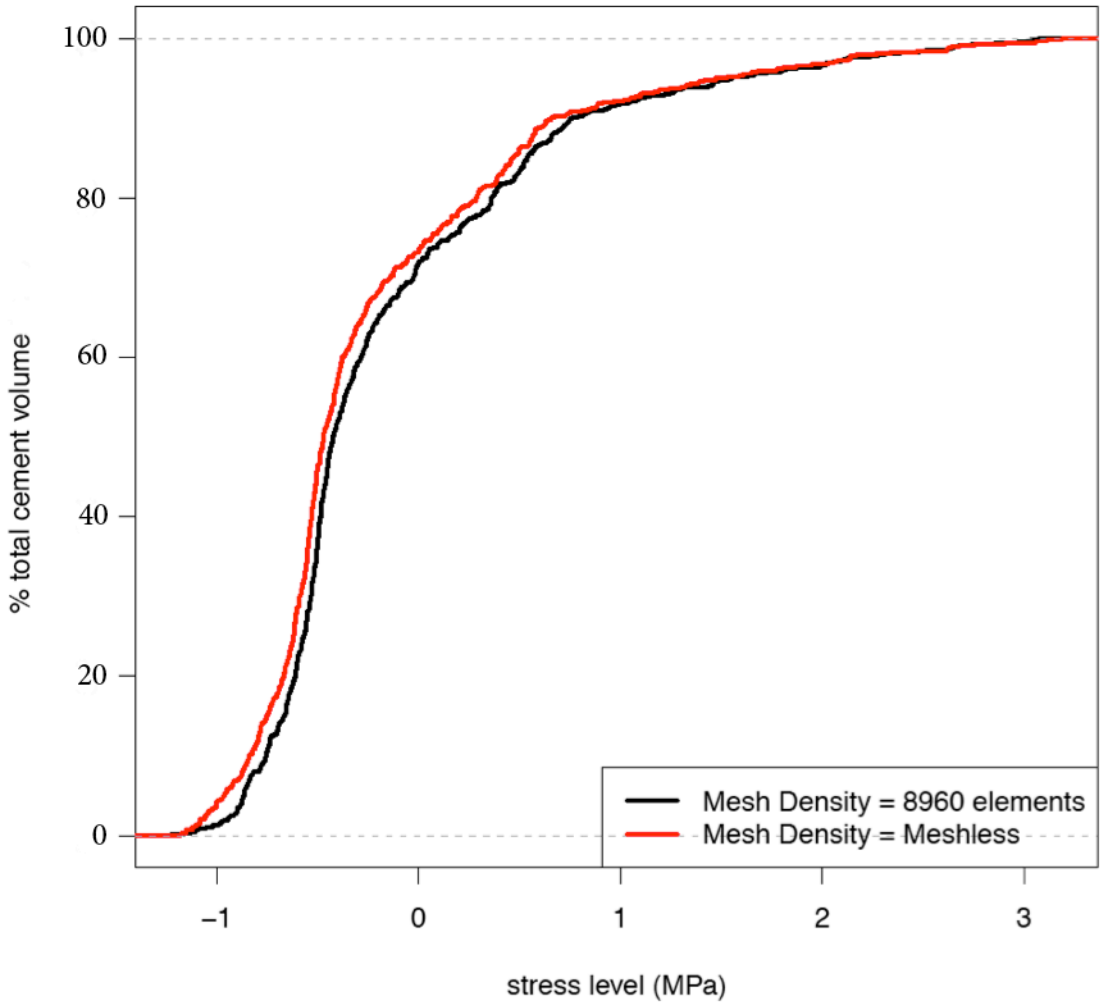

Figure 4.6.b. tensile stress distribution 0.165 seconds after heel strike during walking gait for fine mesh and meshless models.

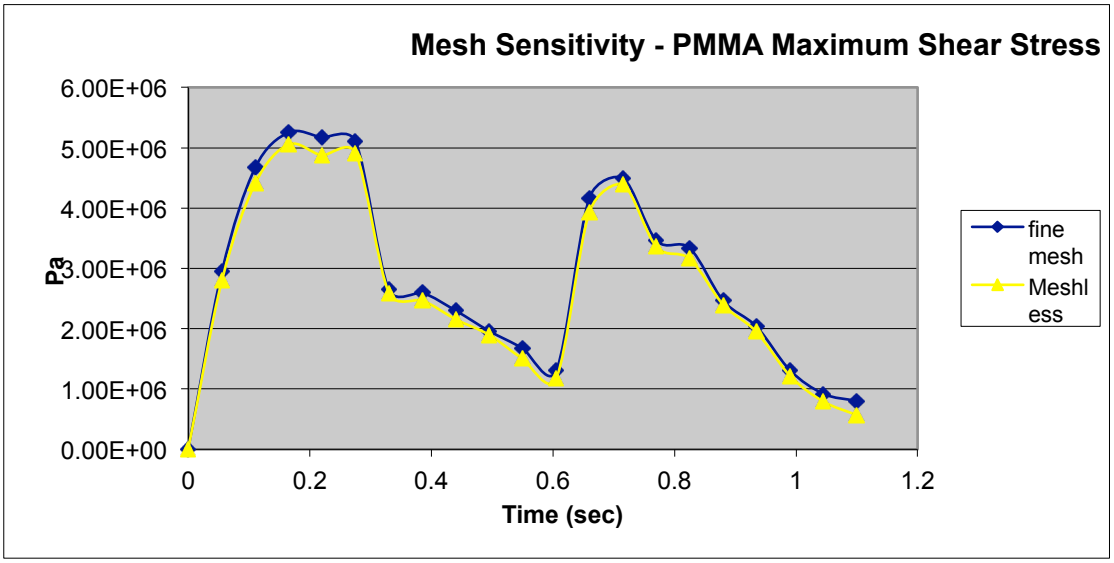

Figure 4.6.c. Maximum shear stresses during walking gait for fine mesh and meshless models.

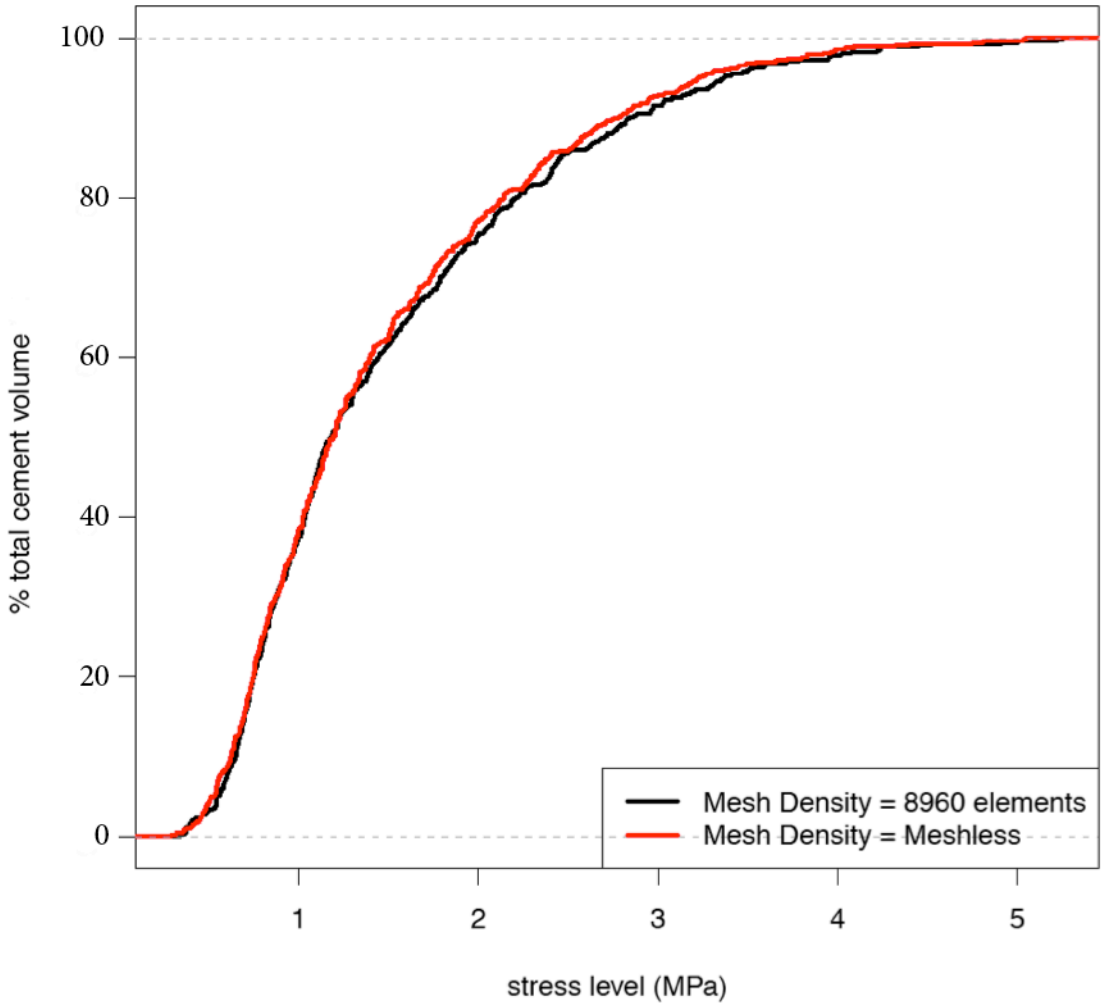

Figure 4.6.d. Shear stress distribution 0.165 seconds after heel strike during walking gait for fine mesh and meshless models.

From Figures 4.6.a to 4.6.d, it can be seen that the results for the fine mesh and meshless models are in close agreement, allowing the selection of the fine mesh model to perform the Finite Element Analysis for this study.

4.6 Sensitivity Analysis

4.6.1 Mass scaling

The run analysis time for the shortest dynamic Finite Element Analysis model (walking gait) was found to be around nine days. Mass scaling was used as a tool to optimise the run analysis time. The run analysis time depends on the minimum element size and more importantly the time step. The basic relationship between time step and wave speed is defined as:

$$\Delta t = \frac{L}{c} = \frac{L}{\sqrt{E/\rho}}$$

The time step can be modified increasing the material density (ρ) and consequently modifying the mass. This optimisation technique should be used carefully because an appreciable change in material density can affect the dynamic respond of the model (NAFEMS, 2002).

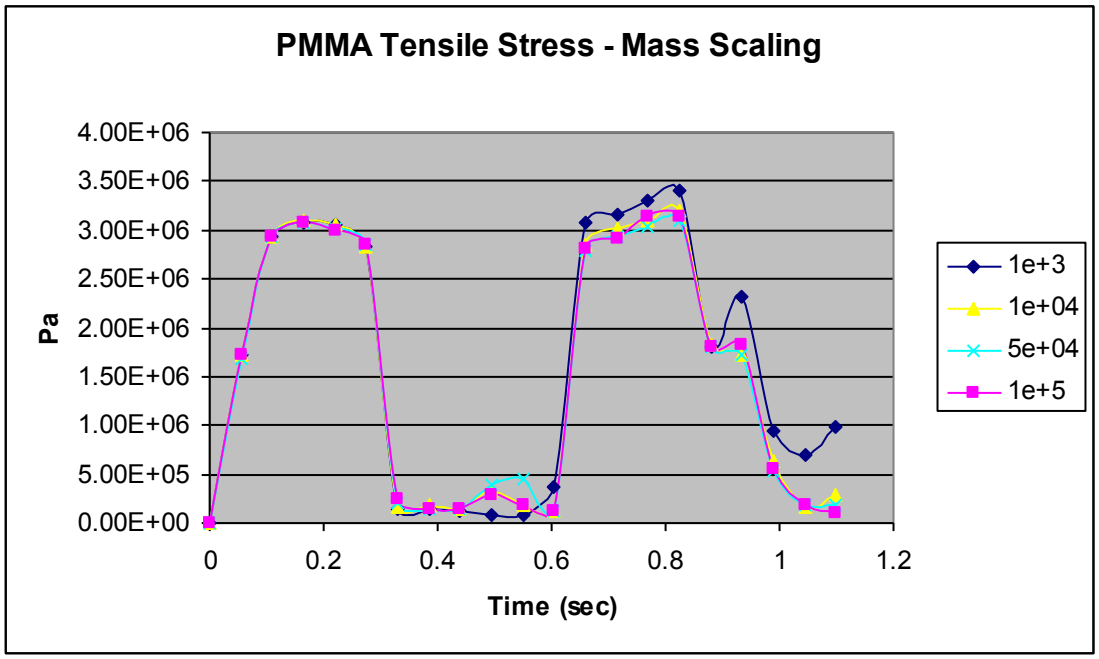

Figure 4.7.a. Maximum tensile stresses during walking gait for different material densities.

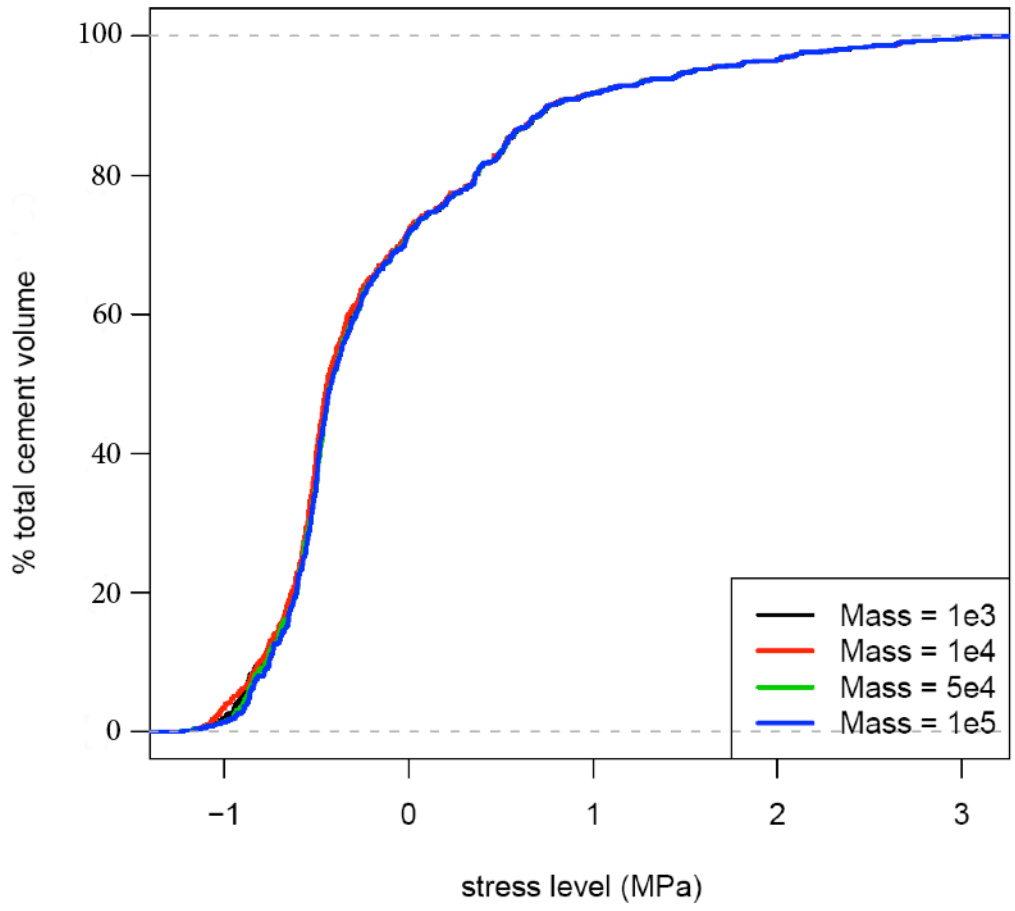

Figure 4.7.b. Tensile stress distribution 0.165 seconds after heel strike during walking gait for different material densities.

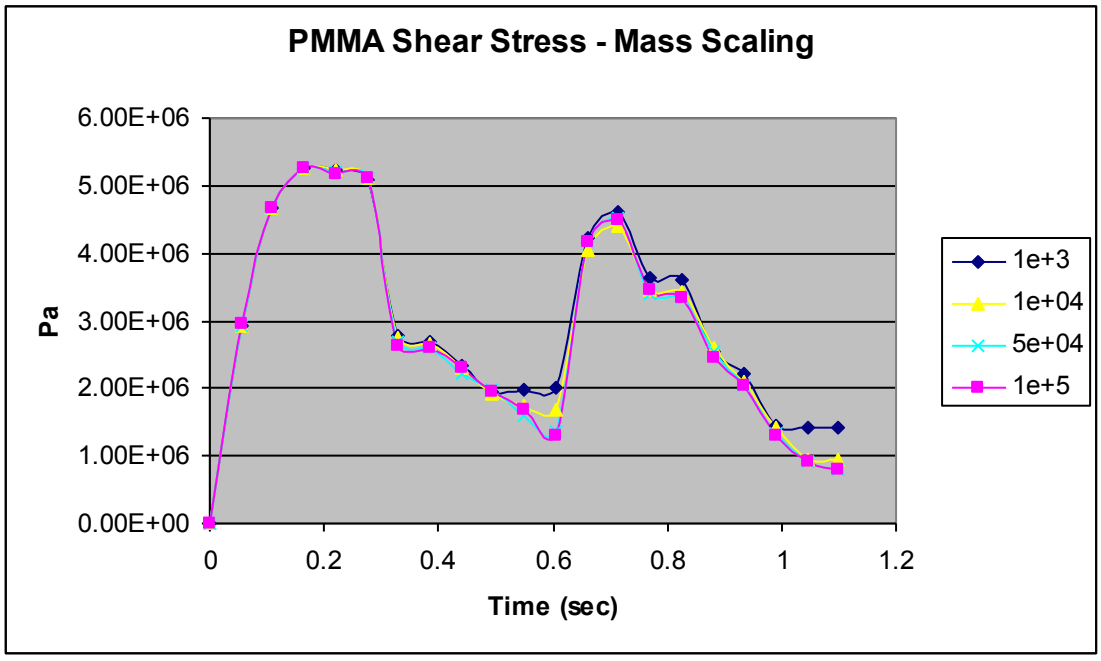

Figure 4.7.c. Maximum shear stresses during walking gait for different material densities.

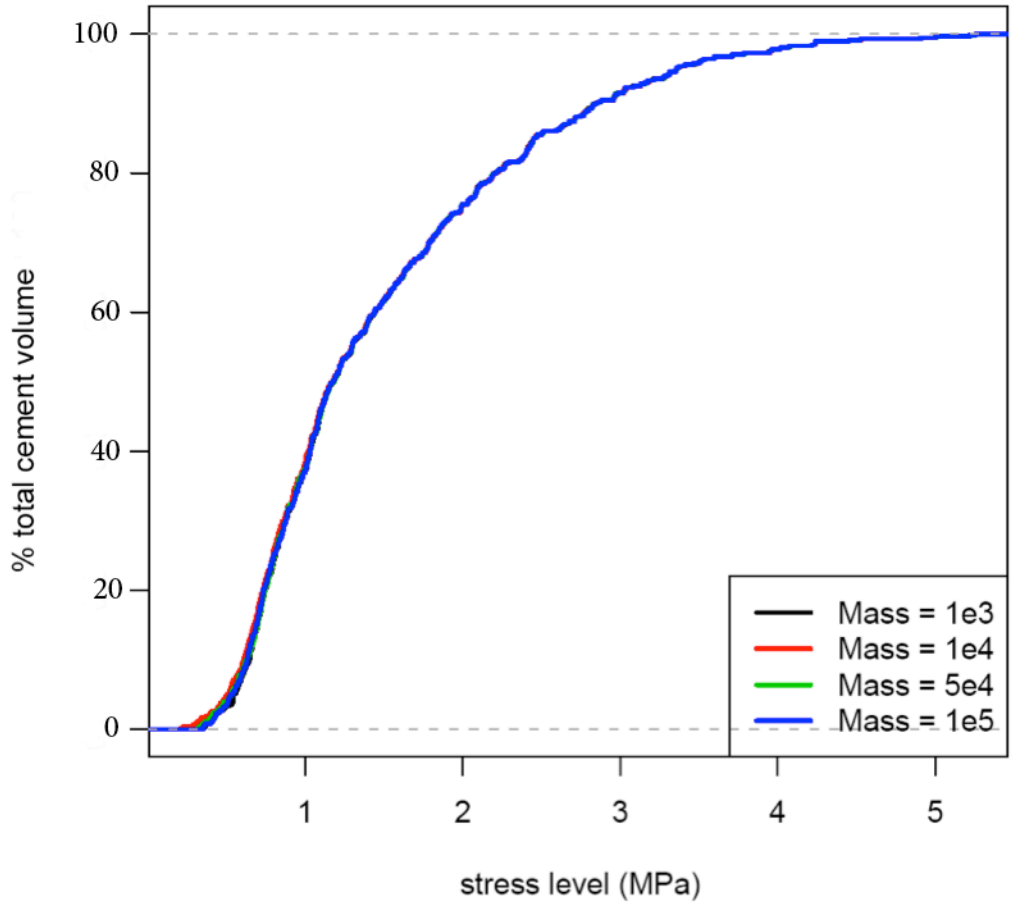

Figure 4.7.d. Shear stress distribution 0.165 seconds after heel strike during walking gait for different material densities.

Four finite element analyses were solved using *LS-Dyna* with material densities equal to 1e3, 1e4, 5e4 and 1e5 to increase the time step and lower the run analysis time. The Finite Element Analysis models were solved for walking gait and with boundary conditions as described in Section 4.4.

The run analysis time was reduced from around nine days to around two days after an increase in material density from 1e3 to 1e5. Figure 4.7.a to Figure 4.7.c show the result of peak PMMA tensile and shear stress values to demonstrate that the effect of changing the material density imply a small change in the PMMA bone cement stress results. Furthermore, the stress distribution for tensile and shear stresses in the PMMA bone cement is shown in Figure 4.7.b to Figure 4.7.d for 0.165 seconds after heel strike during walking gait, demonstrating that the change in material density has little influence in the stress distribution.

4.6.2 Sensitivity to metal-PMMA friction

The coefficient of friction for the contact interface between the metal femoral implant and the PMMA bone cement is proposed as 0.42 following mechanical testing carried out by the author previous to this research (Jimenez-Bescos, 2004). Nevertheless, it was considered beneficial to understand the sensitivity of the Finite Element Analysis model to a variation of this coefficient of friction and more importantly its effect on the PMMA bone cement stresses.

Five finite element analyses were solved using *LS-Dyna* with metal-PMMA coefficient of frictions equal to 0.3, 0.35, 0.42, 0.45 and 0.5.

Figure 4.8.a and Figure 4.8.c show the results of peak PMMA bone cement tensile and shear stress values for different metal-PMMA coefficient of friction during walking with a metal-on-metal friction of 0.098. A maximum variation of 7% of the maximum peak value for PMMA bone cement tensile stress was observed after a reduction of metal-PMMA friction from 0.42 to 0.3. In the case of PMMA bone cement shear stress, a maximum variation of 4% was shown due to a reduction of metal-PMMA friction from 0.42 to 0.3. A maximum variation of 7% of the maximum peak value for PMMA bone cement tensile stress was observed after an increase of metal-PMMA friction from 0.42 to 0.5. In the case of PMMA bone cement shear stress, a maximum variation of 4% was shown due to an increase of metal-PMMA friction from 0.42 to 0.5. The points to calculate the variations on PMMA bone cement peak stresses were taken from the maximum PMMA bone cement stress values during the walking gait cycle.

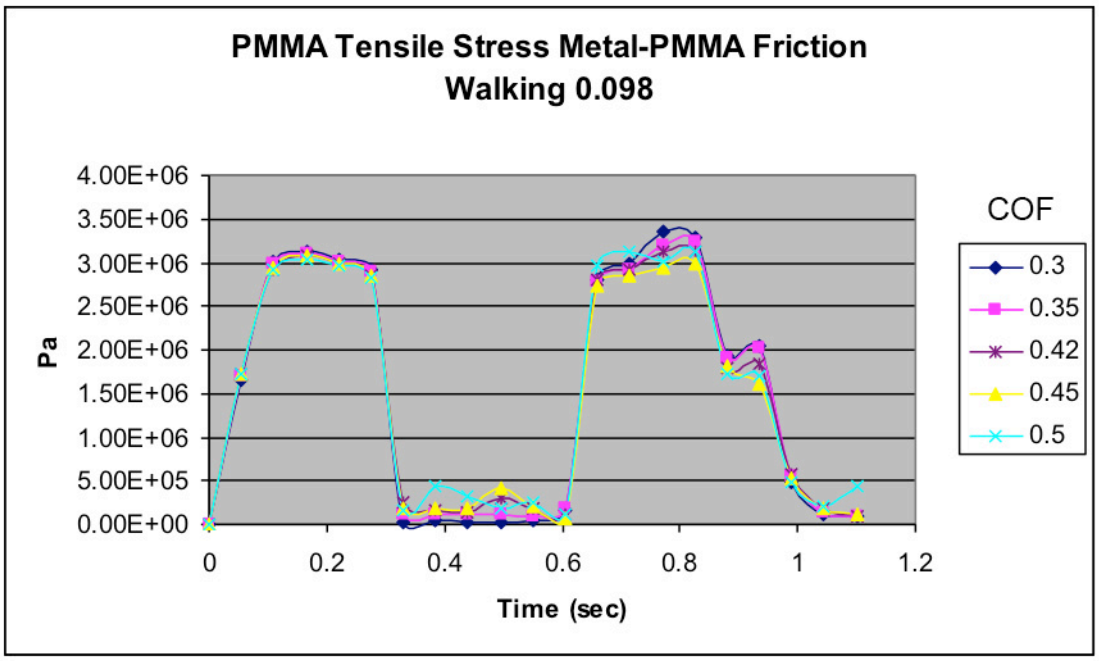

Figure 4.8.a. Maximum tensile stresses during walking gait for different metal-PMMA coefficient of friction.

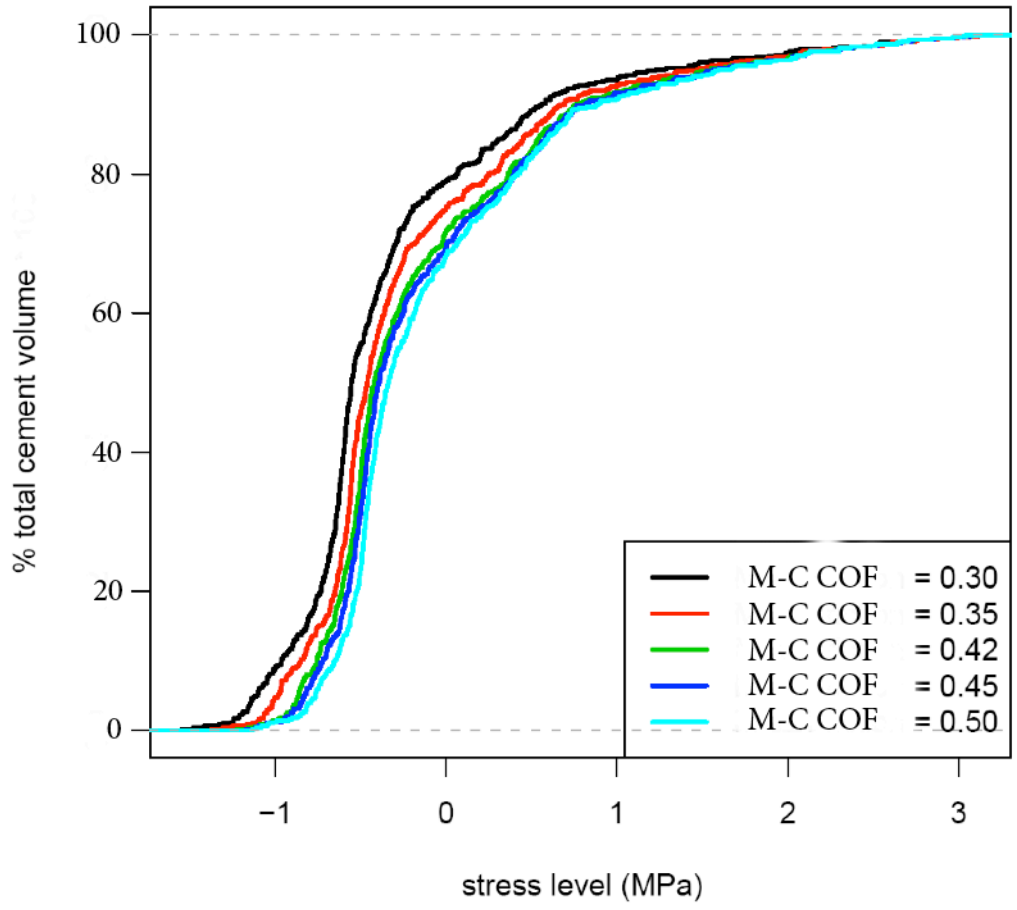

Figure 4.8.b. Tensile stress distribution 0.165 seconds after heel strike during walking gait for different metal-PMMA coefficient of friction.

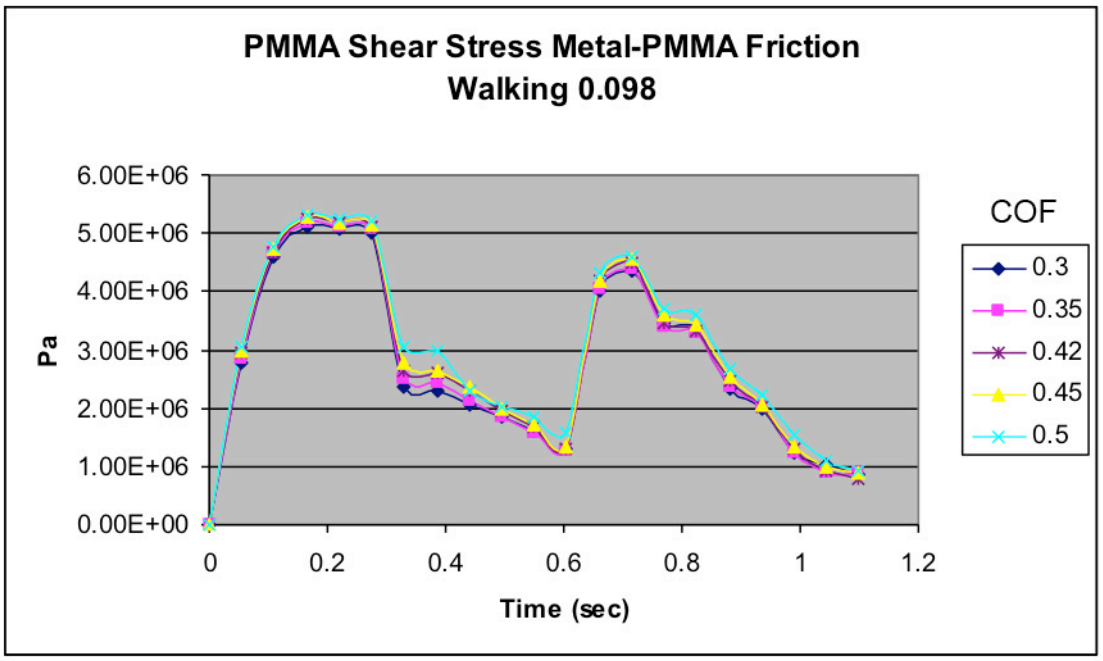

Figure 4.8.c. Maximum shear stresses during walking gait for different metal-PMMA coefficient of friction.

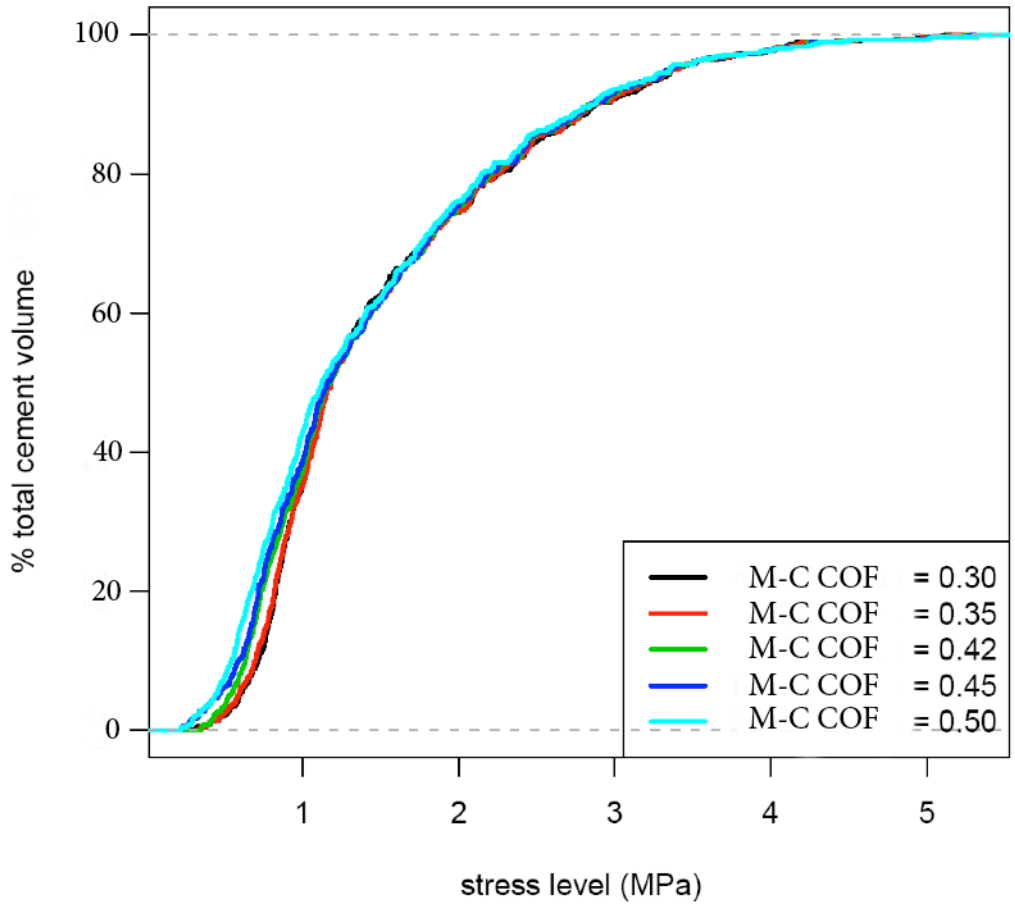

Figure 4.8.d. Shear stress distribution 0.165 seconds after heel strike during walking gait for different metal-PMMA coefficient of friction.

Furthermore, the stress distribution for tensile and shear stresses in the PMMA bone cement is shown in Figure 4.8.b and Figure 4.8.d for 0.165 seconds after heel strike during walking gait. Greater variation was found in the tensile distribution compared to the shear stress distribution. Nevertheless, the variations could be considered small for the purpose of this research.

4.6.3 Sensitivity to metal-bone friction

According to Section 4.4.1, the coefficient of friction for contact interface between the metal femoral peg and the cancellous bone was taken as 0.15. Nevertheless, it was considered beneficial to understand the sensitivity of the Finite Element Analysis model to a variation of this coefficient of friction and more importantly its effect on the PMMA bone cement stresses.

Five finite element analyses were solved using *LS-Dyna* with metal-bone coefficient of frictions equal to 0.1, 0.15, 0.2, 0.3 and 0.4.

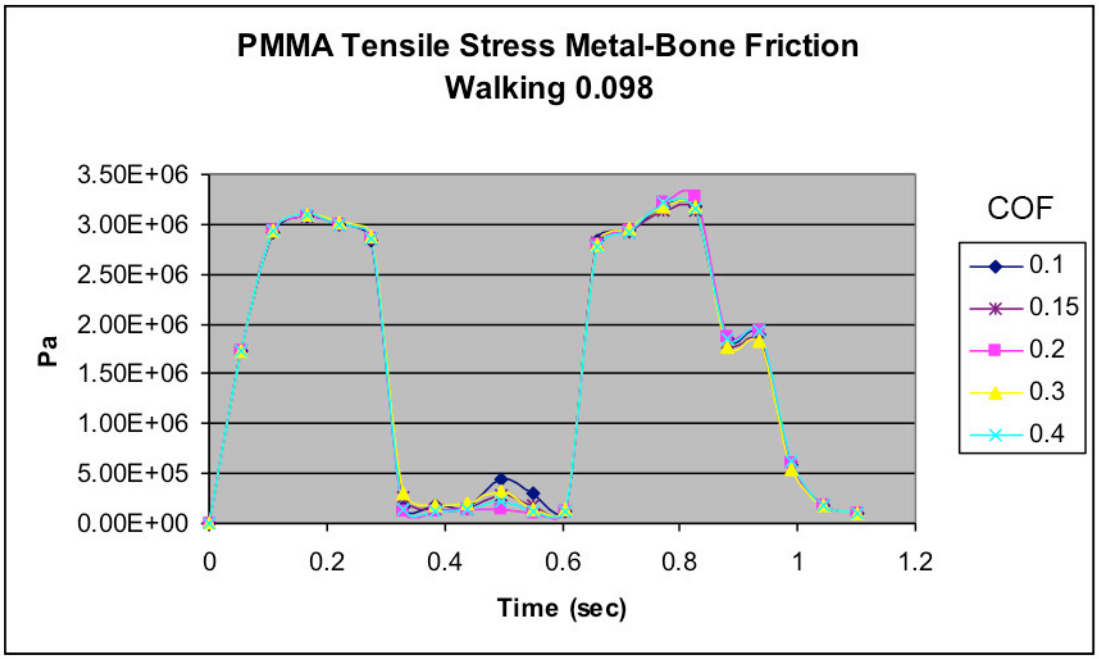

Figure 4.9.a. Maximum tensile stresses during walking gait for different metal-bone coefficient of friction.

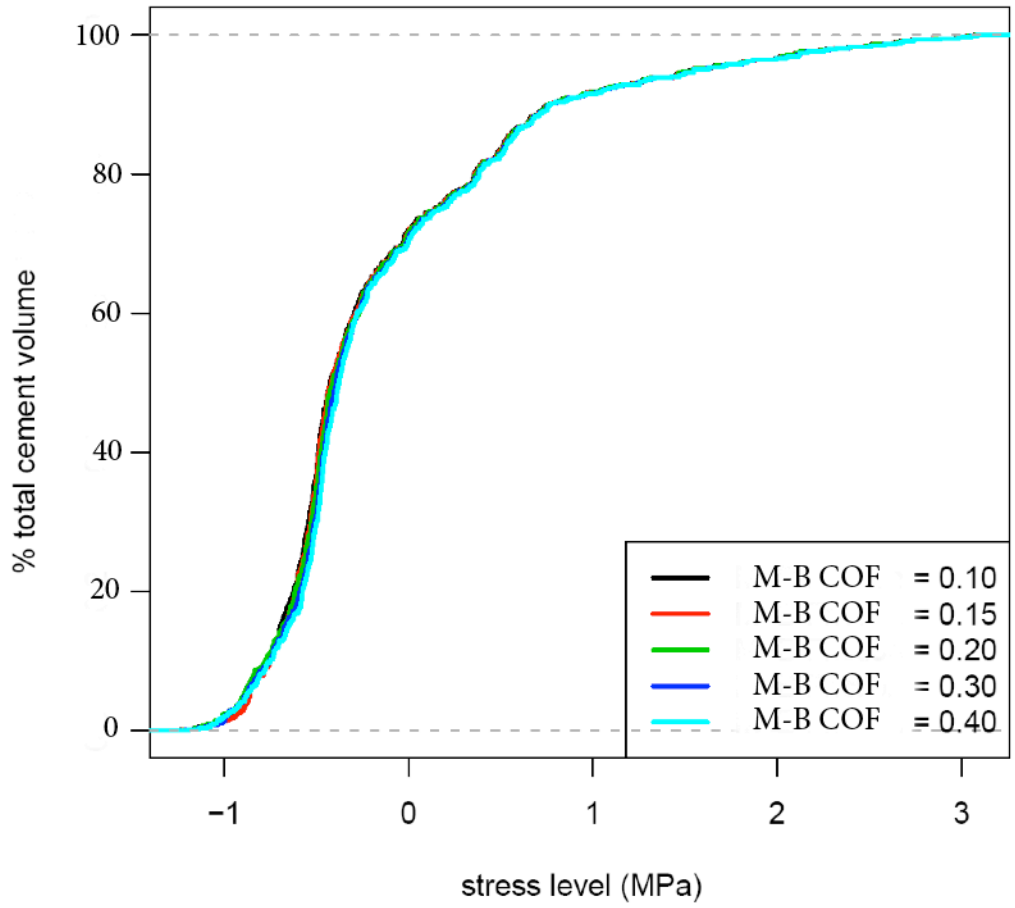

Figure 4.9.b. Shear stress distribution 0.165 seconds after heel strike during walking gait for different metal-bone coefficient of friction.

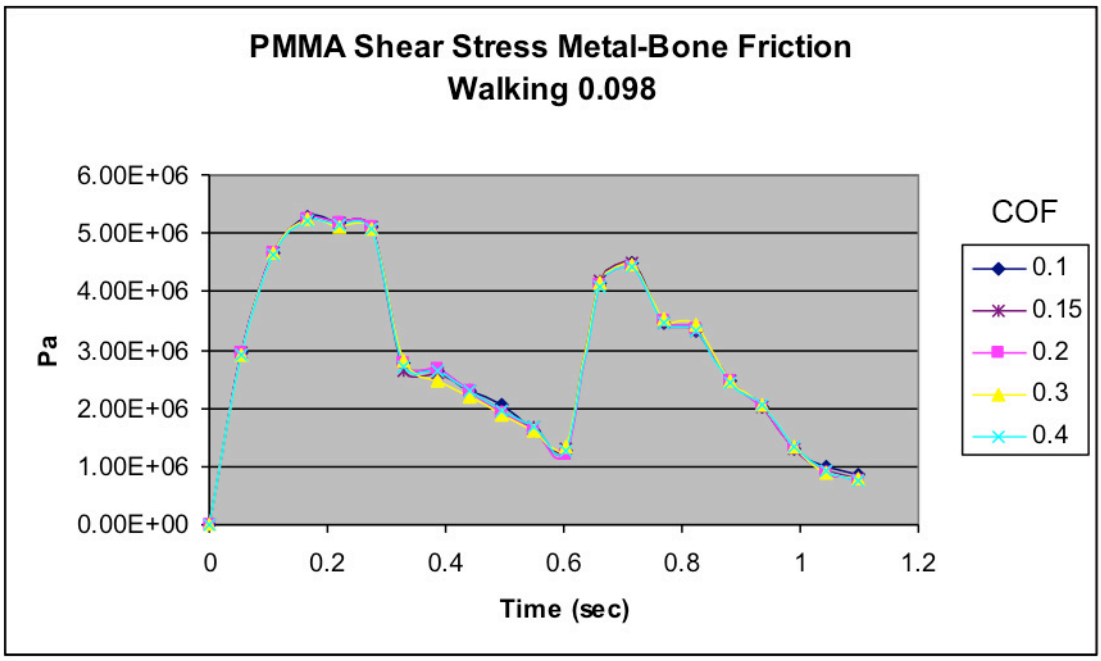

Figure 4.9.c. Maximum shear stresses during walking gait for different metal-bone coefficient of friction.

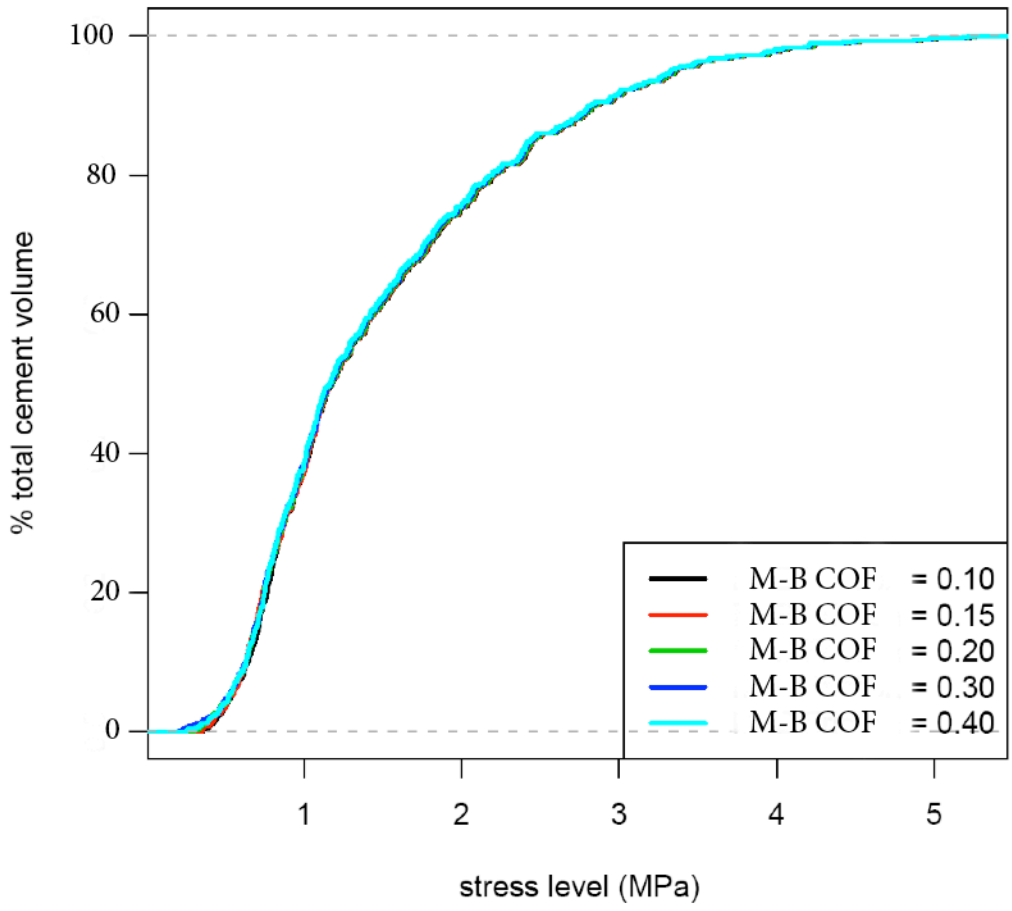

Figure 4.9.d. Shear stress distribution 0.165 seconds after heel strike during walking gait for different metal-bone coefficient of friction.

Figure 4.9.a and Figure 4.9.c show the result of peak PMMA bone cement tensile and shear stress values for different metal-bone coefficient of friction during walking with a metal-on-metal friction of 0.098. A maximum variation of 2% of the maximum peak value for PMMA bone cement tensile stress was observed after a reduction of metal-bone friction from 0.15 to 0.1. In the case of PMMA bone cement shear stress, a maximum variation of less than 1% was shown due to a reduction of metal-bone friction from 0.15 to 0.1. A maximum variation of 3% of the maximum peak value for PMMA bone cement tensile stress was observed after an increase of metal-bone friction from 0.15 to 0.4. In the case of PMMA bone cement shear stress, a maximum variation of less than 1% was shown due to an increase of metal-bone friction from 0.15 to 0.4. The points to calculate the variations on PMMA bone cement peak stresses were taken from the maximum PMMA bone cement stress values during the walking gait cycle.

Furthermore, the stress distribution for tensile and shear stresses in the PMMA bone cement is shown in Figure 4.9.b and Figure 4.9.d for 0.165 seconds after heel strike

during walking gait. Very little variation can be seen in the stress distribution for tensile and shear stress. Finally, it could be said that a variation in PMMA-bone friction is assumed to have no significant consequence to this research.

4.7 Corroboration of Finite Element Analysis Model

As the Finite Element Analysis model is a mathematical model representing reality with assumptions and limitations as presented in this chapter, the model had to be corroborated to find out if the model was representing the behaviour of hip resurfacing in real events and the output data be used to draw conclusions related to these real events.

The first point of corroboration for the Finite Element Analysis model used for this study was related to the output PMMA bone cement stresses. The boundary condition input, hip contact forces and flexion-extension rotation, can be compared to the post-processing result from *LS-Dyna*, PMMA bone cement tensile and shear stresses. The comparison of input (boundary conditions) and output (PMMA stresses) is shown in Figure 4.10, simulating normal walking gait.

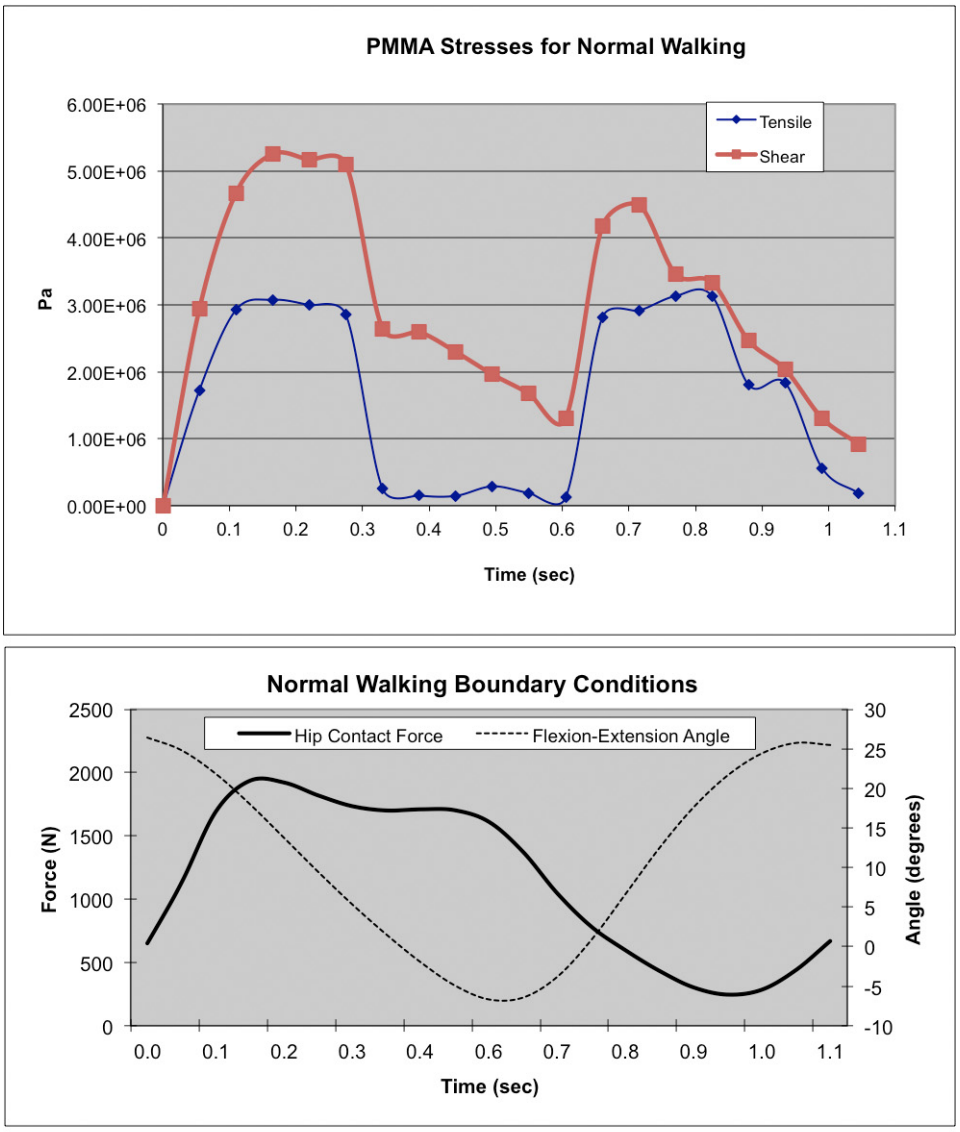

Figure 4.10. PMMA bone cement tensile and shear stress (top) and hip contact force and flexion-extension rotation for normal walking gait.

Comparing the PMMA stresses results in Figure 4.10 with the boundary conditions for normal walking, the first part of the walking gait (from heel strike to around 0.4 seconds into the gait) was driven by the high contact forces and rotation. It can be said that between 0.4 and 0.7 seconds into the gait, the response of the PMMA stresses were taken into account the very small rotation during this period. Finally, the last part of the walking gait (swing phase) was corresponding with an increase in PMMA stresses driven by the high-speed rotation in a short time scale and the hip contact forces due to muscle and tendons during this phase. The PMMA stresses results obtained from Finite Element Analysis can be explained by the boundary conditions applied to the Finite Element Analysis.

4.7.1 Contact mechanics

Contact stress can be modelled using the theory of contact mechanics or Hertzian mechanics if the contact is small, which it will happen for low stresses (Johnson, 1985). According to Johnson, low stress can be described as stress that results in a contact arc of less than 52 degrees in total, which means an angle of α of less than 26 degrees.

The key symbols and equations (taken from Johnson, 1985) that have been used for this corroboration are as follow:

P = Force applied

R = Relative radius of curvature

$$R = \frac{R_1 \cdot R_2}{R_2 - R_1}$$

R_1 = Radius of hole

R_2 = Radius of pin

a = Contact radius

α = Half the angle subtended by the contact radius.

Po = Maximum pressure

ν = Poisson's ratio

E* = Effective Young's modulus

$$\frac{1}{E^*} = \frac{1-\nu_1^2}{E_1} + \frac{1-\nu_2^2}{E_2}$$

The maximum pressure can be calculated as:

$$P_o = \sqrt[3]{\frac{6 \cdot P \cdot E^2}{\Pi^3 \cdot R^2}}$$

Contact radius (a) is equal to:

$$a = \frac{\Pi \cdot R \cdot P_o}{2 \cdot E}$$

α can be calculated as follows to satisfy having an angle smaller than 26 degrees:

$$\alpha = a\sin\left(\frac{a}{R_1}\right)$$

For a more detail description of the Hertzian mechanics, the reader can refer to the work of Walker (2007).

The contact pressures calculated from the Hertzian mechanics were compared to the contact pressure taken from the Finite Element Analysis simulating normal walking

gait. The comparison is shown in Figure 4.11, where it can be seen the agreement between both methods.

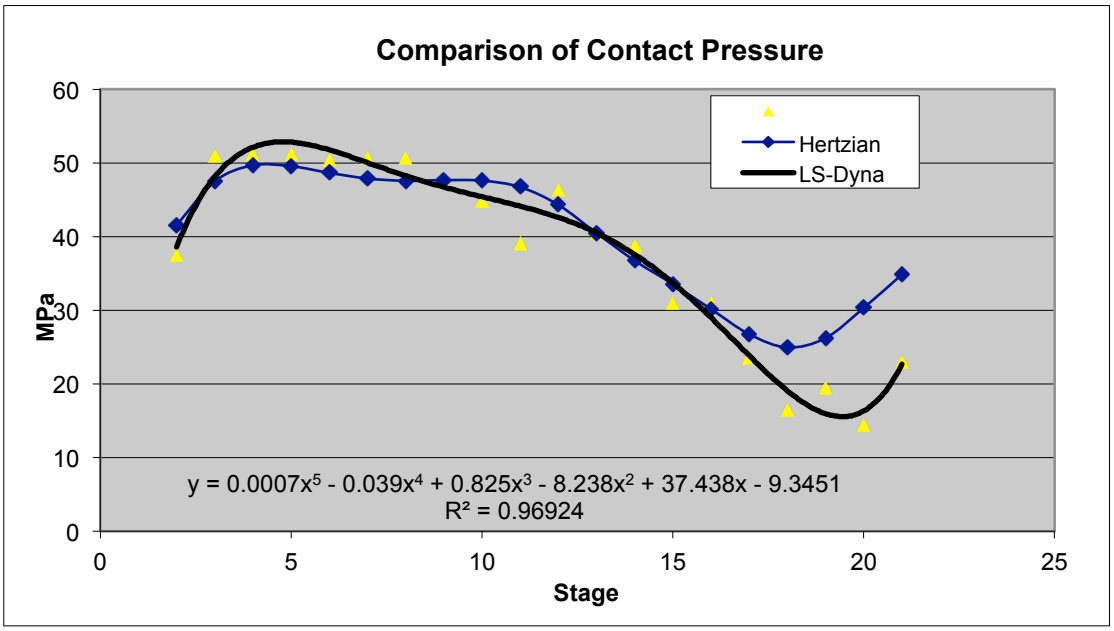

Figure 4.11. Comparison of contact pressure between Finite Element Analysis model and Hertzian mechanics.

The main simplifications in using Hertzian mechanics are the assumptions of large radiuses for the component and thick material, while we are calculating the contact pressure for small diameters in a hip resurfacing system with thin metal components. The small discrepancy between the Hertzian mechanics and the Finite Element Simulation can be explained due to the Hertzian mechanics being a static calculation of the contact pressure, while the Finite Element Analysis is a dynamic simulation and the inertia of the dynamic simulation model at the final stage can we accountable for the small difference.

4.7.2 Corroboration of simulation by comparison with clinical data and published work

The result for PMMA bone cement stresses, which are shown on this study, agrees with the finite element analyses done by other researchers and furthermore with clinical data reported in the literature.

Figure 4.12 shows, on the left hand side, a failure hip resurfacing patient due to femoral neck fracture (Falez, 2007). Note that potential bone damage is hidden under

the femoral implant. On the right hand side of Figure 4.12, it is presenting a picture showing the Von Mises PMMA bone cement stress taken from a Finite Element Analysis simulating the normal walking at 0.165 seconds after heel strike during walking gait. The location of the high stresses in the PMMA bone cement from the Finite Element Analysis is in concordance with the reported fracture. More importantly, it has been reported that the outer wall of the cement mantle is the most important fixation area for resisting torque (Ma, 1983 and Bitsch, 2007).

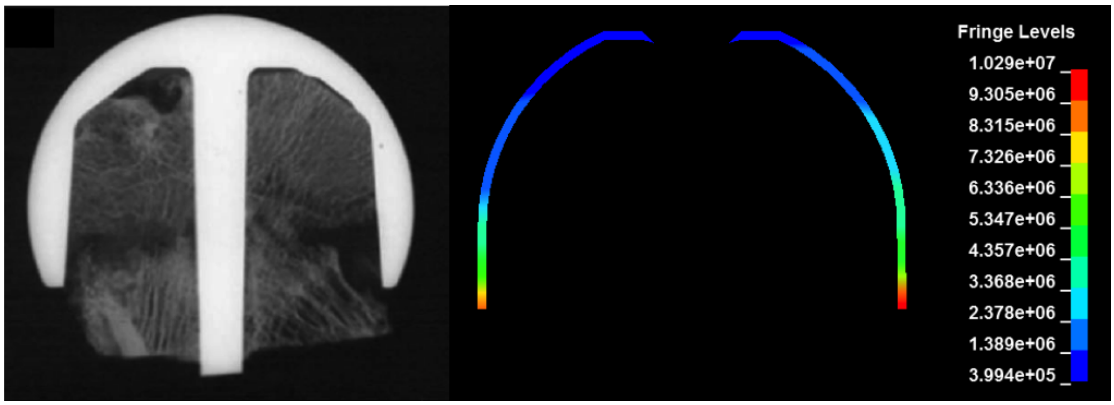

Figure 4.12. Retrieved specimen after femoral neck failure (left) (Falez, 2007) and Von Mises PMMA bone cement stress (Pa) during normal walking at 0.165 seconds after heel strike during walking gait.

Watanabe (2000) reported the transfer of loading to the bone through the prosthesis rim. This phenomenon has been presented by other authors using patient specific Finite Element Analyses (Taylor, 2006 and Radcliffe and Taylor, 2007). The same transfer of load can be appreciated in Figure 4.13, which is showing the Von Mises stresses for cancellous bone during normal walking at 0.165 seconds after heel strike during walking gait. It can be seen from Figure 4.13, that stress shield is happening at the superior part of the femoral head under the cement mantle. Stress and Strain shielding has been reported after finite element analyses (Watanabe, 2000, Taylor, 2006 and Radcliffe and Taylor, 2007).

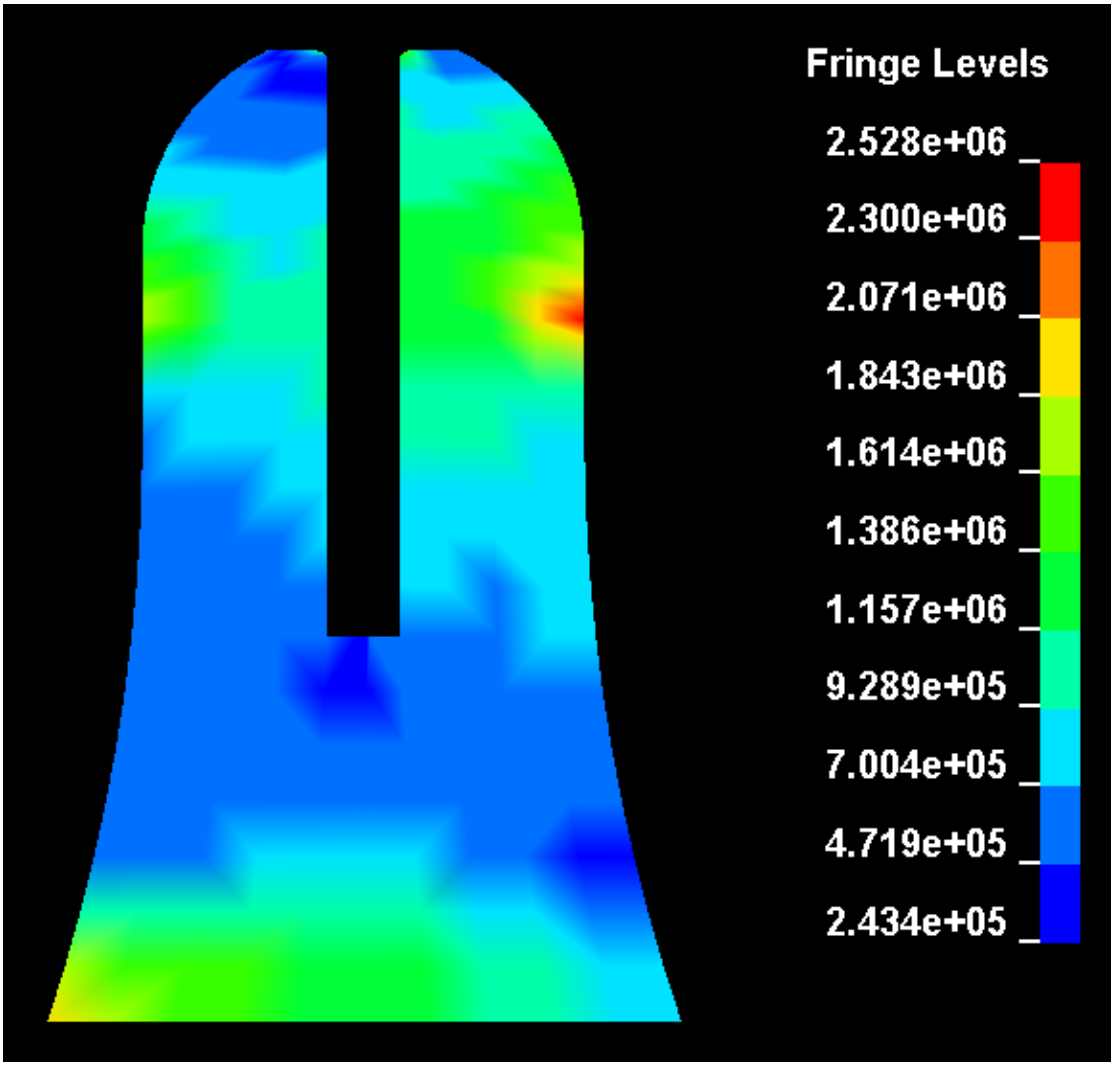

Figure 4.13. Von Mises cancellous bone stress (Pa) during normal walking at 0.165 seconds after heel strike during walking gait.

4.8 Conclusion

The Finite Element Analysis model described in this chapter, which has been corroborated in Section 4.7, is proposed to be used in this study in reference to the post-processing of PMMA bone cement for daily activities.

The next chapter uses the Finite Element model developed in this chapter to explore the role of resting periods, metal-on-metal friction, patient bone quality and PMMA bone cement Young's modulus in the short, medium and long term failure of hip resurfacing arthroplasty according to the drivers presented in Section 3.5.

Chapter 5

Applying the Model to Explore the Role of Resting Periods

This chapter explores and aims to determine the four drivers established in Section 3.5:

- Could high metal-on-metal friction coefficient due to resting periods cause aseptic loosening of femoral hip resurfacing components during daily activities by PMMA bone cement fatigue?

- Could low bone quality affect the stability of the femoral hip resurfacing components due to PMMA stresses?

- Could PMMA Young's modulus affect the stability of the femoral hip resurfacing components due to PMMA stresses?

- Could the torque produce failure on the PMMA-metal interface and loosening of femoral hip resurfacing components?

5.1 Effect of Metal-on-Metal Friction Coefficient Due to Resting Periods During Daily Activities on PMMA Bone Cement Fatigue

This chapter analyses the effect of resting periods in everyday activities on the fatigue performance of PMMA due to the increase in metal-on-metal friction coefficient between the femoral and acetabular component in hip resurfacing.

The duration and frequency of everyday activities are shown in Table 5.1 and are taken from the work of Morlock et al. (2001) as presented in HIP98-workpackage 5. The number of cycles were normalized to 12 hours per day. Cycles per month for normal load are the median multiplied by 30.5 days in a month.

The selected everyday activities were walking, descending stairs and standing up from a chair.

Table 5.1. Frequency of everyday activities (Morlock et al., 2001).

	Cycles per Day	Cycles per Month
Activity	**Median**	**Normal load**
Walking	7,583.70	240,000
Descending Stairs	108.9	3,400
Standing Up	27.3	840

The relation between number of cycles for walking and descending stairs in Table 5.1 was used as an activity weighting factor to assign the frequency of resting periods as shown in Table 5.2.

According to Table 5.2, for a resting duration between 2 to 5 seconds, the frequency of resting periods equal 99.4 per hour. This short resting period is assumed to happen during walking and before descending stairs, such as, for example, when we are walking in the street and stopped by somebody to ask the time or, perhaps, when we are asked a question by a colleague before starting descending stairs.
According to the Table 5.1, the proportion of everyday activities is 240.000 walking cycles per month versus 3.400 cycles descending stairs. This would mean a ratio of 1.4 descending stairs cycles for every 100 walking cycles per month, as calculated below.

$$Walking\ 240{,}000 \implies 100$$
$$Decending\ Stairs\ 3{,}400 \implies X\ ;\ X = 1.41$$

Following this 1.4 ratio of descending cycles to walking cycles, out of the 99.4 total resting periods per hour available, 1.4 resting periods per hour are assigned to descending stairs and (99.4 – 1.4) = 98 to walking. This is shown in Table 5.2 in the 'weighted frequency' column as 98 / 1.4.

The same process is applied for a resting duration between 5 to 10 seconds to calculate the amount of resting periods per hour for walking and descending stairs activities.

Resting durations lasting between 10 and 30 second are assumed to happen only in walking activities. While resting durations higher than 30 seconds are only considered to happen in standing up activities after periods of sitting.

The resting durations and frequencies were taken from the work of Nassutt et al. (2003) and matched to the everyday activities by the weighting factor explained above.

Table 5.2. Duration and frequency of resting periods.

Resting Duration (Seconds)	Frequency of Resting Periods (Nassutt et al., 2003) (Number per Hour)	Everyday Activity	Weighted Frequency
2 to 5	99.4 ± 43.1	Walking / Descending Stairs	98 / 1.4
5 to 10	35.6 ± 14.2	Walking / Descending Stairs	35.1 / 0.5
10 to 30	25.6 ± 13.7	Walking	25.6
30 to 60	6.4 ± 3.6	Standing Up	
60 to 180	3.6 ± 2.4	Standing Up	10
All durations	170.6 ± 36.4		

The metal-on-metal friction coefficients for the selected resting periods are shown in Table 5.3.

Table 5.3. Metal-on-metal friction for resting periods (Nassutt et al., 2003).

Resting Duration (Seconds)	Metal-on-metal friction coefficient
0	0.098
5	0.189
10	0.219
30	0.251
60	0.285

According to the resting duration, frequency of resting periods (Table 5.2) and metal-on-metal friction coefficients (Table 5.3), the following Finite Element Analysis were performed as shown in Table 5.4.

Table 5.4. Finite element models to solve according to MoM friction coefficient.

Everyday Activity	Resting Duration (Seconds)	Metal-on-metal friction coefficient
Walking	**0**	0.098
	5	0.189
	10	0.219
	30	0.251
Descending Stairs	**0**	0.098
	5	0.189
	10	0.219
Standing Up	**0**	0.098
	60	0.285

Using Table 5.4 the metal-on-metal friction coefficient can be estimated for different activities after a resting period and from Table 5.2 the frequency of the estimated resting periods can be assessed. This means that for example after a resting period of 5 seconds, there are 98 cycles per hour when walking has a metal-on-metal friction of 0.189 instead of assuming that every single cycle in walking has the friction of 0,098.

The frequencies of resting periods in Table 5.2 are converted to number of cycles per month and year when hip resurfacing patients will experience the increased metal-on-metal friction coefficients. To achieve this goal, the frequency of resting periods per hour are multiplied by 12 hours per day, by 30.5 days in a month and finally by 12 months in a year.

The number of cycles per month for the dynamic metal-on-metal friction (0.098) is calculated as total number of cycles per month as for Table 5.1 minus all the number of cycles per month when metal-on-metal friction is higher than the dynamic one. Table 5.5 shows the total cycles per year according to metal-on-metal friction and everyday activities.

Table 5.5. Cycles per year according to MoM friction coefficient and activity.

Everyday Activity	MoM friction coefficient	Frequency of Resting Periods (Table 5.2) (Number per Hour)	Cycles per month (x12 x30.5)	Cycles per year (x12)
Walking	0.098		181915.8	2182989.6
	0.189	98	35868	430416
	0.219	35.1	12846.6	154159.2
	0.251	25.6	9369.6	112435.2
Descending Stairs	0.098		2704.6	32455.2
	0.189	1.4	512.4	6148.8
	0.219	0.5	183	2196
Standing Up	0.285	10	3660	43920

Taking as an example from Table 5.5 the walking cycle, walking cycle with a metal-on-metal friction of 0.251 will occur for resting durations of 30 seconds. According to the weighted frequency presented in Table 5.2 for resting periods of 10 to 30 seconds, there is a frequency of 25.6 resting periods per hour. Subsequently, there will be 25.6 walking cycles per hour, in which the metal-on-metal friction will have a value of 0.251. To calculate how many walking cycles at the 0.251 metal-on-metal friction will be happening per month, the value of 25.6 walking cycles per hour is multiply by 12 hours of activities per day and 30.5 days in a month to achieve a total of 9369.6 walking cycles per month at 0.251 metal-on-metal friction.

The same procedure will be applied to calculate the walking cycles per month for metal-on-metal frictions of 0.219 and 0.189. To calculate the amount of walking cycles at dynamic metal-on-metal friction (0.098), the total number of walking cycles per month of 240.000 cycles (Table 5.1) is used and the number of cycles per month for metal-on-metal frictions of 0.251,0.219 and 0.189 is subtracted to achieve a total number of walking cycles per month at dynamic metal-on-metal friction (0.098) of 181915.8 cycles.

Furthermore, following advice from Professor Morlock (2005), it was suggested that the high metal-on-metal friction will take only 2 to 3 cycles to return to the dynamic

metal-on-metal friction value of 0.098, so this would have a knocking on effect of a bigger number of cycles at higher metal-on-metal friction that assumed in Table 5.5.

Taking as an example from Table 5.5 the walking cycle, this means that 9369.6 walking cycles per month with a metal-on-metal friction of 0.251 will have 9369.6 walking cycles at 0.219 friction and 9369.6 walking cycles at 0.189 friction. In similar way, 12846.6 walking cycles per month with a metal-on-metal friction of 0.219 will have 12846.6 walking cycles at 0.189 friction as well. The total number of walking cycles per month at dynamic metal-on-metal friction (0.098) is calculated in the same way as described to Table 5.5.

Table 5.6 shows the total cycles per year according to metal-on-metal friction and everyday activities with the adjustment regarding the recovery from high metal-on-metal friction to dynamic friction.

Table 5.6. Adjusted cycles per year according to MoM friction coefficient and activity.

Everyday Activity	MoM friction coefficient	Frequency of Resting Periods (Number per Hour)	Cycles per month (x12 x30.5)	Cycles per year (x12)
Walking	0.098		150330	1803960
	0.189	98	58084.2	697010.4
	0.219	35.1	22216.2	266594.4
	0.251	25.6	9369.6	112435.2
Descending Stairs	0.098		2521.6	30259.2
	0.189	1.4	695.4	8344.8
	0.219	0.5	183	2196
Standing Up	0.285	10	3660	43920

5.1.1 Finite Element Analysis results for walking

The Finite Element model developed in Chapter 4 was used to assess the effect of resting periods during walking.

Hip forces and flexion-extension rotation were applied to the model to simulate walking; total hip force and flexion-extension rotation are shown in Figure 5.1.

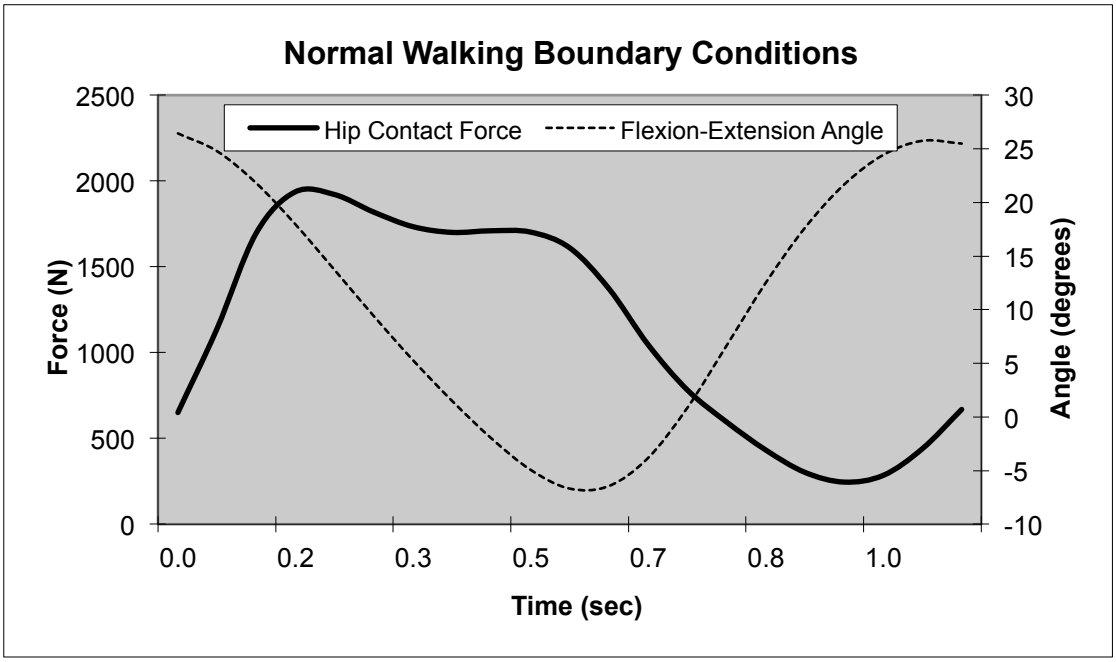

Figure 5.1. Hip contact force and flexion-extension rotation for normal walking gait.

Four Finite Element models were solved according to the metal-on-metal friction coefficient due to resting periods for walking as shown in Table 5.7.

Table 5.7. MoM friction due to resting periods for walking.

Everyday Activity	Resting Duration (Seconds)	Metal-on-metal friction coefficient
Walking	**0**	0.098
	5	0.189
	10	0.219
	30	0.251

Tensile and shear stresses in the PMMA cement mantle were plotted in *LS-Dyna* and the raw data extracted for further analysis.

The maximum tensile and shear stresses for PMMA bone cement according to varying metal-on-metal friction coefficient due to resting periods are shown in Table 5.8. Furthermore, Table 5.8 shows the equations to predict tensile and shear stresses according to metal-on-metal friction coefficient.

Table 5.8. PMMA maximum tensile and shear stresses for different MoM friction coefficients during walking.

Everyday Activity	Metal-on-metal COF	Tensile Stress (MPa)	Shear Stress (MPa)	Stress Equations
Walking	**0.098**	3.13	5.25	Tensile Stress = 44.46 * μ - 1.338
	0.189	6.81	8.34	
	0.219	8.37	9.72	Shear Stress = 38.35 * μ + 1.368
	0.251	10	11.2	

Maximum tensile stresses in the PMMA bone cement occur for the four FEA models at the prosthesis rim area as shown in Figure 5.2.

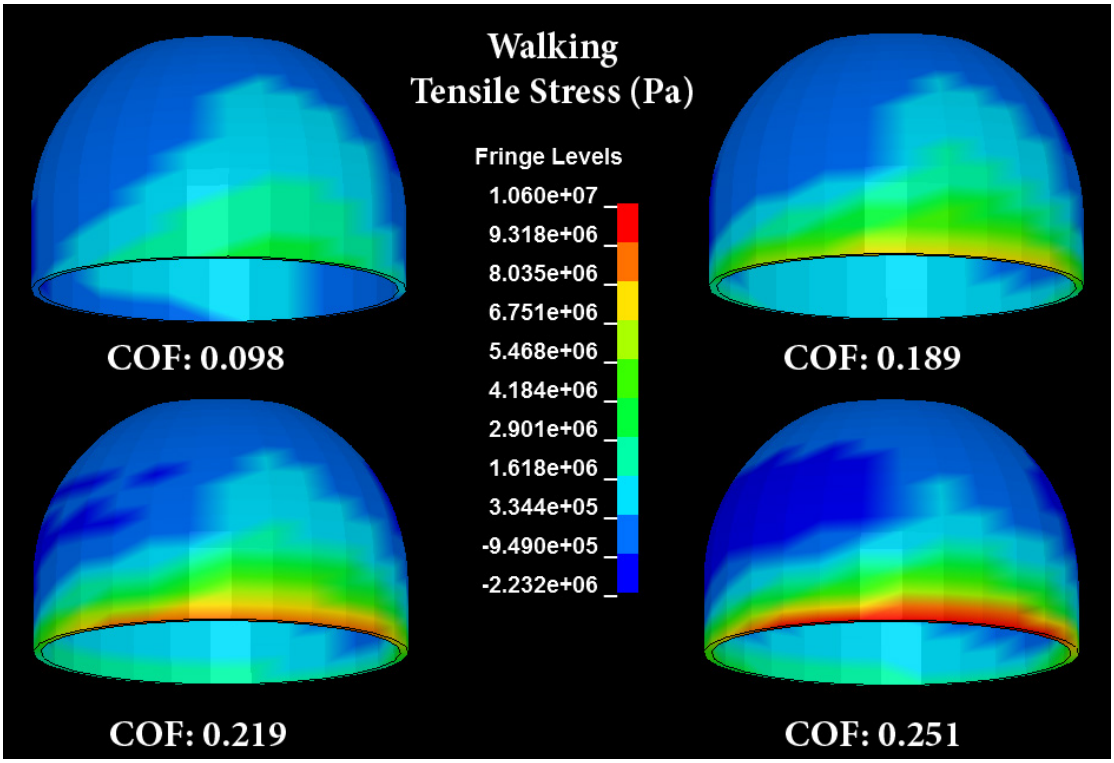

Figure 5.2. PMMA bone cement tensile stresses (Pa) 0.165 seconds into the walking gait for four different metal-on-metal friction coefficients.

Figure 5.3 shows maximum shear stresses happening in the prosthesis rim area. As metal-on metal (MoM) friction coefficient increases from 0.098 to 0.251, the peak tensile stress for the PMMA cement mantle increases from 3.13 MPa to 10 MPa, representing an increase of 319.49 %. In a similar way, the peak shear stress

increases from 5.25 MPa to 11.2 MPa as MoM friction increases from 0.098 to 0.251, representing an increase of 213.33 %.

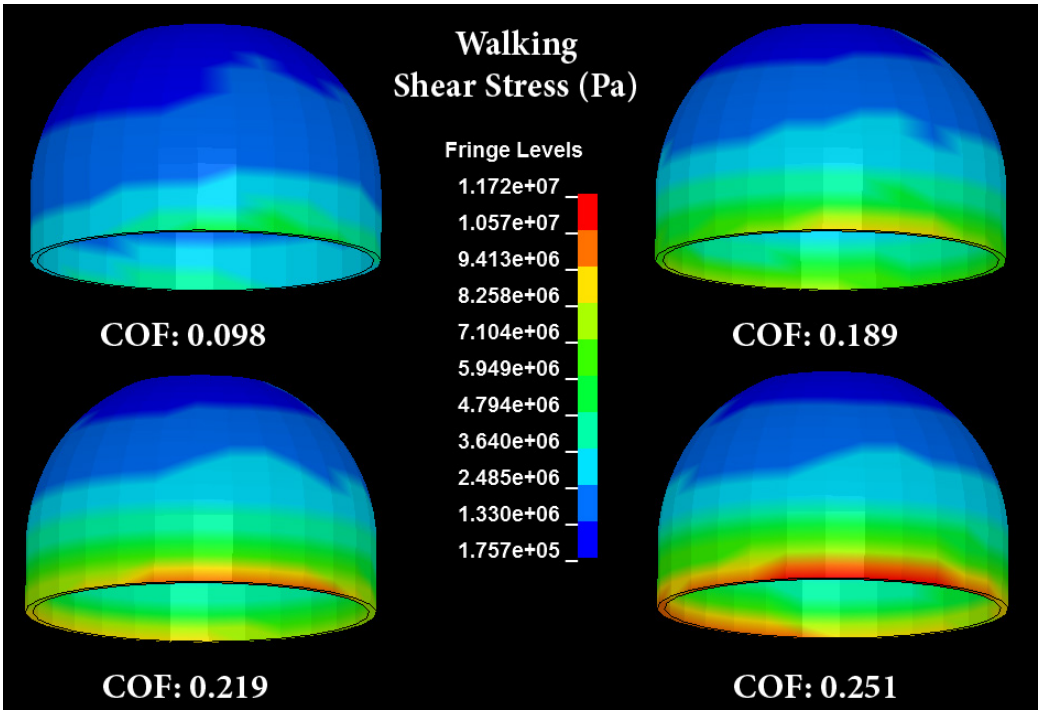

Figure 5.3. PMMA bone cement shear stresses (Pa) 0.165 seconds into the walking gait for four different metal-on-metal friction coefficients.

The range of maximum tensile and shear stresses along the walking cycle are shown in Figure 5.4.a and Figure 5.4.c for different metal-on-metal friction coefficients.

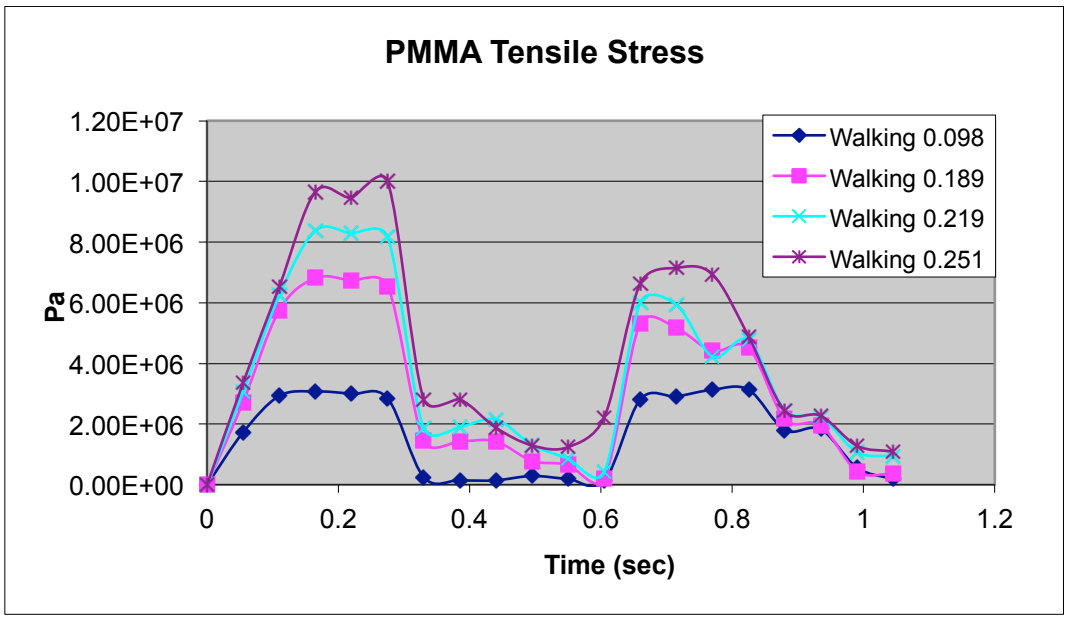

Figure 5.4.a. Maximum tensile stresses during walking gait for different MoM friction coefficient.

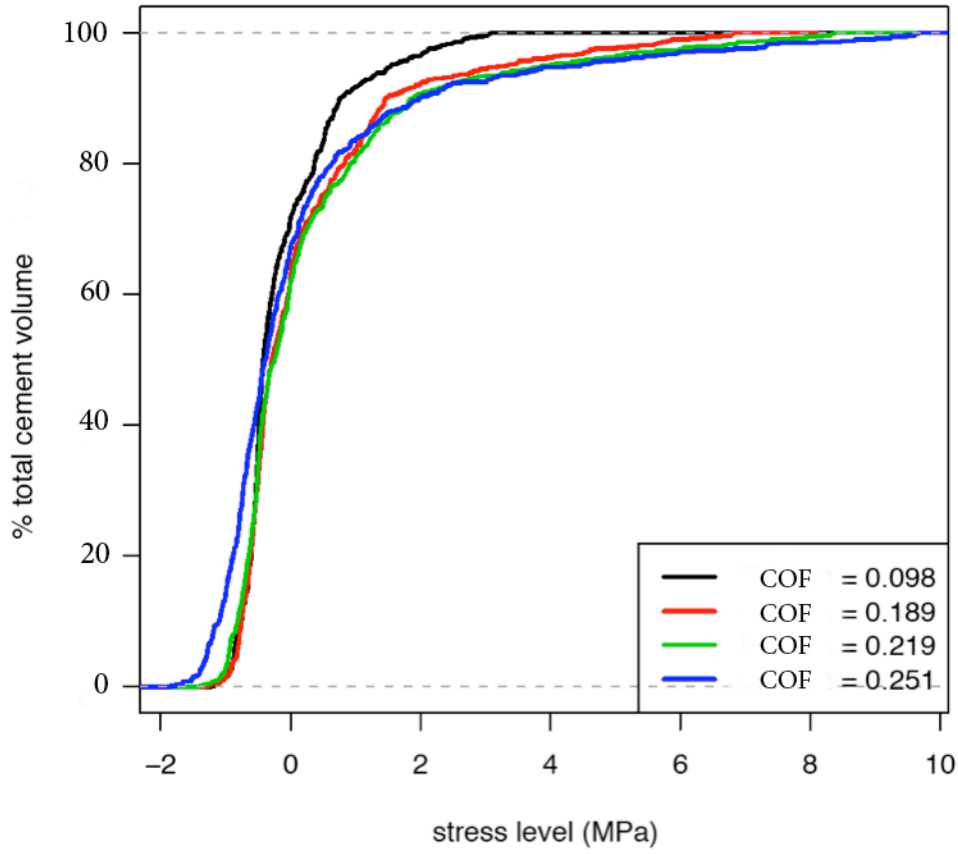

Figure 5.4.b. Tensile stress distribution 0.165 seconds after heel strike during walking gait for different MoM friction coefficient.

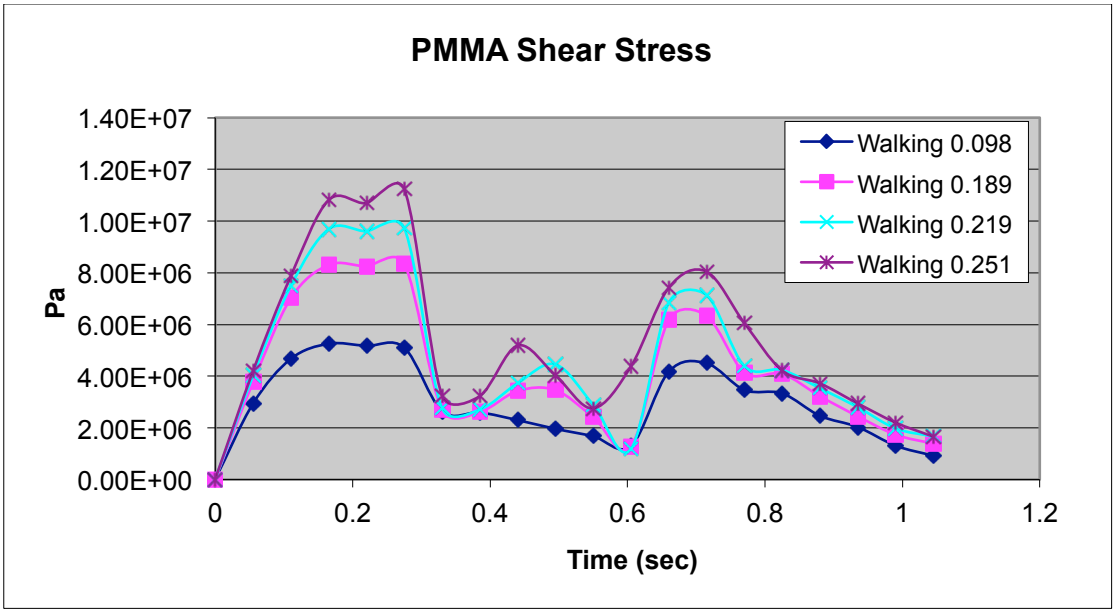

Figure 5.4.c. Maximum shear stresses during walking gait for different MoM friction coefficient.

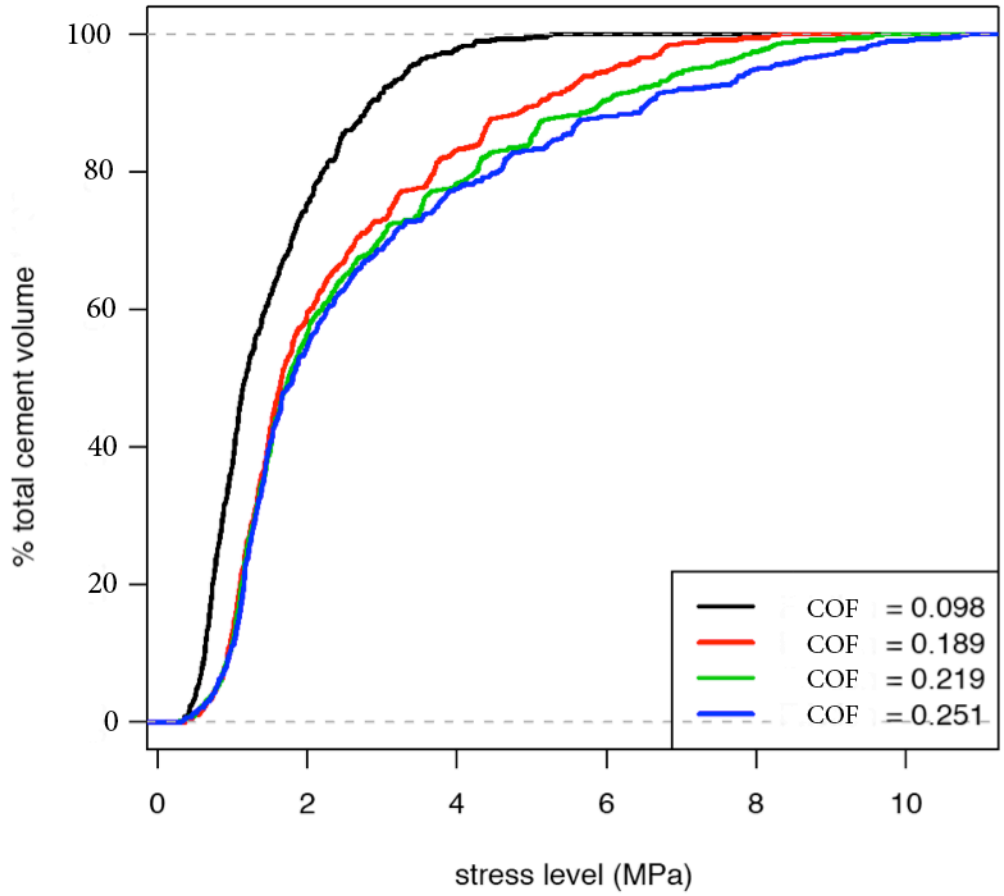

Figure 5.4.d. Shear stress distribution 0.165 seconds after heel strike during walking gait for different MoM friction coefficient.

Furthermore, from the tensile and shear stress distribution graphs in Figures 5.4.b and 5.4.d, it can be observed that around 10% of the total volume of PMMA bone cement is subjected to a tensile stress above the maximum peak tensile stress for the dynamic friction case, which is 3.13 MPa for 0.098 MoM friction. In the case of shear stress distribution, around 17% of the total volume of PMMA bone cement is subjected to a shear stresses above the maximum peak shear stress for the dynamic friction case, which is 5.25 MPa for 0.098 MoM friction.

5.1.2 Finite Element Analysis results for descending stairs

Hip forces and flexion-extension rotation were applied to the Finite Element model to simulate descending stairs; total hip force and flexion-extension rotation are shown in Figure 5.5.

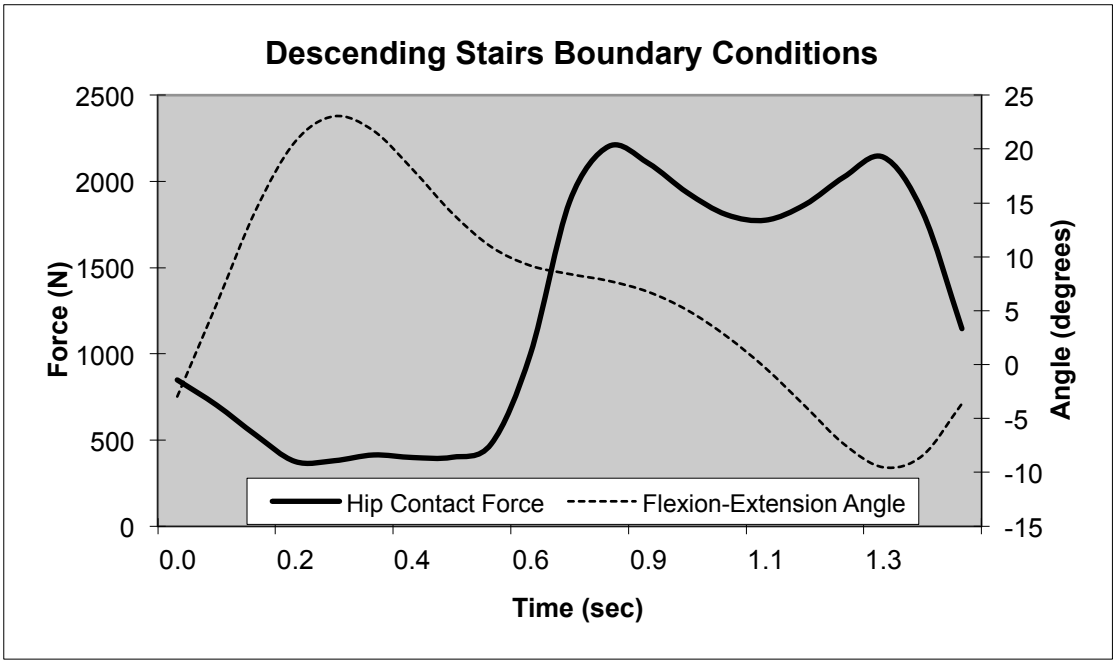

Figure 5.5. Hip contact force and flexion-extension rotation for descending stairs gait.

Three Finite Element models were solved according to the metal-on-metal friction coefficient due to resting periods for descending stairs as shown in Table 5.9.

Table 5.9. MoM friction due to resting periods for descending stairs.

Everyday Activity	Resting Duration (Seconds)	Metal-on-metal friction coefficient
Descending Stairs	**0**	0.098
	5	0.189
	10	0.219

The maximum tensile and shear stresses for PMMA bone cement according to varying metal-on-metal friction coefficient due to resting periods are shown in Table 5.10. Furthermore, Table 5.10 shows the equations to predict tensile and shear stresses according to metal-on-metal friction coefficient.

Table 5.10. PMMA maximum tensile and shear stresses for different MoM friction coefficients during descending stairs.

Everyday Activity	Metal-on-metal COF	Tensile Stress (MPa)	Shear Stress (MPa)	Stress Equations
Descending Stairs	0.098	2.86	4.67	Tensile Stress = 37.23 * μ - 0.81
	0.189	6.16	7.46	Shear Stress = 31.36 * μ + 1.58
	0.219	7.4	8.49	

Maximum tensile stresses in the PMMA bone cement happens for the three FEA models at the prosthesis rim area as shown in Figure 5.6.

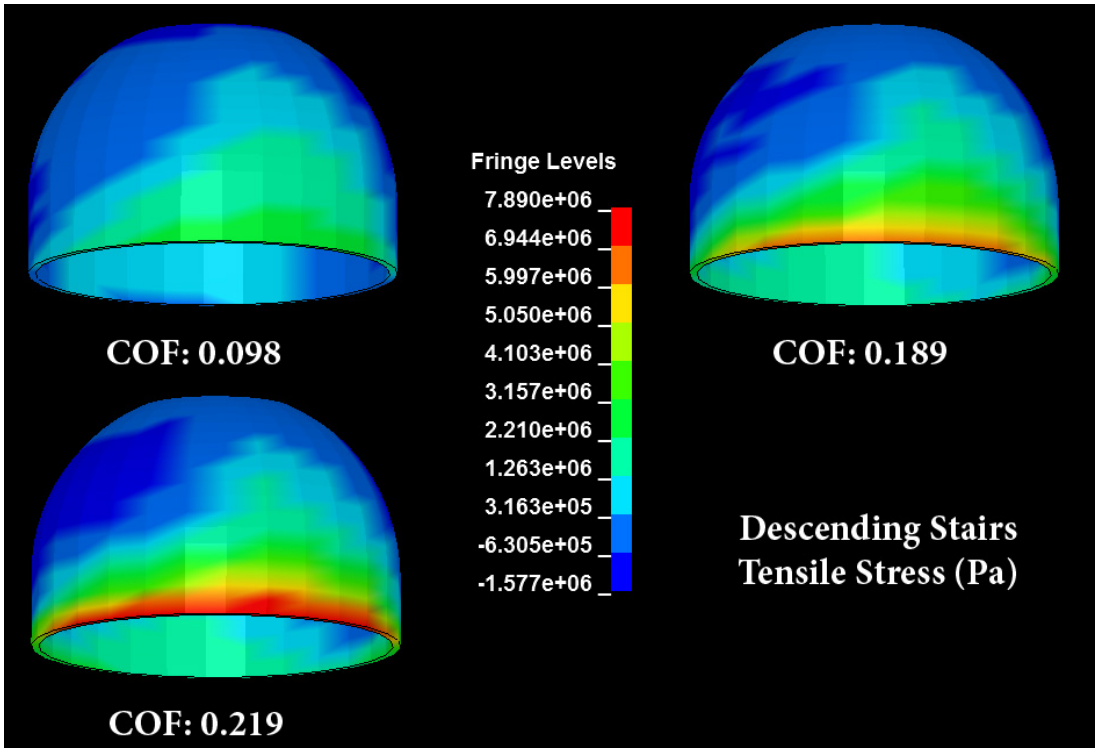

Figure 5.6. PMMA bone cement tensile stresses (Pa) 1.152 seconds into the descending stairs gait for three different metal-on-metal friction coefficients.

Figure 5.7 shows maximum shear stresses occurring in the prosthesis rim area.

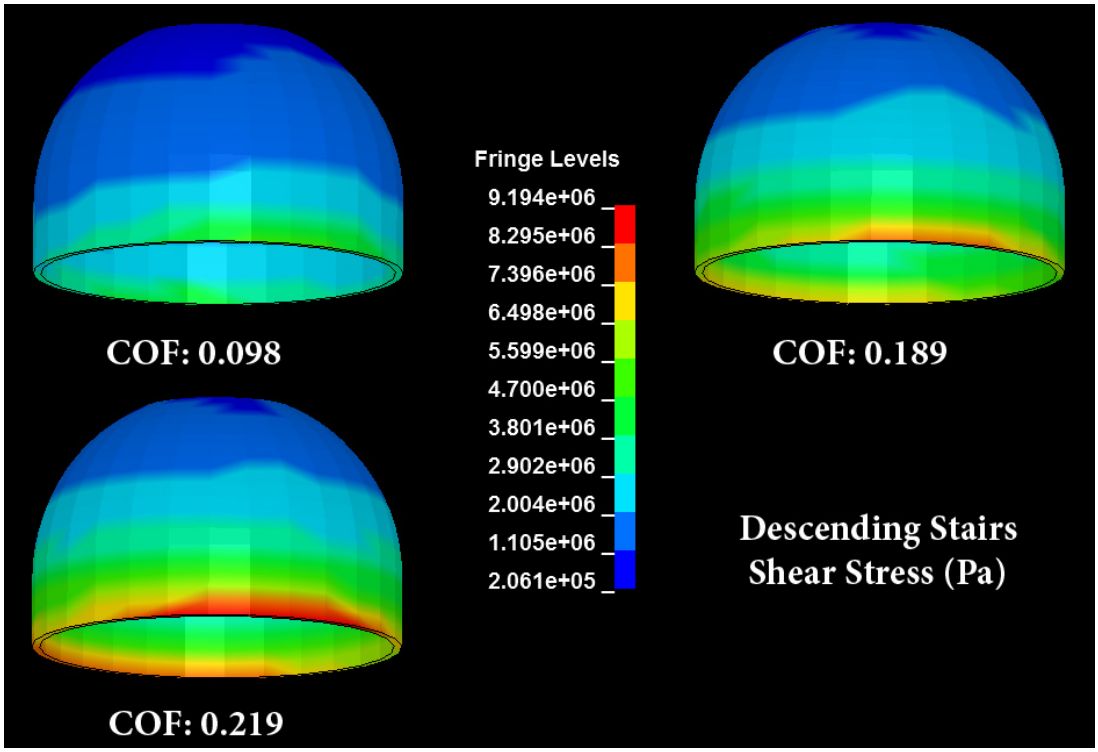

Figure 5.7. PMMA bone cement shear stresses (Pa) 1.152 seconds into the descending stairs gait for three different metal-on-metal friction coefficients.

As metal-on metal (MoM) friction coefficient increases from 0.098 to 0.219, the maximum tensile stress for the PMMA cement mantle increases from 2.86 MPa to 7.4 MPa, representing an increase of 258.74 %. In a similar way, the maximum shear stress increases from 4.67 MPa to 8.49 MPa as MoM friction increases from 0.098 to 0.219, representing an increase of 181.8 %.

The range of maximum tensile and shear stresses across the descending stair cycle are shown in Figure 5.8.a and Figure 5.8.c for different metal-on-metal friction coefficients.

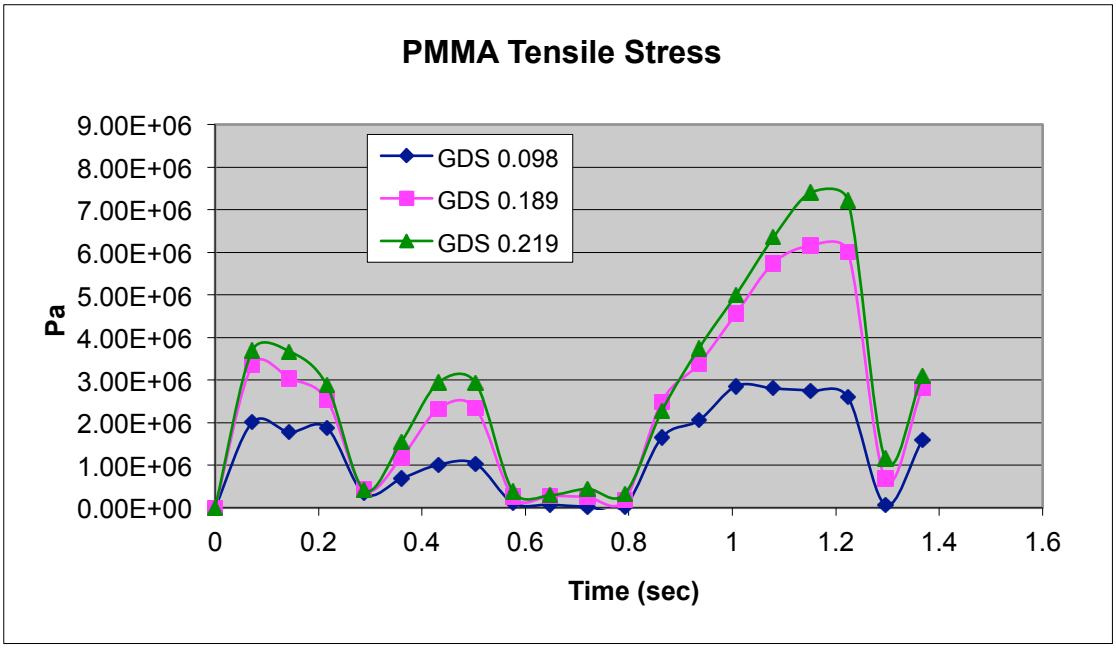

Figure 5.8.a. Maximum tensile stresses during descending stairs for different MoM friction coefficient.

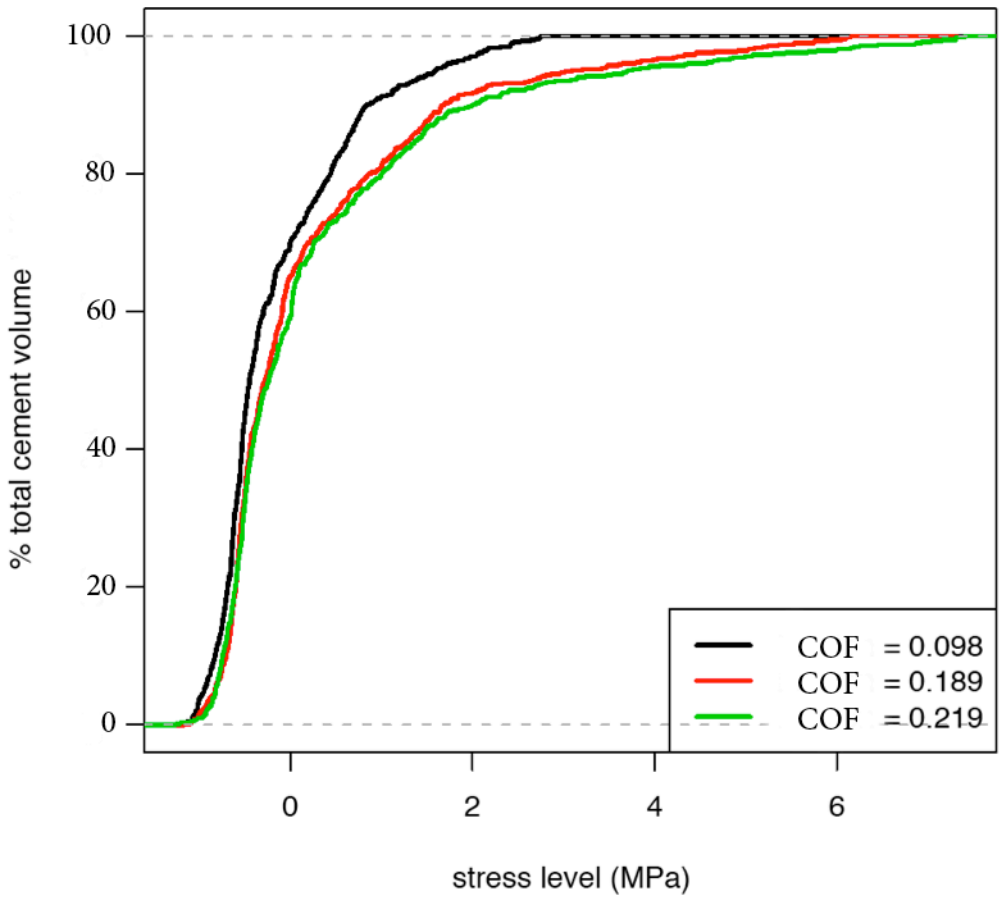

Figure 5.8.b. Tensile stress distribution 1.152 seconds into the descending stairs gait cycle for different MoM friction coefficient.

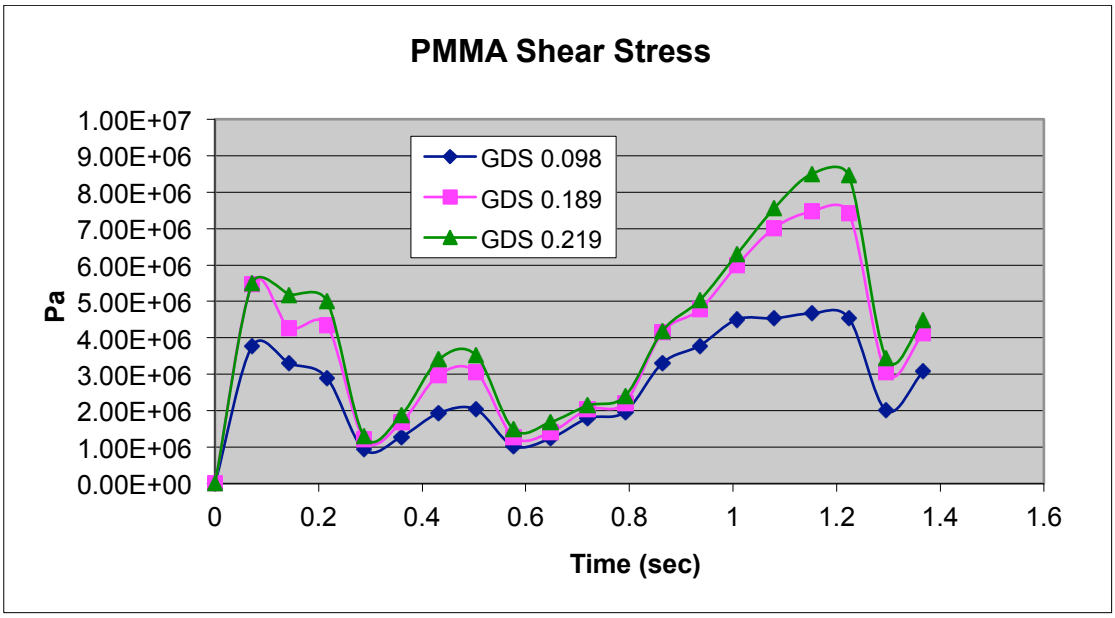

Figure 5.8.c. Maximum shear stresses during descending stairs for different MoM friction coefficient.

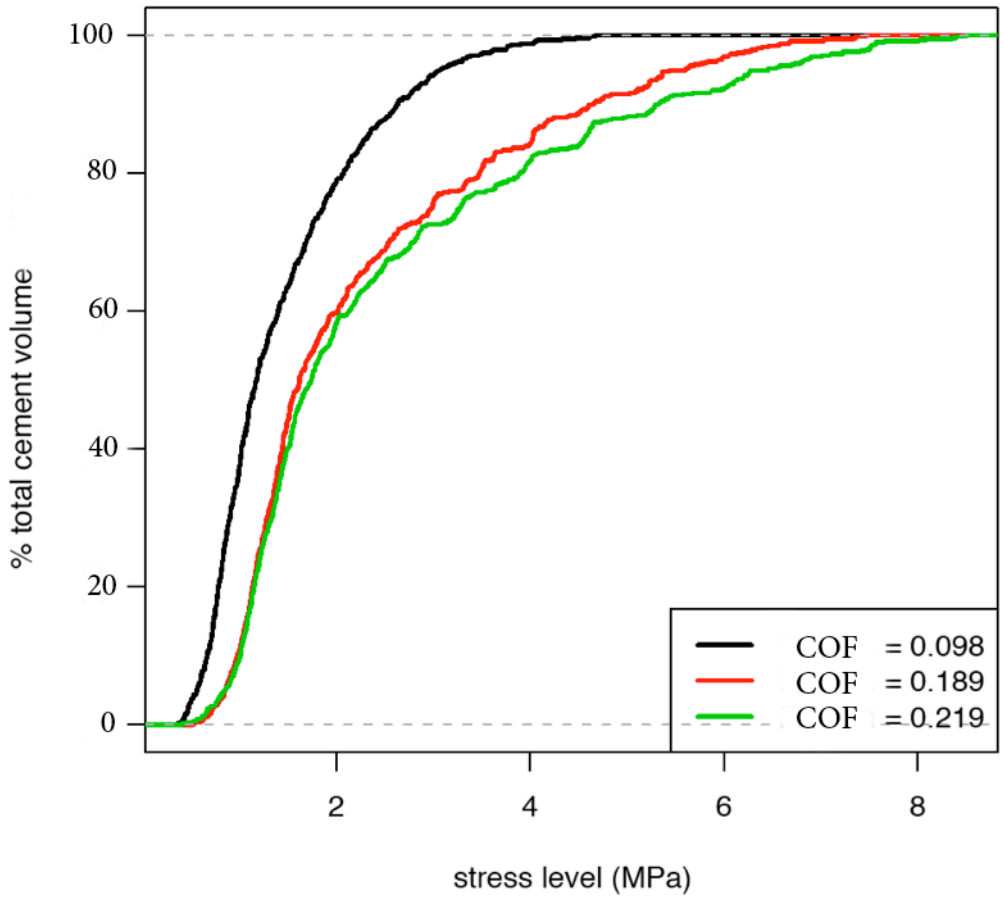

Figure 5.8.d. Tensile stress distribution 1.152 seconds into the descending stairs gait cycle for different MoM friction coefficient.

Furthermore, from the tensile and shear stress distribution graphs in Figure 5.8.b and 5.8.d, it can be observed that around 10% of the total volume of PMMA bone cement is subjected to a tensile stress above the maximum peak tensile stress for the dynamic friction case, which is 2.86 MPa for 0.098 MoM friction coefficient. In the case of shear stress distribution, around 16% of the total volume of PMMA bone cement is subjected to a tensile stress above the maximum peak tensile stress for the dynamic friction case, which is 4.67 MPa for 0.098 MoM friction.

5.1.3 Finite Element Analysis results for standing up

The Finite Element model developed in Chapter 4 was used to assess the effect of resting periods during standing up from a chair.

Hip forces and flexion-extension rotation were applied to the model to simulate standing up, total hip force and flexion-extension rotation are shown in Figure 5.9.

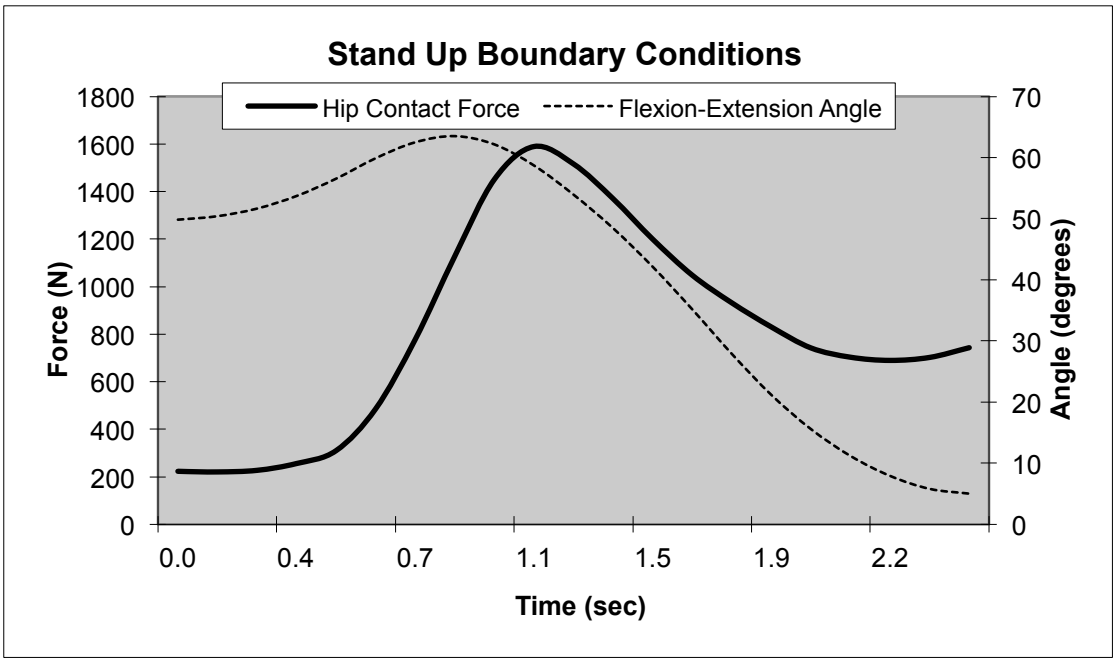

Figure 5.9. Hip contact force and flexion-extension rotation for normal standing up.

Two Finite Element models were solved according to the metal-on-metal friction coefficient due to resting periods for walking as shown in Table 5.11.

Table 5.11. MoM friction due to resting periods for standing up.

Everyday Activity	Resting Duration (Seconds)	Metal-on-metal friction coefficient
Standing Up	**0**	0.098
	60	0.285

The maximum tensile and shear stresses for PMMA bone cement according to varying metal-on-metal friction coefficient due to resting periods are shown in Table 5.12. Furthermore, Table 5.12 shows the equations to predict tensile and shear stresses according to metal-on-metal friction coefficient.

Table 5.12. PMMA maximum tensile and shear stresses for different MoM friction coefficients during walking.

Everyday Activity	Metal-on-metal COF	Tensile Stress (MPa)	Shear Stress (MPa)	Stress Equations
Standing Up	**0.098**	2.16	3.61	Tensile Stress = 33.31 * μ - 1.104
	0.285	8.39	9.36	Shear Stress = 30.74 * μ + 0.596

Maximum tensile stresses in the PMMA bone cement occur for the two FEA models at the prosthesis rim area as shown in Figure 5.10.

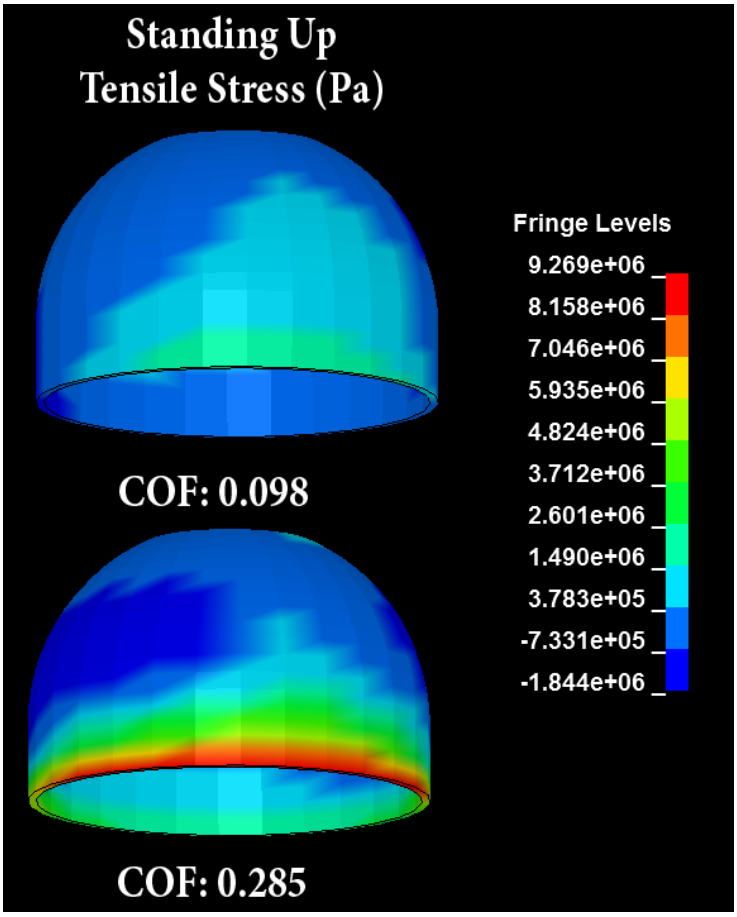

Figure 5.10. PMMA bone cement tensile stresses (Pa) 1.245 seconds into the standing up gait for two different metal-on-metal friction coefficients.

Figure 5.11 shows maximum shear stresses occurring in the prosthesis rim area. As metal-on metal (MoM) friction coefficient increases from 0.098 to 0.285, the peak tensile stress for the PMMA cement mantle increases from 2.16 MPa to 8.39 MPa, representing an increase of 388.43 %. In a similar way, the peak shear stress increases from 3.61 MPa to 9.36 MPa as MoM friction increases from 0.098 to 0.285, representing an increase of 259.28 %.

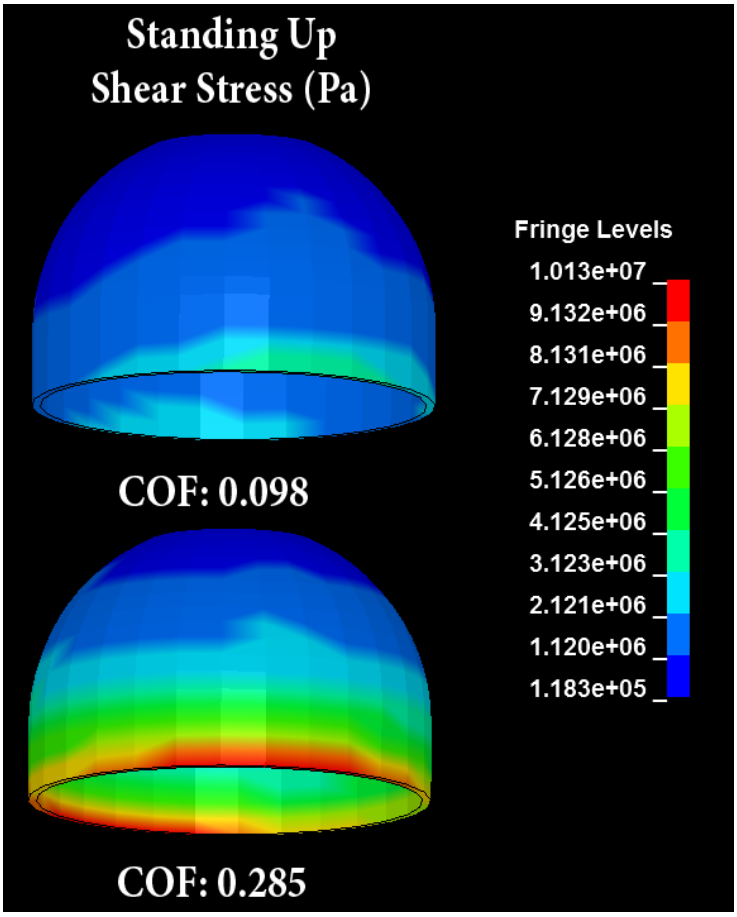

Figure 5.11. PMMA bone cement shear stresses (Pa) 1.245 seconds into the standing up gait for two different metal-on-metal friction coefficients.

The range of maximum tensile and shear stresses for the standing up cycle are shown in Figure 5.12.a and Figure 5.12.c for different metal-on-metal friction coefficients.

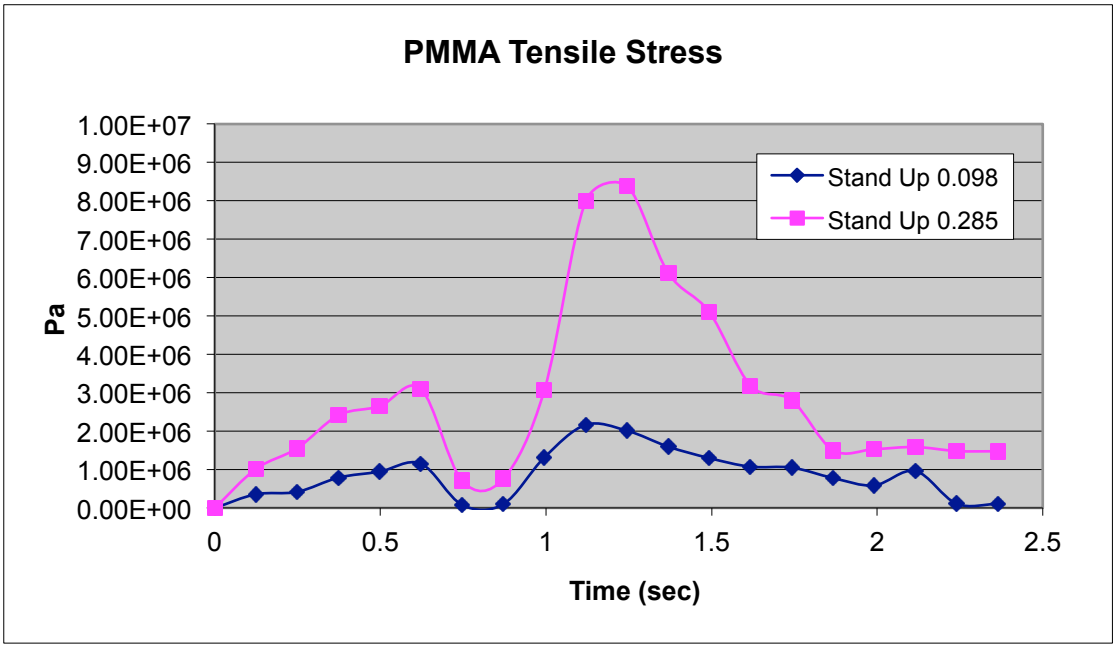

Figure 5.12.a. Maximum tensile stresses at standing up cycle for different MoM friction coefficient.

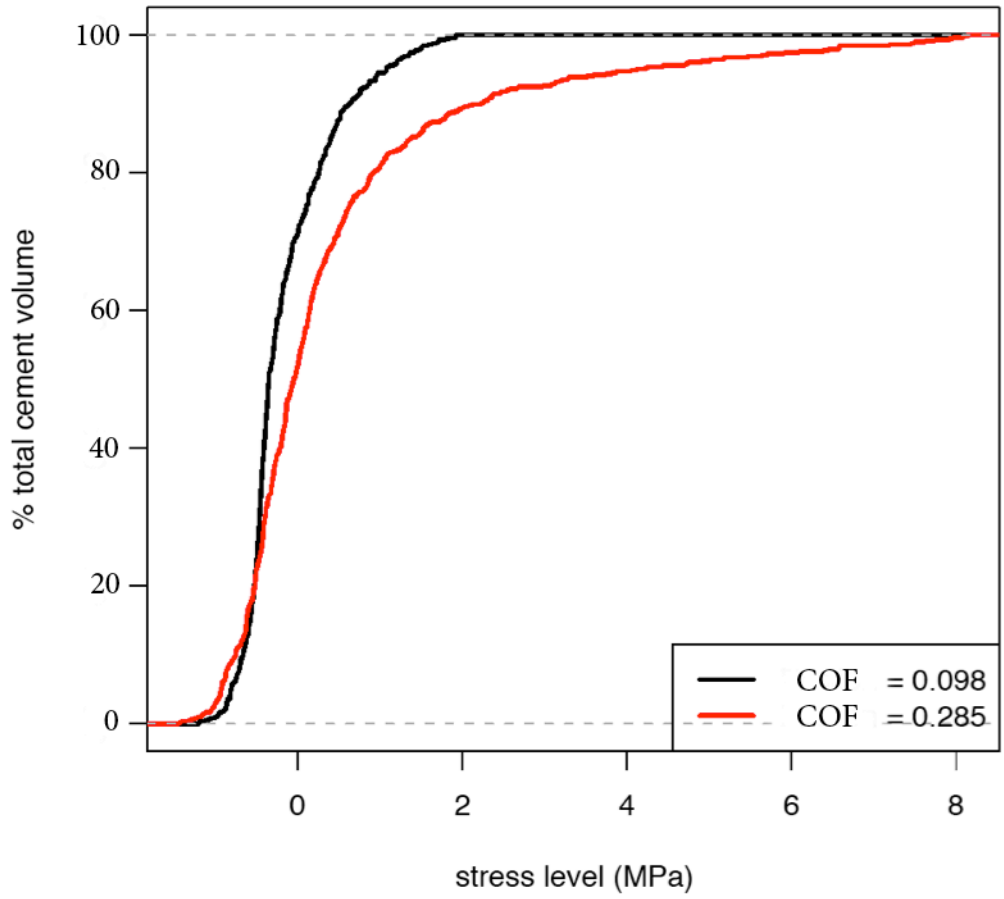

Figure 5.12.b. Tensile stress distribution 1.245 seconds into the standing up cycle for different MoM friction coefficient.

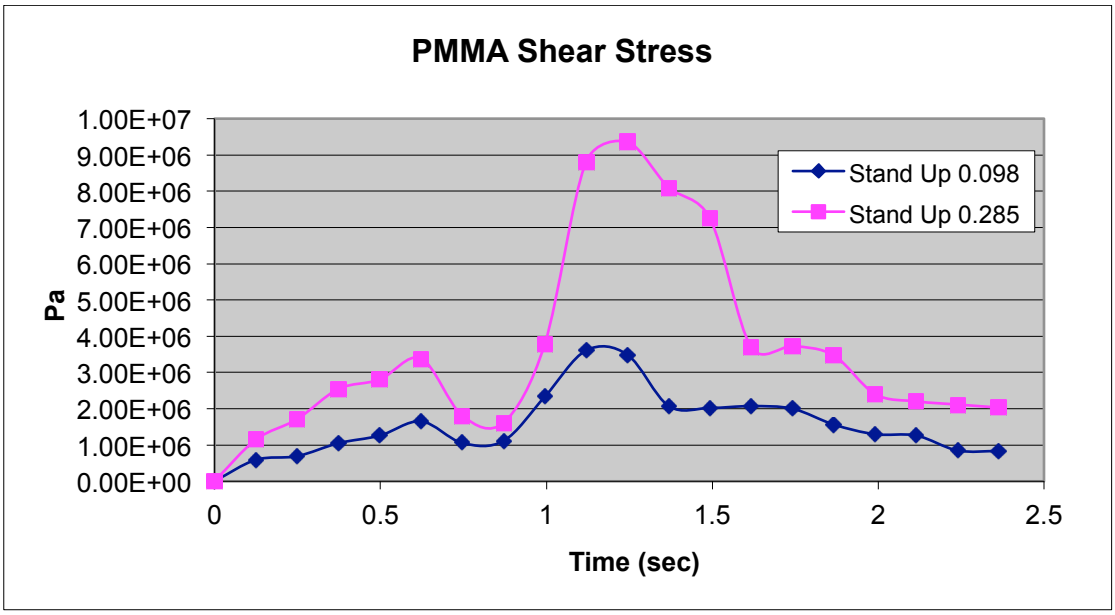

Figure 5.12.c. Maximum shear stresses at standing up cycle for different MoM friction coefficient.

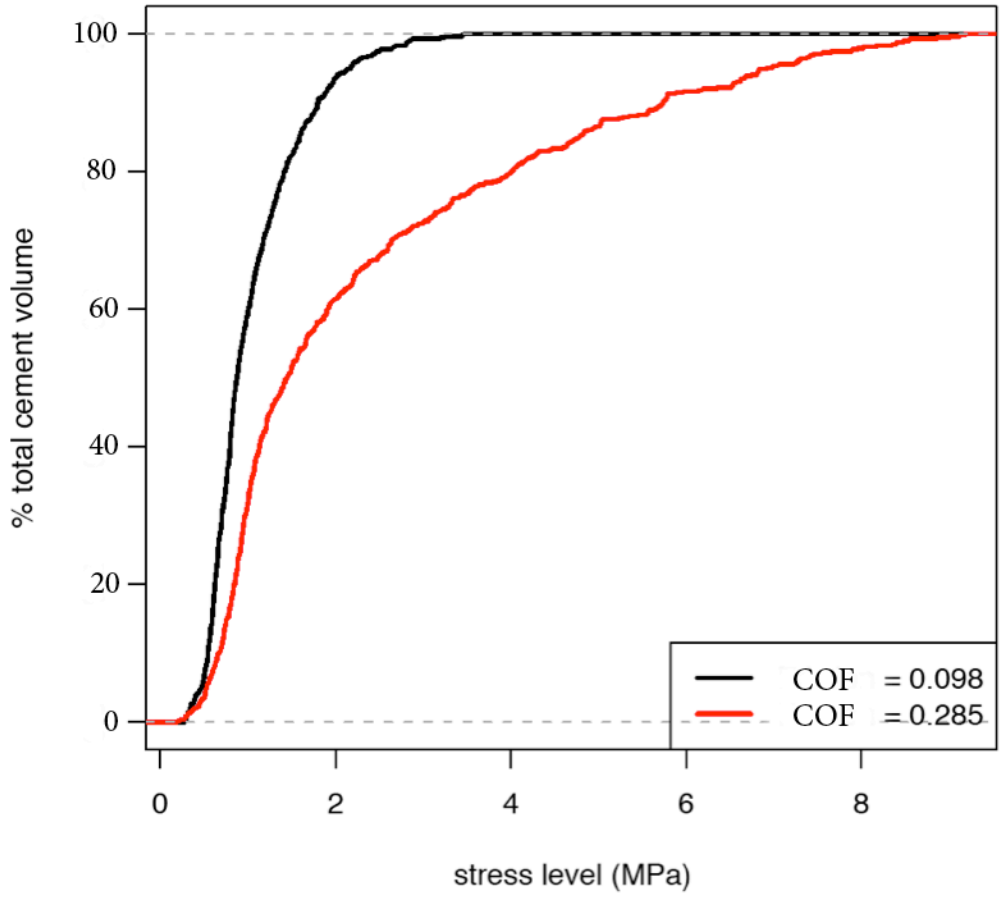

Figure 5.12.d. Shear stress distribution 1.245 seconds into the standing up cycle for different MoM friction coefficient.

Furthermore, from the tensile and shear stress distribution graphs in Figures 5.12.b and 5.12.d, it can be observed that around 15% of the total volume of PMMA bone cement is subjected to a tensile stress above the maximum peak tensile stress for the dynamic friction case, which is 2.16 MPa for 0.098 MoM friction coefficient. In the case of shear stress distribution, around 25% of the total volume of PMMA bone cement is subjected to a tensile stress above the maximum peak tensile stress for the dynamic friction case, which is 3.61 MPa for 0.098 MoM friction coefficient.

5.1.4 Fatigue analysis

The fatigue analysis was performed using the Miner's cumulative damage rule (Miner, 1945). The main reason for the use of the Miner's cumulative damage rule was the strong relation between the number of applied stress cycles (n_i) and the cycles to failure at that stress level (N_f). As it can be observed in Figure 5.4.a, the PMMA bone cement maximum tensile stress for the whole walking cycle is compound of two main peaks of tensile stress. If only the maximum tensile stress for the whole walking gait was taken to calculate the fatigue life of the PMMA bone cement, the damage causes by the second peak of tensile stress will not be taking into account and the fatigue life prediction would be overestimated. Miner's rule allowed accounting for the cumulative damage causes by all the stress cycles across the whole gait and furthermore, allow the calculated the fatigue life to be compiled together the damage cause by different daily activities at different metal-on-metal friction coefficients due to resting periods.

$$Miner's\ rule \implies \sum \frac{n_i}{N_f} = 1$$

Miner's cumulative damage rule implies the following assumptions taking from Suresh (1998):

- The damage fraction is calculated as the number of stresses imposed to the component expressed as a percentage of the total number of stress cycles of the same amplitude to cause damage.

- The fatigue life is not affected by the order in which the order of stress blocks of different amplitudes is applied, not taking into account the loading sequence of stress cycles.

- Failure will happen when the linear sum of the damage for each stress block reach the value of 1.

Figure 5.13 shows a cyclic stress load with standard nomenclature.

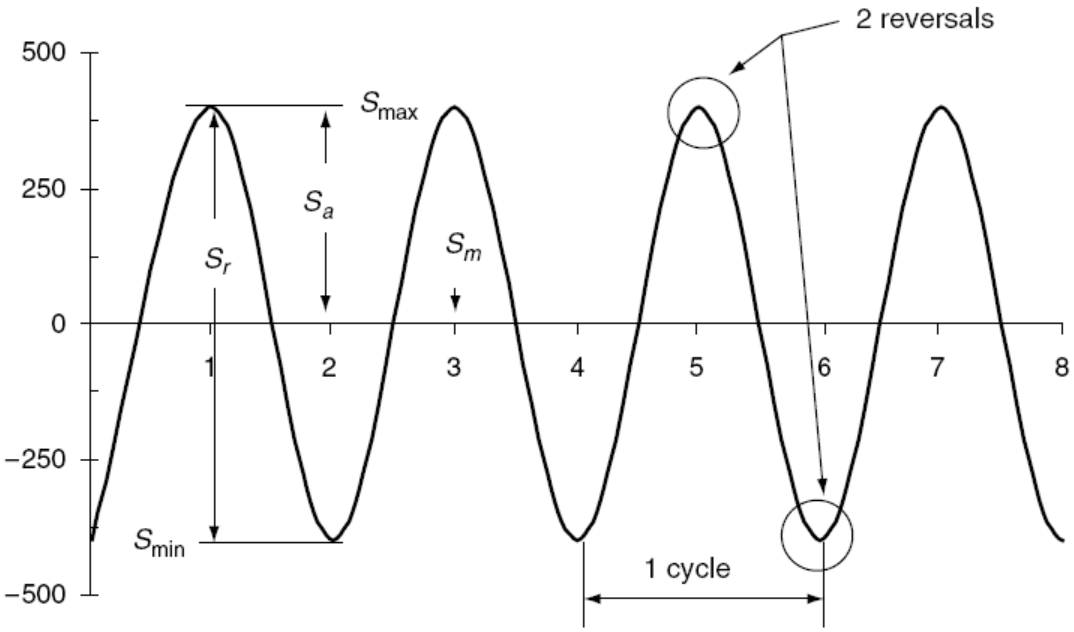

Figure 5.13. Cyclic stress load (Lee et al, 2005)

Some important parameters for cyclic stress loads are:

$$Stress\ range \implies S_r = S_{max} - S_{min}$$

$$Stress\ amplitude \implies S_a = \frac{S_r}{2} = \frac{(S_{max} - S_{min})}{2}$$

$$Mean\ stress \implies S_m = \frac{(S_{max} + S_{min})}{2}$$

$$Stress\ ratio \implies R = \frac{S_{min}}{S_{max}}$$

Stress life approach to fatigue is mostly performed using a fully reversal loading, meaning that the mean stress will be equal to zero and the values of S_{max} and S_{min} will be identical with opposite signs as shown in Figure 5.13.

According to Suresh (1998), the mean stress of fatigue cycles plays an important role in the fatigue behaviour of the material. The Finite Element Analysis stress cycles and the PMMA fatigue data have variable mean stresses and do not equal to zero. A

modified Goodman relation was used to transform all the cyclic stresses into a zero stress mean, allowing to account for the effect of mean stresses and compare Finite Element Analysis stress results with PMMA fatigue testing data to calculate the cycles to failure for every given stress cycle in the Finite Element Analysis stress results using the graphs and equations in Figure 5.13.

$$Modified\ Goodman\ Relation\ \Longrightarrow S_a = S_{a|S_m=0}\left\{1 - \frac{S_m}{S_{TS}}\right\}$$

Where:

$$S_a = Stress\ amplitude\ for\ non\ zero\ mean$$

$$S_{a|S_m=0} = Stress\ amplitude\ for\ zero\ mean$$

$$S_m = Mean\ stress\ amplitude$$

$$S_{TS} = Tensile\ strength\ of\ the\ material$$

5.1.4.1 PMMA fatigue data

Murphy and Prendergast (2000) performed fatigue experiments using *Cemex Rx* bone cement (low viscosity) producing data for vacuum mixed and hand mixed bone cement.

The fatigue test were performed in pure tension at four different stress levels (13 MPa, 17 MPa, 21 MPa and 25 MPa) in cycling loading with a stress ratio R=0.1.
They provided a linear fatigue equation to estimate the fatigue life of PMMA for a range of stresses under hand or vacuum mix based (Figure 5.14) on the assumption of a linear relation between stress and cycles to failure (Davies et al., 1987) and no fatigue limit (Huiskes, 1993).

The linear regressions shown in Figure 5.15 provides a better interpretation of the results by fitting the regression line to the average $\log_{10}(Nf)$ for the four stress levels.
A similar approach was used by Jeffers (2005) to perform PMMA fatigue analysis.

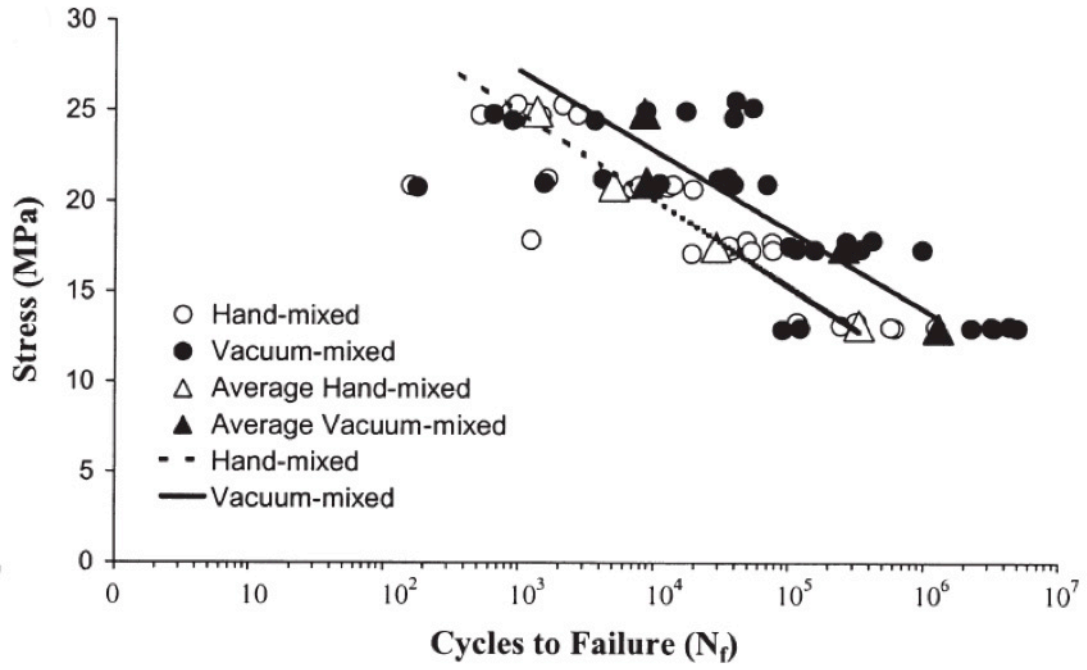

Figure 5.14. Stress versus number of cycles to failure curves for vacuum-mixed and hand-mixed *Cemex Rx* bone cement for average $\log_{10}$ (Nf) values for the four stress levels (Murphy and Prendergast, 2000)

Dr. Murphy very kindly provided the original data from the fatigue testing for use in this research.

The PMMA fatigue data was transformed to a zero mean to be able to compare the stress levels from Finite Element Analysis to the fatigue data using the modified Goodman approach as described in Section 5.1.4.

The equations below show the regression lines equations for zero mean as shown in Figure 5.15.

$$Hand\ mixed \Longrightarrow S_a = -1.72 \cdot Ln(N_f) + 29.27 \Longrightarrow R^2 = 0.983$$

$$Vacuum\ mixed \Longrightarrow S_a = -1.70 \cdot Ln(N_f) + 32.14 \Longrightarrow R^2 = 0.89$$

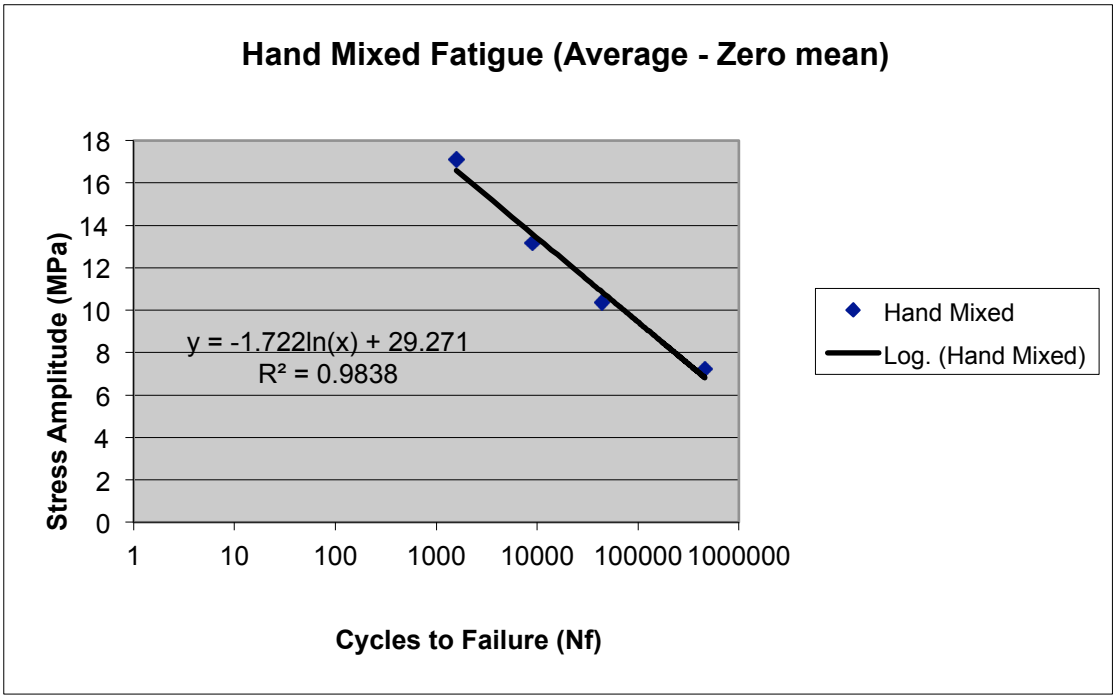

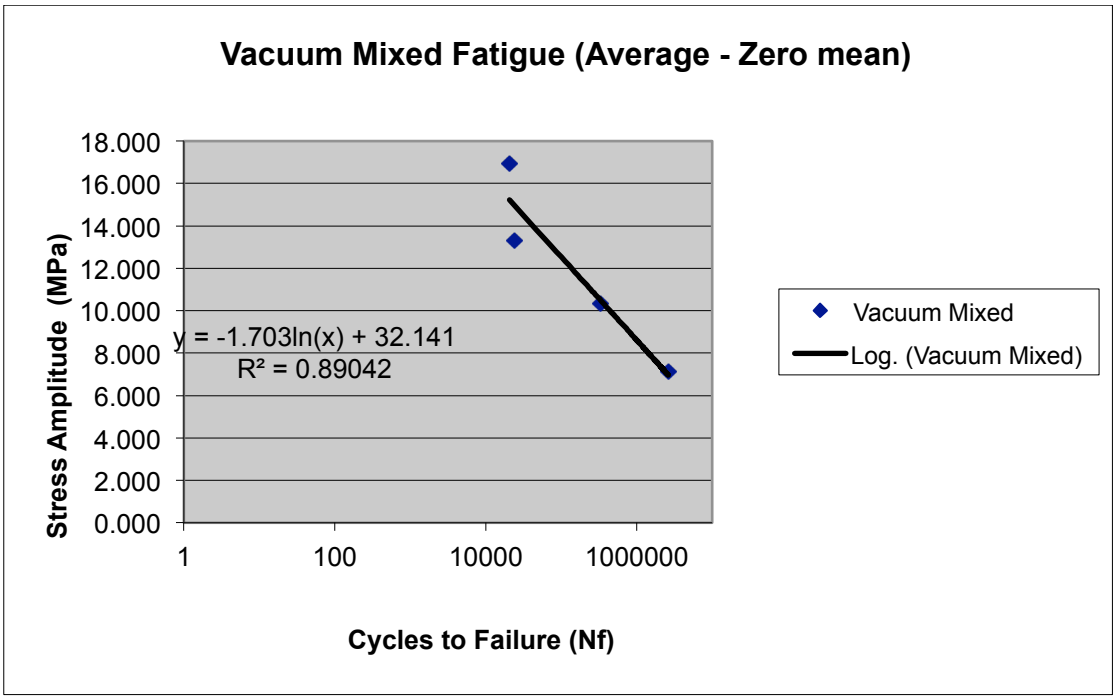

Figure 5.15. Stress versus number of cycles to failure curves for vacuum-mixed and hand-mixed *Cemex Rx* for zero mean stress.

These equations were used to calculate the number of cycles to failure (N_f) for the stress cycles obtained from the Finite Element Analysis for walking, descending stairs and standing up for different metal-on-metal friction coefficients due to resting periods.

5.1.4.2 Rainflow counting method

Rainflow counting is a widely used technique in fatigue analysis for data reduction (SAE AE-22, 1997) and it allows the reduction of an unstructured loading pattern into identifiable stress cycles.

The process is explained below by using the maximum tensile stress results for walking with a metal-on-metal friction coefficient of 0.098 (Figure 5.16).

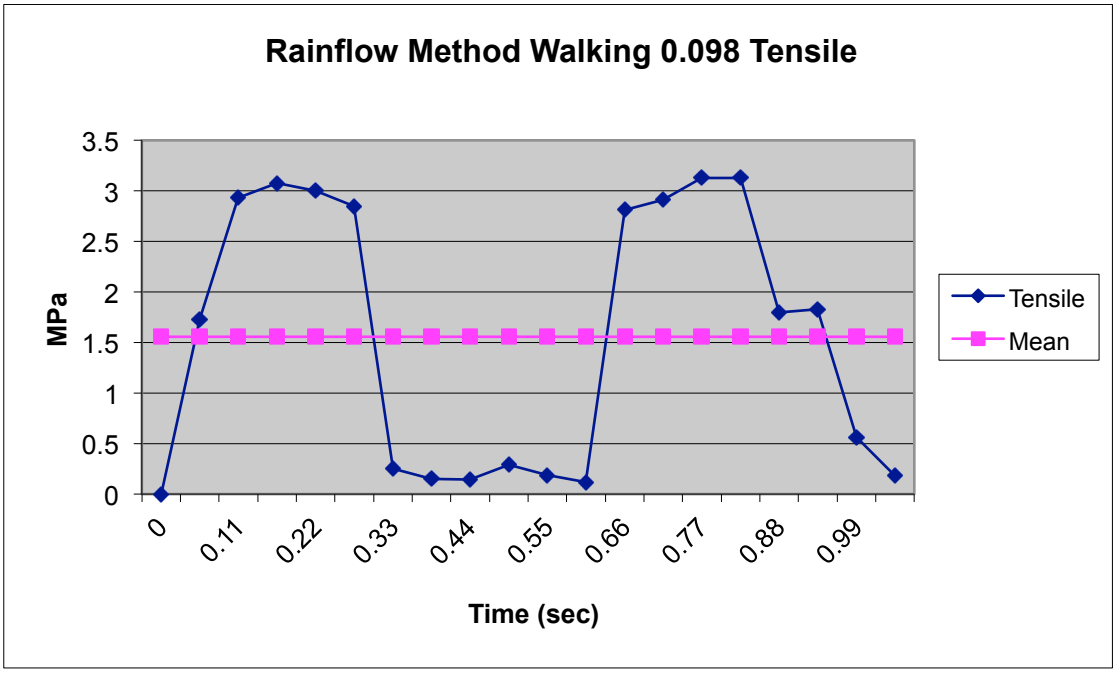

Figure 5.16. Maximum tensile stress for walking with MoM coefficient of friction of 0.098.

First, the tensile stress results are reduced to low and high peak stress values in the gait as shown in Figure 5.17, with the stress values for each point presented in Table 5.13.

Table 5.13. Tensile stress for points in Figure 5.17.

Point	Stress (MPa)
A	0
B	3.08
C	0.121
D	3.13
E	0.185

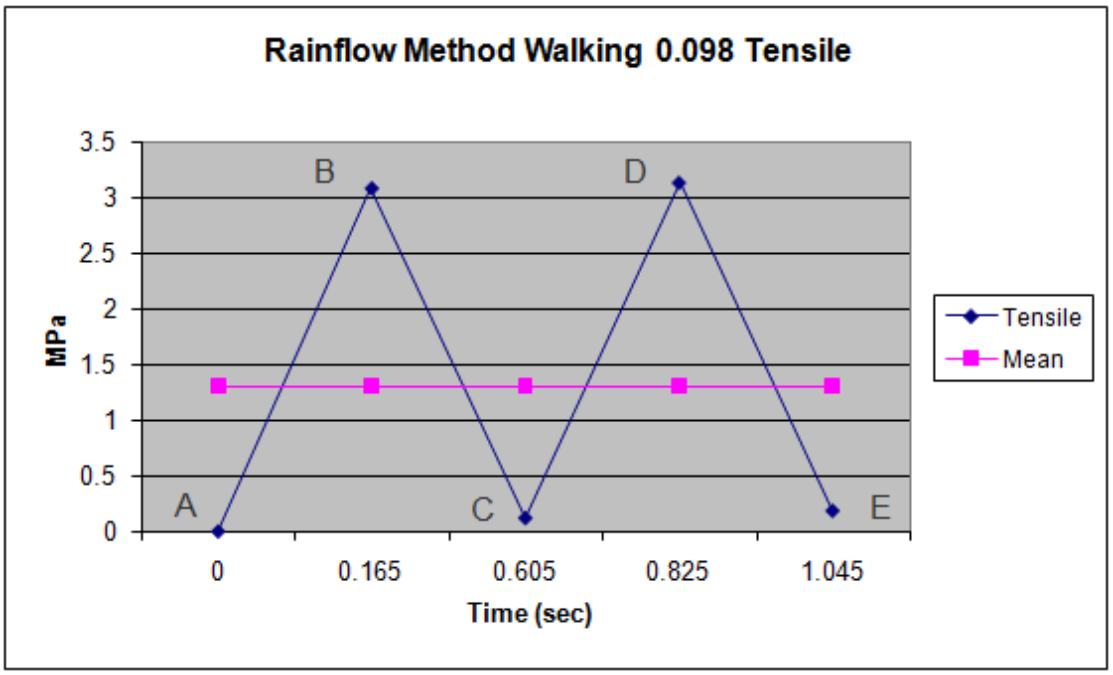

Figure 5.17. Maximum tensile stress reduced to low and high peaks.

The process starts in point A and move along to the next point. When two segments are read, they are compared and if the latter segment is smaller than the first segment, then the latter segment is selected as the stress range and the mean stress can be calculated.

In our example, segment A-B = B – A = 3.08 MPa – 0 MPa = 3.08 MPa while segment B-C = B – C = 3.08 MPa – 0.121 MPa = 2.959 MPa. Segment B-C is smaller than segment A-B, so segment B-C is our first cycle with a stress amplitude of 2.959 MPa and a mean stress of 1.6005 MPa.

$$Mean\ Stress = \frac{B + C}{2} = \frac{3.08\ MPa + 0.121\ MPa}{2} = 1.6005\ MPa$$

Next, stress points B and C are taking away from the cycle as shown in Figure 5.18 and the process starts again.

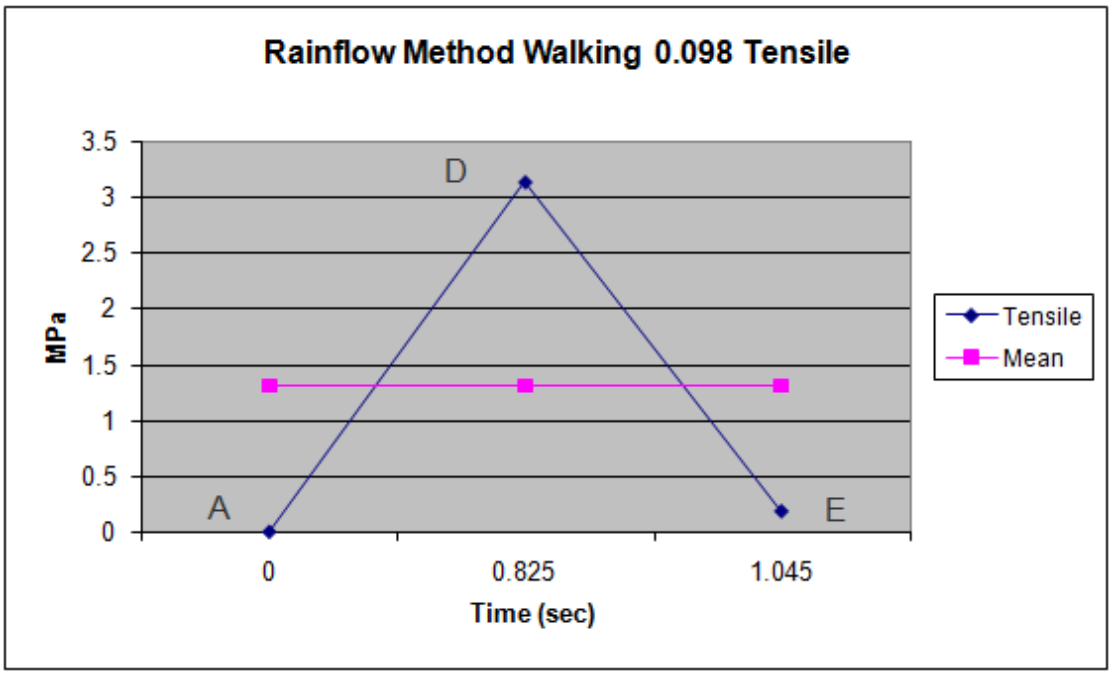

Figure 5.18. Maximum tensile stress reduced after first cycle has been calculated.

Starting again from point A, segment A-D = D – A = 3.13 MPa – 0 MPa = 3.13 MPa while segment D-E = D – E = 3.13 MPa – 0.185 MPa = 2.945 MPa. Segment D-E is smaller than segment A-D, so segment D-E is our second and final cycle with a stress amplitude of 2.945 MPa and a mean stress of 1.6575 MPa.

$$Mean\ Stress = \frac{D+E}{2} = \frac{3.13\ MPa + 0.185\ MPa}{2} = 1.6575\ MPa$$

After the rainflow counting method, the maximum tensile stress graph in Figure 5.16 was reduced to two loading cycles.

$$1^{st}\ Stress\ cycle \implies S_r = 2.959\ MPa\ ; S_m = 1.6005\ MPa$$
$$2^{nd}\ Stress\ cycle \implies S_r = 2.945\ MPa\ ; S_m = 1.6575\ MPa$$

The same rainflow counting method was applied to the Finite Element Analysis maximum tensile stress results for walking gait, descending stairs and standing up for different metal-on-metal frictions as presented in Section 5.1.1, Section 5.1.2 and Section 5.1.3.

Furthermore, when all the first and second cycles for walking at different metal-on-metal frictions are calculated, the stress amplitudes and mean stresses can be

plotted and a regression line plotted to be able to interpolate for new values of metal-on-metal friction. This is very much the case to account for pre-wear and post-wear metal-on-metal friction due to resting periods (Wimmer et al., 2006) after the running in period.

Figure 5.19 shows the first stress cycle and mean stress regression line and equations for the walking cycles as an example.

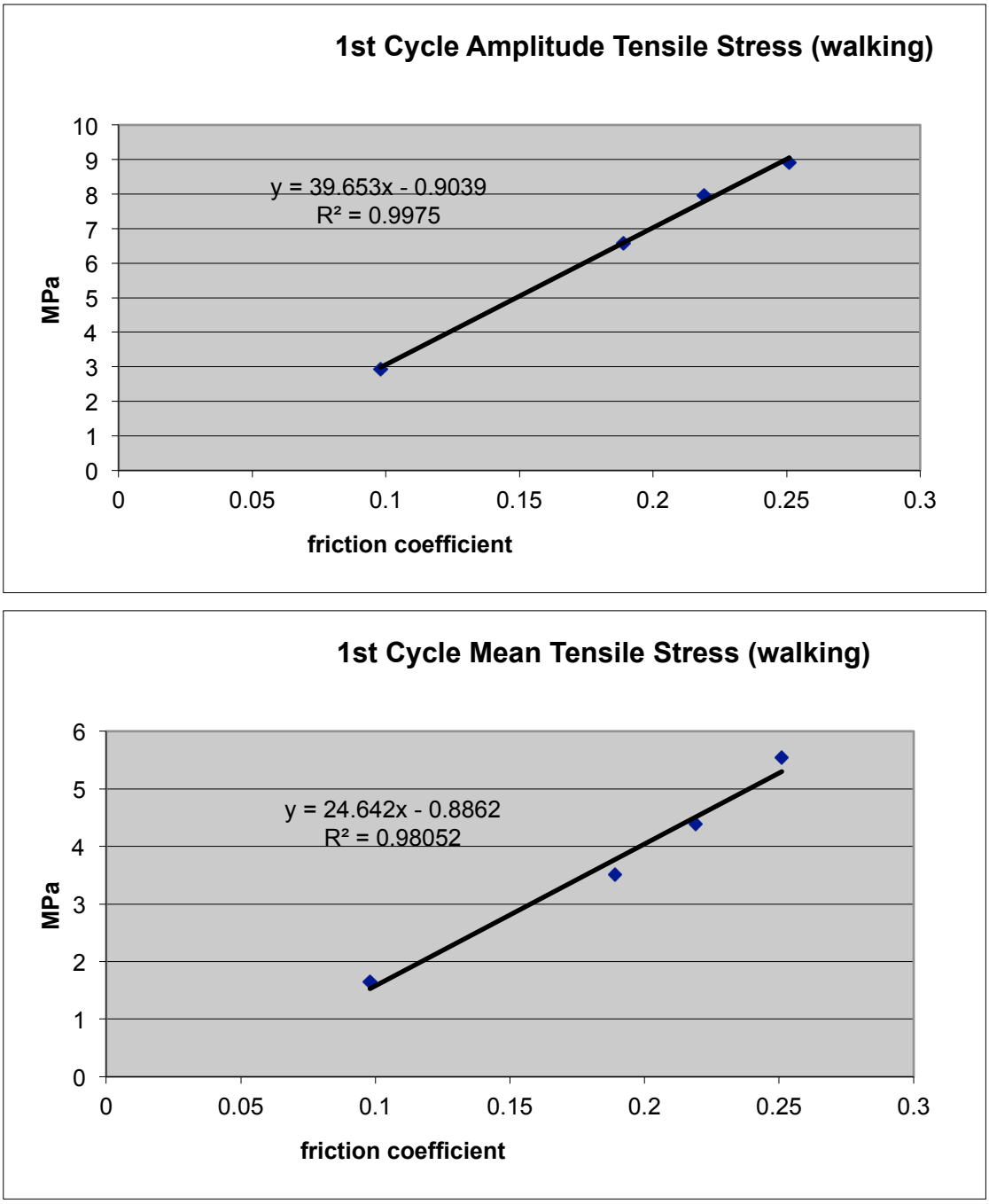

Figure 5.19. Regression lines and equations for first cycle amplitude tensile stress and mean stress for walking.

Equations for the different stress amplitude and mean stress cycles for everyday activities and different metal-on-metal friction coefficients due to resting periods are shown in Table 5.14.

Table 5.14. Equations for amplitude and mean tensile and shear stress cycles in MPa for everyday activities due to metal-on-metal friction coefficient.

	Cycle	Tensile Amplitude (MPa)	Tensile Mean (MPa)	Shear Amplitude (MPa)	Shear Mean (MPa)
Walking	1st cycle	39.653 * μ - 0.904	24.642 * μ - 0.8862	34.278 * μ + 0.8824	21.22 * μ + 0.9268
	2nd cycle	18.784 * μ + 1.1674	16.545 * μ - 0.1052	15.037 * μ + 1.8792	15.236 * μ + 1.2565
Descending Stairs	1st cycle	28.817 * μ - 0.023	22.819 * μ - 0.7943	19.453 * μ + 0.7557	21.632 * μ + 1.2065
	2nd cycle	13.185 * μ - 0.5896	8.7083 * μ + 0.1012	12.091 * μ + .7207	9.159 * μ + 1.4885
	3rd cycle	14.675 * μ - 0.7719	8.0981 * μ - 0.1175	8.5895 * μ + 0.1579	7.8763 * μ + 0.7449
Standing Up	1st cycle	26.011 * μ - 0.493	20.31 * μ - 0.8584	24.358 * μ + 0.3879	18.57 * μ + 0.4027
	2nd cycle	7.056 * μ + 0.378	6.8997 * μ - 0.061	6.3102 * μ - 0.0284	6.1497 * μ + 0.7523

Tables 5.15 to 5.17 show the breakdown of amplitude tensile cycles and mean tensile cycles for walking, descending stairs and standing up for pre-wear and post wear metal-on-metal friction according to the regression equations in Table 5.14. These values are converted to a zero mean equivalent using the modifies Goodman relation as it was done with the PMMA fatigue data in Section 5.1.4.1, to be able to calculate the cycles to failure for each tensile cycle.

Table 5.15. Amplitude and mean tensile stress cycles in MPa for walking due to resting periods.

Resting period (seconds)	Pre-wear	1st amplitude tensile cycle (MPa)	2nd amplitude tensile cycle (MPa)	1st mean tensile stress (MPa)	2nd mean tensile stress (MPa)
dynamic	**0.098**	2.982	3.008	1.529	1.516
5	**0.189**	6.591	4.718	3.771	3.022
10	**0.219**	7.780	5.281	4.510	3.518
30	**0.251**	9.049	5.882	5.299	4.048
	Post-wear				
dynamic	**0.098**				
5	**0.185**	6.432	4.642	3.673	2.956
10	**0.204**	7.185	4.999	4.141	3.270
30	**0.239**	8.573	5.657	5.003	3.849

Table 5.16. Amplitude and mean tensile stress cycles in MPa for descending stairs due to resting periods.

Resting period (seconds)	Pre-wear	1st amplitude tensile cycle (MPa)	2nd amplitude tensile cycle (MPa)	3rd amplitude tensile cycle (MPa)	1st mean tensile stress (MPa)	2nd mean tensile stress (MPa)	3rd mean tensile stress (MPa)
dynamic	**0.098**	2.801	1.882	0.666	1.442	0.955	0.676
5	**0.189**	5.424	3.081	2.002	3.518	1.747	1.413
10	**0.219**	6.288	3.477	2.442	4.203	2.008	1.656
	Post-wear						
dynamic	**0.098**						
5	**0.185**	5.308	3.029	1.943	3.427	1.712	1.381
10	**0.204**	5.856	3.279	2.222	3.861	1.878	1.535

Table 5.17. Amplitude and mean tensile stress cycles in MPa for standing up due to resting periods.

Resting period (seconds)	Pre-wear	1st amplitude tensile cycle (MPa)	2nd amplitude tensile cycle (MPa)	1st mean tensile stress (MPa)	2nd mean tensile stress (MPa)
dynamic	**0.098**	2.056	1.069	1.132	0.615
60	**0.285**	6.920	2.389	4.930	1.906
	Post-wear				
dynamic	**0.098**				
60	**0.274**	6.634	2.311	4.707	1.830

5.1.4.3 Results

Miner's cumulative damage rule is applied to all the tensile cycles for walking, descending stairs and standing up presented in Tables 5.15 to 5.17. The number of applied stress cycles (n_i) for every activity and metal-on-metal friction were taken from Table 5.5. The cycles to failure for every stress level (N_i) were calculated after transforming all the stress cycles to a zero mean using the modified Goodman relation and comparing the stress level to the fatigue data shown in Figure 5.15 to obtain N_f (cycles to failure).

$$Miner's\ rule \implies \sum \frac{n_i}{N_f} = 1$$

The process from the modified Goodman relation to the calculation of the damage per year is presented in Tables 5.18 to 5.21.

The fatigue analysis is calculated for a running in phase and a post running in phase (pre-wear and post-wear) for hand mixed and vacuum mixed PMMA bone cement.

According to Table 5.18, for hand mixed PMMA bone cement the damage process will have been completed in one year.

In the case of vacuum mixed PMMA bone cement, during the first year (running in phase) the damage will be around 0.1571 after which the damage will be completed in less than seven years according to Tables 5.20 and 5.21.

Table 5.18. Damage per year calculation for hand mixed bone cement during running in phase.

Friction	Walking	S amp	Smax	Smin	Smean	S amp-eq	Smax-eq	Smin-eq	Smean-eq	cycles/year	N_f	damage/year
0.098	1st cycle	1.416	2.945	0.112	1.529	1.473	1.473	-1.473	0	1803960.0	1.04E+07	0.172795784
	2nd cycle	1.429	2.945	0.087	1.516	1.485	1.485	-1.485	0	1803960.0	1.04E+07	0.174048663
0.189	1st cycle	3.130	6.902	0.641	3.771	3.457	3.457	-3.457	0	697010.4	3.29E+06	0.21157666
	2nd cycle	2.241	5.263	0.781	3.022	2.424	2.424	-2.424	0	697010.4	6.00E+06	0.116078625
0.219	1st cycle	3.696	8.206	0.815	4.510	4.166	4.166	-4.166	0	266594.4	2.18E+06	0.122210539
	2nd cycle	2.509	6.027	1.010	3.518	2.751	2.751	-2.751	0	266594.4	4.97E+06	0.053679957
0.251	1st cycle	4.298	9.597	1.001	5.299	4.955	4.955	-4.955	0	112435.2	1.38E+06	0.081572121
	2nd cycle	2.794	6.842	1.254	4.048	3.109	3.109	-3.109	0	112435.2	4.03E+06	0.027881757
	Descending Stairs											
0.098	1st cycle	1.330	2.772	0.112	1.442	1.380	1.380	-1.380	0	30259.2	1.10E+07	0.002746589
	2nd cycle	0.894	1.889	0.101	0.995	0.917	0.917	-0.917	0	30259.2	1.44E+07	0.002097779
	3rd cycle	0.316	0.992	0.360	0.676	0.322	0.322	-0.322	0	30259.2	2.04E+07	0.001484322
0.189	1st cycle	2.576	6.094	0.942	3.518	2.825	2.825	-2.825	0	8344.8	4.76E+06	0.001754559
	2nd cycle	1.463	2.876	-0.050	1.413	1.517	1.517	-1.517	0	8344.8	1.02E+07	0.000820168
	3rd cycle	0.951	2.959	1.057	2.008	1.001	1.001	-1.001	0	8344.8	1.37E+07	0.000607646
0.219	1st cycle	2.987	7.190	1.216	4.203	3.338	3.338	-3.338	0	2196.0	3.53E+06	0.000622092
	2nd cycle	1.652	3.660	0.356	2.008	1.739	1.739	-1.739	0	2196.0	8.94E+06	0.000245546
	3rd cycle	1.160	2.816	0.496	1.656	1.210	1.210	-1.210	0	2196.0	1.22E+07	0.00018055
	Stand Up											
0.285	1st cycle	3.287	8.217	1.643	4.930	3.750	3.750	-3.750	0	43920.0	2.78E+06	0.015807404
	2nd cycle	1.135	3.040	0.771	1.906	1.192	1.192	-1.192	0	43920.0	1.23E+07	0.003572352
											Total	0.9897831114
	Sa = -1.72ln(Nf) + 29.27										**Years**	1.010322348

Table 5.19. Damage per year calculation for hand mixed bone cement after running in phase.

Friction	Walking	S amp	Smax	Smin	Smean	S amp-eq	Smax-eq	Smin-eq	Smean-eq	cycles/year	N_f	damage/year
0.098	1st cycle	1.4165	2.945	0.112	1.529	1.472	1.472	-1.472	0	1803960.0	1.04E+07	0.172728844
	2nd cycle	1.4289	2.945	0.087	1.516	1.485	1.4846	-1.4846	0	1803960.0	1.04E+07	0.173981247
0.185	1st cycle	3.0552	6.728	0.617	3.673	3.360	3.36049	-3.36049	0	697010.4	3.48E+06	0.200064959
	2nd cycle	2.2052	5.161	0.750	2.956	2.379	2.379128	-2.37913	0	697010.4	6.16E+06	0.113078551
0.204	1st cycle	3.413	7.554	0.728	4.141	3.803	3.802572	-3.80257	0	266594.4	2.69E+06	0.098948041
	2nd cycle	2.3747	5.645	0.895	3.270	2.584	2.583707	-2.58371	0	266594.4	5.47E+06	0.0487133
0.239	1st cycle	4.0723	9.075	0.931	5.003	4.648	4.647532	-4.64753	0	112435.2	1.65E+06	0.068203712
	2nd cycle	2.687	6.536	1.162	3.849	2.970	2.969769	-2.96977	0	112435.2	4.37E+06	0.02571452
Descending Stairs												
0.098	1st cycle	1.3305	2.772	0.112	1.442	1.380	1.380	-1.380	0	30259.2	1.10E+07	0.00274565
	2nd cycle	0.894	1.889	0.101	0.995	0.917	0.917	-0.917	0	30259.2	1.44E+07	0.002097454
	3rd cycle	0.3164	0.992	0.360	0.676	0.322	0.322	-0.322	0	30259.2	2.04E+07	0.001484268
0.185	1st cycle	2.5214	5.949	0.906	3.4272	2.755	2.755	-2.755	0	8344.8	4.95E+06	0.001684485
	2nd cycle	1.4386	3.151	0.274	1.7122	1.502	1.502	-1.502	0	8344.8	1.03E+07	0.000813123
	3rd cycle	0.9229	2.304	0.458	1.3806	0.956	0.956	-0.956	0	8344.8	1.41E+07	0.00059171
0.204	1st cycle	2.7815	6.642	1.079	3.8608	3.075	3.075	-3.075	0	2196.0	4.11E+06	0.000533993
	2nd cycle	1.5576	3.435	0.320	1.8777	1.634	1.634	-1.634	0	2196.0	9.51E+06	0.000230946
	3rd cycle	1.0554	2.590	0.479	1.5345	1.097	1.097	-1.097	0	2196.0	1.30E+07	0.00016906
Stand Up												
0.274	1st cycle	3.1512	7.858	1.555	4.7065	3.566	3.566	-3.566	0	43920.0	3.09E+06	0.014210022
	2nd cycle	1.0979	2.928	0.732	1.8296	1.150	1.150	-1.150	0	43920.0	1.26E+07	0.003486912
											Total	0.9294807799
	Sa = -1.72ln(Nf) + 29.27										**Years**	1.075869454

Table 5.20. Damage per year calculation for vacuum mixed bone cement during running in phase.

Friction	Walking	S amp	Smax	Smin	Smean	S amp-eq	Smax-eq	Smin-eq	Smean-eq	cycles/year	N_f	damage/year
0.098	1st cycle	1.416	2.945	0.112	1.529	1.472	1.472	-1.472	0	1803960.0	6.62E+07	0.027264932
	2nd cycle	1.429	2.945	0.087	1.516	1.485	1.485	-1.485	0	1803960.0	6.57E+07	0.02746459
0.189	1st cycle	3.130	6.902	0.641	3.771	3.453	3.453	-3.453	0	697010.4	2.07E+07	0.033700438
	2nd cycle	2.241	5.263	0.781	3.022	2.422	2.422	-2.422	0	697010.4	3.79E+07	0.018399333
0.219	1st cycle	3.696	8.206	0.815	4.510	4.160	4.160	-4.160	0	266594.4	1.37E+07	0.019523656
	2nd cycle	2.509	6.027	1.010	3.518	2.748	2.748	-2.748	0	266594.4	3.13E+07	0.008520897
0.251	1st cycle	4.298	9.597	1.001	5.299	4.947	4.947	-4.947	0	112435.2	8.60E+06	0.013071155
	2nd cycle	2.794	6.842	1.254	4.048	3.105	3.105	-3.105	0	112435.2	2.54E+07	0.004432463
	Descending Stairs											
0.098	1st cycle	1.330	2.772	0.112	1.442	1.380	1.380	-1.380	0	30259.2	6.99E+07	0.000433165
	2nd cycle	0.894	1.889	0.101	0.995	0.917	0.917	-0.917	0	30259.2	9.17E+07	0.00033002
	3rd cycle	0.316	0.992	0.360	0.676	0.322	0.322	-0.322	0	30259.2	1.30E+08	0.000232739
0.189	1st cycle	2.576	6.094	0.942	3.518	2.822	2.822	-2.822	0	8344.8	3.00E+07	0.000278617
	2nd cycle	1.463	2.876	-0.050	1.413	1.516	1.516	-1.516	0	8344.8	6.45E+07	0.000129448
	3rd cycle	0.951	2.959	1.057	2.008	1.001	1.001	-1.001	0	8344.8	8.73E+07	9.56218E-05
0.219	1st cycle	2.987	7.190	1.216	4.203	3.333	3.333	-3.333	0	2196.0	2.22E+07	9.89993E-05
	2nd cycle	1.652	3.660	0.356	2.008	1.738	1.738	-1.738	0	2196.0	5.66E+07	3.87948E-05
	3rd cycle	1.160	2.816	0.496	1.656	1.210	1.210	-1.210	0	2196.0	7.72E+07	2.84465E-05
	Stand Up											
0.285	1st cycle	3.287	8.217	1.643	4.930	3.744	3.744	-3.744	0	43920.0	1.74E+07	0.002519286
	2nd cycle	1.135	3.040	0.771	1.906	1.191	1.191	-1.191	0	43920.0	7.80E+07	0.000562753
											Total	0.157125352
	Sa = -1.7031Ln(Nf) + 32.141										**Years**	6.364345319

Table 5.21. Damage per year calculation for hand mixed bone cement after running in phase.

Friction	Walking	S amp	Smax	Smin	Smean	S amp-eq	Smax-eq	Smin-eq	Smean-eq	cycles/year	N_f	damage/year
0.098	1st cycle	1.4165	2.945	0.112	1.529	1.472	1.472	-1.472	0	1803960.0	6.62E+07	0.027264932
	2nd cycle	1.4289	2.945	0.087	1.516	1.485	1.4846	-1.4846	0	1803960.0	6.57E+07	0.02746459
0.185	1st cycle	3.0552	6.728	0.617	3.673	3.360	3.36049	-3.3605	0	697010.4	2.18E+07	0.031925804
	2nd cycle	2.2052	5.161	0.750	2.956	2.379	2.37913	-2.3791	0	697010.4	3.88E+07	0.017942882
0.204	1st cycle	3.413	7.554	0.728	4.141	3.803	3.80257	-3.8026	0	266594.4	1.68E+07	0.015830173
	2nd cycle	2.3747	5.645	0.895	3.270	2.584	2.58371	-2.5837	0	266594.4	3.44E+07	0.007738773
0.239	1st cycle	4.0723	9.075	0.931	5.003	4.648	4.64753	-4.6475	0	112435.2	1.03E+07	0.010964872
	2nd cycle	2.687	6.536	1.162	3.849	2.970	2.96977	-2.9698	0	112435.2	2.75E+07	0.004094211
Descending Stairs												
0.098	1st cycle	1.3305	2.772	0.112	1.442	1.380	1.380	-1.380	0	30259.2	6.99E+07	0.000433165
	2nd cycle	0.894	1.889	0.101	0.995	0.917	0.917	-0.917	0	30259.2	9.17E+07	0.00033002
	3rd cycle	0.3164	0.992	0.360	0.676	0.322	0.322	-0.322	0	30259.2	1.30E+08	0.000232739
0.185	1st cycle	2.5214	5.949	0.906	3.4272	2.755	2.755	-2.755	0	8344.8	3.12E+07	0.000267868
	2nd cycle	1.4386	3.151	0.274	1.7122	1.502	1.502	-1.502	0	8344.8	6.50E+07	0.000128372
	3rd cycle	0.9229	2.304	0.458	1.3806	0.956	0.956	-0.956	0	8344.8	8.96E+07	9.31223E-05
0.204	1st cycle	2.7815	6.642	1.079	3.8608	3.075	3.075	-3.075	0	2196.0	2.58E+07	8.5073E-05
	2nd cycle	1.5576	3.435	0.320	1.8777	1.634	1.634	-1.634	0	2196.0	6.02E+07	3.64884E-05
	3rd cycle	1.0554	2.590	0.479	1.5345	1.097	1.097	-1.097	0	2196.0	8.25E+07	2.66281E-05
Stand Up												
0.274	1st cycle	3.1512	7.858	1.555	4.7065	3.566	3.566	-3.566	0	43920.0	1.93E+07	0.002270291
	2nd cycle	1.0979	2.928	0.732	1.8296	1.150	1.150	-1.150	0	43920.0	7.99E+07	0.00054938
											Total	0.147679385
	Sa = -1.7031Ln(Nf) + 32.141										**Years**	6.77142583

Figure 5.20 shows a comparison of the damage per year for hand and vacuum mixed PMMA bone cement during the running in phase. The damage per year for hand mixed bone cement is very much greater than for vacuum mixed.

Furthermore, Figure 5.20 shows that the main contribution to damage is due to walking; producing close to a 97% of the damage as it is the most performed everyday activity.

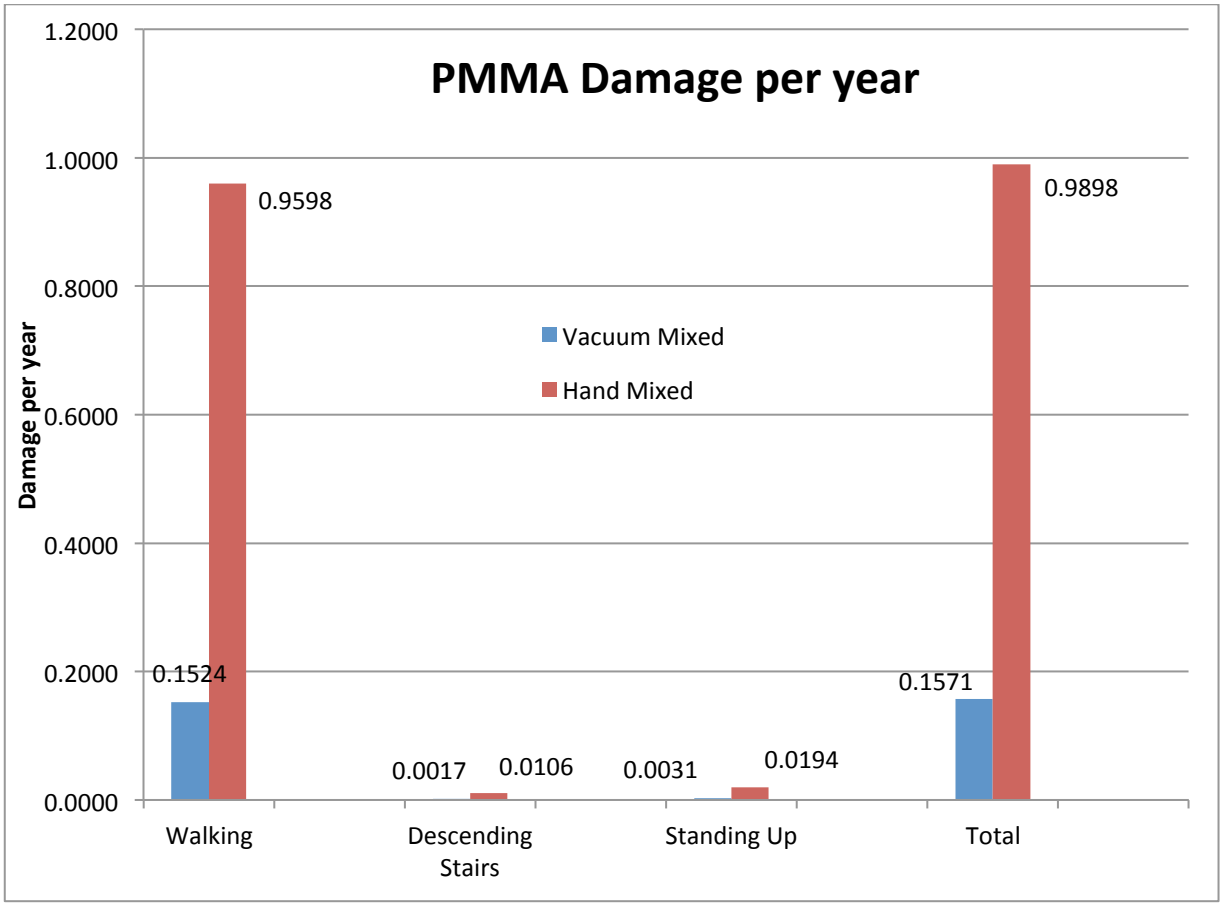

Figure 5.20. Total damage per year for hand and vacuum mixed PMMA bone cement.

Focusing in the activity of walking, Figure 5.21 shows that the effect of resting periods produces around 64% of the total damage per year due to walking, with 36% of damage due to dynamic metal-on-metal friction (0.098). Highlighting the effect of resting periods and the consequent increase in metal-on-metal friction coefficient play in the fatigue damage of PMMA bone cement.

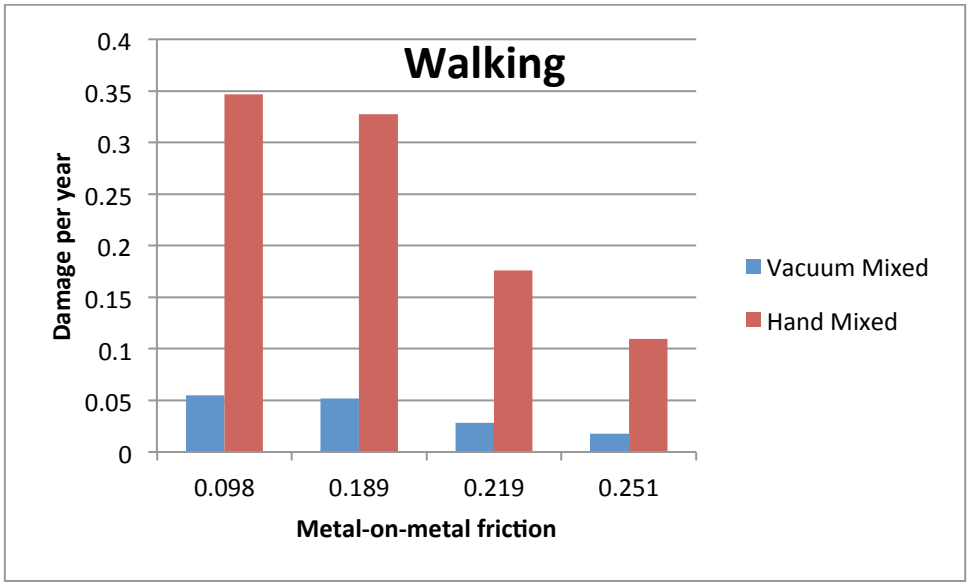

Figure 5.21. Damage per year for hand and vacuum mixed PMMA bone cement for walking due to metal-on-metal friction.

In a similar approach for descending stairs, the effect of resting periods accounts for 40% of the damage per year as shown in Figure 5.22.

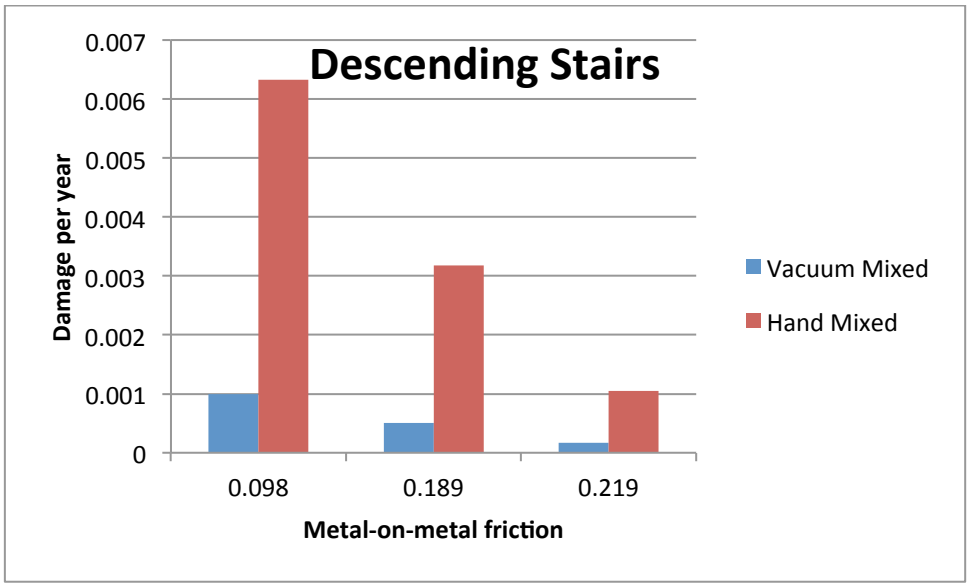

Figure 5.22. Damage per year for hand and vacuum mixed PMMA bone cement for descending stairs due to metal-on-metal friction.

5.2 Effect of Bone Quality on PMMA Bone Cement Stresses

Bone quality is one of the main factors in patient selection as it was discussed in Section 2.13.1. Appropriate screening and selection should aim to preclude patients likely to feature low bone quality in order to maximise the potential for successful hip resurfacing arthroplasty.

Furthermore, the initial research presented in Section 1.2 shows the results for the effect of bone quality in the tensile and shear stresses of PMMA bone cement. A similar approach was used later on by Little et al (2007) to investigate hip resurfacing arthroplasty.

The Finite Element model developed in Chapter 4 was used to assess the effect of bone quality and resting periods during everyday activities.

Every Finite Element model simulated in Section 5.1 for different metal-on-metal friction was further solved to incorporate a 60%, 80% and 120% bone quality model. Cancellous and cortical bone Young's modulus in the Finite Element models were changed as shown in Table 5.22 to incorporate different bone quality to the Finite Element Analysis.

Table 5.22. Cancellous and cortical bone Young's modulus according to different bone quality.

	Poisson's Ratio	Young's Modulus (GPa)			
		60%	80%	100%	120%
Cancellous Bone	0.3	0.48	0.64	0.8	0.96
Cortical Bone	0.2	10.2	13.6	17	20.4

The reasoning behind simulating up to 120% of normal bone material properties is firstly to be able to interpolate between the Finite Element results and secondly due to the fact that very active people develop higher bone quality with high loads in their bones. Hip resurfacing arthroplasty were aimed to young and very active patients, such as Dr Scott Clark's testimonial of climbing high peaks after hip resurfacing surgery (Hospital for Special Surgery).

5.2.1 Finite Element Analysis results for walking

Sixteen Finite Element models were solved according to the metal-on-metal friction coefficient due to resting periods for walking and simulated different bone quality as

shown in Table 5.23. Following this approach, the study is not just a parametric study varying just one variable but a multi-parametric approach allowing variable bone quality for every Finite Element model according to metal-on-metal friction coefficient due to resting periods.

Table 5.23 presents the comparison of maximum tensile and shear stresses in the PMMA bone cement according to varying metal-on-metal friction coefficient and patient bone quality. Furthermore, Table 5.23 shows the equations to predict maximum tensile and shear PMMA bone cement stresses according to the parameters previously mentioned.

Table 5.23. PMMA maximum tensile and shear stresses due to varying MoM friction coefficient and bone quality during walking.

Everyday Activity	Metal-on-metal COF	Bone Quality	Tensile Stress (MPa)	Shear Stress (MPa)	Stress Equations
Walking	0.098	60%	3.55	5.9	Tensile Stress = -0.954 * BQ + 4.073
		80%	3.25	5.53	
		100%	3.13	5.25	Shear Stress = -1.463 * BQ + 6.739
		120%	2.96	5.02	
	0.189	60%	8.12	9.75	Tensile Stress = -2.71 * BQ + 9.649
		80%	7.4	8.99	
		100%	6.81	8.34	Shear Stress = -3.085 * BQ + 11.52
		120%	6.51	7.91	
	0.219	60%	9.57	11.4	Tensile Stress = -2.815 * BQ + 11.17
		80%	8.78	10.4	
		100%	8.37	9.72	Shear Stress = -3.775 * BQ + 13.55
		120%	7.83	9.11	
	0.251	60%	11.2	12.8	Tensile Stress = -3.185 * BQ +13.16
		80%	10.7	12.1	
		100%	10	11.2	Shear Stress = -3.9 * BQ + 15.16
		120%	9.31	10.5	

Figure 5.23 and 5.24 shows the comparison of PMMA maximum tensile and shear stresses for different metal-on-metal friction and patient bone quality as shown in Table 5.23.

As described in section 5.1.1 and Figure 5.2 and 5.3, maximum tensile and shear stresses in the PMMA bone cement occur at the prosthesis rim area for all Finite Element Analysis models.

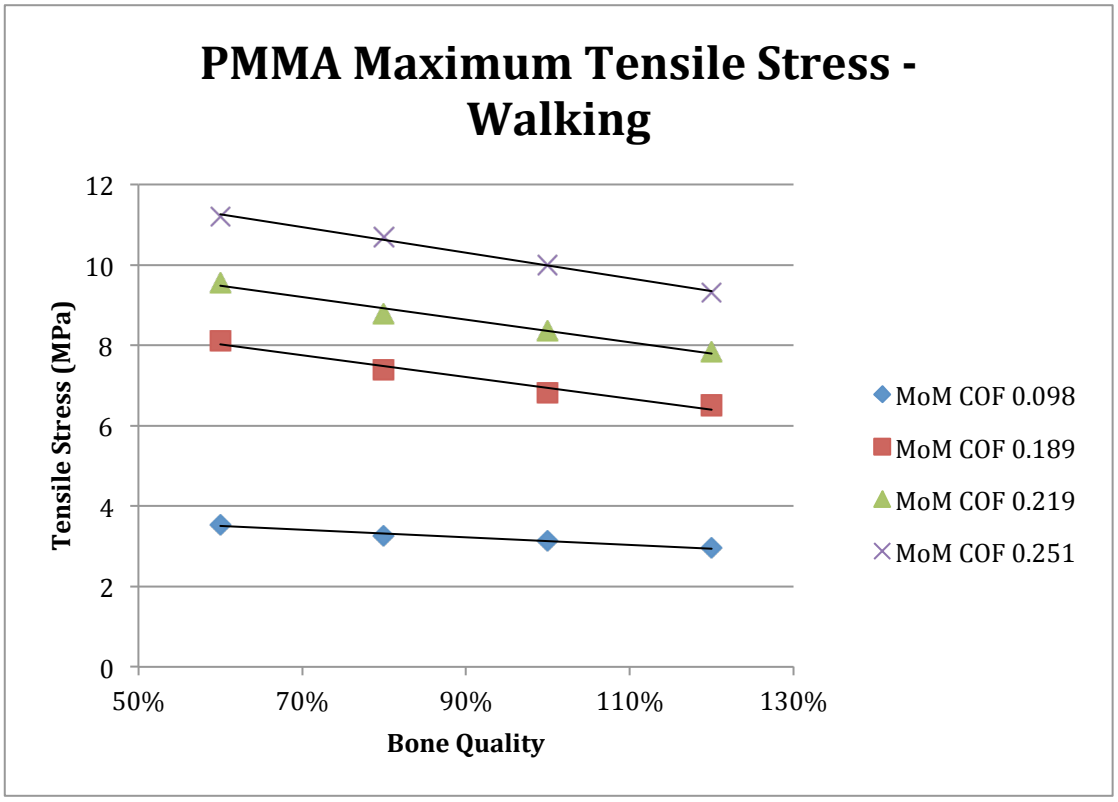

Figure 5.23. Comparison of PMMA maximum tensile stress (MPa) according to different metal-on-metal friction coefficients and patient bone quality during walking gait.

From Figure 5.23, it can be observed that a decrease in patient bone quality has a greater effect at higher metal-on-metal friction coefficients producing higher maximum tensile stresses in the PMMA bone cement.

A similar effect on PMMA maximum shear stress values can be appreciated in Figure 5.24, higher metal-on-metal friction coefficients show greater maximum shear stresses in the PMMA bone cement when patient bone quality is reduced.

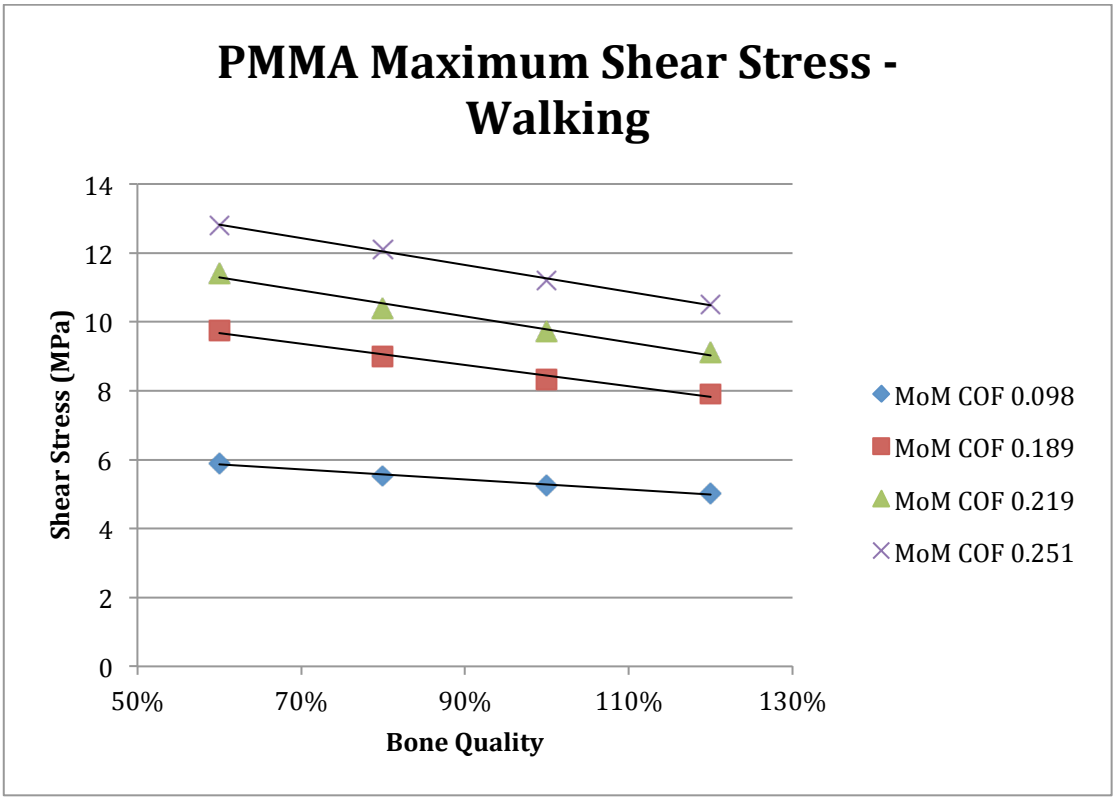

Figure 5.24. Comparison of PMMA maximum shear stress (MPa) according to different metal-on-metal friction coefficients and patient bone quality during walking gait.

Figure 5.25 and 5.26 show a different approach to deducting maximum tensile and shear stresses in PMMA bone cement due to metal-on-metal friction and bone quality using a two dimensional graphical approach.

$$Tensile\ Stress = 0.8369 + 45.858 \cdot \mu - 2.4138 \cdot BQ$$

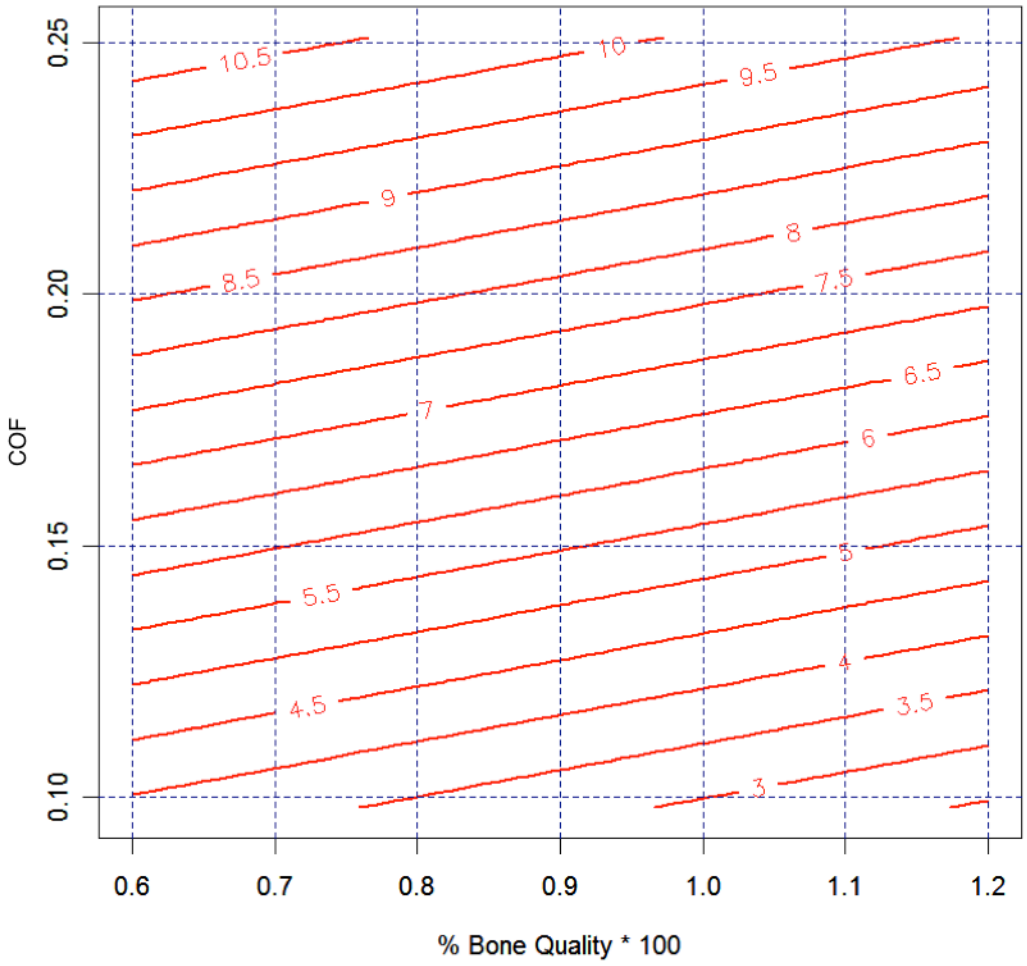

Figure 5.25. Two dimensional PMMA bone cement tensile stresses (MPa) due to walking for varying metal-on-metal friction coefficient and bone quality.

$$Shear\ Stress = 4.1256 + 40.2584 \cdot \mu - 3.055 \cdot BQ$$

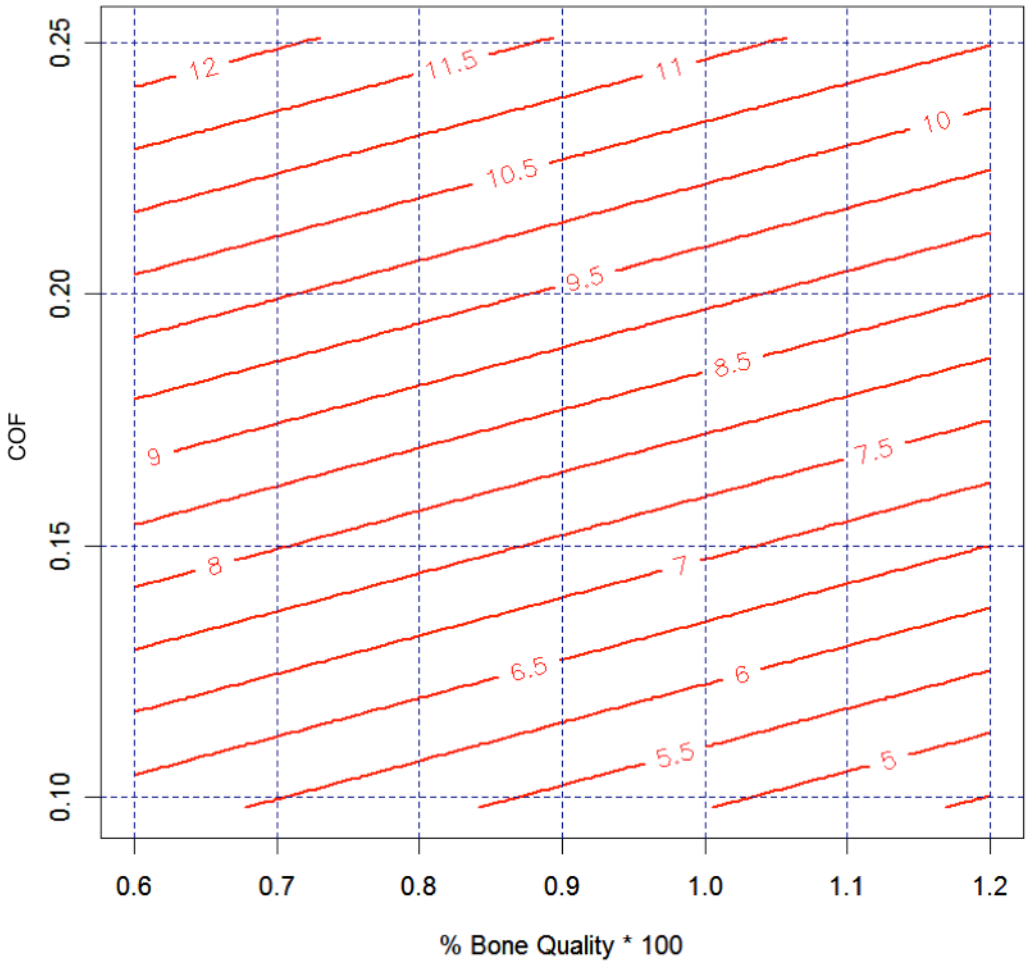

Figure 5.26. Two dimensional PMMA bone cement shear stresses (MPa) due to walking for varying metal-on-metal friction coefficient and bone quality.

Figures 5.27 and 5.28 show the PMMA maximum tensile and shear stresses during the whole walking gait for different metal-on-metal friction coefficients with 60% and 120% patient bone qualities. As observed previously in Figure 5.23 and 5.24, the increase of maximum tensile and shear stresses in the PMMA bone cement due to a reduction of patient bone quality is greater at higher levels of metal-on-metal friction coefficients.

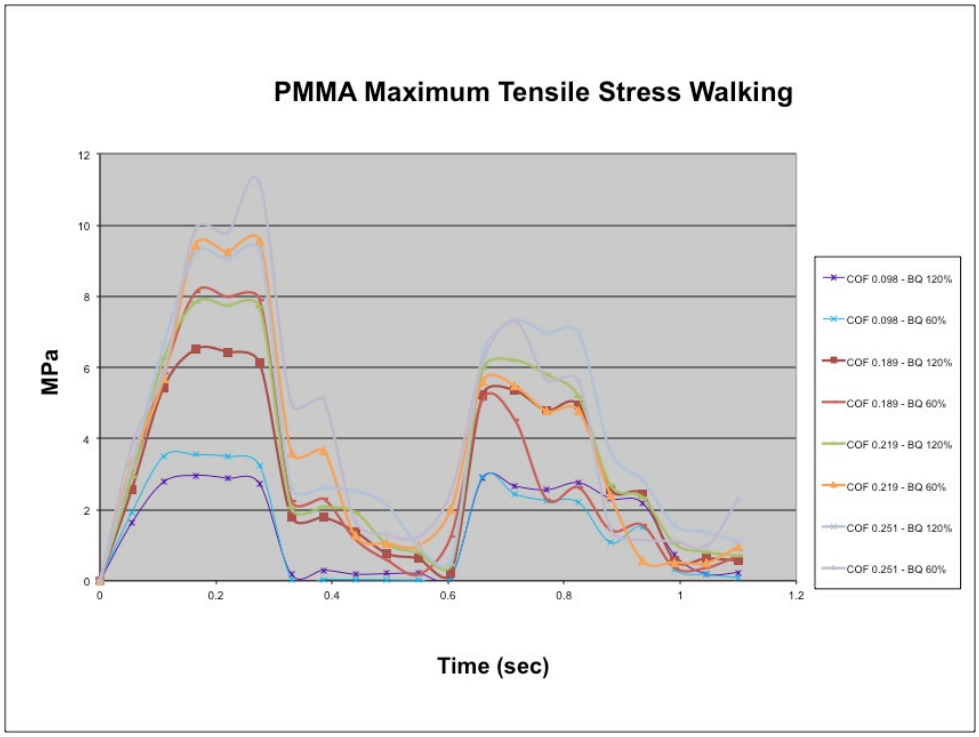

Figure 5.27. PMMA maximum tensile stresses during walking gait for different MoM friction coefficient and respective patient bone qualities 0f 60% and 120%.

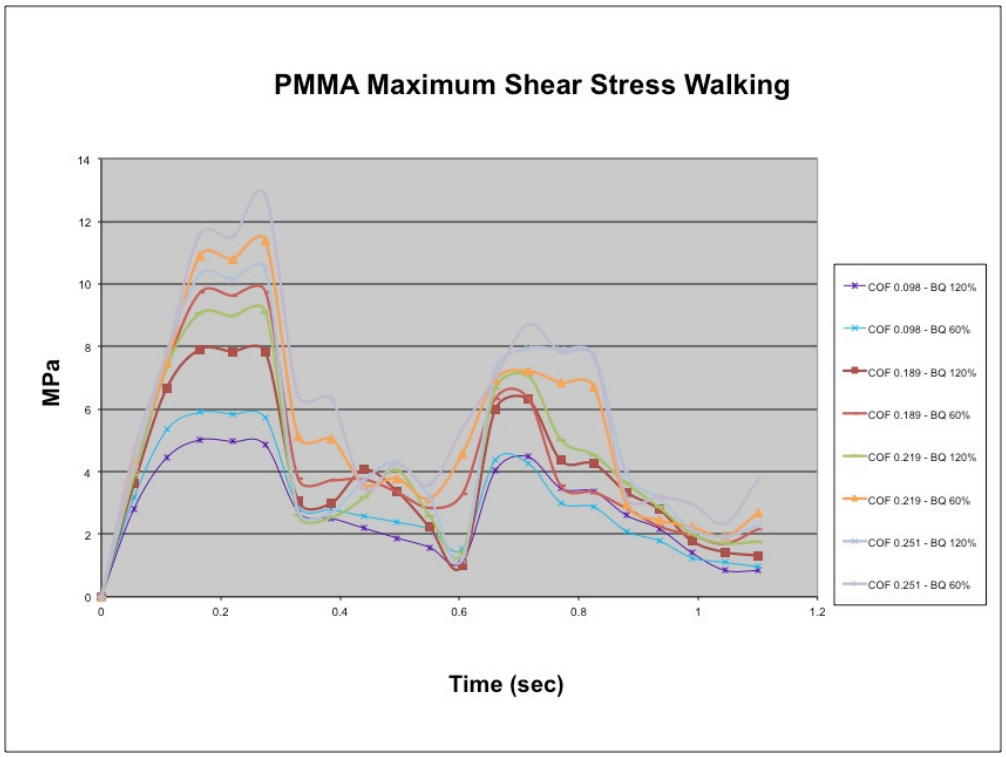

Figure 5.28. PMMA maximum shear stresses during walking gait for different MoM friction coefficient and respective patient bone qualities 0f 60% and 120%.

5.2.2 Finite Element Analysis results for descending stairs

Twelve Finite Element models were solved according to the metal-on-metal friction coefficient due to resting periods for descending stairs and simulated different bone quality as shown in Table 5.24. Following this approach, the study is not only a parametric varying just one variable but more of a multi-parametric approach due to the varying bone quality for every Finite Element model according to metal-on-metal friction due to resting periods.

Table 5.24. PMMA maximum tensile and shear stresses due to varying MoM friction coefficient and bone quality during descending stairs.

Everyday Activity	Metal-on-metal COF	Bone Quality	Tensile Stress (MPa)	Shear Stress (MPa)	Stress Equations
Descending Stairs	0.098	60%	3.44	5.32	Tensile Stress = -1.32 * BQ + 4.198
		80%	3.1	4.96	
		100%	2.86	4.67	Shear Stress = -1.435 * BQ + 6.144
		120%	2.64	4.46	
	0.189	60%	6.82	8.54	Tensile Stress = -1.82 * BQ + 7.998
		80%	6.68	8.01	
		100%	6.16	7.46	Shear Stress = -2.585 * BQ + 10.07
		120%	5.78	7	
	0.219	60%	7.96	9.39	Tensile Stress = -1.63 * BQ + 8.962
		80%	7.66	8.91	
		100%	7.4	8.49	Shear Stress = -2.31 * BQ + 10.77
		120%	6.96	7.99	

Figure 5.23 and 5.24 shows the comparison of PMMA maximum tensile and shear stresses for different metal-on-metal friction and patient bone quality as shown in Table 5.24.

As described in section 5.1.2 and Figures 5.6 and 5.7, maximum tensile and shear stresses in the PMMA bone cement occur at the prosthesis rim area for all Finite Element Analysis models.

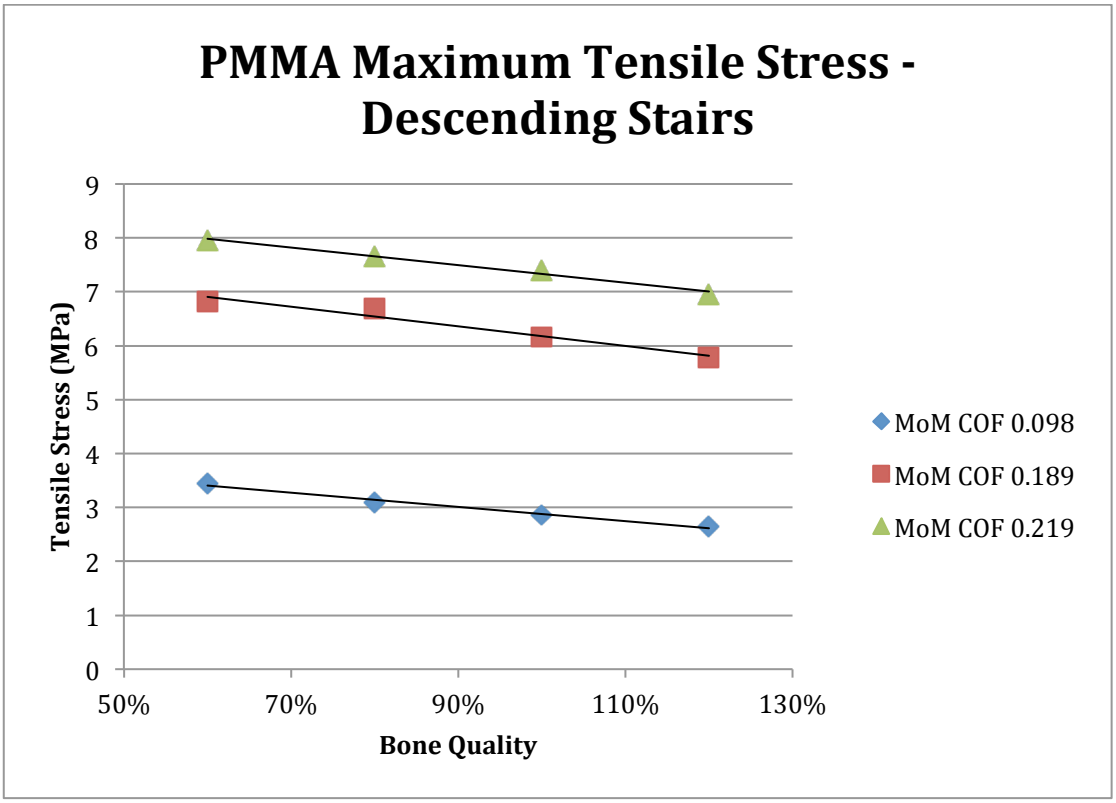

Figure 5.29. Comparison of PMMA maximum tensile stress (MPa) according to different metal-on-metal friction coefficients and patient bone quality during descending stairs.

From Figure 5.29, it can be observed that a decrease in patient bone quality has a greater effect at higher metal-on-metal friction coefficients producing higher maximum tensile stresses in the PMMA bone cement.

A similar effect on PMMA maximum shear stress values can be appreciated in Figure 5.30, higher metal-on-metal friction coefficients show greater maximum shear stresses in the PMMA bone cement when patient bone quality is reduced.

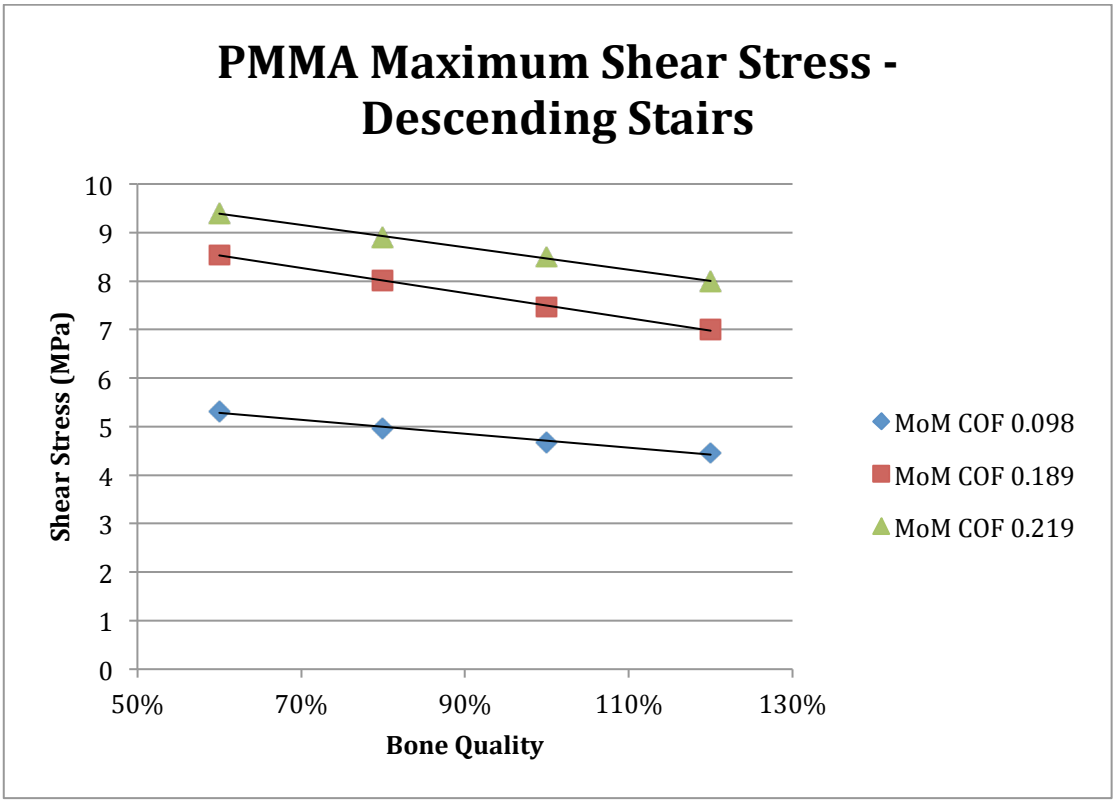

Figure 5.30. Comparison of PMMA maximum shear stress (MPa) according to different metal-on-metal friction coefficients and patient bone quality during descending stairs.

Figure 5.31 and 5.32 show a different approach to deducting maximum tensile and shear stresses in PMMA bone cement for descending stairs due to metal-on-metal friction and bone quality using a two dimensional graphical approach.

$$Tensile\ Stress = 0.8108 + 37.0072 \cdot \mu - 1.59 \cdot BQ$$

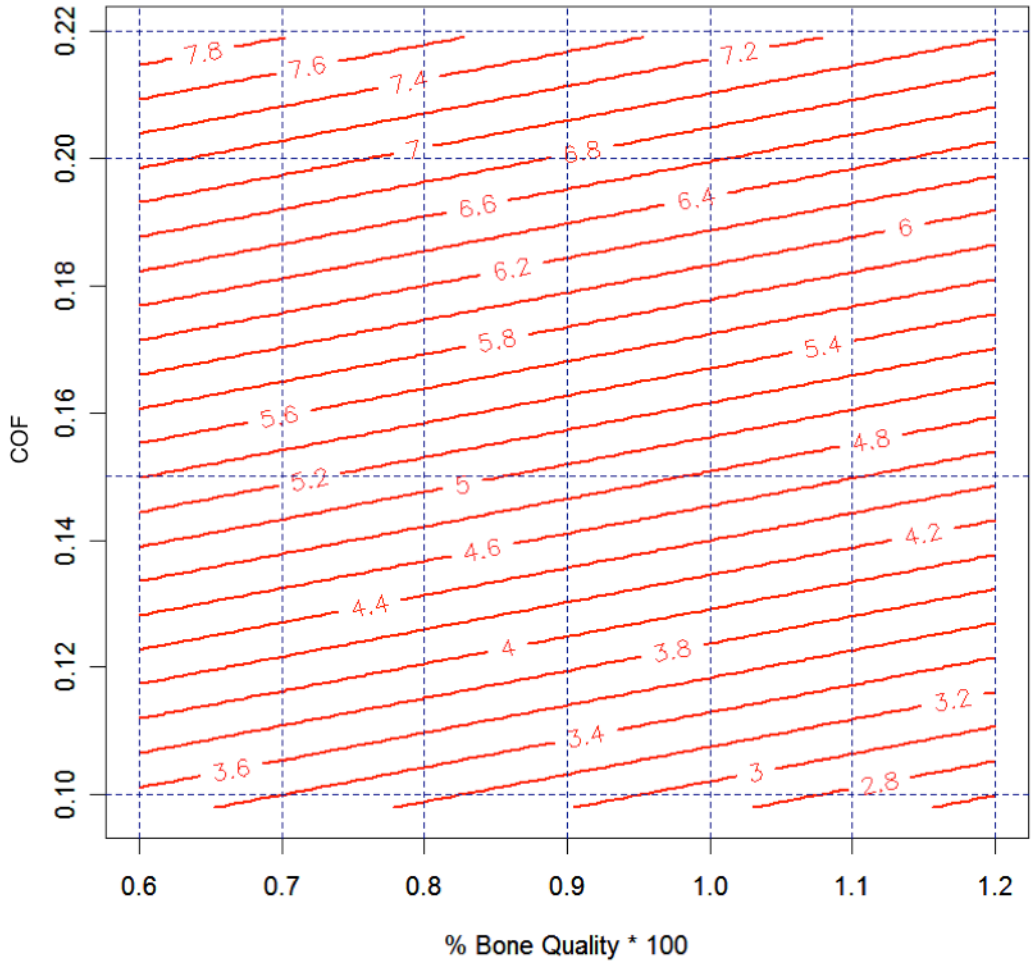

Figure 5.31. Two dimensional PMMA bone cement tensile stresses (MPa) due to descending stairs for varying metal-on-metal friction coefficient and bone quality.

$$Shear\ Stress = 3.6384 + 31.7823 \cdot \mu - 2.11 \cdot BQ$$

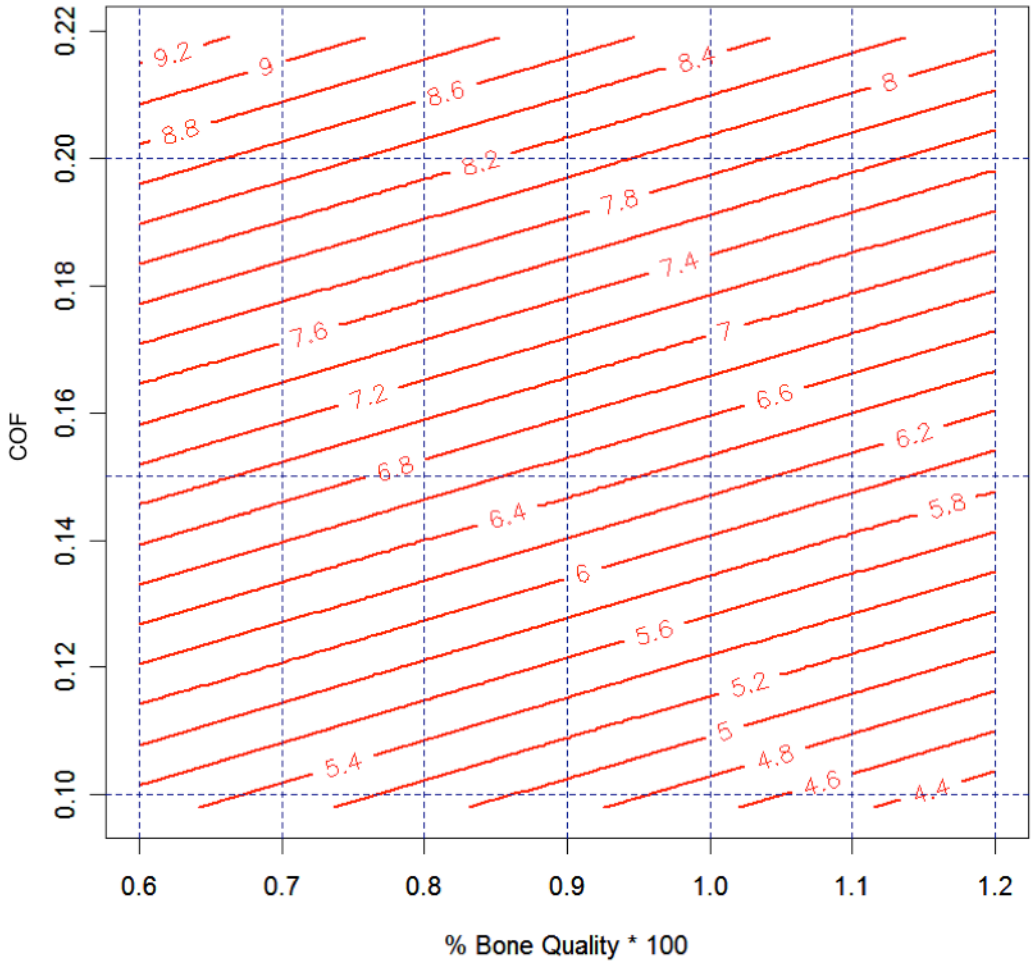

Figure 5.32. Two dimensional PMMA bone cement shear stresses (MPa) due to descending stairs for varying metal-on-metal friction coefficient and bone quality.

Figures 5.33 and 5.34 show the PMMA maximum tensile and shear stresses during the whole descending stairs cycle for different metal-on-metal friction coefficients with 60% and 120% patient bone qualities. As observed previously in Figure 5.29 and 5.30, the increase of maximum tensile and shear stresses in the PMMA bone cement due to a reduction of patient bone quality is greater at higher levels of metal-on-metal friction coefficients.

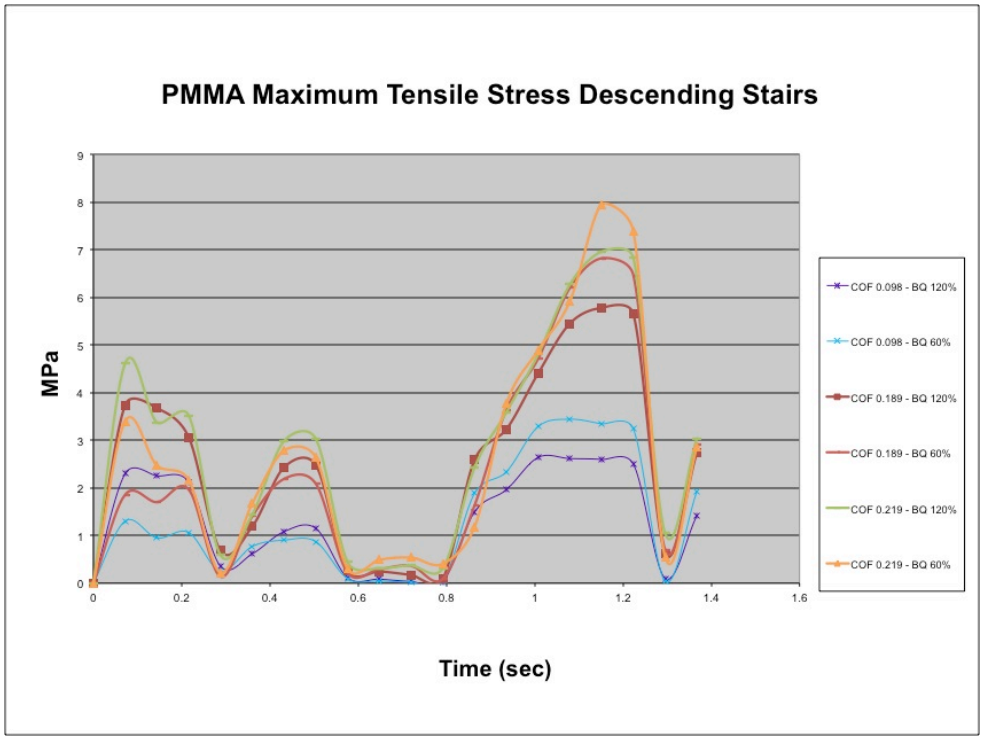

Figure 5.33. PMMA maximum tensile stresses during descending stairs for different MoM friction coefficient and respective patient bone qualities of 60% and 120%.

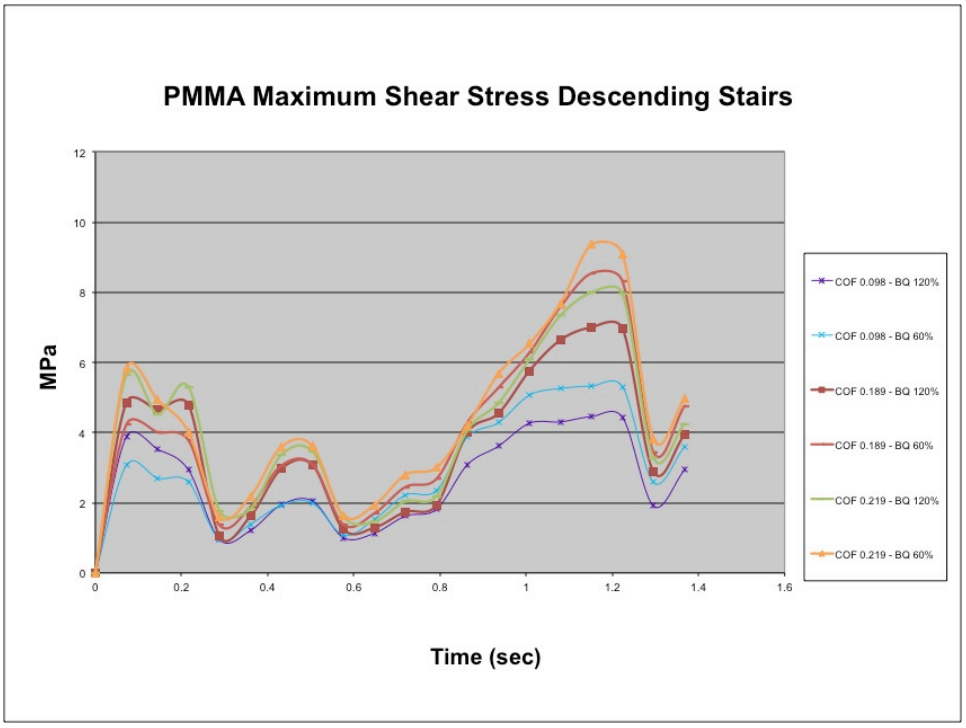

Figure 5.34. PMMA maximum shear stresses during descending stairs for different MoM friction coefficient and respective patient bone qualities of 60% and 120%.

5.2.3 Finite Element Analysis results for standing up

Eight Finite Element models were solved according to the metal-on-metal friction coefficient due to resting periods for standing up and simulated different bone quality as shown in Table 5.25. Following this approach, the study is not only a parametric varying just one variable but more of a multi-parametric approach due to the varying bone quality for every Finite Element model according to metal-on-metal friction due to resting periods.

Table 5.25. PMMA maximum tensile and shear stresses due to varying MoM friction coefficient and bone quality during standing up.

Everyday Activity	Metal-on-metal COF	Bone Quality	Tensile Stress (MPa)	Shear Stress (MPa)	Stress Equations
Standing Up	0.098	60%	2.67	4.22	Tensile Stress = -1.045 * BQ + 3.328
		80%	2.33	3.81	
		100%	2.16	3.61	Shear Stress = -1.285 * BQ + 4.924
		120%	2.03	3.43	
	0.285	60%	10.3	11.2	Tensile Stress = -4.14 * BQ + 12.681
		80%	9.29	10.2	
		100%	8.39	9.36	Shear Stress = -4.305 * BQ + 13.717
		120%	7.84	8.61	

Figure 5.35 and 5.36 shows the comparison of PMMA maximum tensile and shear stresses for different metal-on-metal friction and patient bone quality as shown in Table 5.25.

As described in section 5.1.3 and Figures 5.10 and 5.11, maximum tensile and shear stresses in the PMMA bone cement occur at the prosthesis rim area for all Finite Element Analysis models.

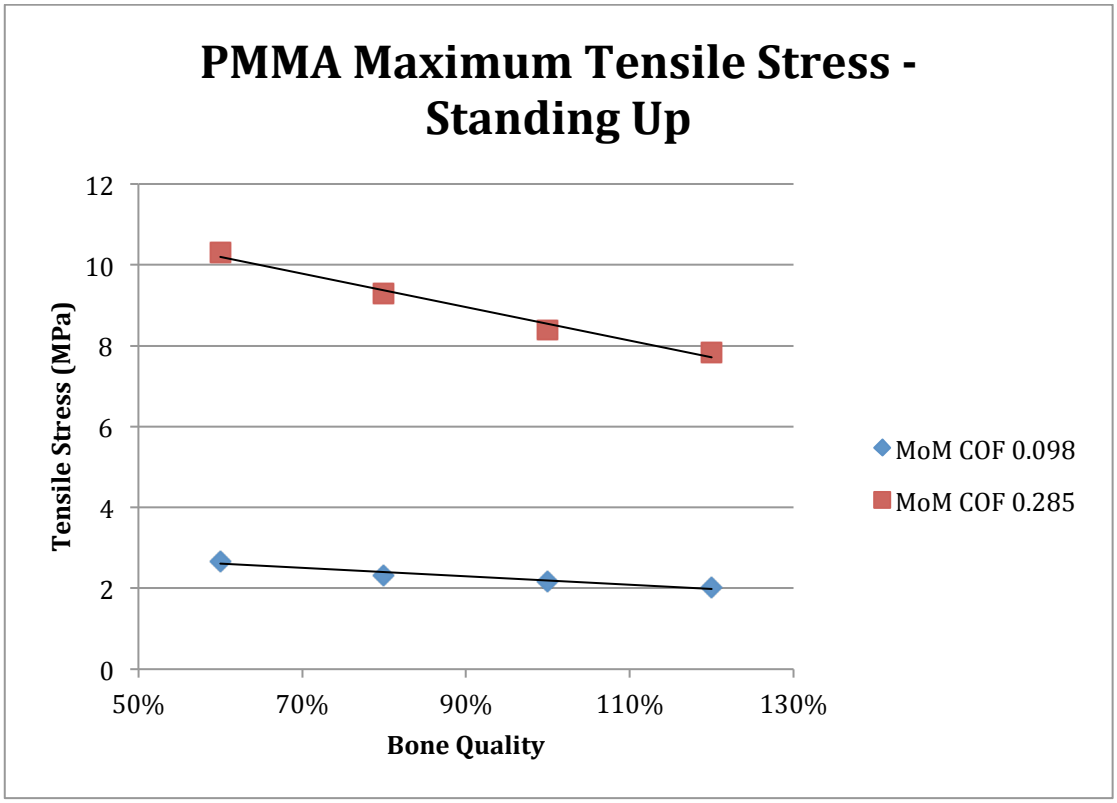

Figure 5.35. Comparison of PMMA maximum tensile stress (MPa) according to different metal-on-metal friction coefficients and patient bone quality during standing up.

From Figure 5.35, it can be observed that a decrease in patient bone quality has a greater effect at a metal-on-metal friction coefficient of 0.251 producing higher maximum tensile stresses in the PMMA bone cement than at dynamic metal-on-metal friction coefficient of 0.098.

A similar effect on PMMA maximum shear stress values can be appreciated in Figure 5.36, higher metal-on-metal friction coefficients show greater maximum shear stresses in the PMMA bone cement when patient bone quality is reduced.

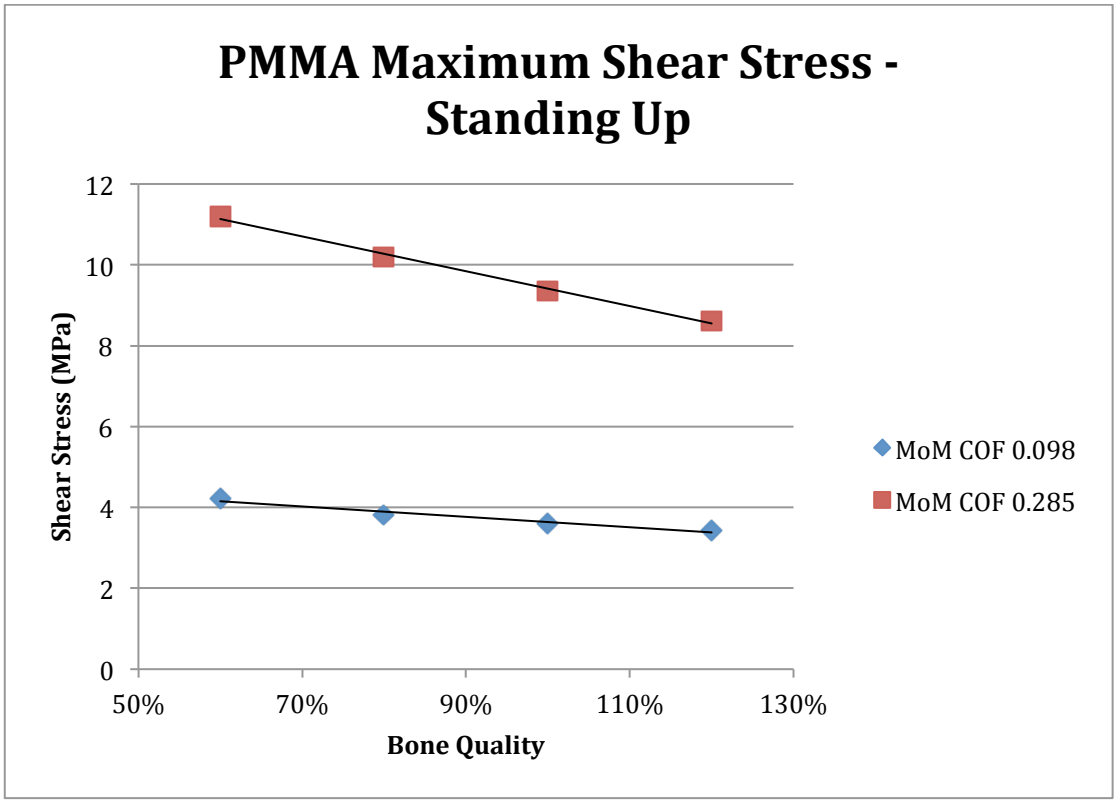

Figure 5.36. Comparison of PMMA maximum shear stress (MPa) according to different metal-on-metal friction coefficients and patient bone quality during standing up.

Figure 5.37 and 5.38 show a different approach to deducting maximum tensile and shear stresses in PMMA bone cement for standing up due to metal-on-metal friction and bone quality using a two dimensional graphical approach.

$$Tensile\ Stress = 1.1418 + 35.6016 \cdot \mu - 2.5925 \cdot BQ$$

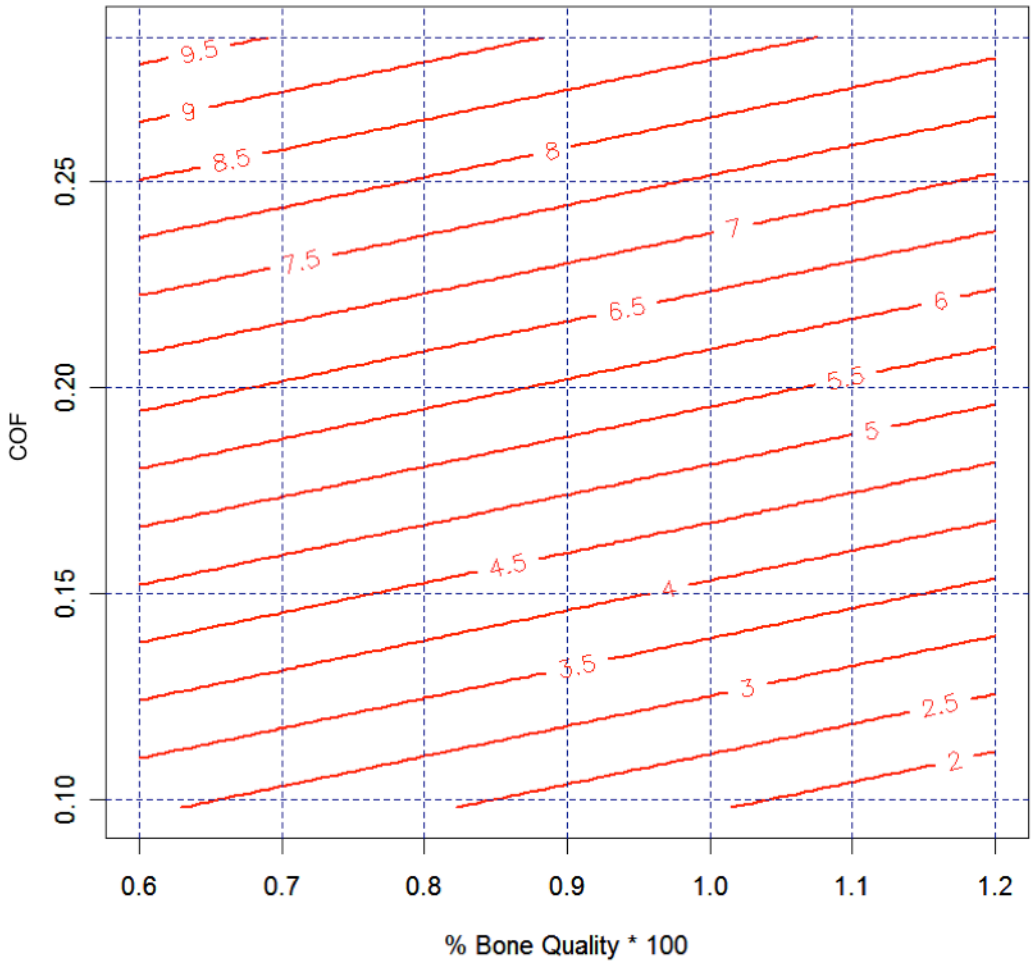

Figure 5.37. Two dimensional PMMA bone cement tensile stresses (MPa) due to descending stairs for varying metal-on-metal friction coefficient and bone quality.

$$Shear\ Stress = 3.0993 + 32.4866 \cdot \mu - 2.795 \cdot BQ$$

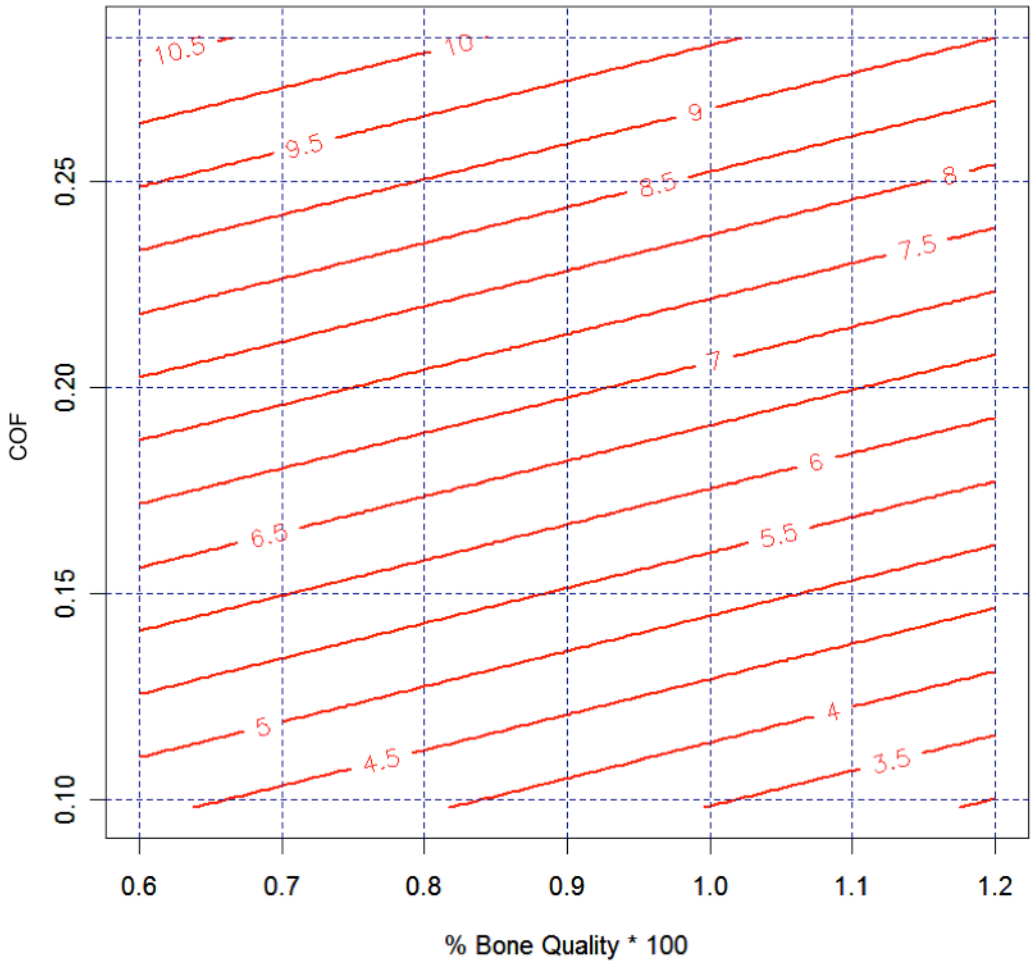

Figure 5.38. Two dimensional PMMA bone cement shear stresses (MPa) due to descending stairs for varying metal-on-metal friction coefficient and bone quality.

Figures 5.39 and 5.40 show the PMMA maximum tensile and shear stresses during the whole standing up cycle for different metal-on-metal friction coefficients with 60% and 120% patient bone qualities. As observed previously in Figures 5.35 and 5.36, the increase of maximum tensile and shear stresses in the PMMA bone cement due to a reduction of patient bone quality is greater at higher levels of metal-on-metal friction coefficients.

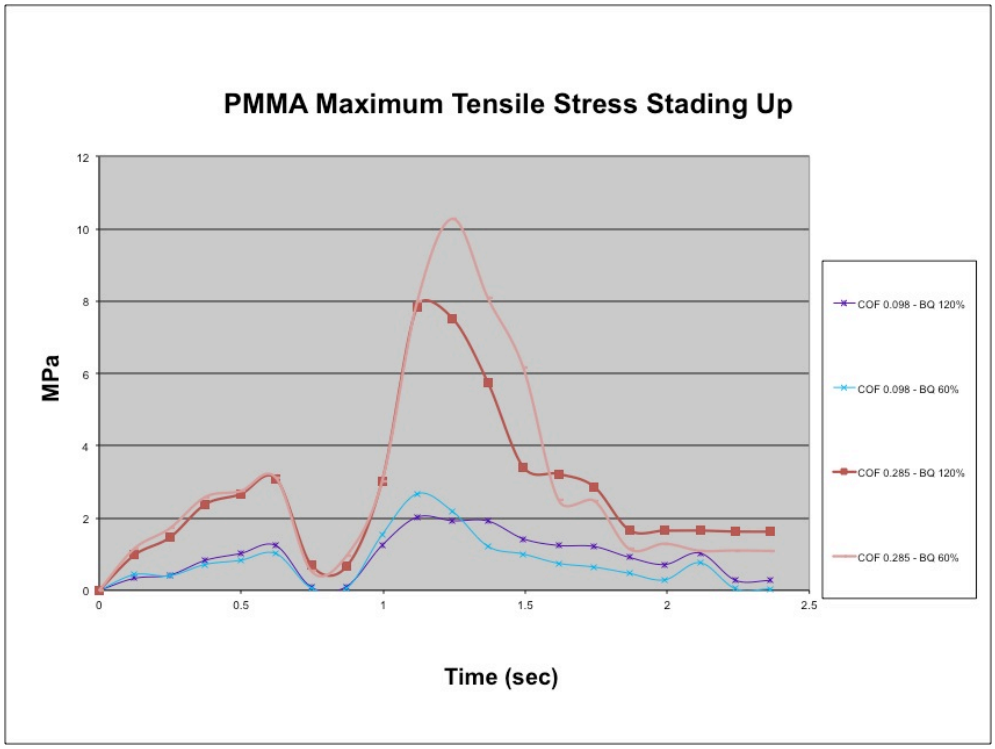

Figure 5.39. PMMA maximum tensile stresses during standing up for different MoM friction coefficient and respective patient bone qualities of 60% and 120%.

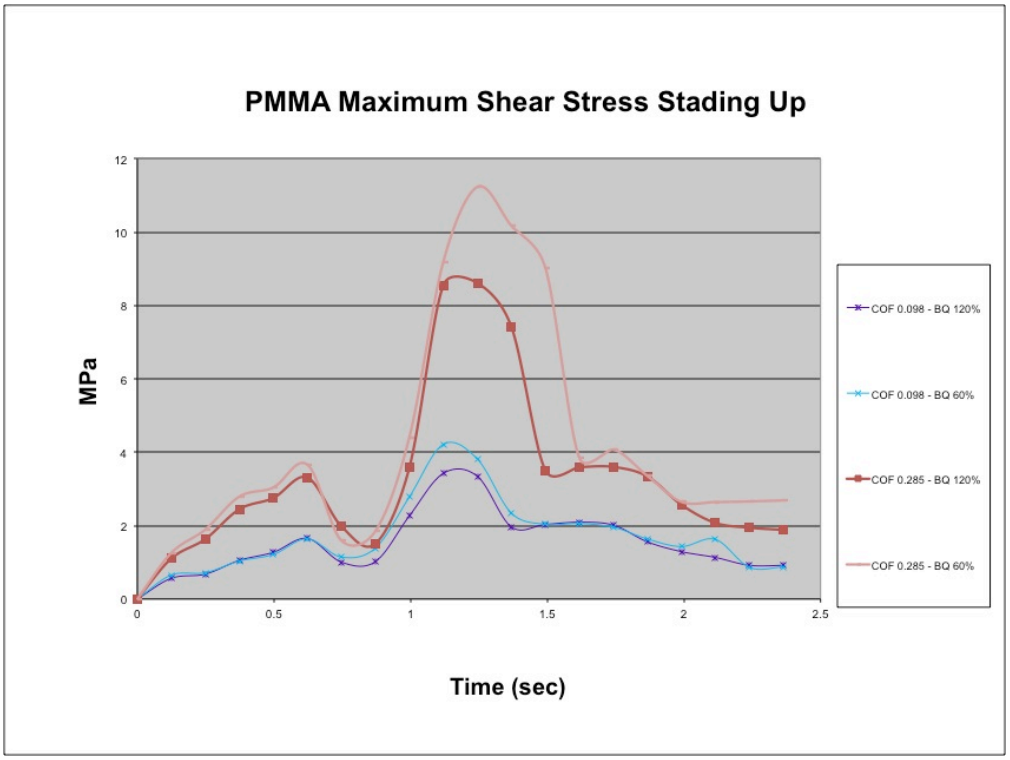

Figure 5.40. PMMA maximum tensile stresses during standing up for different MoM friction coefficient and respective patient bone qualities of 60% and 120%.

5.3 Effect of PMMA Young's Modulus on PMMA Bone Cement Stresses

As it was presented in Section 4.1.5.2, the Young's modulus value for PMMA bone cement used in Finite Element Analysis varies between 1 GPa and 4 GPa (Schmoelz, 2001) while PMMA bone cement Young's modulus through mechanical testing varies between 1.5 GPa and 4.1 GPa (Lewis, 1997).

Different manufacturers of PMMA bone cement produce different mechanical properties and Young's modulus due to the use of slightly different constituents and molecular weight. Furthermore, the same model of hip resurfacing arthroplasty will be fixed with different PMMA bone cement by different surgeons performing the operation and hence producing different PMMA mechanical properties.

The Finite Element model developed in Chapter 4 was used to assess the effect of PMMA bone cement Young's modulus according to bone quality and resting periods during everyday activities.

Every Finite Element model simulated in Section 5.2, and consequently in Section 5.1, was analysed simulating a PMMA bone cement Young's modulus of 2.75 GPa, 2 GPa and 1.25 GPa.

5.3.1 Finite Element Analysis results for walking

Forty-eight Finite Element models were solved according to the metal-on-metal friction coefficient due to resting periods for walking, simulated different bone quality and PMMA bone cement Young's modulus. Following this approach, the study is not simply parametric (with one variable) but allows a multi-parametric approach involving different PMMA young's modulus for varying bone quality whilst every Finite Element model is also varied according to metal-on-metal friction due to resting periods.

The maximum tensile and shear stresses can be calculated according to the metal-on-metal friction, bone quality of the patient and PMMA bone cement Young's modulus as:

$$Tensile\ Stress = -2.3129 + 44.9284 \cdot \mu - 2.3933 \cdot BQ + 1.5712 \cdot E_{PMMA}$$

$$Shear\ Stress = -0.2611 + 39.2683 \cdot \mu - 2.9625 \cdot BQ + 2.1425 \cdot E_{PMMA}$$

To facilitate a much better graphical display of the results, the bone quality will be fixed in the intervals of 60%, 80%, 100% and 120%.

Figures 5.41 to 5.44 show predicting graphs to calculate tensile stresses in PMMA bone cement according to metal-on-metal friction and PMMA bone cement Young's modulus.

$$Tensile\ Stress = -3.7489 + 44.9284 \cdot \mu - 2.3933 \cdot BQ + 1.5712 \cdot E_{PMMA} \Rightarrow 60\%\ BQ$$

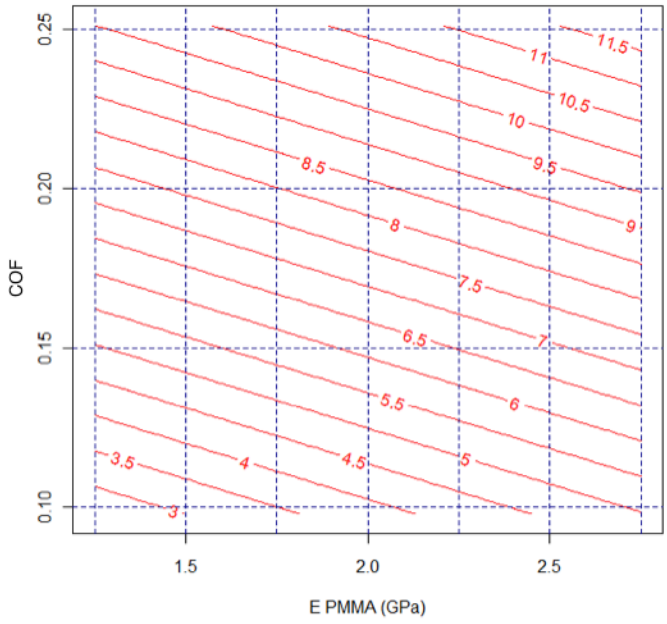

Figure 5.41. Two dimensional PMMA bone cement tensile stresses (MPa) due to walking for varying metal-on-metal friction coefficient and PMMA Young's modulus for 60% bone quality.

$$Tensile\ Stress = -4.2275 + 44.9284 \cdot \mu - 2.3933 \cdot BQ + 1.5712 \cdot E_{PMMA} \Rightarrow 80\%\ BQ$$

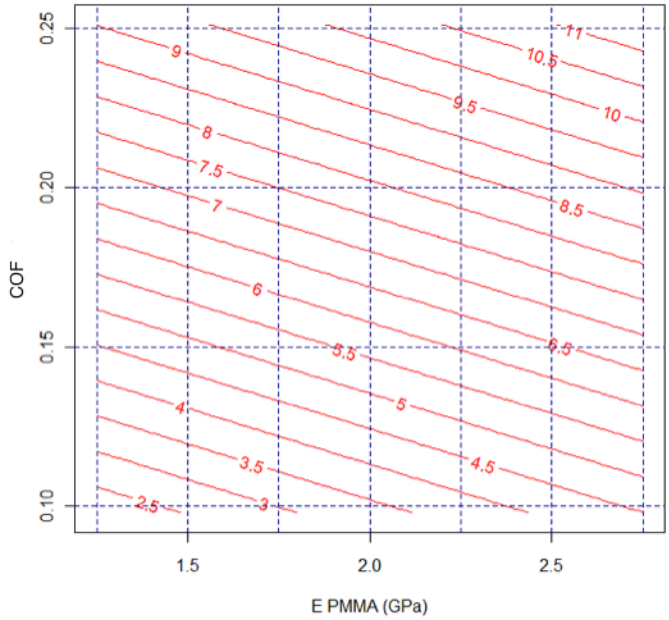

Figure 5.42. Two dimensional PMMA bone cement tensile stresses (MPa) due to walking for varying metal-on-metal friction coefficient and PMMA Young's modulus for 80% bone quality.

$$Tensile\ Stress = -4.7062 + 44.9284 \cdot \mu - 2.3933 \cdot BQ + 1.5712 \cdot E_{PMMA} \Rightarrow 100\%\ BQ$$

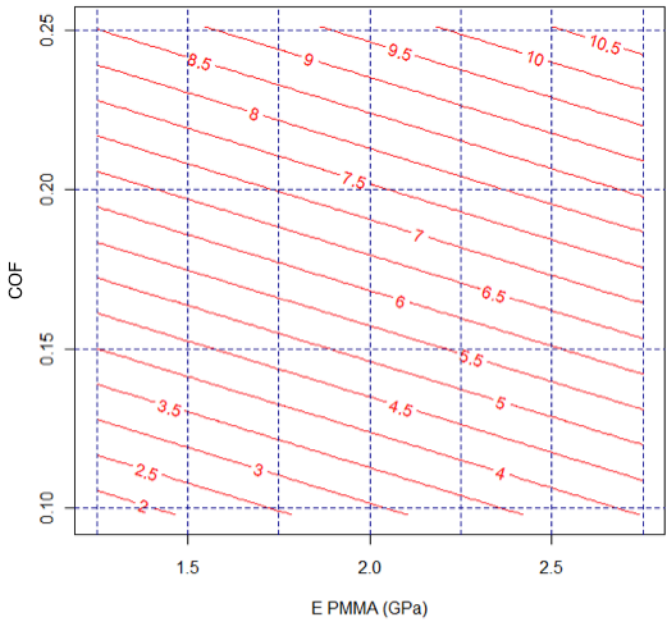

Figure 5.43. Two dimensional PMMA bone cement tensile stresses (MPa) due to walking for varying metal-on-metal friction coefficient and PMMA Young's modulus for 100% bone quality.

$$Tensile\ Stress = -5.1849 + 44.9284 \cdot \mu - 2.3933 \cdot BQ + 1.5712 \cdot E_{PMMA} \Rightarrow 120\%\ BQ$$

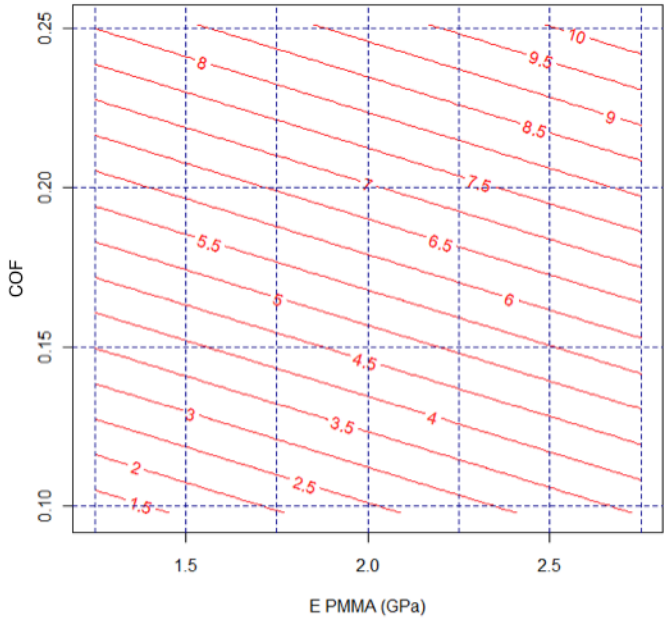

Figure 5.44. Two dimensional PMMA bone cement tensile stresses (MPa) due to walking for varying metal-on-metal friction coefficient and PMMA Young's modulus for 120% bone quality.

Figures 5.45 to 5.48 show predicting graphs to calculate shear stresses in PMMA bone cement according to metal-on-metal friction and PMMA bone cement Young's modulus.

$$Shear\ Stress = -2.0386 + 39.2683 \cdot \mu - 2.9625 \cdot BQ + 2.1425 \cdot E_{PMMA} \Rightarrow 60\%\ BQ$$

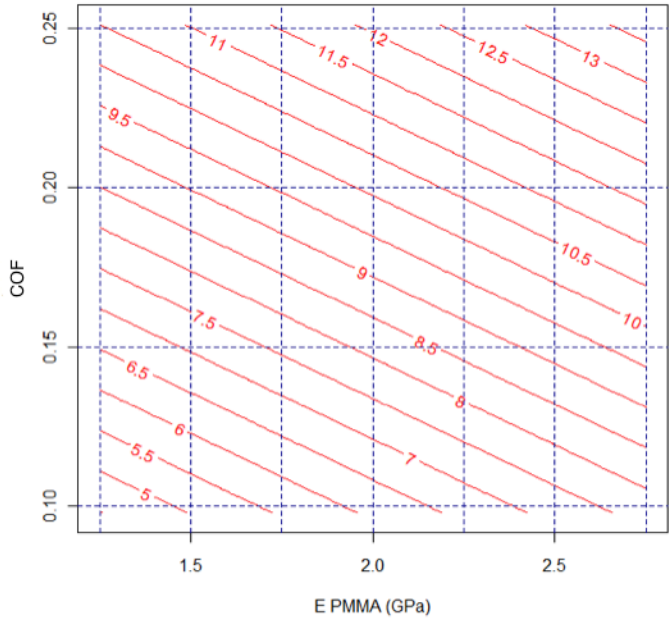

Figure 5.45. Two dimensional PMMA bone cement shear stresses (MPa) due to walking for varying metal-on-metal friction coefficient and PMMA Young's modulus for 60% bone quality.

$$Shear\ Stress = -2.6311 + 39.2683 \cdot \mu - 2.9625 \cdot BQ + 2.1425 \cdot E_{PMMA} \Rightarrow 80\%\ BQ$$

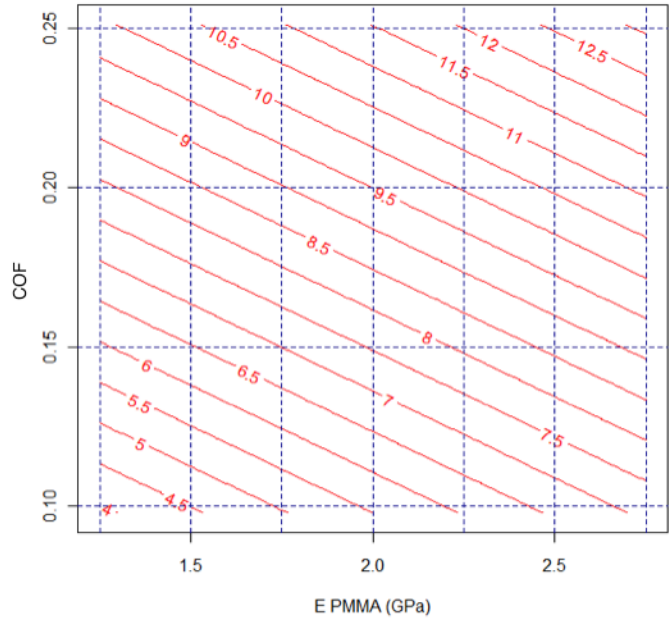

Figure 5.46. Two dimensional PMMA bone cement shear stresses (MPa) due to walking for varying metal-on-metal friction coefficient and PMMA Young's modulus for 80% bone quality.

$$Shear\ Stress = -3.2236 + 39.2683 \cdot \mu - 2.9625 \cdot BQ + 2.1425 \cdot E_{PMMA} \Rightarrow 100\%\ BQ$$

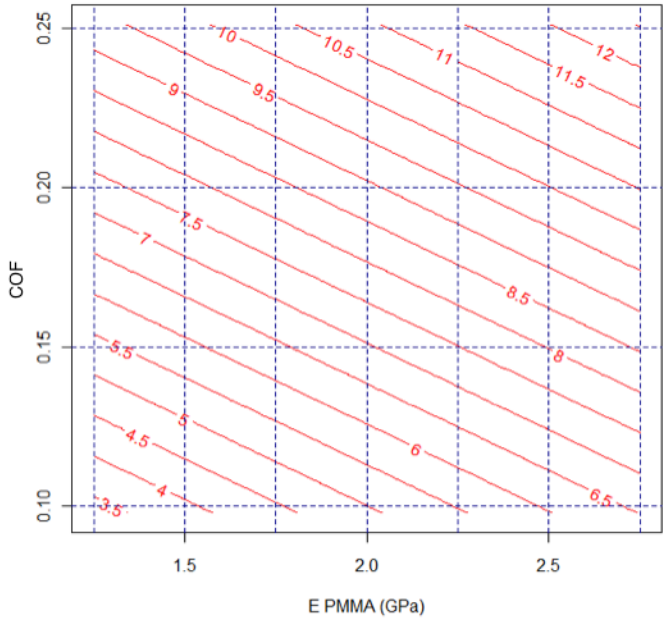

Figure 5.47. Two dimensional PMMA bone cement shear stresses (MPa) due to walking for varying metal-on-metal friction coefficient and PMMA Young's modulus for 100% bone quality.

$$Shear\ Stress = -3.8161 + 39.2683 \cdot \mu - 2.9625 \cdot BQ + 2.1425 \cdot E_{PMMA} \Rightarrow 120\%\ BQ$$

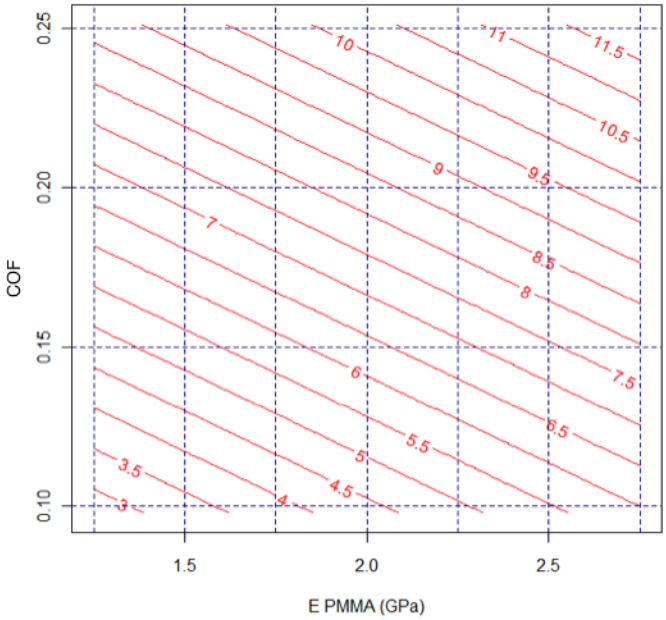

Figure 5.48. Two dimensional PMMA bone cement shear stresses (MPa) due to walking for varying metal-on-metal friction coefficient and PMMA Young's modulus for 120% bone quality.

Table 5.26 presents the comparison of maximum tensile and shear stresses in the PMMA bone cement according to varying metal-on-metal friction, patient bone quality and PMMA Young's modulus. Furthermore, Table 5.26 shows the equations to predict maximum tensile and shear PMMA bone cement stresses according to the parameters previously mentioned.

Table 5.26. PMMA tensile and shear stresses due to varying MoM friction coefficient, bone quality and PMMA Young's modulus during walking.

Everyday Activity	Metal-on-metal COF	Bone Quality	E_{PMMA} (Gpa)	Tensile Stress (Mpa)	Shear Stress (Mpa)	Stress Equations
Walking	0.098	60%	1.25	2.92	4.85	Tensile Stress = 0.686 * E_{PMMA} + 2.1
			2	3.55	5.9	Shear Stress = 1.14 * E_{PMMA} + 3.49
			2.75	3.95	6.56	
		80%	1.25	2.65	4.42	Tensile Stress = 0.686 * E_{PMMA} + 1.82
			2	3.25	5.53	Shear Stress = 1.226 * E_{PMMA} + 2.95
			2.75	3.68	6.26	
		100%	1.25	2.55	4.1	Tensile Stress = 0.633 * E_{PMMA} + 1.793
			2	3.13	5.25	Shear Stress = 1.293 * E_{PMMA} + 2.543
			2.75	3.5	6.04	
		120%	1.25	2.36	3.87	Tensile Stress = 0.693 * E_{PMMA} + 1.52
			2	2.96	5.02	Shear Stress = 1.326 * E_{PMMA} + 2.263
			2.75	3.4	5.86	
	0.189	60%	1.25	6.72	8.01	Tensile Stress = 1.14 * E_{PMMA} + 5.476
			2	8.12	9.75	Shear Stress = 1.926 * E_{PMMA} + 5.7
			2.75	8.43	10.9	
		80%	1.25	5.91	7.17	Tensile Stress = 1.446 * E_{PMMA} + 4.236
			2	7.4	8.99	Shear Stress = 1.953 * E_{PMMA} + 4.846
			2.75	8.08	10.1	
		100%	1.25	5.43	6.55	Tensile Stress = 1.573 * E_{PMMA} + 3.53
			2	6.81	8.34	Shear Stress = 2.053 * E_{PMMA} + 4.066
			2.75	7.79	9.63	
		120%	1.25	5.08	6.05	Tensile Stress = 1.646 * E_{PMMA} + 3.086
			2	6.51	7.91	Shear Stress = 2.126 * E_{PMMA} + 3.48
			2.75	7.55	9.24	
	0.219	60%	1.25	8.15	9.16	Tensile Stress = 1.766 * E_{PMMA} + 5.073
			2	9.57	11.4	Shear Stress = 2.36 * E_{PMMA} + 6.366
			2.75	10.8	12.7	
		80%	1.25	7.28	8.3	Tensile Stress = 1.88 * E_{PMMA} + 4.96
			2	8.78	10.4	Shear Stress = 2.4 * E_{PMMA} + 5.4
			2.75	10.1	11.9	
		100%	1.25	6.53	7.58	Tensile Stress = 1.92 * E_{PMMA} + 4.263
			2	8.37	9.72	Shear Stress = 2.413 * E_{PMMA} + 4.673
			2.75	9.41	11.2	
		120%	1.25	6.1	6.99	Tensile Stress = 1.866 * E_{PMMA} + 3.876
			2	7.83	9.11	Shear Stress = 2.406 * E_{PMMA} + 4.086
			2.75	8.9	10.6	
	0.251	60%	1.25	8.97	10.1	Tensile Stress = 2.553 * E_{PMMA} + 5.883
			2	11.2	12.8	Shear Stress = 3 * E_{PMMA} + 6.5
			2.75	12.8	14.6	
		80%	1.25	8.68	9.43	Tensile Stress = 2.28 * E_{PMMA} + 5.933
			2	10.7	12.1	Shear Stress = 2.98 * E_{PMMA} + 5.85
			2.75	12.1	13.9	
		100%	1.25	7.98	8.67	Tensile Stress = 2.213 * E_{PMMA} + 5.333
			2	10	11.2	Shear Stress = 2.82 * E_{PMMA} + 5.283
			2.75	11.3	12.9	
		120%	1.25	7.37	8.02	Tensile Stress = 2.153 * E_{PMMA} + 4.786
			2	9.31	10.5	Shear Stress = 2.853 * E_{PMMA} + 4.566
			2.75	10.6	12.3	

Figure 5.49 and 5.50 shows the comparison of PMMA tensile and shear stresses for different metal-on-metal friction, patient bone quality and PMMA Young's modulus as shown in Table 5.26.

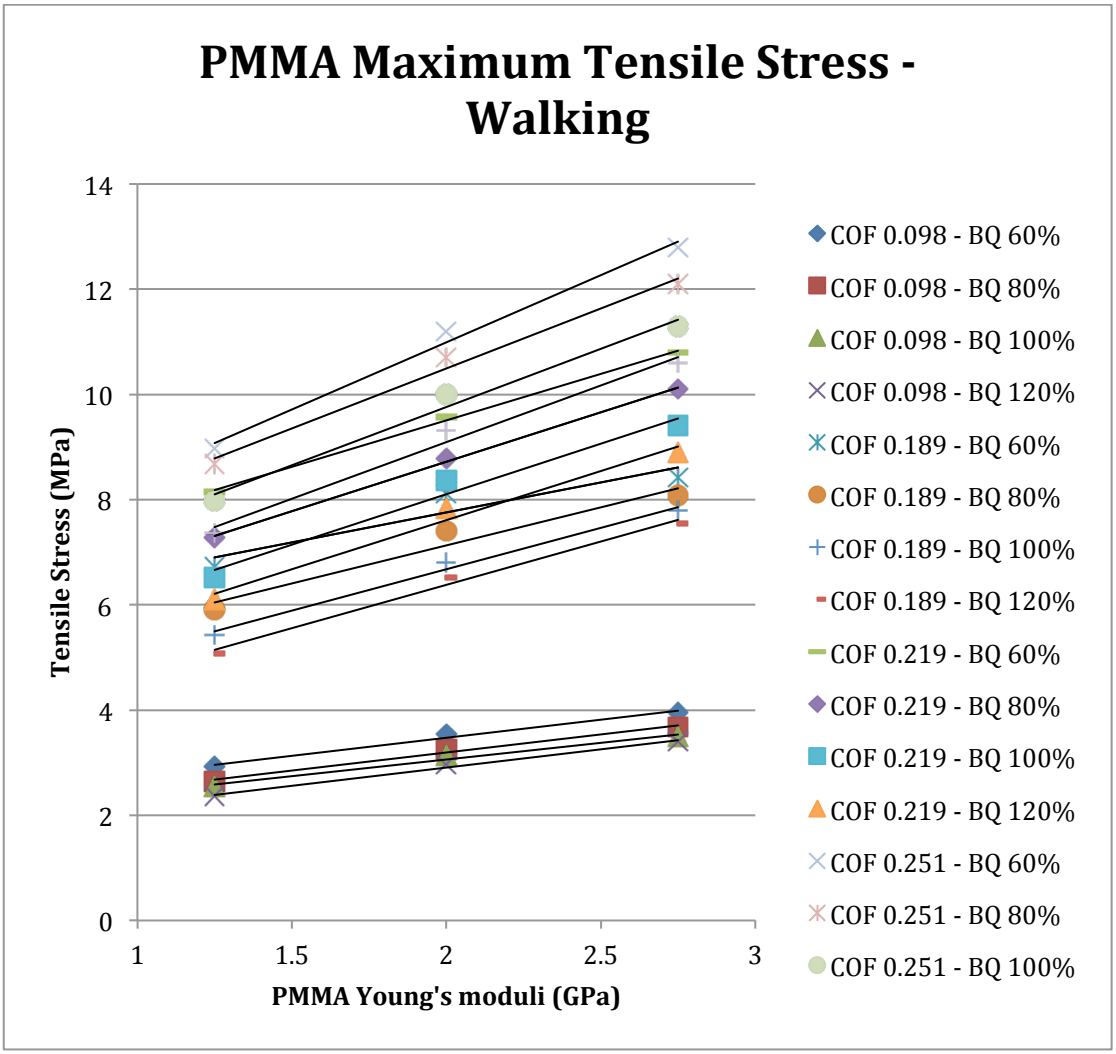

Figure 5.49. Comparison of PMMA tensile stress (MPa) according to different metal-on-metal friction coefficients, patient bone quality and PMMA Young's modulus during walking.

From Figure 5.49, it can be observed that a decrease in PMMA Young's Modulus produces a decrease in maximum tensile stresses in the PMMA bone cement, and this reduction is more accentuated at higher metal-on-metal friction coefficient and lower patient bone quality.

A similar effect on PMMA maximum shear stress values can be appreciated in Figure 5.50, lower PMMA Young's Modulus for higher metal-on-metal friction coefficients and lower patient bone quality show a greater reduction on maximum shear stresses in the PMMA bone cement.

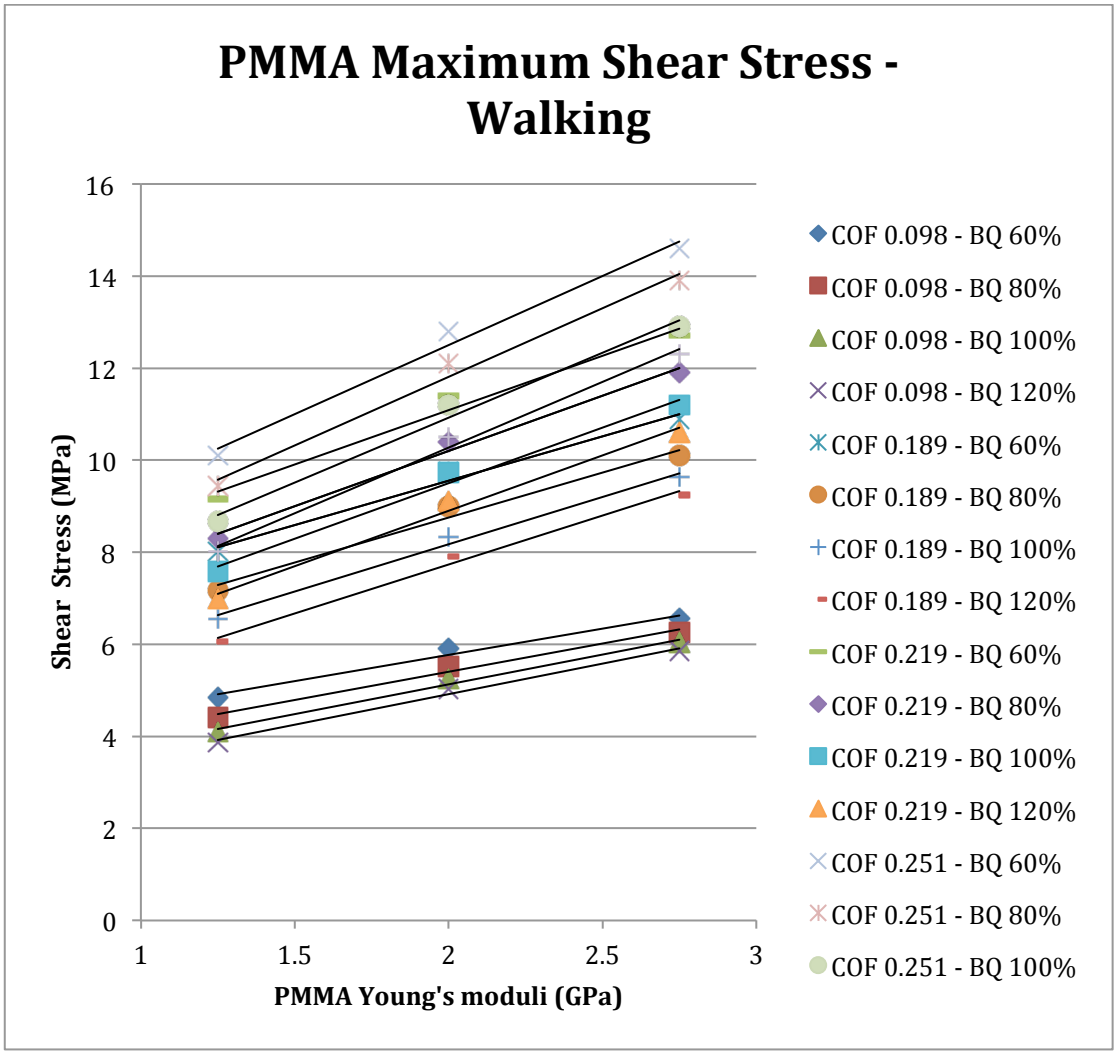

Figure 5.50. Comparison of PMMA shear stress (MPa) according to different metal-on-metal friction coefficients, patient bone quality and PMMA Young's modulus during walking.

5.3.2 Finite Element Analysis results for descending stairs

Thirty-six Finite Element models were solved according to the metal-on-metal friction coefficient due to resting periods for descending stairs, simulated different bone quality and PMMA bone cement Young's modulus. Following this approach, the study is not simply parametric (with one variable) but allows a multi-parametric approach involving different PMMA young's modulus for varying bone quality whilst every Finite Element model is also varied according to metal-on-metal friction due to resting periods.

The maximum tensile and shear stresses can be calculated according to the metal-on-metal friction, bone quality of the patient and PMMA bone cement Young's modulus as:

$$Tensile\ Stress = -1.83884 + 35.64727 \cdot \mu - 1.555 \cdot BQ + 1.35278 \cdot E_{PMMA}$$

$$Shear\ Stress = -0.21689 + 30.59158 \cdot \mu - 2.05556 \cdot BQ + 1.69833 \cdot E_{PMMA}$$

To facilitate a much better graphical display of the results, the bone quality will be fixed in the intervals of 60%, 80%, 100% and 120%.

Figures 5.51 to 5.54 show predicting graphs to calculate tensile stresses in PMMA bone cement according to metal-on-metal friction and PMMA bone cement Young's modulus.

$$Tensile\ Stress = -2.7718 + 35.64727 \cdot \mu + 1.35278 \cdot E_{PMMA} \Rightarrow 60\%\ BQ$$

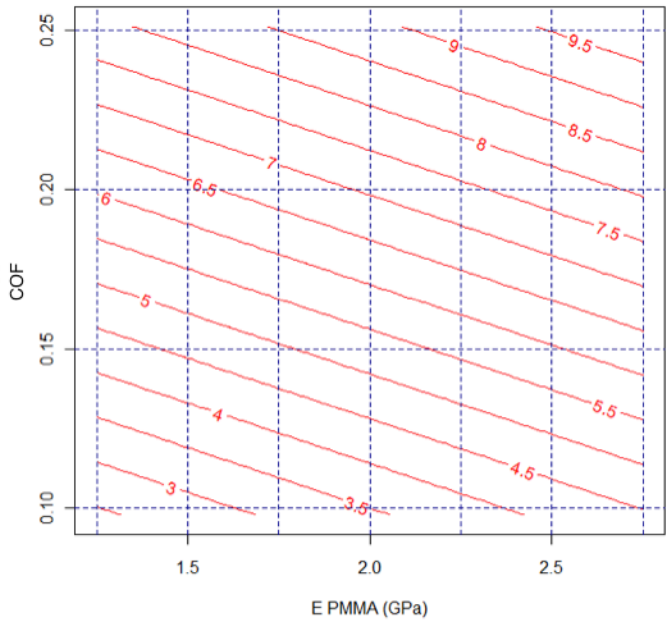

Figure 5.51. Two dimensional PMMA bone cement tensile stresses (MPa) due to descending stairs for varying metal-on-metal friction coefficient and PMMA Young's modulus for 60% bone quality.

$$Tensile\ Stress = -3.0828 + 35.64727 \cdot \mu + 1.35278 \cdot E_{PMMA} \Rightarrow 80\%\ BQ$$

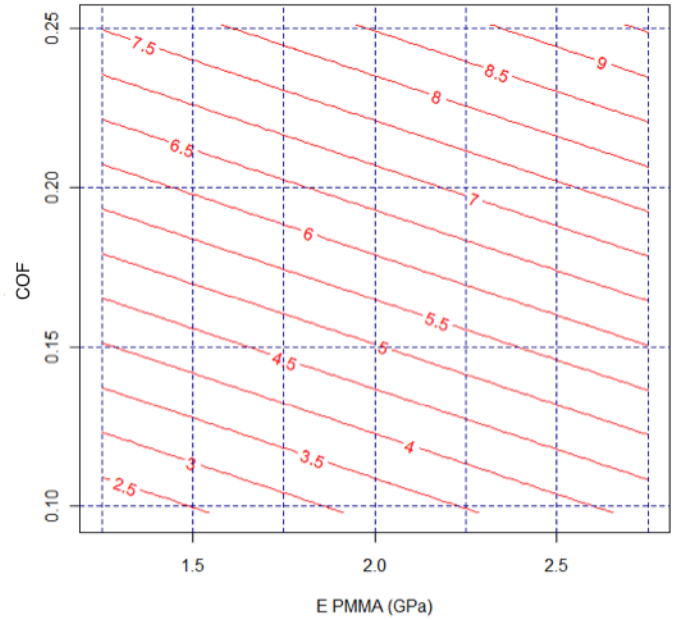

Figure 5.52. Two dimensional PMMA bone cement tensile stresses (MPa) due to descending stairs for varying metal-on-metal friction coefficient and PMMA Young's modulus for 80% bone quality.

$$Tensile\ Stress = -3.3938 + 35.64727 \cdot \mu + 1.35278 \cdot E_{PMMA} \Rightarrow 100\%\ BQ$$

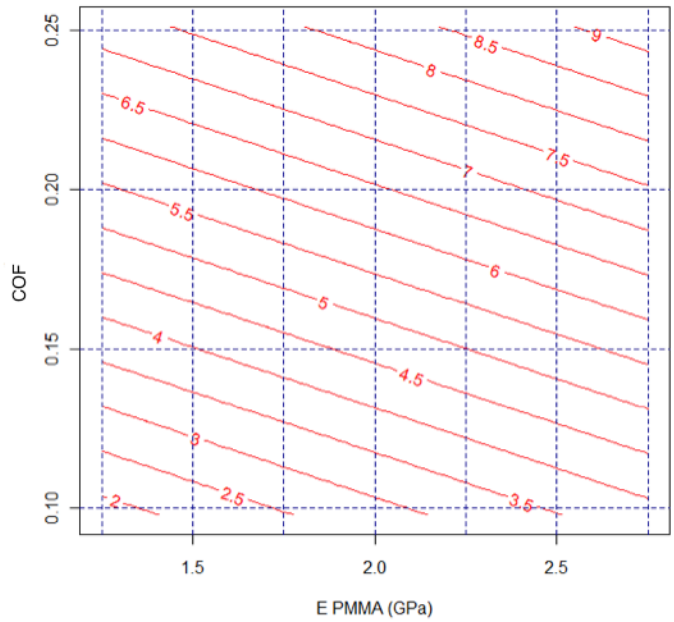

Figure 5.53. Two dimensional PMMA bone cement tensile stresses (MPa) due to descending stairs for varying metal-on-metal friction coefficient and PMMA Young's modulus for 100% bone quality.

$$Tensile\ Stress = -3.7048 + 35.64727 \cdot \mu + 1.35278 \cdot E_{PMMA} \Rightarrow 120\%\ BQ$$

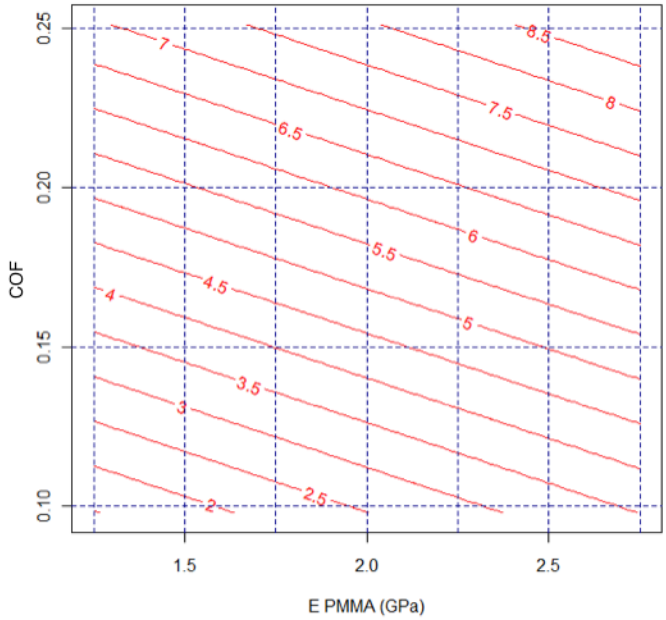

Figure 5.54. Two dimensional PMMA bone cement tensile stresses (MPa) due to descending stairs for varying metal-on-metal friction coefficient and PMMA Young's modulus for 120% bone quality.

Figures 5.55 to 5.58 show predicting graphs to calculate shear stresses in PMMA bone cement according to metal-on-metal friction and PMMA bone cement Young's modulus.

$$Shear\ Stress = -1.4502 + 30.59158 \cdot \mu + 1.69833 \cdot E_{PMMA} \Rightarrow 60\%\ BQ$$

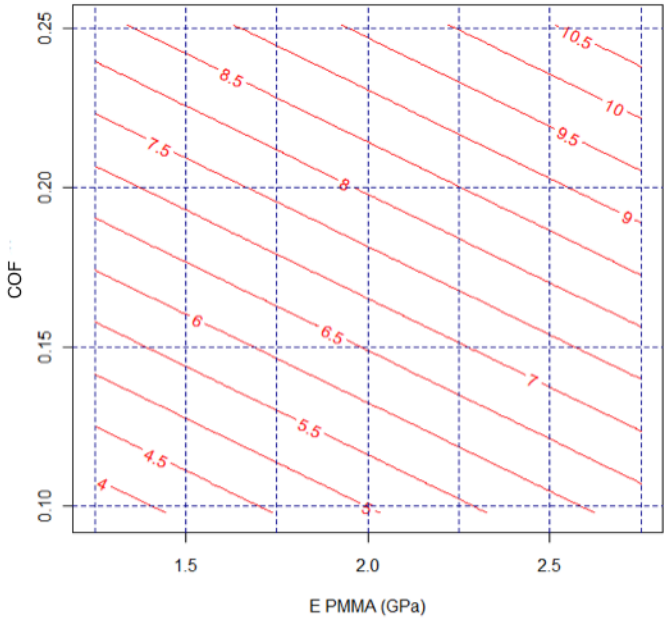

Figure 5.55. Two dimensional PMMA bone cement shear stresses (MPa) due to descending stairs for varying metal-on-metal friction coefficient and PMMA Young's modulus for 60% bone quality.

$$Shear\ Stress = -1.8613 + 30.59158 \cdot \mu + 1.69833 \cdot E_{PMMA} \Rightarrow 80\%\ BQ$$

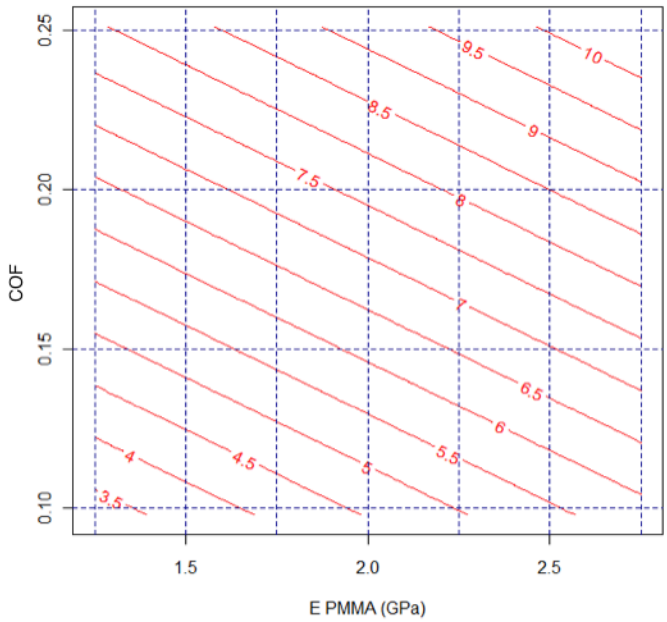

Figure 5.56. Two dimensional PMMA bone cement shear stresses (MPa) due to descending stairs for varying metal-on-metal friction coefficient and PMMA Young's modulus for 80% bone quality.

$$Shear\ Stress = -2.2725 + 30.59158 \cdot \mu + 1.69833 \cdot E_{PMMA} \Rightarrow 100\%\ BQ$$

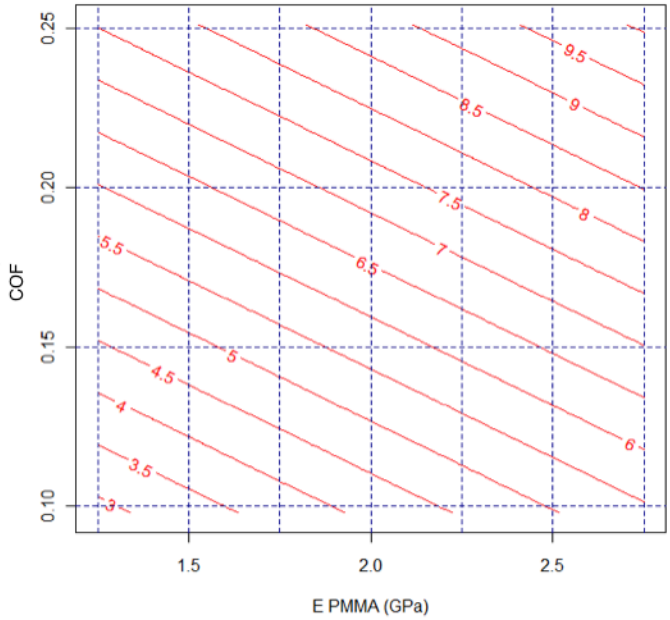

Figure 5.57. Two dimensional PMMA bone cement shear stresses (MPa) due to descending stairs for varying metal-on-metal friction coefficient and PMMA Young's modulus for 100% bone quality.

$$Shear\ Stress = -2.6836 + 30.59158 \cdot \mu + 1.69833 \cdot E_{PMMA} \Rightarrow 120\%\ BQ$$

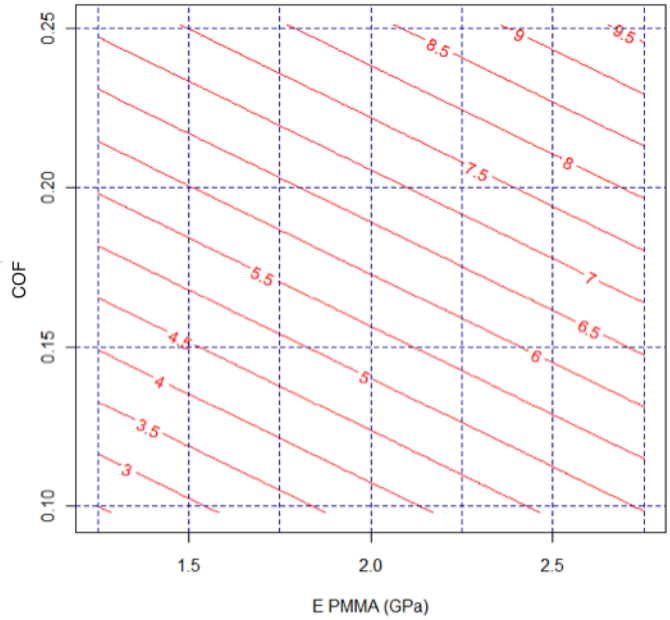

Figure 5.58. Two dimensional PMMA bone cement shear stresses (MPa) due to descending stairs for varying metal-on-metal friction coefficient and PMMA Young's modulus for 120% bone quality.

Table 5.27 presents the comparison of maximum tensile and shear stresses according to varying metal-on-metal friction, patient bone quality and PMMA Young's modulus. Furthermore, Table 5.27 shows the equations to predict tensile and shear stresses according to the parameters previously mentioned.

Table 5.27. PMMA tensile and shear stresses due to varying MoM friction coefficient, bone quality and PMMA Young's modulus during descending stairs.

Everyday Activity	Metal-on-metal COF	Bone Quality	E_{PMMA} (Gpa)	Tensile Stress (Mpa)	Shear Stress (Mpa)	Stress Equations
Descending Stairs	0.098	60%	1.25	2.8	4.44	Tensile Stress = 0.68 * E_{PMMA} + 1.993
			2	3.44	5.32	Shear Stress = 1 * E_{PMMA} + 3.233
			2.75	3.82	5.94	
		80%	1.25	2.4	3.97	Tensile Stress = 0.793 * E_{PMMA} + 1.443
			2	3.1	4.96	Shear Stress = 1.093 * E_{PMMA} + 2.66
			2.75	3.59	5.61	
		100%	1.25	2.26	3.76	Tensile Stress = 0.713 * E_{PMMA} + 1.39
			2	2.86	4.67	Shear Stress = 1.073 * E_{PMMA} + 2.453
			2.75	3.33	5.37	
		120%	1.25	2.04	3.41	Tensile Stress = 0.72 * E_{PMMA} + 1.16
			2	2.64	4.46	Shear Stress = 1.166 * E_{PMMA} + 2.01
			2.75	3.12	5.16	
	0.189	60%	1.25	5.69	6.9	Tensile Stress = 1.573 * E_{PMMA} + 3.706
			2	6.82	8.54	Shear Stress = 1.846 * E_{PMMA} + 4.676
			2.75	8.05	9.67	
		80%	1.25	5.33	6.34	Tensile Stress = 1.486 * E_{PMMA} + 3.55
			2	6.68	8.01	Shear Stress = 1.853 * E_{PMMA} + 4.116
			2.75	7.56	9.12	
		100%	1.25	4.83	5.79	Tensile Stress = 1.486 * E_{PMMA} + 3.043
			2	6.16	7.46	Shear Stress = 1.873 * E_{PMMA} + 3.536
			2.75	7.06	8.6	
		120%	1.25	4.5	5.37	Tensile Stress = 1.34 * E_{PMMA} + 2.916
			2	5.78	7	Shear Stress = 1.766 * E_{PMMA} + 3.263
			2.75	6.51	8.02	
	0.219	60%	1.25	5.96	7.22	Tensile Stress = 1.926 * E_{PMMA} + 3.736
			2	7.96	9.36	Shear Stress = 2.253 * E_{PMMA} + 4.553
			2.75	8.85	10.6	
		80%	1.25	5.88	6.95	Tensile Stress = 1.813 * E_{PMMA} + 3.753
			2	7.66	8.91	Shear Stress = 2.1 * E_{PMMA} + 4.453
			2.75	8.6	10.1	
		100%	1.25	5.72	6.51	Tensile Stress = 1.86 * E_{PMMA} + 3.49
			2	7.4	8.49	Shear Stress = 2.193 * E_{PMMA} + 3.88
			2.75	8.51	9.8	
		120%	1.25	5.32	6.09	Tensile Stress = 1.84 * E_{PMMA} + 3.106
			2	6.96	7.99	Shear Stress = 2.16 * E_{PMMA} + 3.483
			2.75	8.08	9.33	

Figure 5.59 and 5.60 shows the comparison of PMMA tensile and shear stresses for different metal-on-metal friction, patient bone quality and PMMA Young's modulus as shown in Table 5.27.

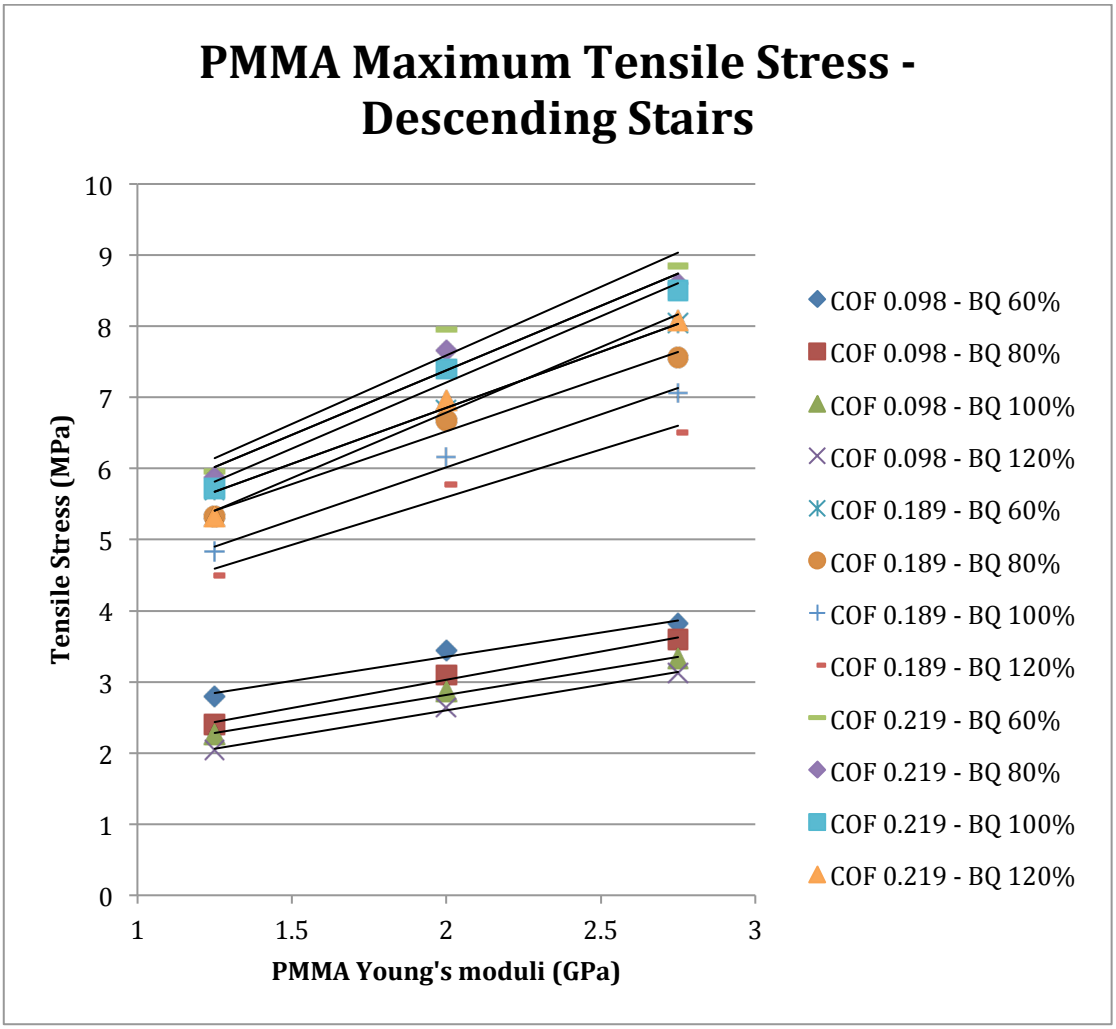

Figure 5.59. Comparison of PMMA tensile stress (MPa) according to different metal-on-metal friction coefficients, patient bone quality and PMMA Young's modulus during descending stairs.

From Figure 5.59, it can be observed that a decrease in PMMA Young's Modulus produces a decrease in maximum tensile stresses in the PMMA bone cement, and this reduction is more accentuated at higher metal-on-metal friction coefficient and lower patient bone quality.

A similar effect on PMMA maximum shear stress values can be appreciated in Figure 5.60, lower PMMA Young's Modulus for higher metal-on-metal friction coefficients and lower patient bone quality show a greater reduction on maximum shear stresses in the PMMA bone cement.

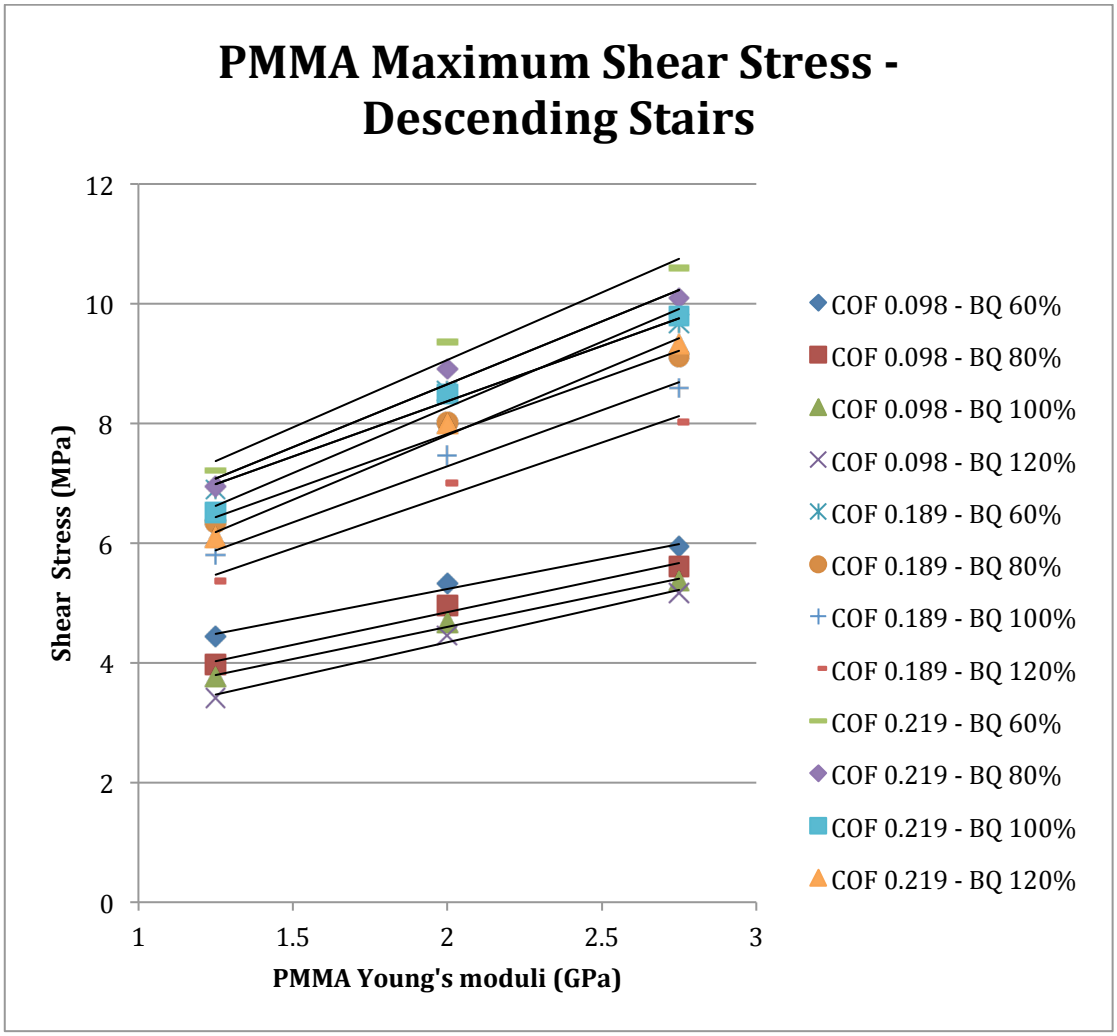

Figure 5.60. Comparison of PMMA shear stress (MPa) according to different metal-on-metal friction coefficients, patient bone quality and PMMA Young's modulus during descending stairs.

5.3.3 Finite Element Analysis results for standing up

Twenty-four Finite Element models were solved according to the metal-on-metal friction coefficient due to resting periods for standing up, simulated different bone quality and PMMA bone cement Young's modulus. Following this approach, the study is not simply parametric (with one variable) but allows a multi-parametric approach involving different PMMA young's modulus for varying bone quality whilst every Finite Element model is also varied according to metal-on-metal friction due to resting periods.

The maximum tensile and shear stresses can be calculated according to the metal-on-metal friction, bone quality of the patient and PMMA bone cement Young's modulus as:

$$Tensile\ Stress = -1.3673 + 34.4786 \cdot \mu - 2.3758 \cdot BQ + 1.1917 \cdot E_{PMMA}$$
$$Shear\ Stress = -0.17 + 31.738 \cdot \mu - 2.7133 \cdot BQ + 1.5933 \cdot E_{PMMA}$$

To facilitate a much better graphical display of the results, the bone quality will be fixed in the intervals of 60%, 80%, 100% and 120%.

Figures 5.61 to 5.64 show predicting graphs to calculate tensile stresses in PMMA bone cement according to metal-on-metal friction and PMMA bone cement Young's modulus.

$$Tensile\ Stress = -2.7928 + 34.4786 \cdot \mu + 1.1917 \cdot E_{PMMA} \Rightarrow 60\%\ BQ$$

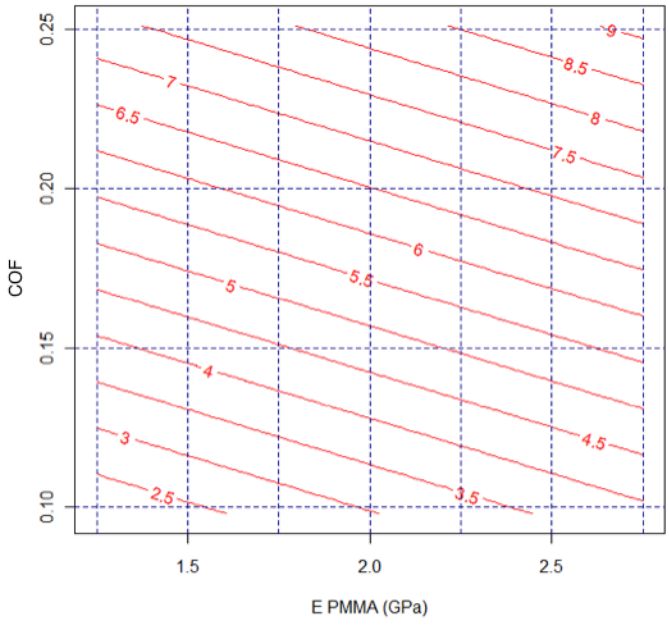

Figure 5.61. Two dimensional PMMA bone cement tensile stresses (MPa) due to standing up for varying metal-on-metal friction coefficient and PMMA Young's modulus for 60% bone quality.

$$Tensile\ Stress = -3.2679 + 34.4786 \cdot \mu + 1.1917 \cdot E_{PMMA} \Rightarrow 80\%\ BQ$$

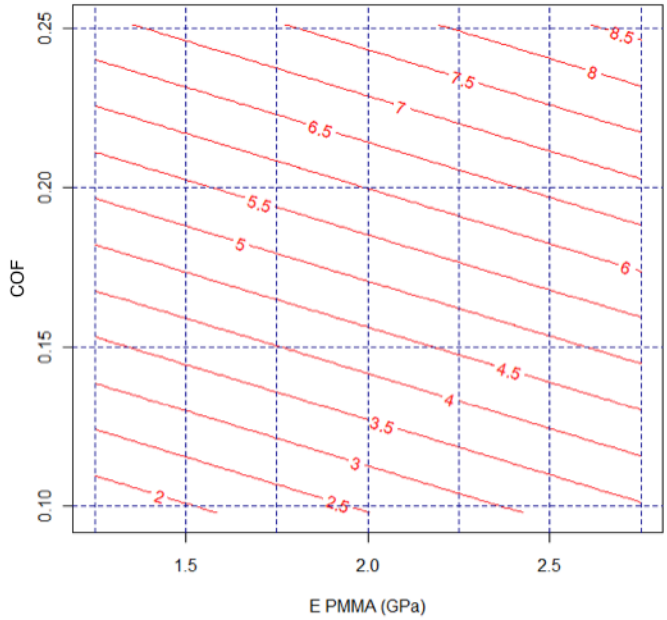

Figure 5.62. Two dimensional PMMA bone cement tensile stresses (MPa) due to standing up for varying metal-on-metal friction coefficient and PMMA Young's modulus for 80% bone quality.

$$Tensile\ Stress = -3.7431 + 34.4786 \cdot \mu + 1.1917 \cdot E_{PMMA} \Rightarrow 100\%\ BQ$$

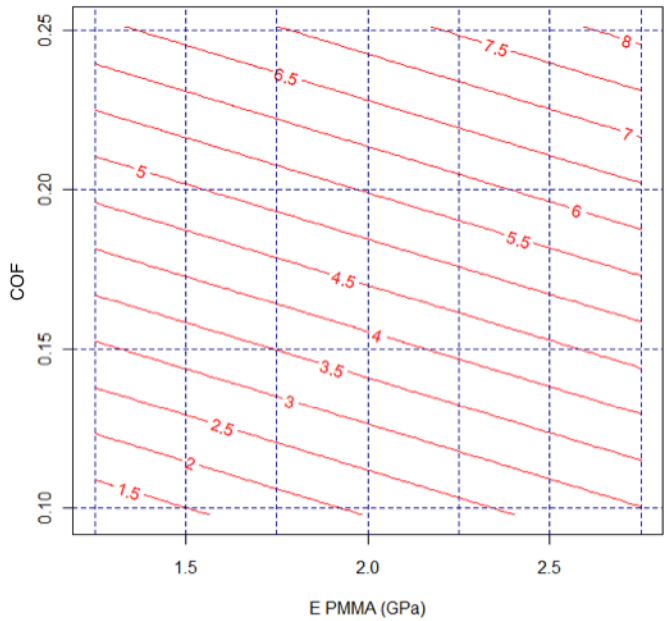

Figure 5.63. Two dimensional PMMA bone cement tensile stresses (MPa) due to standing up for varying metal-on-metal friction coefficient and PMMA Young's modulus for 100% bone quality.

$$Tensile\ Stress = -4.2183 + 34.4786 \cdot \mu + 1.1917 \cdot E_{PMMA} \Rightarrow 120\%\ BQ$$

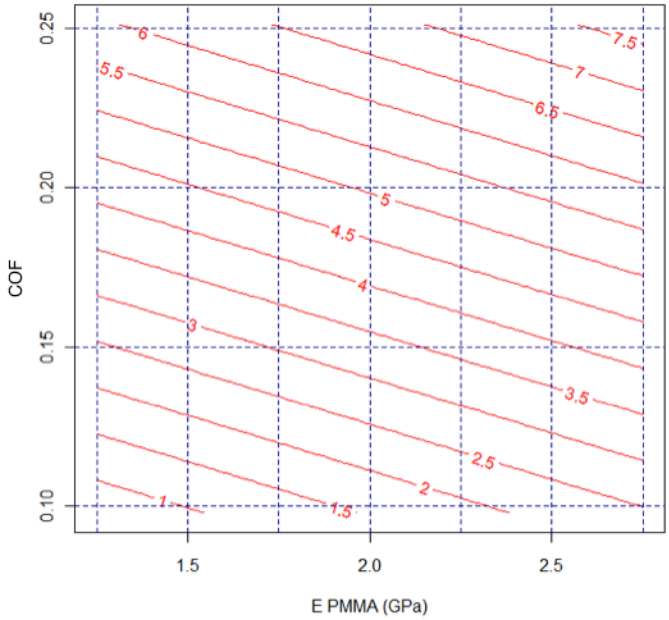

Figure 5.64. Two dimensional PMMA bone cement tensile stresses (MPa) due to standing up for varying metal-on-metal friction coefficient and PMMA Young's modulus for 120% bone quality.

Figures 5.65 to 5.68 show predicting graphs to calculate shear stresses in PMMA bone cement according to metal-on-metal friction and PMMA bone cement Young's modulus.

$$Shear\ Stress = -1.798 + 31.738 \cdot \mu + 1.5933 \cdot E_{PMMA} \Rightarrow 60\%\ BQ$$

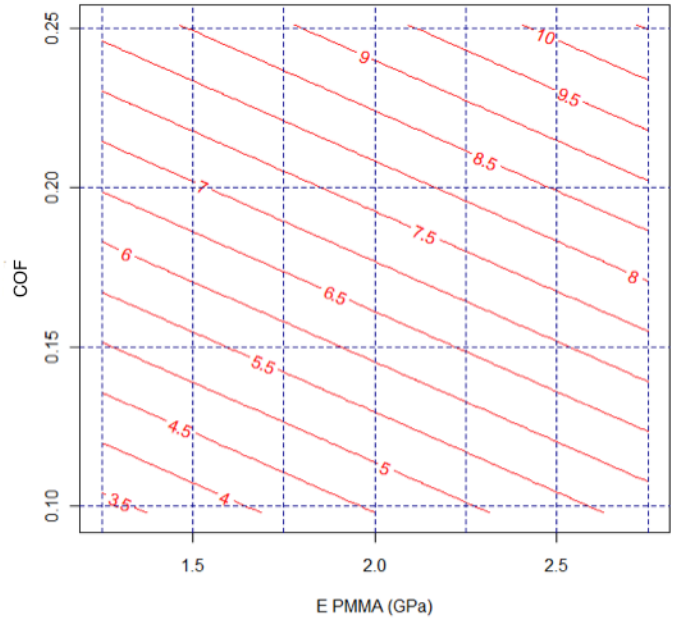

Figure 5.65. Two dimensional PMMA bone cement shear stresses (MPa) due to standing up for varying metal-on-metal friction coefficient and PMMA Young's modulus for 60% bone quality.

$$Shear\ Stress = -2.3406 + 31.738 \cdot \mu + 1.5933 \cdot E_{PMMA} \Rightarrow 80\%\ BQ$$

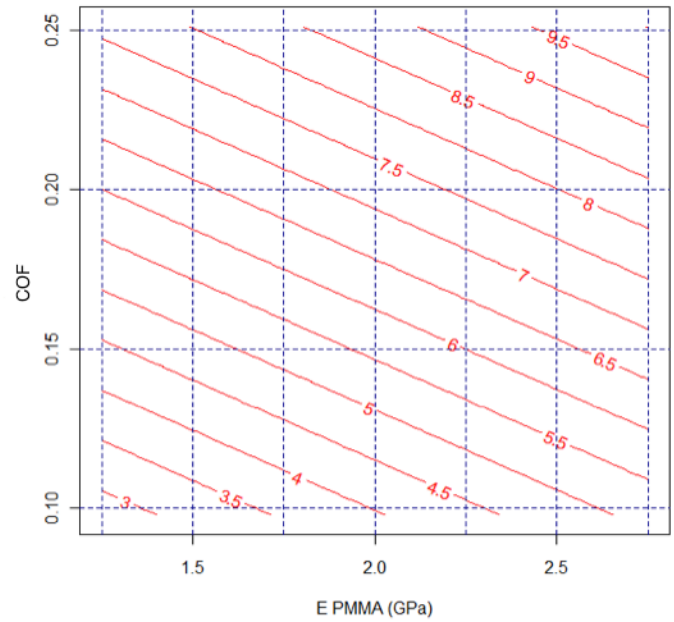

Figure 5.66. Two dimensional PMMA bone cement shear stresses (MPa) due to standing up for varying metal-on-metal friction coefficient and PMMA Young's modulus for 80% bone quality.

$$Shear\ Stress = -2.8833 + 31.738 \cdot \mu + 1.5933 \cdot E_{PMMA} \Rightarrow 100\%\ BQ$$

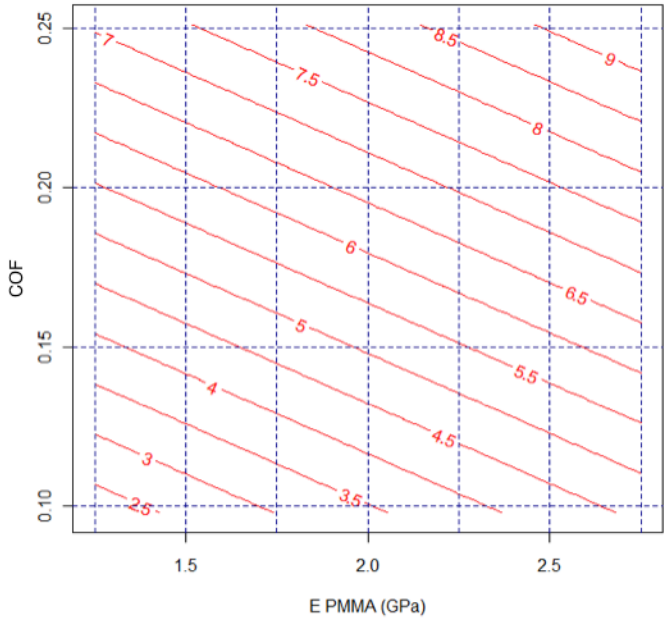

Figure 5.67. Two dimensional PMMA bone cement shear stresses (MPa) due to standing up for varying metal-on-metal friction coefficient and PMMA Young's modulus for 100% bone quality.

$$Shear\ Stress = -3.426 + 31.738 \cdot \mu + 1.5933 \cdot E_{PMMA} \Rightarrow 120\%\ BQ$$

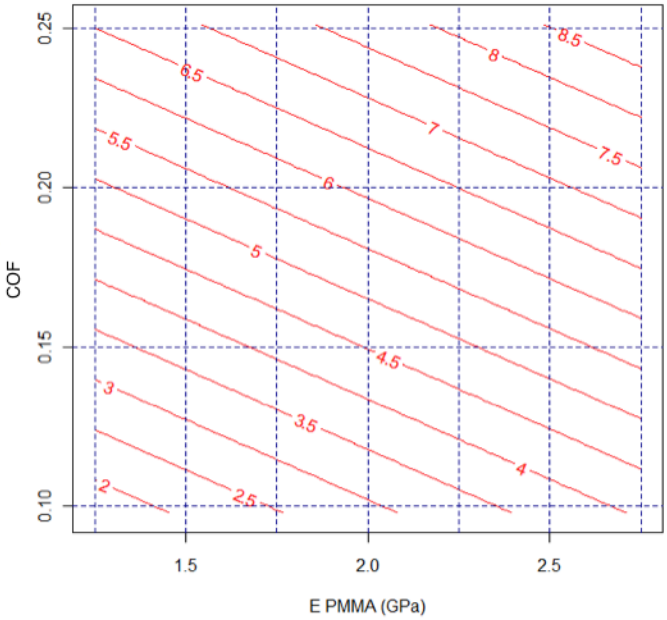

Figure 5.68. Two dimensional PMMA bone cement shear stresses (MPa) due to standing up for varying metal-on-metal friction coefficient and PMMA Young's modulus for 120% bone quality.

Table 5.28 presents the comparison of maximum tensile and shear stresses according to varying metal-on-metal friction, patient bone quality and PMMA Young's modulus. Furthermore, Table 5.28 shows the equations to predict tensile and shear stresses according to the parameters previously mentioned.

Table 5.28. PMMA tensile and shear stresses due to varying MoM friction coefficient, bone quality and PMMA Young's modulus during standing up.

Everyday Activity	Metal-on-metal COF	Bone Quality	E_{PMMA} (Gpa)	Tensile Stress (Mpa)	Shear Stress (Mpa)	Stress Equations
Standing Up	0.098	60%	1.25	2.17	3.49	Tensile Stress = 0.56 * E_{PMMA} + 1.496
			2	2.67	4.22	Shear Stress = 0.78 * E_{PMMA} + 2.563
			2.75	3.01	4.66	
		80%	1.25	1.9	3.15	Tensile Stress = 0.526 * E_{PMMA} + 1.253
			2	2.33	3.81	Shear Stress = 0.773 * E_{PMMA} + 2.21
			2.75	2.69	4.31	
		100%	1.25	1.68	2.84	Tensile Stress = 0.54 * E_{PMMA} + 1.03
			2	2.16	3.61	Shear Stress = 0.853 * E_{PMMA} + 1.816
			2.75	2.49	4.12	
		120%	1.25	1.57	2.6	Tensile Stress = 0.54 * E_{PMMA} + 0.913
			2	2.03	3.43	Shear Stress = 0.92 * E_{PMMA} + 1.496
			2.75	2.38	3.98	
	0.285	60%	1.25	8.34	8.93	Tensile Stress = 1.84 * E_{PMMA} + 6.233
			2	10.3	11.2	Shear Stress = 2.446 * E_{PMMA} + 6.016
			2.75	11.1	12.6	
		80%	1.25	7.42	8.05	Tensile Stress = 1.92 * E_{PMMA} + 5.163
			2	9.29	10.2	Shear Stress = 2.433 * E_{PMMA} + 5.116
			2.75	10.3	11.7	
		100%	1.25	6.82	7.3	Tensile Stress = 1.706 * E_{PMMA} + 4.783
			2	8.39	9.36	Shear Stress = 2.333 * E_{PMMA} + 4.486
			2.75	9.38	10.8	
		120%	1.25	6.21	6.69	Tensile Stress = 1.9 * E_{PMMA} + 3.903
			2	7.84	8.61	Shear Stress = 2.206 * E_{PMMA} + 4.02
			2.75	9.06	10	

Figure 5.69 and 5.70 shows the comparison of PMMA tensile and shear stresses for different metal-on-metal friction, patient bone quality and PMMA Young's modulus as shown in Table 5.28.

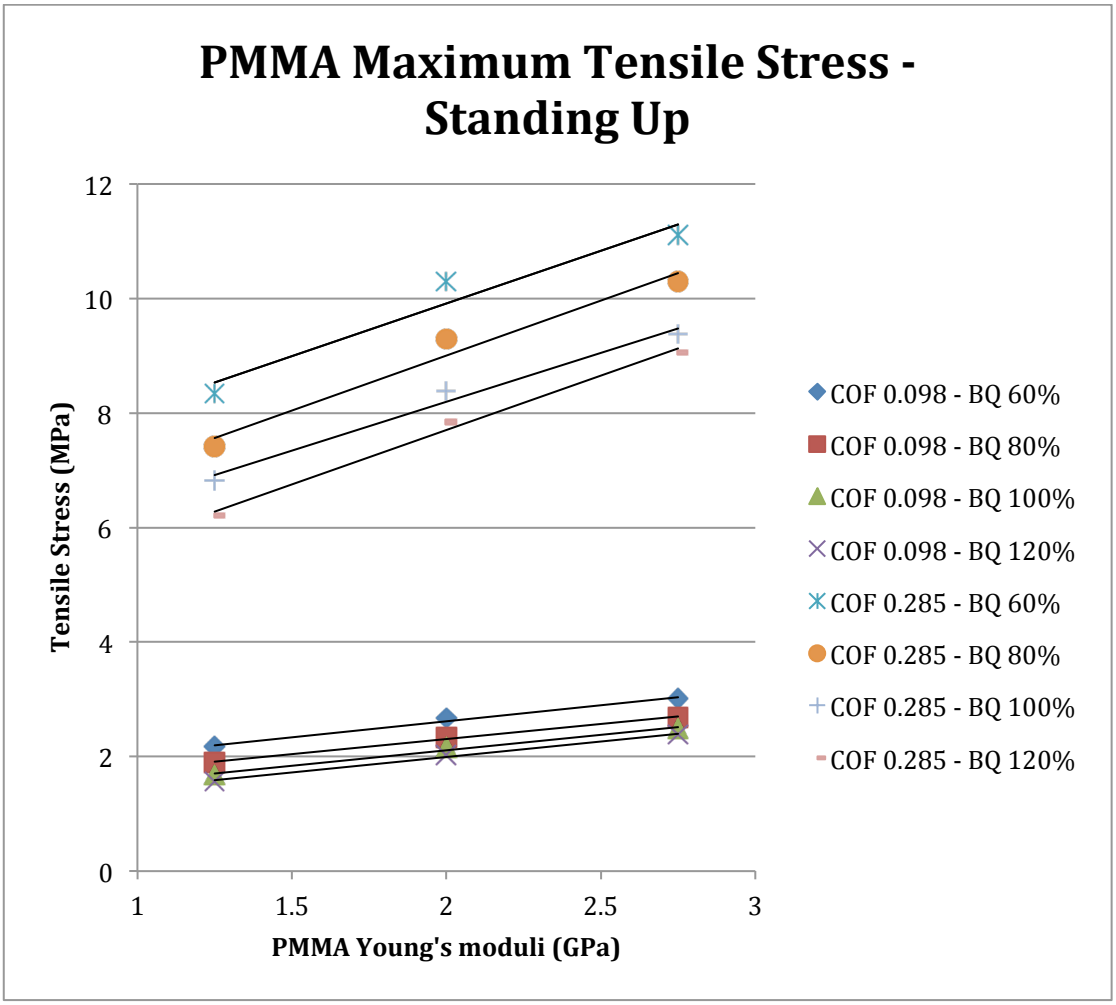

Figure 5.69. Comparison of PMMA tensile stress (MPa) according to different metal-on-metal friction coefficients, patient bone quality and PMMA Young's modulus during standing up.

From Figure 5.69, it can be observed that a decrease in PMMA Young's Modulus produces a decrease in maximum tensile stresses in the PMMA bone cement, and this reduction is more accentuated at higher metal-on-metal friction coefficient and lower patient bone quality.

A similar effect on PMMA maximum shear stress values can be appreciated in Figure 5.70, lower PMMA Young's Modulus for higher metal-on-metal friction coefficients and lower patient bone quality show a greater reduction on maximum shear stresses in the PMMA bone cement.

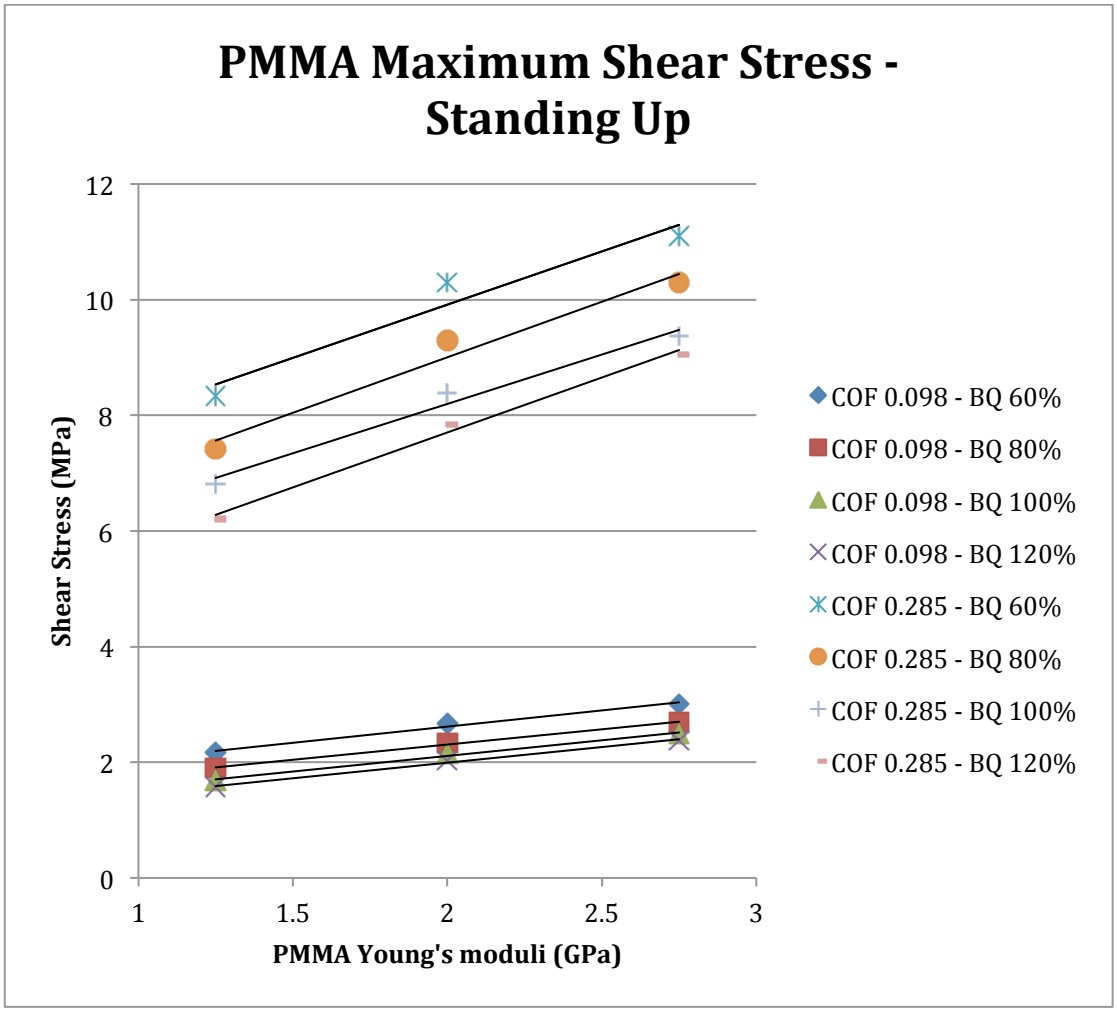

Figure 5.70. Comparison of PMMA shear stress (MPa) according to different metal-on-metal friction coefficients, patient bone quality and PMMA Young's modulus during standing up.

5.4 PMMA Mechanical Testing

This section shows the results of the mechanical testing performed to illustrate the use of Finite Element Analysis results to understand the behaviour of hip resurfacing arthroplasty due to PMMA bone cement and metal interface failure.

The materials and surface finishes do not comply with those used in hip resurfacing arthroplasty. The reader should take forward the methodology to use the Finite Element Analysis results presented previously in chapter 5 and not the actual results from the mechanical testing.

5.4.1 PMMA - metal interface

PMMA-Metal interface testing was performed using custom made metal jigs and metal plates. The main objective of the testing was to investigate the behaviour of the PMMA-metal interface under pure shear stress to illustrate the use of the Finite Element Analysis results previously presented in this chapter. The jigs were built from steel with dimensions of 80 mm by 80 mm and a thickness of 20 mm. The jig consists of two parts, one holding the PMMA bone cement as shown in Figure 5.71 and a counterpart with a plain steel metal surface. The surface roughness of the metal interface did not match the surface roughness of the inside of hip resurfacing femoral components. Two versions of the jigs were created, three jigs with a square area and another three jigs with a circular area of contact with the metal face. The jigs were reused after each testing and carefully clean of any residues of PMMA bone cement before preparation for a new testing sample. Figure 5.71 shows both versions of the jig after testing and Table 5.29 shows the contact area between PMMA bone cement and metal for the interface testing.

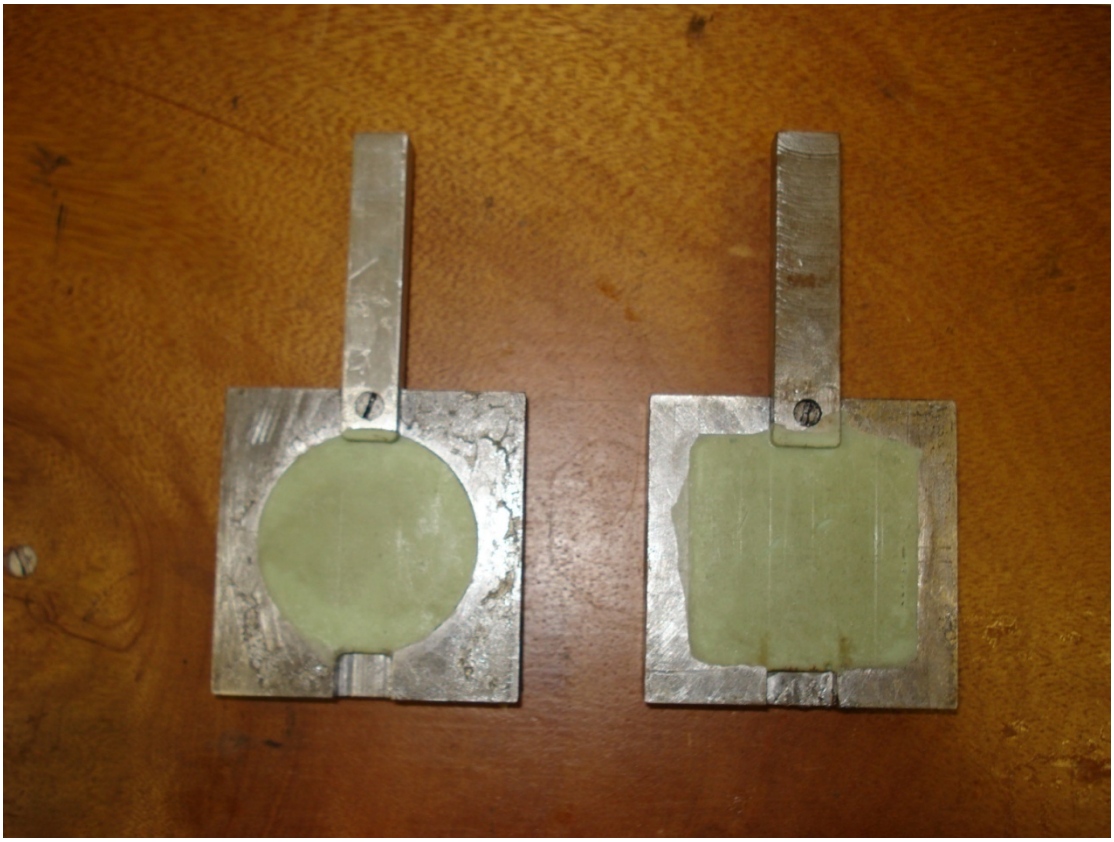

Figure 5.71. Interface testing jigs after testing.

Table 5.29. Interface testing jigs areas.

	Total Area [mm^2]
Jig 1	2583.60
Jig 2	2620.55
Jig 3	2539.06
Jig 4	1954.67
Jig 5	1928.51
Jig 6	1972.34

The first interface test was performed using vacuum mixed *Palacos LV* PMMA bone cement. The testing jigs were kept for an average of 8 days in an oven at 37 degrees centigrade for curing. According to the review of PMMA bone cement properties from Lewis (1997), PMMA bone cement performance has small differences after curing for at least 7 days.

Before implantation, metal-on-metal surfaces to be in contact during the test were coated on Vaseline to avoid any friction during the testing. Furthermore, during testing a metal bracing was used to assure that only pure shear stress would be responsible for the failure. The contact surfaces between the brace and the jig were coated with Vaseline to avoid any resistance friction. The mechanical testing was performed using an *Instron* testing machine (5KN load cell and speed of 5 mm/min) and later on a *Hounsfield* testing machine (5KN load cell and speed of 5 mm/min). Figure 5.72 shows one of the jigs during testing. The interface testing was developed to estimate the ultimate interface shear stress with the purpose of illustrating the use of the Finite Element results previously presented in Chapter 5.

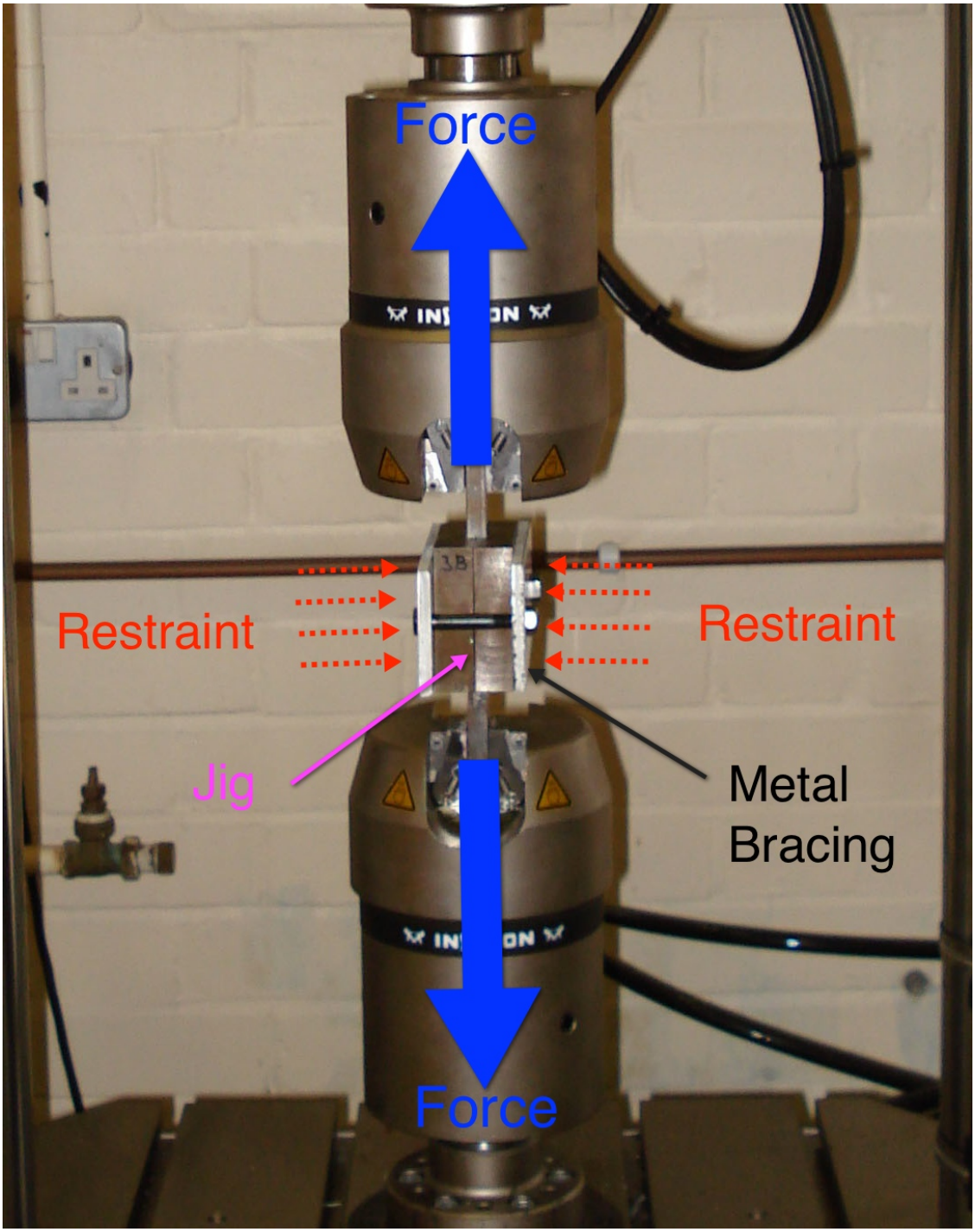

Figure 5.72. Interface testing jig during mechanical testing in *Instron* testing machine.

Figure 5.73 shows the ultimate interface shear stress results for *Palacos LV* PMMA bone cement. The mean ultimate interface shear stress indicated by this test is equal to 0.925 MPa with a standard deviation of 0.143 for a sample of 10 tests.

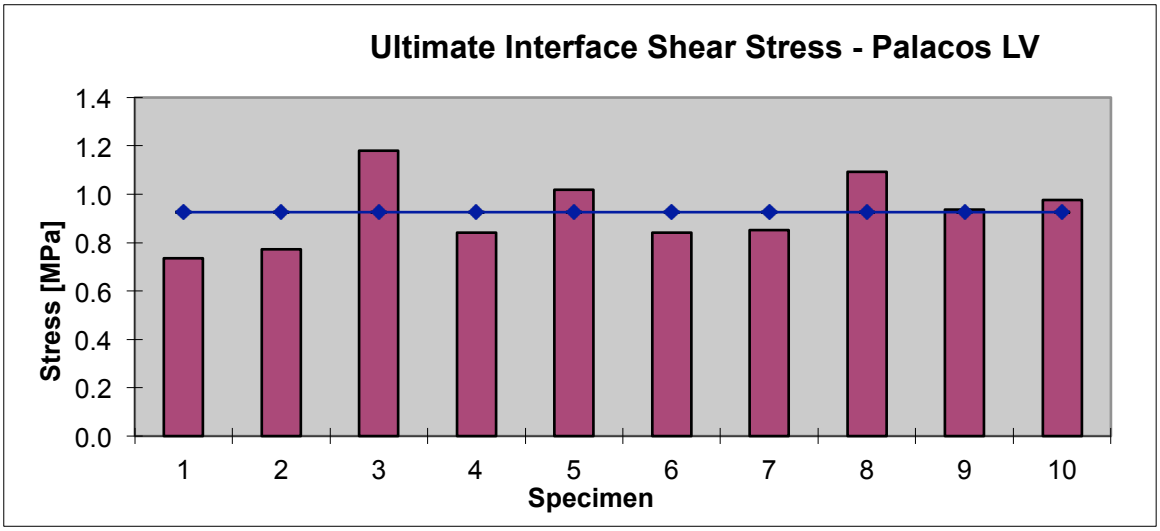

Figure 5.73. Ultimate interface shear stress for *Palacos LV* PMMA bone cement.

This experimentally derived ultimate shear stress of 0.925 MPa provides a benchmark for interpreting the Finite Element Analysis results presented in Sections 5.1 to 5.3.

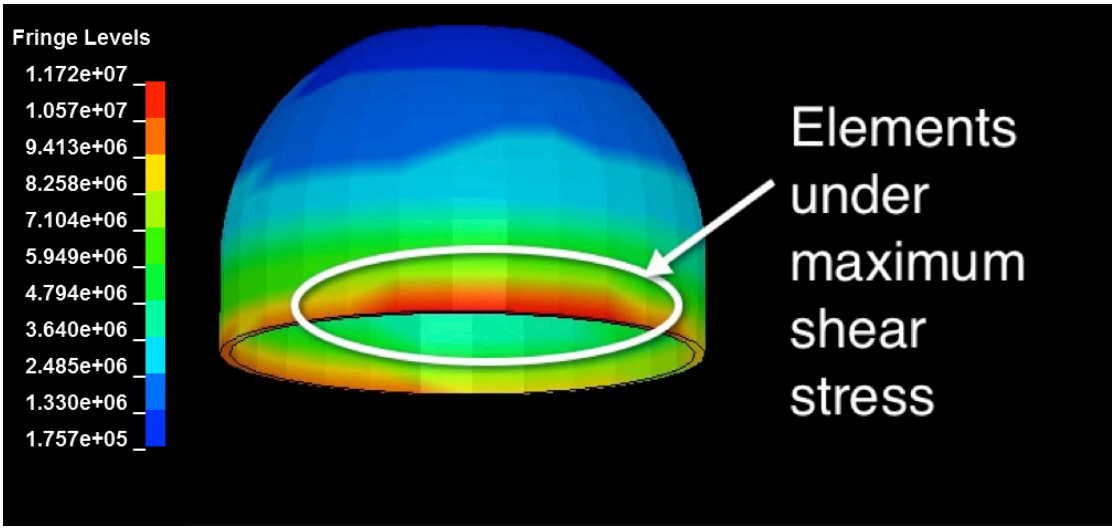

Figure 5.74. PMMA shear stress during walking gait.

For comparison with the Finite Element results of PMMA shear stress, the total area of elements affected by maximum shear stress equals to 98.51 mm^2 (around 10 elements as shown in Figure 5.74, each FEA element is 9.85 mm^2) in *Ls-Dyna* and an average load to failure during mechanical testing was 1973.899 N for the 10 tests presented in Figure 5.73. If an average load of 1973.899 N (mechanical testing) is applied to the 98.51 mm^2 area (Figure 5.73), the maximum shear stress required for

failure during the interface mechanical testing can calculated as 20.04 MPa. As this value (20.04 MPa) represents the failure of samples during mechanical testing, it can be suggested that a shear stress higher than 20.04 MPa could be expected to initiate failure of the Metal-PMMA bone cement interface.

$$Shear\ Stress = \frac{Shear\ Force}{Area} = \frac{1973.899\ N}{98.51\ m^2} = 20.04\ MPa$$

Further testing was performed using *Simplex P* PMMA bone cement following the same approach as presented above for *Palacos LV* PMMA bone cement.

Figure 5.75 shows the ultimate interface shear stress results for *Simplex P* PMMA bone cement. The mean ultimate interface shear stress value was equal to 0.377 MPa with a standard deviation of 0.204 for a sample of 22 tests.

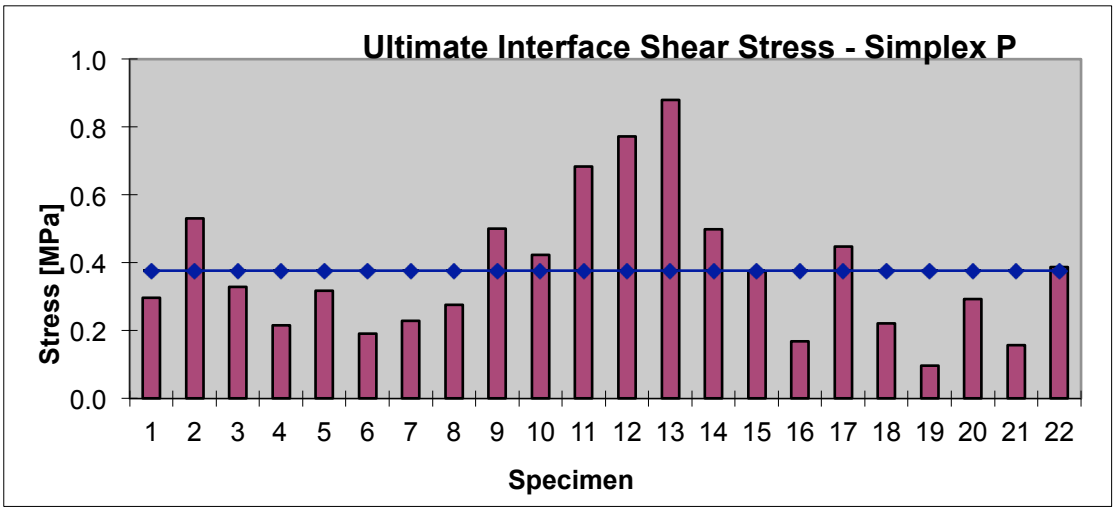

Figure 5.75. Ultimate interface shear stress for *Simplex P* PMMA bone cement.

Providing a benchmark ultimate shear stress for the Finite Element Analysis, the total area of elements affected by maximum shear stress equals 98.51 mm^2 in *Ls-Dyna* (Figure 5.74) and an average load to failure during interface mechanical testing of 585.486 N, it can therefore be suggested that a shear stress higher than 5.94 MPa would be expected to initiate failure of the Metal-PMMA bone cement interface.

$$Shear\ Stress = \frac{Shear\ Force}{Area} = \frac{585.486\ N}{98.51\ m^2} = 5.94\ MPa$$

5.4.2 Torque testing

Torque testing was carried out using *Sawbone* composite bone. *Sawbone* composite bones are widely used in orthopaedic research and have similar properties to natural bones (Heiner, 2008). Five aluminium resurfacing heads with an internal diameter of 0.04048 meters were manufactured to match the head size of the femoral *Sawbone* sample following the *Biomet Recap* technical design rationale (*Biomet*, 2005).

As explained before in section 5.4 and 5.4.1, the materials and surface finishes do not comply with those used in hip resurfacing arthroplasty. As explained in section 5.4, the mechanical testing is performed to illustrate the use of Finite Element Analysis results to understand the behaviour of hip resurfacing arthroplasty due to PMMA bone cement and metal interface failure.

The femoral *Sawbone* samples were sectioned at femoral neck level and reamed using a manual lathe to match the aluminium heads.

Fixation was performed using vacuum mixed *Simplex P* bone cement. The testing samples were kept for 13 days in an oven at 37 degrees centigrade for curing (Lewis, 1997).

The torque test was performed using a torque wrench while the base of the testing sample was firmly fixed.

Figure 5.76 shows the result of the torque testing for the ten samples. The mean torque value is equal to 15.98 Nm with a standard deviation of 6.88 for a sample of 10 tests.

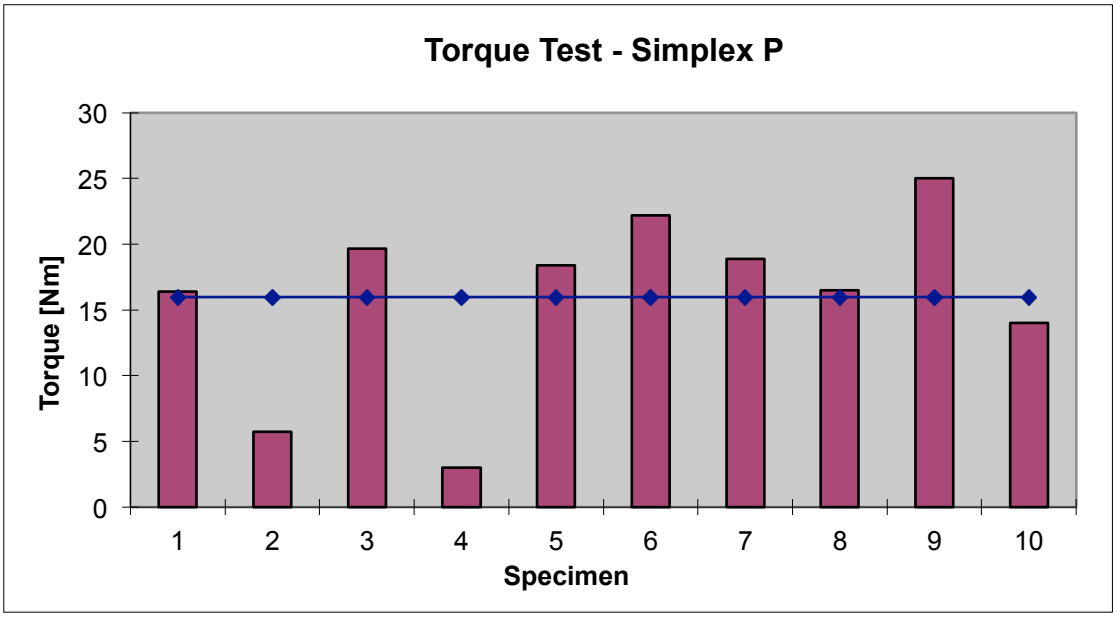

Figure 5.76 Torque testing results for ten testing samples.

Sawbone test samples were cut in half after testing and closely inspected to examine the state of the PMMA bone cement mantle and assure even coverage of the head. Figure 5.77 shows a test sample cut in half during inspection.

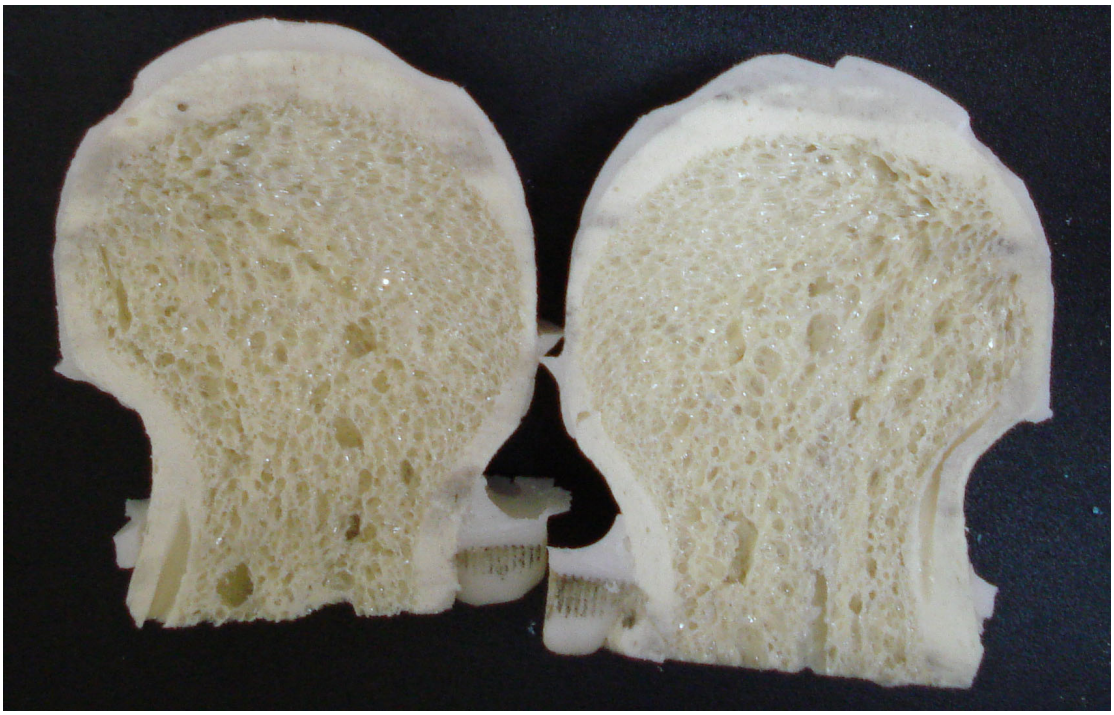

Figure 5.77. Test sample during inspection.

Samples number 2 and 4 were disregarded due to insufficient PMMA bone cement coverage of the femoral heads during implantation and more precisely, the outer wall of the cement mantle. As described in Section 2.8, the outer wall of the cement mantle is the most important fixation area for resisting torque in hip resurfacing arthroplasty (Ma, 1983 and Bitsch, 2007), as such samples number 2 and 4 were excluded from the study due to unsatisfactory coverage of the area.

Figure 5.78 shows the result of the torque testing for the final eight samples.

The final mean torque value is equal to 18.88 Nm with a standard deviation of 3.48 for a sample of 8 tests.

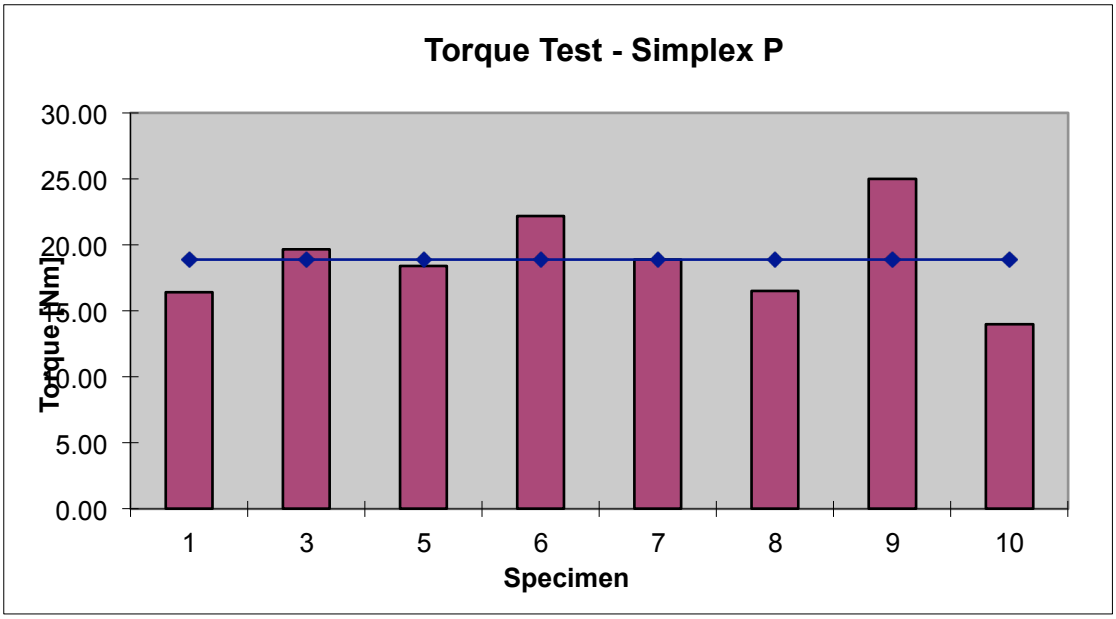

Figure 5.78. Torque testing results for eight testing samples.

Using the 18.88 Nm torque for a 0.02024 meters internal radius of the aluminium femoral head, the force presents in the interface is equal to 932.806 N.

$$Shear\ Force = \frac{Torque}{Distance} = \frac{18.88\ Nm}{0.02024\ m} = 932.806\ N$$

Providing a benchmark ultimate shear stress for the Finite Element Analysis, the total area of elements affected by maximum shear stress equals 98.51 mm^2 in *Ls-Dyna*, it

can be said that a shear stress higher than 9.47 MPa will start the failure mechanism of the Metal-PMMA bone cement interface.

$$Shear\ Stress = \frac{Shear\ Force}{Area} = \frac{932.806\ N}{98.51\ m^2} = 9.47\ MPa$$

These results for the Metal-PMMA bone cement interface agree with previously published data investigating UHMWPE-PMMA bone cement interface (10.1 MPa) (Park et al, 2003).

Chapter 6

Discussion

This study investigates the short, medium and long term performance of PMMA bone cement, for the femoral component in hip resurfacing arthroplasty from the point of view of analysing the failure of Poly Methyl Methacrylate (PMMA) bone cement to provide understanding, awareness and potentially inform lifestyle options. To achieve this aim, dynamic Finite Element Analysis and mechanical testing were performed to address the following drivers in the light of the controlled variables presented in Section 3.5.

- Could high metal-on-metal friction coefficient due to resting periods cause aseptic loosening of femoral hip resurfacing components during daily activities by PMMA bone cement fatigue?

- Could low bone quality affect the stability of the femoral hip resurfacing components due to PMMA stresses?

- Could PMMA Young's modulus affect the stability of the femoral hip resurfacing components due to PMMA stresses?

- Could the torque produce failure on the PMMA-metal interface and loosening of femoral hip resurfacing components?

A forensic engineering approach was used in this study due to the lack of independent medium and long term follow-ups and the unknown aseptic loosening mechanism in the medium and long term. (Sharma et al., 2005 and Yue et al., 2009).

Currently the National Joint Registry (NJR) for England and Wales has a follow-up for hip resurfacing of 7 years with a revision rate of 11.8%, almost four times higher than cemented prostheses (3% at 7 years). Further adding to the lack of clarity in the performance of stemmed metal-on metal bearings (total hip replacement) with a revision rate of 13.6% at 7 years (NJR, 2011). The Swedish National Hip Arthroplasty Register (2011) has reported the risk of revision within five years to be more than doubled in the use of resurfacing.

The feeling of the bioengineering community regarding hip resurfacing arthroplasty can be expressed by the following extract from the Swedish National Hip Arthroplasty register (2010) presenting concerns for the understanding of modern era hip resurfacing arthroplasty:

> "In general the use of resurfacing prostheses are associated with an increased risk of early revision. This problem could mainly be related to the design of certain prostheses or related factors such as the design of the instrumentation and the training of individual surgeons, factors that cannot be evaluated in the registry."

The recent events regarding revision rates have materialised in the voluntary recall by DePuy in August 2010 of its ASR Hip Resurfacing System, due to a revision rate of 12% after 5 years (DePuy, 2011) and higher revision risks reported in the literature (Seppanen et al., 2012).

Radiographic pictures of hip resurfacing arthroplasty do not provide any internal information or any indication of the state of the PMMA cement mantle under the femoral component as the metal component obscure or blurs the X-ray, as it can be observed in radiographs from Loughead et al. (2005). Watters et al. (2010) highlighted the difficulties in diagnosing femoral component loosening. The most likely way to assess the state of the PMMA cement mantle after implantation is undesirable: by removal of the femoral component after failure.

The Finite Element model presented in Chapter 4 answers the research questions summarised in page 35. The Finite Element model used a simplified geometry of the bone, while the PMMA bone cement was modelled as a uniform thickness and hip resurfacing components modelled form *Biomet* templates. The main feature of the Finite Element model was to be able to perform a dynamic simulation of daily activities, such as walking, descending stairs and standing up from a chair.

The Finite Element model could incorporate the effect of hip forces and flexion-extension rotation to provide a tool to study the effect of metal-on-metal friction on the PMMA cement mantle.

Previous Finite Element Analysis of hip resurfacing arthroplasty has used a static approach (Taylor, 2006). The dynamic approach used in this study explored the phenomena of more accurate simulation of metal-on-metal friction and furthermore, understand that maximum hip forces are not correlated with maximum stresses. For example, in the case of descending stairs the maximum hip contact force (2203.57 N) happened at 0.7917 seconds into the gait, while the maximum tensile (2.74 MPa) and shear (4.67 MPa) stresses in the PMMA bone cement appeared 1.1516 seconds into the gait. This was due to the Finite Element model accounting for hip forces, flexion-extension rotation and metal-on-metal friction.

6.1 Effect of Metal-on-Metal Friction Coefficient Due to Resting Periods During Daily Activities on PMMA Bone Cement Fatigue

To address the first driver, if high metal-on-metal friction coefficient due to resting periods could cause aseptic loosening of femoral hip resurfacing components during daily activities, the Finite Element Analysis model presented in Chapter 4 was applied to daily activities (walking, descending stairs and standing up) with different metal-on-metal friction coefficients according to the work of Nassutt (2003).

Nassutt et al. (2003) published *in vitro* results for mechanical testing, which identify a 'stick phenomena' related to resting periods. The 'stick phenomena' increases the metal-on-metal friction after resting periods as small as 1 second. The resting periods and consequent values for metal-on-metal friction coefficient were shown in Table 5.3. Furthermore, Wimmer et al. (2006) investigated the stick phenomena after the running in period with agreeable results to Nassutt et al. (2003).

From the point of view of PMMA bone cement maximum tensile stresses, it can be said that the higher metal-on-metal friction coefficient due to resting periods provokes an increase of tensile stress of 319.9% for the walking gait, an increase of 258.74% for descending stairs and an increase of 388.43% for standing up.

The PMMA maximum tensile stress values according to the dynamic metal-on-metal friction of 0.098 are relatively low with a maximum value for walking of only 3.13 MPa, which from the point of view of catastrophic failure or fatigue failure of the PMMA bone cement provide very small chances of happening. This research shows that the effect of resting periods during daily activities produces much higher PMMA maximum tensile stresses and PMMA tensile stress distributions than under the assumption of dynamic metal-on-metal friction.

Furthermore, PMMA maximum tensile stresses after improvement to metal-on-metal friction coefficient in the future can be predicted by the linear regression equations provide in this study.

This study proposes an eye-opener upon the effect of resting periods with its consequent higher metal-on-metal friction on the PMMA bone cement stresses.

To understand in more detail the effect of resting periods on the PMMA bone cement stresses, a fatigue analysis was performed using the Finite Element tensile stress results. The fatigue analysis presented in this study connects together the following variables: resting periods (metal-on-metal friction), cycles per year for daily activities, PMMA bone cement fatigue data and Finite Element maximum tensile stresses.

The process by which all these variables were linked is explained in Section 5.1 and 5.1.4.

PMMA fatigue data from Murphy and Prendergast (2000) was reconverted to a zero mean to be able to assess the cycles to failure for the Finite Element tensile stresses. The Finite Element maximum tensile stresses presented through section 5.1 went through a rainflow counting method to be able to capture all the damage performed by the PMMA tensile stress cycles through the whole gait and not only the damage due to the PMMA maximum tensile stress.

The rainflow counting method provided as well a prediction tool throughout linear regression equations, presented in Table 5.14, to take into account future developments in metal-on-metal friction.

The fatigue analysis described in this study was performed using Miner's cumulative damage rule (Miner, 1945) to account for the cumulative damage causes by all the stress cycles across the whole gait and furthermore, allowing to calculate the fatigue life compiling together the damage cause by different daily activities at different metal-on-metal friction coefficients due to resting periods.

The result of the fatigue analysis showed that hand mixed PMMA bone cement can be expected to initiate fatigue failure in one year after implantation, while vacuum mixed PMMA bone cement would be expected to take seven years.

It must be noted that current revision rates for hip resurfacing have escalated to 11.8% at 7 years for hip resurfacing and 13.6% at 7 years for stemmed metal-on metal bearings (total hip replacement) (NJR, 2011). The high increase in revision could be caused by several reasons but the main commonality for both systems (hip resurfacing and total hip replacement) is the metal-on-metal bearings. This study shows that high metal-on-metal friction coefficients due to resting periods may have a big influence in the medium and long term performance of metal-on metal bearing systems.

It must be noted that Miner's cumulative damage rule will not be able to give a reliable estimation of the exact moment of failure but it indicates that taking into effect the resting periods, PMMA bone cement failure will happen far sooner than previously expected.

To put these facts into perspective, previously used fatigue estimation might solely rely on static Finite Element analysis and would be limited to use the PMMA maximum tensile stress for dynamic friction (3.13 MPa in this case) during walking, which would produce damage per year of 0.0099 and it would show that 100 years are needed to produce PMMA fatigue in hand mixed bone cement and even longer life for vacuum mixed PMMA bone cement. This approach may be responsible for the high expectations on hip resurfacing arthroplasty neglecting the importance of PMMA fatigue for the survival of the femoral hip resurfacing component.

From the three daily activities simulated in this study, walking is with a difference the activity mostly responsible for the PMMA fatigue damage with 96.97% of the damage per year. This behaviour was expected as from the three daily activities selected from the work of Morlock et al. (2001), walking accounted for 98.26% of the total cycles.

The effect of resting periods and higher metal-on-metal friction can be observed in Figures 5.20 and 5.21 for walking gait and descending stairs. During walking, resting periods are responsible for around 64% of the damage per year and during descending stairs, resting periods are responsible for around 40% of the damage per year reducing the considerably the fatigue life of PMMA bone cement.

The fatigue analysis technique proposed in this study provides a way to take into account all the damaging PMMA tensile cycles and provide a realistic picture of the influence of resting periods on the PMMA fatigue failure.

Furthermore, this fatigue analysis technique could be applied to any replacement arthroplasty design because the technique is not linked only to hip resurfacing arthroplasty but, alternatively, could be adapted to Total Hip Replacement, Knee replacement and any arthoplasty where a detailed understanding of PMMA fatigue is needed.

As an illustrated way of showing the application of the Finite Element Analysis results for PMMA maximum shear stresses due to resting periods and the consequent higher metal-on-metal friction, when comparing the PMMA maximum shear stresses to the shear stress limit of 9.47 MPa calculated by the torque testing describe in section 5.4.2: Finite Element Analysis results for PMMA maximum shear stress (for dynamic metal-on-metal friction) are very much below the interface failure limits, with maximum shear stress values of 5.25 MPa for walking, 4.67 MPa for descending stairs and 3.61 MPa for standing up.

If resting periods are taking into account a very different picture is drawn, with resting periods over 10 seconds during walking reaching a higher PMMA maximum shear stress value than the torque testing shear stress limit and descending stairs getting very close to the limit as well, same as standing up.

Furthermore, the debonding of the PMMA-metal interface could produce the squeaky noise reported in private conversations with practitioners during conferences as it was experienced by the author during torque mechanical testing.

In a similar way to PMMA tensile stresses, PMMA maximum shear stresses after improvement to metal-on-metal friction in the future could be predicted by the linear regression equations provide in this study.

The Finite Element Analysis results for PMMA tensile and shear stresses show how much the effect of resting periods can influence the survival of the femoral hip resurfacing component and the outcome of the procedure.

This study recommends that patients with hip resurfacing arthroplasty should be made aware of high metal-on-metal friction situations, which could lead to early failure. Due to the fact of high metal-on-metal friction coefficients being restored to dynamic friction values after only 2 or 3 cycles (Morlock, 2005), the author suggest to hip resurfacing patients to rotate the resurfaced leg without weight bearing after any resting periods. This would reinstate the fluid film lubrication in between the femoral and acetabular hip resurfacing components and, when the walking or descending stairs gait starts, the metal-on-metal lubrication will be dynamic with very low risk of interface failure and PMMA bone cement failure. After long periods seated, this study suggests that resurfaced hip-patients might benefit from reducing the weight borne by the resurfaced hip by improving their posture during standing-up.

6.2 Effect of Bone Quality on PMMA Bone Cement Stresses

Patient Bone quality is a very important factor for the success of hip resurfacing (Currey, 1998). Bone quality is one of the parameters used for patient selection to have hip resurfacing arthroplasty (Pollard et al., 2006, Siebel et al., 2006 and Amstutz et al., 2004).

During the preliminary research of this study, static Finite Element Analysis simulated a decrease in bone quality to understand the effect on the PMMA bone cement (Jimenez-Bescos et al., 2005), resulting in an increase in PMMA bone cement stresses due to the decrease in bone quality.

To address the second driver, if low bone quality affects the stability of the femoral hip resurfacing components due to PMMA stresses during daily activities, the Finite Element model presented in Chapter 4 was applied to daily activities (walking, descending stairs and standing up) with different metal-on metal friction coefficient and varying the bone quality. A multi-parametric approach was used during the Finite Element Analysis.

This study provides an easy to use relationship between PMMA maximum tensile and shear stress; according to varying metal-on-metal due to resting periods and patient bone quality. These comparisons are presented as equations, two-dimensional graphs and two-dimensional templates which increases the usability of the results as shown in along section 5.2. The two-dimensional templates are thought to be a practical tool to predict in situ PMMA tensile and shear stresses; for example in the operating theatre once bone quality had been evaluated by the surgeon.

A decrease in patient bone quality from 120% to 60% produced an increase of PMMA maximum tensile stresses between 120% and 124% during walking and between 117% and 125% for PMMA maximum shear stresses. During descending stairs, a decrease in patient bone quality produced an increase of PMMA maximum tensile stresses between 114% and 130% and between 117% and 122% for PMMA maximum shear stresses. During standing up, a decrease in patient bone quality produced an increase of PMMA maximum tensile stresses around 131% and between 123% and 130% for PMMA maximum shear stresses.

Furthermore, a decrease in patient bone quality has a greater effect at higher metal-on-metal friction coefficients producing higher maximum tensile stresses in the PMMA bone cement.

According to these results, patients should be advised to be careful during descending stairs and standing up due to having the biggest increases in PMMA stresses.

An increase of PMMA maximum tensile stresses due to reduced bone quality would produce higher tensile stress cycles, which will reduce the PMMA fatigue life, leading to failure of the PMMA bone cement in an earlier stage than predicted just for resting periods.

As an illustrated way of showing the application of the Finite Element Analysis results for PMMA maximum shear stresses, taking into account patients bone quality and resting periods on the effect on PMMA maximum shear stresses, with resting periods over 5 seconds during walking, a higher value than the torque testing shear stress limit will be reached. Additionally the limit is approached during descending stairs. In the case of standing up, the torque shear stress limit would be far exceeded. These scenarios could produce the initiation of PMMA-metal interface failure.

PMMA maximum tensile and shear stresses after improvement to metal-on-metal friction in the future and for different patient bone quality could be predicted by the linear regression equations provide in this study according to daily activity, metal-on-metal friction and bone quality.

This study on the effect of bone quality on PMMA bone cement stresses provide evidence to support the important of bone quality during patient selection as presented in the literature review in sections 2.13.1 and 2.13.2.

Bone quality could be reduced due to stress shielding in the bone and according to this study, this reduction could provoke PMMA bone cement failure by fatigue or interface failure due to an increase of PMMA tensile and shear stresses. PMMA tensile and shear stresses can increase up to 19% and 17% respectively due a reduction of bone quality to 60% during walking, up to 20% and 14% respectively during descending stairs and up to 23% and 20% respectively during standing up.

6.3 Effect of PMMA Young's Modulus on PMMA Bone Cement Stresses

The third driver, if PMMA bone cement Young's modulus could affect the stability femoral hip resurfacing components due to PMMA stresses during daily activities; was addressed using the Finite Element model presented in Chapter 4 for different daily activities (walking, descending stairs and standing up). With varying metal-on metal friction coefficient, varying the bone quality and varying PMMA Young's modulus. A multi-parametric approach was achieved during the Finite Element Analysis.

PMMA bone cement Young's modulus values used in Finite Element Analysis varies between 1 GPa and 4 GPa (Schmoelz, 2001) while PMMA bone cement Young's modulus through mechanical testing varies between 1.5 GPa and 4.1 GPa (Lewis, 1997).

Different manufacturers of PMMA bone cement produce different mechanical properties and Young's modulus through different PMMA bone cement compositions. Furthermore, a hip resurfacing arthroplasty design will be fixed with different PMMA

bone cement by different surgeons performing the operation and hence producing different PMMA mechanical properties and outcomes to the operation.

The results of this study regarding a comparison of PMMA tensile and shear stresses according to varying metal-on-metal, due to resting periods, patient bone quality and PMMA Young's modulus are presented as a prediction tool in the form of equations, two-dimensional graphs and two-dimensional templates within Section 5.3.

The influence of PMMA Young's modulus on the PMMA maximum tensile and shear stresses can be observed from Figures 5.49 and 5.50 during walking. PMMA maximum tensile and shear stresses can be reduced or managed by the composition of PMMA bone cement. These reductions are higher as the metal-on-metal friction is increased, suggesting it could be a way forward to reduce the risk of interface failure and PMMA bone cement failure. Similar trends in PMMA maximum tensile and shear stresses are observed for descending stairs and standing up.

PMMA maximum tensile and stresses after improvement to metal-on-metal friction in the future for different patient bone quality and PMMA bone cements could be predicted by the linear regression equations provide in this study according to daily activity, metal-on-metal friction, bone quality and PMMA Young's modulus.

This study suggests that the use of low PMMA Young's modulus could reduce the risk of interface failure and PMMA bone cement failure due to resting periods and patient bone quality. According to the findings of this study, the use of low PMMA Young's modulus could be the answer to a long lasting outcome of hip resurfacing arthroplasty as long as they do not compromise other PMMA bone cement properties, such as fatigue strength for example.

By using PMMA bone cement with a low Young's modulus, PMMA tensile and shear stresses would be reduced in the PMMA bone cement lowering the risk of PMMA fatigue failure and PMMA-metal interface failure and avoiding premature failure of the femoral hip resurfacing component in the medium and long term. This reduction effect in PMMA stresses due to low PMMA Young's modulus is more accentuated at high metal-on-metal friction values, helping to reduce the effect of resting periods in hip resurfacing arthroplasty.

6.4 PMMA Mechanical Testing

This research used mechanical testing to address the four driver presented in section 3.5 by investigating the behaviour and failure of the PMMA-metal interface, which might be instrumental in promoting failure in the femoral hip resurfacing component by torque. The research developed a protocol to test the PMMA-metal interface in pure shear as a way to illustrate the application of the Finite Element Analysis results for PMMA maximum shear stresses.

The PMMA-metal interface results were matched to Finite Element Analysis shear stress results as shown in Figure 5.74 to calculate the maximum PMMA shear stress to initiate interface damage.

The PMMA-metal interface mechanical testing involved two different PMMA bone cement: *Palacos LV* and *Simplex P*. The results of the mechanical testing (section 5.4.1) showed that a maximum PMMA shear stress over 20.04 MPa would produce PMMA-metal interface failure for *Palacos LV* bone cement, while for Simplex P bone cement the PMMA shear stress to initiate PMMA-metal interface failures 5.94 MPa.

Torque testing was performed using *Simplex P* PMMA bone cement to evaluate the torque implications in failure of the PMMA-metal interface and loosening of the hip resurfacing femoral component. Torque in early development of hip resurfacing was reported to be higher than for conventional total hip arthroplasty (Ma et al., 1983).

After matching the torque testing results (section 5.4.2) to the Finite Element Analysis results, a PMMA maximum shear stress over 9.47 MPa would initiate loosening of the PMMA-metal interface.

Mechanical torque testing revealed two important phenomena: First, it appeared that a femoral hip resurfacing component could become loose at the PMMA-metal interface, allowing it to freely rotate, while still being attached to the femoral neck. This phenomenon could not have been detected during post-operative radiographic follow-ups as explained above. This phenomenon could produce erosion of the PMMA bone cement with the production of particles and could lead to failure as presented by Bell et al. (1985) while studying the failure of the Wagner resurfacing arthroplasty. This failure mechanism was presented by Huiskes et al (1985) as failure caused by high sensitivity to interface loosening, followed by failure propagation.

Debonding of the PMMA-metal interface has been long understood as a mechanism of initiation of failure in total hip arthroplasty (Davies et al., 1992). As presenting previously in this chapter, PMMA bone cement could be suggested to torque failure due to higher metal-on-metal friction coefficients and further accentuated by a decrease in bone quality.

Second, the phenomenon of free rotation was noted to be accompanied by a squeaky noise, which was linked to high metal-on-metal friction and will be further explained in this chapter.

According to Bitsch et al. (2007), the outer wall of the femoral hip resurfacing component is the most important area for torque resistance. This was observed during the mechanical torque testing with two specimens failing at a very early stage due to insufficient coverage of the outer wall during implantation, which could happen using a low viscosity cementing technique (Chandler, 2006, Falez et al., 2010 and Falez et al., 2011). Morlock et al. (2006) reported thicker PMMA bone cement thickness around the pole than the sides of retrieved femoral hip resurfacing components due to failure.

The mechanical testing in this study ratified the importance of PMMA bone cement coverage in the outer wall of the femoral hip resurfacing component to prevent interface loosening and failure propagation.

Chapter 7

Conclusions and Recommendations

Following a review of the current status of hip resurfacing arthroplasty and the variables affecting its outcome, a gap in knowledge regarding resting periods, bone quality, dynamic loading and stresses within cementing agents was identified. The aim of the study was to investigate the short, medium and long term performance of PMMA bone cement of the femoral component in hip resurfacing arthroplasty from the point of view of analysing the failure of the bone cement to provide understanding, awareness and potentially inform upon lifestyle options following hip resurfacing arthroplasty.

7.1 Effect of Metal-on-Metal Friction Coefficient Due to Resting Periods During Daily Activities on PMMA Bone Cement Fatigue

The literature review suggests that dynamic Finite Element Analysis is yet to be used to investigate the effect of resting periods during daily activities on the failure mechanisms of PMMA bone cement and as such it forms the gap in knowledge. The Finite Element model developed in Chapter 4 was used to investigate the drivers to achieve the objectives and aim of this study.

Finite Element Analysis was performed for three different daily activities: walking, descending stairs and standing up from a chair. The Finite Element Analysis used hip contact forces and flexion-extension rotation to be able to simulate metal-on-metal friction variations according to resting periods. The Finite Element Analysis was dynamic to capture the whole effect of the forces and rotation instead of a static analysis that focus in the point of maximum hip contact force.

A fatigue analysis study based on Miner's cumulative damage rule was developed to be able to understand if PMMA fatigue failure would occur. Resting periods, metal-on-metal friction, frequency of daily activities and PMMA fatigue data were compiled together to be able to analyse the results of the Finite Element Analysis developed in Section 5.1.

The fatigue analysis technique proposed in this study provides a way to take into account all the damaging PMMA tensile cycles and provide a realistic picture of the influence of resting periods on the PMMA fatigue failure. The fatigue analysis shows that resting periods could promote PMMA fatigue failure much earlier than expected by static Finite Element studies (Watanabe, 2000) and draws attention into the importance of the understanding of PMMA fatigue for the survival of the femoral hip resurfacing component.

PMMA fatigue will develop faster in hand mixed bone cement because of a lower fatigue life; hence this study recommends the use of vacuum mixed bone cement within hip resurfacing arthroplasty procedures.

The fatigue analysis technique shown in this study could be applied to any replacement arthroplasty design. It could be adapted to total hip replacement, Knee replacement and any arthoplasty where a detailed indicative understanding of PMMA fatigue is necessary.

Resting periods over 10 seconds during walking could produce a higher stress value (around 3%) than the torque testing shear stress limit calculated in this study. Descending stairs and the action of standing up approaches this limit. Exceeding the shear stress limit would lead to failure of the PMMA-metal interface and subsequent failure of the hip resurfacing arthroplasty.

This study suggests that occupational therapist and patients with hip resurfacing arthroplasty should be aware of high metal-on-metal friction situations, which could lead to early failure. It is suggested that hip resurfacing patients rotate the resurfaced leg without weight bearing after any resting periods. This would reinstate the fluid film lubrication in between the femoral and acetabular hip resurfacing components and avoid the higher PMMA bone cement stresses due to resting periods. When the walking or descending stairs gait starts, the metal-on-metal lubrication will be dynamic with very low risk of interface failure or PMMA bone cement failure. After long periods seated, the findings of the study suggest that hip resurfacing patients could benefit from reducing the weight borne by the resurfaced hip; perhaps by improved posture or behavioural therapy to reduce hip-stresses.

7.2 Effect of Bone Quality on PMMA Bone Cement Stresses

This study shows the combined, multi-variant effect of patient bone quality and resting periods on the PMMA bone cement stresses. A decrease in bone quality added to the effect of resting periods will increase the risk of PMMA fatigue failure and PMMA-metal interface failure due to an increase of PMMA tensile and shear stresses, suggesting that patients with low bone quality should avoid hip resurfacing procedure.

7.3 Effect of PMMA Young's Modulus on PMMA Bone Cement Stresses

This study identifies that the use of low PMMA Young's modulus could reduce the risk of interface failure and PMMA bone cement failure due to resting periods and patient bone quality. The use of low PMMA Young's modulus could greatly enhance the long term success of hip resurfacing arthroplasty, as long as they do not compromise other PMMA bone cement properties, such as fatigue strength for example.

A prediction tool to assess failure in PMMA bone cement via an easy to use relationship between PMMA maximum tensile and shear stress according to varying metal-on-metal (resting periods), patient bone quality, and PMMA Young's modulus has been analysed and discussed in this thesis. These prediction tools are presented as equations, two-dimensional graphs and two-dimensional templates which increases the usability of the results as shown along Section 5.4. The two-dimensional templates are thought to offer a practical tool to predict the PMMA tensile and shear stresses and the optimal PMMA Young's modulus, for example in the operating theatre, once bone quality had been established.

In a private conversation with Professor Kevin Cheah FRCS on 7th May 2007, orthopaedic surgeons are starting to show concerns regarding hip resurfacing arthroplasty in private conversations, due to rise in the number of premature failure that they are experiencing. These concerns start to become clearer in the statistics shown by the National Joint Registry for England and Wales and the Swedish National Hip Arthroplasty Register, with a revision rate of 11.8% at 7 years for hip resurfacing and a reduction in hip resurfacing operations.

This study shows that there are various parameters that affect the PMMA bone cement stresses, including resting periods, metal-on-metal friction, patient bone quality and PMMA Young's modulus. Moreover, this study shows that the consequence of PMMA fatigue failure and PMMA-metal interface failure must be included in the design, patient selection, screening process, post-operative rehabilitation and long term lifestyle attributes.

Finite Element Analysis has been used to address the effect of resting periods during daily activities, patients bone quality and PMMA bone cement Young's modulus on the PMMA bone cement stresses of the femoral hip resurfacing component.

7.4 PMMA Mechanical Testing

Mechanical testing was used to investigate the failure of the PMMA-metal interface in hip resurfacing. Mechanical interface testing was performed using *Palacos LV* and *Simplex P* PMMA bone cement. The interface testing showed how different PMMA bone cement formulation reacts to the interface testing, with a high variation of interface shear stress limit.

The mechanical testing on this study included torque testing. The torque testing results put into context the effect of PMMA shear stress on the PMMA-metal interface failure in hip resurfacing arthroplasty. The torque testing results were matched to the Finite Element results in this study, concluding that the shear stress interface limit in the PMMA bone cement could be as low as 9.47 MPa.

The study therefore enhances the understanding of the effect of resting periods, metal-on-metal friction, patient bone quality and PMMA bone cement mechanical properties to improve the short, medium and long term performance of hip resurfacing arthroplasty.

Chapter 8

Recommendations for further work

8.1 Developing the Application to Other Procedures

This study investigated several parameters that could affect the stability of hip resurfacing arthroplasty through the failure of PMMA bone cement. However, the mechanical testing and Finite Element Analysis could be further refined, developed, and extended to other designs of hip resurfacing arthroplasty designs and also to total hip arthroplasty.

8.2 Fatigue, Torque and Mechanical Test Databases

The mechanical testing used in this study to understand the PMMA-metal interface failure was developed to provide data regarding the ultimate pure shear stress to failure. It is suggested that PMMA-metal interface testing should be performed to provide fatigue data regarding the PMMA-metal interface. The interface fatigue data could be used for a fatigue analysis similar to the one used in this study to understand the PMMA fatigue failure.

In a similar way, the torque mechanical testing would benefit from a fatigue study and from using femoral hip resurfacing components provide by manufacturers.

It would be beneficial for the whole bioengineering community to have available a database containing all the mechanical testing raw data for PMMA bone cements available in the market as step forward from the work of Kühn (2000). Moreover, with all the data collected using the same equipment and experimental protocols to make easier the comparison of performance between different PMMA bone cements.

8.3. Limitations and Refinement of the Finite Element Model

The Finite Element Analysis used in this study used an ideal shape and homogenous material properties to represent the femur. It is suggested that the next step would be to apply the effect of resting periods to a heterogeneous model created from CT-scan data. The study could be extrapolated to a musculoskeletal three dimensional model blending together hard and soft tissue from CT-scan and MRI data. The limitations for these approaches include the amount of elements to be solved in a dynamic Finite Element Analysis; these require enormous computing power that may become more readily achievable in the future.

The multi-parametric forensic engineering approach developed in this study could be applied to the *Birmingham* hip resurfacing system for direct comparison. Preliminary research (Jimenez-Bescos et al., 2005) already showed similarities between the PMMA stresses for both hip resurfacing systems.

The multi-parametric approach combining the effects of resting periods, bone quality and PMMA Young's modulus could be further developed by deploying a Monte Carlo probabilistic approach. This would enhance understanding of the interrelations between these parameters now that this study has shown their importance.

It is suggested that the effect of resting periods should be studied on metal-on-metal total hip arthroplasty because of the high metal-on-metal friction generated during resting periods as supported by the high revision rates for stemmed metal-on metal bearings of 13.6% at 7 years (NJR, 2011). This could greatly affect the outcome of the total hip procedure as it has been shown in this study for hip resurfacing arthroplasty.

Methods of reducing static friction after rest periods should be investigated and provisional results from research at Anglia Ruskin University show that surface texturing by simulating plateau honing is a promising development.

This study could be further enhanced by from more data regarding frequency and duration of daily activities and resting periods, which would generate more accurate prediction of PMMA bone cement fatigue.

References

Active Joints Orthopedics. http://activejointsortho.com/procedure.htm. Accessed in 2012.

Adams, D. & Quigley, S. 2005. Hip Resurfacing: Past, present and future. Journal of Orthopaedic Nursing 9, 87-94.

Amstutz, H. C. Grigoris, P. & Dorey, F. J. 1998, Evolution and future of surface replacement of the hip, *Journal of Orthopaedic Science*, issue 3. pp. 169-186.

Amstutz, H. C., Beaule, P. E., Dorey, F. J., Le Duff, M. J., Campbell, P. A., & Gruen, T. A. 2004, Metal-on-metal hybrid surface arthroplasty: two to six-year follow-up study, *J.Bone Joint Surg.Am.*, vol. 86-A, no. 1, pp. 28-39.

Amstutz, H. C., Campbell, P. A., & Le Duff, M. J. 2004, "Fracture of the neck of the femur after surface arthroplasty of the hip", *J.Bone Joint Surg.Am.*, vol. 86-A, no. 9, pp. 1874-1877.

Amstutz, H. C., Su, E. P., & Le Duff, M. J. 2005, Surface arthroplasty in young patients with hip arthritis secondary to childhood disorders, *Orthop.Clin.North Am.*, vol. 36, no. 2, pp. 223-230.

Amstutz, H. C. & Le Duff, M. J. 2006, Background of metal-on-metal resurfacing, *Proc.Inst.Mech.Eng [H.]*, vol. 220, no. 2, pp. 85-94.

Amstutz, H. C., Le Duff, M. J., & Johnson, A. J. 2012, "Socket position determines hip resurfacing 10-year survivorship", *Clin.Orthop Relat Res.*, vol. 470, no. 11, pp. 3127-3133.

Beaule, P. E., Lee, J. L., Le Duff, M. J., Amstutz, H. C., & Ebramzadeh, E. 2004, Orientation of the femoral component in surface arthroplasty of the hip. A biomechanical and clinical analysis, *J.Bone Joint Surg.Am.*, vol. 86-A, no. 9, pp. 2015-2021.

Beaule, P. E., Campbell, P. A., Hoke, R., & Dorey, F. 2006, Notching of the femoral neck during resurfacing arthroplasty of the hip: a vascular study, *J.Bone Joint Surg.Br.*, vol. 88, no. 1, pp. 35-39.

Beaule, P. E., Matar, W. Y., Poitras, P., Smit, K., & May, O. 2009, "2008 Otto Aufranc Award: component design and technique affect cement penetration in hip resurfacing", *Clin.Orthop Relat Res.*, vol. 467, no. 1, pp. 84-93.

Bell, R. S., Schatzker, J., Fornasier, V. L., & Goodman, S. B. 1985, A study of implant failure in the Wagner resurfacing arthroplasty, *J.Bone Joint Surg.Am.*, vol. 67, no. 8, pp. 1165-1175.

Bergmann, G., Deuretzbacher, G., Heller, M., Graichen, F., Rohlmann, A., Strauss, J., & Duda, G. N. 2001, Hip contact forces and gait patterns from routine activities, *J.Biomech.*, vol. 34, no. 7, pp. 859-871.

Biomet Europe. 2005. *ReCap* product rationale.

Biomet Europe. 2005. *ReCap* Operative Technique.

Biomet Europe. 2005. *ReCap* technical design rationale.

Biggam, J. Succeeding with you Master's Dissertation: A Step-by-Step Handbook: A Step-by-step Guide. 2008. Open University Press.

Bitsch, R. G., Heisel, C., Silva, M., & Schmalzried, T. P. 2007, Femoral cementing technique for hip resurfacing arthroplasty, *J.Orthop.Res.*, vol. 25, no. 4, pp. 423-431

Bitsch, R. G., Jager, S., Lurssen, M., Loidolt, T., Schmalzried, T. P., & Clarius, M. 2010, "Influence of bone density on the cement fixation of femoral hip resurfacing components", *J.Orthop Res.*, vol. 28, no. 8, pp. 986-991.

Bitsch, R. G., Loidolt, T., Heisel, C., & Schmalzried, T. P. 2011, "Cementing techniques for hip resurfacing arthroplasty: in vitro study of pressure and temperature", *J.Arthroplasty*, vol. 26, no. 1, pp. 144-151.

Bitsch, R. G., Obermeyer, B. J., Rieger, J. S., Jager, S., Schmalzried, T. P., & Bischel, O. E. 2013, "What is the upper limit of cement penetration for different femoral hip resurfacing components?", *J.Arthroplasty*, vol. 28, no. 4, pp. 654-662.

Breer, S., Krause, M., Busse, B., Hahn, M., Ruther, W., Morlock, M. M., Amling, M., & Zustin, J. 2012, "Analysis of retrieved hip resurfacing arthroplasties reveals the interrelationship between interface hyperosteoidosis and demineralization of viable bone trabeculae", *J.Orthop Res.* , vol. 30, no. 7, pp. 1155-1161.

Callaghan, J. J., Albright, J. C., Goetz, D. D., Olejniczak, J. P., & Johnston, R. C. 2000, Charnley total hip arthroplasty with cement. Minimum twenty-five-year follow-up, *J.Bone Joint Surg.Am.*, vol. 82, no. 4, pp. 487-497.

Campbell, P., Takamura, K., Lundergan, W., Esposito, C., & Amstutz, H. C. 2009, "Cement technique changes improved hip resurfacing longevity - implant retrieval findings", *Bull.NYU.Hosp.Jt.Dis.*, vol. 67, no. 2, pp. 146-153.

Chandler, M., Kowalski, R. S., Watkins, N. D., Briscoe, A., & New, A. M. 2006, Cementing techniques in hip resurfacing, *Proc.Inst.Mech.Eng [H.]*, vol. 220, no. 2, pp. 321-331.

Charnley, J. Low friction arthroplasty of the hip: theory and practice. 1979. Berlin: Springer-Verlag.

Cheah, K. 2007. Personal communication with Professor Kevin Cheah FRCS, Consultant Orthopaedic Surgeon at Springfield Hospital, Lawn Lane, Springfield, Chelmford, Essex, CM1 7GU, on 7th May 2007.

Coulter, G., Young, D. A., Dalziel, R. E., & Shimmin, A. J. 2012, "Birmingham hip resurfacing at a mean of ten years: results from an independent centre", *J.Bone Joint Surg.Br.*, vol. 94, no. 3, pp. 315-321.

Corten, K. & MacDonald, S. J. 2010, "Hip resurfacing data from national joint registries: what do they tell us? What do they not tell us?", *Clin.Orthop Relat Res.*, vol. 468, no. 2, pp. 351-357.

Cuckler, J. M., Moore, K. D., & Estrada, L. 2004, Outcome of hemiresurfacing in osteonecrosis of the femoral head, *Clin.Orthop.* no. 429, pp. 146-150.

Currey, J. D. 1998, Mechanical properties of vertebrate hard tissues, *Proc.Inst.Mech.Eng H.*, vol. 212, no. 6, pp. 399-411.

Davies, J. P., O'Connor, D. O., Greer, J. A., & Harris, W. H. 1987, Comparison of the mechanical properties of *Simplex P*, Zimmer Regular, and LVC bone cements, *J.Biomed.Mater.Res.*, vol. 21, no. 6, pp. 719-730.

Davies, J. P., Burke, D. W., O'Connor, D. O., & Harris, W. H. 1987. Comparison of the fatigue characteristics of centrifuged and uncentrifuged *Simplex P* bone cement. Journal Orthop Research 5, 366-371.

Davies, J. P., Singer, G., & Harris, W. H. 1992, The effect of a thin coating of polymethylmethacrylate on the torsional fatigue strength of the cement-metal interface, *J.Appl.Biomater*, vol. 3, no. 1, pp. 45-49.

Davis, E. T., Olsen, M., Zdero, R., Papini, M., Waddell, J. P., & Schemitsch, E. H. 2009, "A biomechanical and finite element analysis of femoral neck notching during hip resurfacing", *J.Biomech.Eng*, vol. 131, no. 4, p. 041002.

Davis, E. T., Olsen, M., Zdero, R., Smith, G. M., Waddell, J. P., & Schemitsch, E. H. 2013, "Predictors of femoral neck fracture following hip resurfacing: a cadaveric study", J.Arthroplasty, vol. 28, no. 1, pp. 110-116.

Denscombe, M. The Good Research Guide. 2007. Open University Press.

DePuy. 2011. www.depuy.com/asr-hip-replacement-recall. Accessed in 2012.

Dorr, L. D., Kane, T. J., III, & Conaty, J. P. 1994, Long-term results of cemented total hip arthroplasty in patients 45 years old or younger. A 16-year follow-up study, *J.Arthroplasty*, vol. 9, no. 5, pp. 453-456.

Ebied, A. & Journeaux, S. 2002. Metal-on-Metal hip resurfacing" Current Orthopaedics 16, 420-425.

Esposito, C., Walter, W. L., Campbell, P., & Roques, A. 2010, "Squeaking in metal-on-metal hip resurfacing arthroplasties", *Clin.Orthop Relat Res.*, vol. 468, no. 9, pp. 2333-2339.

Falez, F., Favetti, F., Casella, F., & Panegrossi, G. 2007, Hip resurfacing: why does it fail? Early results and critical analysis of our first 60 cases, *Int.Orthop.*

Falez, F., Favetti, F., Casella, F., Papalia, M., & Panegrossi, G. 2010, "Patterns of cement distribution in total hip resurfacing arthroplasty", *J.Arthroplasty*, vol. 25, no. 7, pp. 1162-1167.

Falez, F., Favetti, F., Casella, F., Papalia, M., & Panegrossi, G. 2011, "Results of hip resurfacing", *Int.Orthop*, vol. 35, no. 2, pp. 239-243.

Fellows, R. & Liu, A. M. M. 2008. Research Methods For Construction. Wiley-blackwell.

Fisher, J. 2002. The Synovial Joint. Leeds:EPSRC.

Freeman, M. A. 1978, Some anatomical and mechanical considerations relevant to the surface replacement of the femoral head, *Clin.Orthop.* no. 134, pp. 19-24.

Furman, B. R., Saha, S., & Kitaoka, K. 1999. Fatigue resistance of selfcuring acrylic bone cement mixed by sonicatio". Trans 25th Ann Mtg, Soc Biomater, Providence, RI , 594.

Gokhale, N. S., Deshpande, S. S., Bedekar, S. V., & Thite, A. N. 2008. Practical Finite Element Analysis. Finite to Infinite.

Goodman, S. 2005, Wear particulate and osteolysis, *Orthop.Clin.North Am.*, vol. 36, no. 1, pp. 41-8, vi.

Grigoris, P., Roberts, P., Panousis, K., & Jin, Z. 2006, Hip resurfacing arthroplasty: the evolution of contemporary designs, *Proc.Inst.Mech.Eng [H.]*, vol. 220, no. 2, pp. 95-105.

Gross, T. P., Liu, F., & Webb, L. A. 2012, "Clinical outcome of the metal-on-metal hybrid Corin Cormet 2000 hip resurfacing system: an up to 11-year follow-up study", *J.Arthroplasty*, vol. 27, no. 4, pp. 533-538.

Heiner, A.D. 2008. Structural properties of fourth-generation composite femurs and tibias, *Journal of Biomechanics*, vol. 41, no. 15, pp. 3282-3284

HIP98 CD. 2001.

Hip joint movements. (https://courses.stu.qmul.ac.uk/smd/kb/grossanatomy/basic_anat/movements_of_the_hip_joint.htm, accessed in October 2010)

Hospital for Special Surgery. www.hss.edu/skys-limit-after-hip-resurfacing.asp. Accessed in 2012.

Howie, D. W., Cornish, B. L., & Vernon-Roberts, B. 1993, The viability of the femoral head after resurfacing hip arthroplasty in humans, *Clin.Orthop.* no. 291, pp. 171-184.

Huiskes, R. 1990, The various stress patterns of press-fit, ingrown, and cemented femoral stems, *Clin.Orthop Relat Res.* no. 261, pp. 27-38.

Huiskes, R. 1993. Mechanical failure in total hip arthroplasty with cement". Current Orthopaedics 7, 239-247.

International Standardization Organization. 2002. ISO 5833:2002, Implants for surgery - acrylic resin cements.

Isaac, G. H., Siebel, T., Schmalzried, T. P., Cobb, A. G., O'Sullivan, T., Oakeshott, R. D., Flett, M., & Vail, T. P. 2006, Development rationale for an articular surface replacement: a science-based evolution, *Proc.Inst.Mech.Eng [H.]*, vol. 220, no. 2, pp. 253-268.

Janssen, D., Srinivasan, P., Scheerlinck, T., & Verdonschot, N. 2012, "Effect of cementing technique and cement type on thermal necrosis in hip resurfacing arthroplasty--a numerical study", *J.Orthop Res.*, vol. 30, no. 3, pp. 364-370.

Jimenez-Bescos, C. 2004. Contact Stress as a Function of Cement Mantle Thickness in Total Hip Replacement. Unpublished BSc Dissertation. Anglia Ruskin University.

Jimenez-Bescos, C., Mootanah, R., Walker, R., Ingle, P., Cheah, K., & Dowell, J. 2005. The effect of varying bone material properties on a resurfaced hip joint. 1, 73-83. Proceedings IInd International Conference on Computational Bioengineering, Lisbon, Portugal.

Jin, Z. M., Dowson, D., & Fisher, J. 1997, Analysis of fluid film lubrication in artificial hip joint replacements with surfaces of high elastic modulus, *Proc.Inst.Mech.Eng [H.]*, vol. 211, no. 3, pp. 247-256.

Johnson, K. L. 1985. Contact mechanics. Cambridge University Press.

Kindt-Larsen, T., Smith, D. B., & Jensen, J. S. 1995, Innovations in acrylic bone cement and application equipment, *J.Appl.Biomater*, vol. 6, no. 1, pp. 75-83.

Kordas, G., Baxter, J., Parsons, N., Costa, M. L., & Krikler, S. J. 2012, "Minimum 5-year follow-up after Cormet hip resurfacing. A single surgeon series of 234 hips", *Hip Int.*, vol. 22, no. 2, pp. 189-194.

Krause, W., Krug, W. H., & Miller, J. E. 1980. The effect of cement types and pressurization on the mechanical properties of acrylic bone cement. Proc.26th Annu.ORS, Atlanta, GA , 253.

Krause, W. & Hofmann, A. 1989. Antibiotic impregnated acrylic bone cements: a comparative study of the mechanical properties. J.Bioactive Compat.Polym. 4, 345-361.

Krause, M., Breer, S., Hahn, M., Ruther, W., Morlock, M. M., Amling, M., & Zustin, J. 2012, "Cementation and interface analysis of early failure cases after hip-resurfacing arthroplasty", *Int.Orthop*, vol. 36, no. 7, pp. 1333-1340.

Kwon, Y. M., Glyn-Jones, S., Simpson, D. J., Kamali, A., McLardy-Smith, P., Gill, H. S., & Murray, D. W. 2010, "Analysis of wear of retrieved metal-on-metal hip resurfacing implants revised due to pseudotumours", *J.Bone Joint Surg.Br.*, vol. 92, no. 3, pp. 356-361.

Kühn, K.D. 2000. Bone cements – Up to date comparison of physical and chemical properties of commercial materials. Springer.

Lee, Y., Pan, J., Hathaway, R.B. & Barkey, M.E. 2005. Fatigue testing and analysis – theory and practice. Elsevier Butterworth-Heinemann.

Lewis, G. 1997, Properties of acrylic bone cement: state of the art review, *J.Biomed.Mater.Res.*, vol. 38, no. 2, pp. 155-182.

Lewis, G. 2003, Fatigue testing and performance of acrylic bone-cement materials: state-of-the-art review, *J.Biomed.Mater.Res.B Appl.Biomater.*, vol. 66, no. 1, pp. 457-486.

Little, C. P., Ruiz, A. L., Harding, I. J., McLardy-Smith, P., Gundle, R., Murray, D. W., & Athanasou, N. A. 2005, Osteonecrosis in retrieved femoral heads after failed resurfacing arthroplasty of the hip, *J.Bone Joint Surg.Br.*, vol. 87, no. 3, pp. 320-323.

Little, J. P., Taddei, F., Viceconti, M., Murray, D. W., & Gill, H. S. 2007, Changes in femur stress after hip resurfacing arthroplasty: Response to physiological loads, *Clin.Biomech.(Bristol., Avon.)*, vol. 22, no. 4, pp. 440-448.

Liu, F., Jin, Z., Roberts, P., & Grigoris, P. 2006, Importance of head diameter, clearance, and cup wall thickness in elastohydrodynamic lubrication analysis of metal-on-metal hip resurfacing prostheses, *Proc.Inst.Mech.Eng [H.]*, vol. 220, no. 6, pp. 695-704.

Loughead, J. M., Chesney, D., Holland, J. P., & McCaskie, A. W. 2005, Comparison of offset in Birmingham hip resurfacing and hybrid total hip arthroplasty, *J.Bone Joint Surg.Br.*, vol. 87, no. 2, pp. 163-166.

Ma, S. M., Kabo, J. M., & Amstutz, H. C. 1983, Frictional torque in surface and conventional hip replacement, *J.Bone Joint Surg.Am.*, vol. 65, no. 3, pp. 366-370.

Macpherson, G. J. & Breusch, S. J. 2011, "Metal-on-metal hip resurfacing: a critical review", *Arch.Orthop Trauma Surg.*, vol. 131, no. 1, pp. 101-110.

Maguire, C. M., Seyler, T. M., Boyd, H. S., Lai, L. P., Delanois, R. E., & Jinnah, R. H. 2009, "Hip resurfacing-keys to success", *Bull.NYU.Hosp.Jt.Dis.*, vol. 67, no. 2, pp. 142-145.

McMinn, D., Treacy, R., Lin, K., & Pynsent, P. 1996, Metal on metal surface replacement of the hip. Experience of the McMinn prothesis, *Clin.Orthop.* no. 329 Suppl, p. S89-S98.

McMinn, D. & Daniel, J. 2006, History and modern concepts in surface replacement, *Proc.Inst.Mech.Eng [H.]*, vol. 220, no. 2, pp. 239-251.

McMinn, D. J. W. 2003. Development of metal/metal hip resurfacing. Hip International 1[Suppl. 2], 541-553.

Mellon, S. J., Kwon, Y. M., Glyn-Jones, S., Murray, D. W., & Gill, H. S. 2011, "The effect of motion patterns on edge-loading of metal-on-metal hip resurfacing", *Med.Eng Phys.*, vol. 33, no. 10, pp. 1212-1220.

Miner, M. A. 1945. Cumulative damage in fatigue. Journal of Applied Mechanics 12, 159-164.

Morlock, M., Schneider, E., Bluhm, A., Vollmer, M., Bergmann, G., Muller, V., & Honl, M. 2001, Duration and frequency of every day activities in total hip patients, *J.Biomech.*, vol. 34, no. 7, pp. 873-881.

Morlock, M. 2005.Email correspondent with Professor Michael Morlock on 15-6-2005.

Morlock, M. M., Bishop, N., Ruther, W., Delling, G., & Hahn, M. 2006, Biomechanical, morphological, and histological analysis of early failures in hip resurfacing arthroplasty, *Proc.Inst.Mech.Eng H.*, vol. 220, no. 2, pp. 333-344.

Murphy, B. P. & Prendergast, P. J. 2000. On the magnitude and variability of teh fatigue strength of acrylic bone cement". International Journal of Fatigue 22, 855-864.

Murtha, P. E., Hafez, M. A., Jaramaz, B., & DiGioia, A. M., III 2008, Variations in acetabular anatomy with reference to total hip replacement, J.Bone Joint Surg.Br., vol. 90, no. 3, pp. 308-313.

NAFEMS. 1992. A finite element primer.

NAFEMS. 2002. An Explicit Finite Element Primer.

Naoum, S. 2007. Dissertation Research and Writing for Construction Students. Butterworth-Heinemann.

Nassutt, R., Wimmer, M. A., Schneider, E., & Morlock, M. M. 2003, "The influence of resting periods on friction in the artificial hip", *Clin.Orthop.Relat Res.* no. 407, pp. 127-138.

National Joint Registry (NJR) for England and Wales. 8th Annual Report. 2011.

Noble, P. C., Alexander, J. W., & Paravic, V. 1995. The fatigue resistance of pre-formed acrylic cement mantles. Trans 21st Ann Mtg, Soc Biomater, San Francisco, CA , 94.

Nunley, R. M., Della Valle, C. J., & Barrack, R. L. 2009, "Is patient selection important for hip resurfacing?", *Clin.Orthop Relat Res*., vol. 467, no. 1, pp. 56-65.

Orthoteers. 2007. *The guiding light in orthopaedic education.* [online] available at: www.orthoteers.com [Accessed in 2007].

Park, K. D., Kim, J., Yang, S. J., Yao, A. and Park, J. B. 2003, Preliminary study of interfacial shear strength between PMMA precoated UHMWPE acetabular cup and PMMA bone cement. *J.Biomed.Mater.Res.B Appl.Biomater.*, vol. 65, no. 2, pp. 272-279.

Pollard, T. C., Baker, R. P., Eastaugh-Waring, S. J., & Bannister, G. C. 2006, Treatment of the young active patient with osteoarthritis of the hip. A five- to seven-year comparison of hybrid total hip arthroplasty and metal-on-metal resurfacing, *J.Bone Joint Surg.Br.*, vol. 88, no. 5, pp. 592-600.

Radcliffe, I. A. & Taylor, M. 2007, Investigation into the effect of varus-valgus orientation on load transfer in the resurfaced femoral head: a multi-femur finite element analysis, *Clin.Biomech.(Bristol., Avon.)*, vol. 22, no. 7, pp. 780-786.

Radcliffe, I. A. & Taylor, M. 2007, Investigation into the affect of cementing techniques on load transfer in the resurfaced femoral head: a multi-femur finite element analysis, *Clin.Biomech.(Bristol., Avon.)*, vol. 22, no. 4, pp. 422-430.

Reito, A., Eskelinen, A., Puolakka, T., & Pajamaki, J. 2013, "Results of metal-on-metal hip resurfacing in patients 40 years old and younger", *Arch.Orthop Trauma Surg*., vol. 133, no. 2, pp. 267-273.

Revell, P. A. & Mayston, V. J. 1986, Immunoglobulin classes in plasma cells of the synovial membrane in chronic inflammatory joint disease, *Ann Rheum.Dis.*, vol. 45, no. 5, pp. 405-408.

SAE AE-22 Fatigue Design Handbook. 1997. Society of Automotive Engineers.

Sandiford, N. A., Muirhead-Allwood, S. K., & Skinner, J. A. 2010, "Revision of failed hip resurfacing to total hip arthroplasty rapidly relieves pain and improves function in the early post operative period", *J.Orthop Surg.Res*., vol. 5, p. 88.

Scheerlinck, T., Delport, H., & Kiewitt, T. 2010, "Influence of the cementing technique on the cement mantle in hip resurfacing: an in vitro computed tomography scan-based analysis", J.Bone Joint Surg.Am. , vol. 92, no. 2, pp. 375-387.

Schmalzried, T. P., Silva, M., de la Rosa, M. A., Choi, E. S., & Fowble, V. A. 2005, Optimizing patient selection and outcomes with total hip resurfacing, *Clin.Orthop.Relat Res.*, vol. 441, pp. 200-204.

Schmoelz, W. 2001. Factors contributing to the loosening of femoral stems in total hip arthroplasty. Glasgow Caledonian University.

Schnurr, C., Nessler, J., Meyer, C., Schild, H. H., Koebke, J., & Konig, D. P. 2009, "Is a valgus position of the femoral component in hip resurfacing protective against spontaneous fracture of the femoral neck?: a biomechanical study", *J.Bone Joint Surg.Br.*, vol. 91, no. 4, pp. 545-551.

Sehatzadeh, S., Kaulback, K., & Levin, L. 2012, "Metal-on-metal hip resurfacing arthroplasty: an analysis of safety and revision rates", *Ont.Health Technol.Assess.Ser.*, vol. 12, no. 19, pp. 1-63.

Seppanen, M., Makela, K., Virolainen, P., Remes, V., Pulkkinen, P., & Eskelinen, A. 2012, "Hip resurfacing arthroplasty: short-term survivorship of 4,401 hips from the Finnish Arthroplasty Register", *Acta Orthop*, vol. 83, no. 3, pp. 207-213.

Sharma, H., Rana, B., Watson, C., Campbell, A. C., & Singh, B. J. 2005, Femoral neck fractures complicating metal-on-metal resurfaced hips: a report of 2 cases, *J.Orthop.Surg.(Hong.Kong.)*, vol. 13, no. 1, pp. 69-72.

Shimmin, A. J. & Back, D. 2005, Femoral neck fractures following Birmingham hip resurfacing: A national review of 50 cases, *J.Bone Joint Surg.Br.*, vol. 87, no. 4, pp. 463-464.

Siebel, T., Maubach, S., & Morlock, M. M. 2006, Lessons learned from early clinical experience and results of 300 ASR hip resurfacing implantations, *Proc.Inst.Mech.Eng [H.]*, vol. 220, no. 2, pp. 345-353.

Silva, M., Lee, K. H., Heisel, C., Dela Rosa, M. A., & Schmalzried, T. P. 2004, The biomechanical results of total hip resurfacing arthroplasty, *J.Bone Joint Surg.Am.*, vol. 86-A, no. 1, pp. 40-46.

SMITH-PETERSEN, M. N. 1948, Evolution of mould arthroplasty of the hip joint, *J.Bone Joint Surg.Br.*, vol. 30B, no. 1, pp. 59-75.

St Nicholas Hospital. http://stnicholashospital.org/BHR/implant.html. Accessed in 2012.

Stachowiak, G.W. & Batchelor, A.W. 2005. Engineering tribology. Elsevier Butterworth-Heinemann

Suresh, S. 1998. Fatigue of Materials. Cambridge University Press.

Swedish national hip arthroplasty register. 2010.

Swedish national hip arthroplasty register. 2011.

Taylor, M., Tanner, K. E., Freeman, M. A., & Yettram, A. L. 1995, Cancellous bone stresses surrounding the femoral component of a hip prosthesis: an elastic-plastic finite element analysis, *Med.Eng Phys.*, vol. 17, no. 7, pp. 544-550.

Taylor, M. 2006, Finite element analysis of the resurfaced femoral head, *Proc.Inst.Mech.Eng [H.]*, vol. 220, no. 2, pp. 289-297.

The McMinn Centre. www.mcminncentre.co.uk/birmingham-hip-resurfacing.html. Accessed in 2012.

Treacy, R. B., McBryde, C. W., & Pynsent, P. B. 2005, Birmingham hip resurfacing arthroplasty. A minimum follow-up of five years, *J.Bone Joint Surg.Br.*, vol. 87, no. 2, pp. 167-170.

Udofia, I. J., Yew, A., & Jin, Z. M. 2004, Contact mechanics analysis of metal-on-metal hip resurfacing prostheses, *Proc.Inst.Mech.Eng [H.]*, vol. 218, no. 5, pp. 293-305.

Walker, R. 2007. The contact stress in the natural knee following autologous chondrocyte implantation. Anglia Ruskin University.

Watanabe, Y., Shiba, N., Matsuo, S., Higuchi, F., Tagawa, Y., & Inoue, A. 2000, Biomechanical study of the resurfacing hip arthroplasty: finite element analysis of the femoral component, *J.Arthroplasty*, vol. 15, no. 4, pp. 505-511.

Wimmer, M. A., Artelt, D., Schneider, E., Kunze, J., Morlock, M. M., & Nassutt, R. 2001. Friction and Wear Properties of Meta l/Metal Hip Joints. Materialwissenschaft und Werkstofftechnik 32[12], 891-896.

Wimmer, M. A., Nassutt, R., Sprecher, C., Loos, J., Tager, G., & Fischer, A. 2006, Investigation on stick phenomena in metal-on-metal hip joints after resting periods, *Proc.Inst.Mech.Eng H.*, vol. 220, no. 2, pp. 219-227.

Yew, A., Udofia, I., Jagatia, M., & Jin, Z. M. 2004, Analysis of elastohydrodynamic lubrication in McKee-Farrar metal-on-metal hip joint replacement, *Proc.Inst.Mech.Eng [H.]*, vol. 218, no. 1, pp. 27-34.

Yue, E. J., Cabanela, M. E., Duffy, G. P., Heckman, M. G., & O'Connor, M. I. 2009, "Hip resurfacing arthroplasty: risk factors for failure over 25 years", *Clin.Orthop Relat Res.*, vol. 467, no. 4, pp. 992-999.

Appendix A

Personal Reflection

An old Spanish proverb says: “no mires cuanto te queda sino lo que has alcanzado”. This means not to look at how much is left to go but at what you have already achieved.

Hence, this reflective report is my look-back at all the experiences that I had during my PhD journey.

This adventure started in September 2004, right after graduating with a first for a BSc (Hons) in Computer Aided Engineering (Mechanical) with a dissertation in bioengineering related to simulations of total hip replacements using Finite Element Analysis.

I certainly had a good idea about what would be expected of me during the PhD but nothing close to reality.

Having previously being working with Finite Element Analysis, the PhD was a fantastic opportunity for me to dig into exploring the possibilities of Finite Element Analysis for bioengineering. In a similar way, the PhD allowed me to not only perform but design my own mechanical testing experiments.

Following this PhD has really helped me to achieve a level of knowledge and approach to Finite Element Analysis and experimental testing, which can be appreciated in my research endeavours regarding building energy simulations and renewable energy simulations. I feel comfortable in having the knowledge to transfer all the learning outcomes from my PhD to new fields.

Perhaps the biggest learning outcome for me came when I met Dr Alan Coday and Dr David Reid in 2008. After all the fun and excitement doing all the computer simulations and mechanical testing and sharing expertise with Dr Robert Walker, I was faced with the daunting task of putting all my work and findings down on paper.
Being an engineer did not make it easy at all. The turning point for me was having to explain to Alan and David all the work I put together in this PhD. That fact made me look at my work totally from the outside and start criticising and justifying my work during the previous years. Undoubtedly, it really helped me to write my thesis keeping in mind the audience.

While in the beginning I would want to have a whole chapter ready and arrange in my head before putting it onto paper, thanks to the help and patience of Alan I learnt techniques and methods to improve my writing and to allow me to develop it even further.

Thanks to my improvement in writing through my PhD, I’m hoping to publish the work presented in this thesis and furthermore, hopefully next year, write a book on AutoCAD for Built Environment students. The writing experience has really changed my confidence in what I can achieve.

Last but not least, the whole research process undertaken to deliver this thesis has helped me to design, perform, analyse, review, write and report in any research field. Currently, I am doing research on generic skill at work, computer visualization techniques, e-learning, renewable energies and building energy simulations. I feel that all the skills gained through this PhD have made me to grow as a person and a as a researcher.